PROTEOMIC STUDIES ON PATIENT RESPONSES TO CHEMOTHERAPY, RADIOTHERAPY AND IMMUNOTHERAPY IN CANCERS

Jessica da Gama Duarte

Thesis Presented for the Degree of

DOCTOR OF PHILOSOPHY

in the Division of Medical Biochemistry

Department of Clinical Laboratory Sciences

Faculty of Health Sciences

UNIVERSITY OF CAPE TOWN

July 2015

DECLARATION

This Thesis is the result of my own work and includes nothing, which is the outcome of work done in collaboration except where specifically indicated in the text. It has not been previously submitted, in part or whole, to any university of institution for any degree, diploma, or other qualification.

In accordance with the Faculty of Health Science's guidelines, this Thesis does not exceed 80000 words in the main text.

Signed:_____

Date:_____

Jessica da Gama Duarte

ABSTRACT

There is increasing evidence that the aberrant expression of cancer-testis (CT) antigens - a family of ca. 150 proteins that are both autoimmunogenic and mainly restricted to tumours in various types of human cancers - makes them attractive immunotherapy targets, as well as possible cancer diagnostic markers.

We carried out a retrospective serological study of primary and secondary autoimmune responses of various cohorts of cancer patients prior to and/or following a variety of distinct treatments (chemotherapy, radiotherapy and immunotherapy), using a large number of archived human serum samples. Our goals were to develop and validate a novel cancer-testis and -associated antigen microarray platform and to then explore its utility and general applicability in the cancer immunology field. In addition, we sought to cross-correlate our protein microarray data from specific cohorts with in vitro T-cell re-stimulation assays for a selected subset of patients. Furthermore, as a means of determining the biological significance of our protein microarray data, we also collected clinical patient data where possible.

The underlying hypothesis of our study was that there were measurable differences in autoantibody repertoires towards tumour-specific and –associated antigens between pre- and post-treated cancer patient samples (using various trial therapies), potentially augmented by prior chemo- or radiotherapy, which would correlate with likelihood of response of individual patients to a given therapeutic treatment – including those treatments that aim to generate T-cell responses – and which would also correlate with the nature and extent of individual patient responses to treatment.

Amongst the four cohorts with acceptable patient numbers and recommended achieved statistical power, we were able to detect abundant autoantibody titres towards 1) NY-ESO-1 and MAGEB1, present in 61% (*n* = 22/36) and 56% (*n* = 20/36) of all patients in the kinase inhibitor treatment cohort, respectively; 2) SILV/gp100 and p53 Q136X, present in 31% (*n* = 19/62) and 21% (*n* = 13/62) of all patients in the pre- or post-operative chemotherapy/radiotherapy treatment cohort, respectively; 3) NY-ESO-1 and CTAG2/LAGE-1b/LAGE-1L, present in 35% (*n* = 17/48) and 25% (*n* = 12/48) of all patients in the apoptosis inhibitor treatment cohort, respectively; and 4) NY-ESO-1 and CTAG2 present in 49% (*n* = 48/98) and 46% (*n* = 45/98) of all patients in the variable treatment cohort, respectively. The remaining two cohorts did not have the necessary patient numbers or statistical power, and thus the findings obtained could not be statistically supported.

We showed that we were in fact able to measure differences in autoantibody titres towards tumour-specific and –associated antigens between cancer patients, both within the same cancer type and across

different cancers, and that these oscillated significantly after distinct treatments, thus supporting our initial hypothesis. Although these autoantibody levels showed preliminary evidence of correlation with associated T-cell and clinical responses across some of the assayed pilot cohorts, larger focussed studies using sufficient patient numbers according to an a priori power calculation estimates are required to verify significant and clinically applicable findings.

In conclusion, we showed that our novel cancer-testis and cancer–associated microarray platform represents a sensitive, high-throughput and readily customizable means to detect and quantify the presence of large panels of cancer-specific human autoantibodies in serum, obtaining consistently robust, high quality and reproducible data, and demonstrating its potential feasibility and inferred biological significance. Applications of this tool include potential use in identifying novel diagnostic, disease progression, prognostic, treatment resistant and even predictive biomarkers, which could aid in the detection and management of cancer. Most importantly, these could lead to the discovery of novel cancer therapeutic targets, patient stratification biomarkers prior to treatment, as well as a means to monitor cancer patient responses to treatment.

ACKNOWLEDGEMENTS

I would like to thank my supervisor, Professor Jonathan Blackburn, for the outstanding opportunities he has given me these past four years, and for successfully moulding me into the independent scientist I have become. I would like to thank Dr. Natasha Beeton-Kempen (CSIR) and Dr. Aubrey Shoko (CPGR) for their assistance regarding the development of the protein microarray platform. Natasha was extremely valuable over these years, assisting me with endless things, including the review of this thesis, and Aubrey was equally appreciated, sharing his expertise with me and always remaining patient, even with my endless and constant questions after our long hours of work together. I would like to thank Dr. Janique Peyper for her assistance with statistical analysis, immunological insight and readiness to help at all times. I would like to thank the Blackburn lab members, both old and new, for their companionship, the many shared lunches and the much needed distractions over these past years.

This Thesis is dedicated to my partner, parents and sister. To my partner in life, Jose Gomes, for supporting me in every possible way, and for always being patient and understanding. To my mother, Madalena Da Gama, for always believing in me, and for her constant desire for me to achieve more. To my father, Antonio Duarte, and sister, Debbie Vermeulen, for their constant care and readiness to help.

CONTENTS

LIST OF TABLES

LIST OF FIGURES

LIST OF ABBREVIATIONS AND ACRONYMS

CIBL: Cancer Immunobiology Laboratory

CPGR: Centre for Proteomic and Genomic Research

CR: complete response

CRC: colorectal cancer

CT: cancer-testis

$CT100^{+}$ array: cancer-testis 100^{+} array

dH_2O: distilled water

FACS: fluorescent activated cell sorting

GSH: Groote Schuur Hospital

h: hour

LICR: Ludwig Institute for Cancer Research

min: minutes

PBMCs: peripheral blood mononuclear cells

PBS: phosphate buffered saline

PD: progressive disease

PPB: Potassium phosphate buffer

PR: partial response

R: resistant

RFU: relative fluorescent units

RT: room temperature

s: seconds

SD: stable disease

SDS-PAGE : Sodium dodecyl sulphate polyacrylamide gel electrophoresis

UCT: University of Cape Town

UZH: University of Zurich Hospital

1 INTRODUCTION

1.1 Global cancer epidemiology

According to the World Health Organization (WHO) 2012 statistics, the ten leading causes of death worldwide were ischemic heart disease (7.4 million deaths, 13.2%), stroke (6.7 million deaths, 11.9%), chronic obstructive pulmonary disease (3.1 million deaths, COPD) (5.6%), lower respiratory infections (3.1 million deaths, 5.5%), trachea, bronchus and lung cancers (1.6 million deaths, 2.9%), HIV/AIDS (1.5 million deaths, 2.7%), diabetes mellitus (1.5 million deaths, 2.7%), diarrhoeal diseases (1.5 million deaths, 2.7%), road injury (1.3 million deaths, 2.2%) and hypertensive heart disease (1.1 million deaths, 2%), as indicated below in Fig. 1.1 (http://apps.who.int/gho/data/).

Figure 1.1: Top ten leading causes of death worldwide (percentage contribution to all-cause mortality). This pie chart indicates the top ten leading causes of death, with each cause indicated by a distinct colour and inserted percentage.

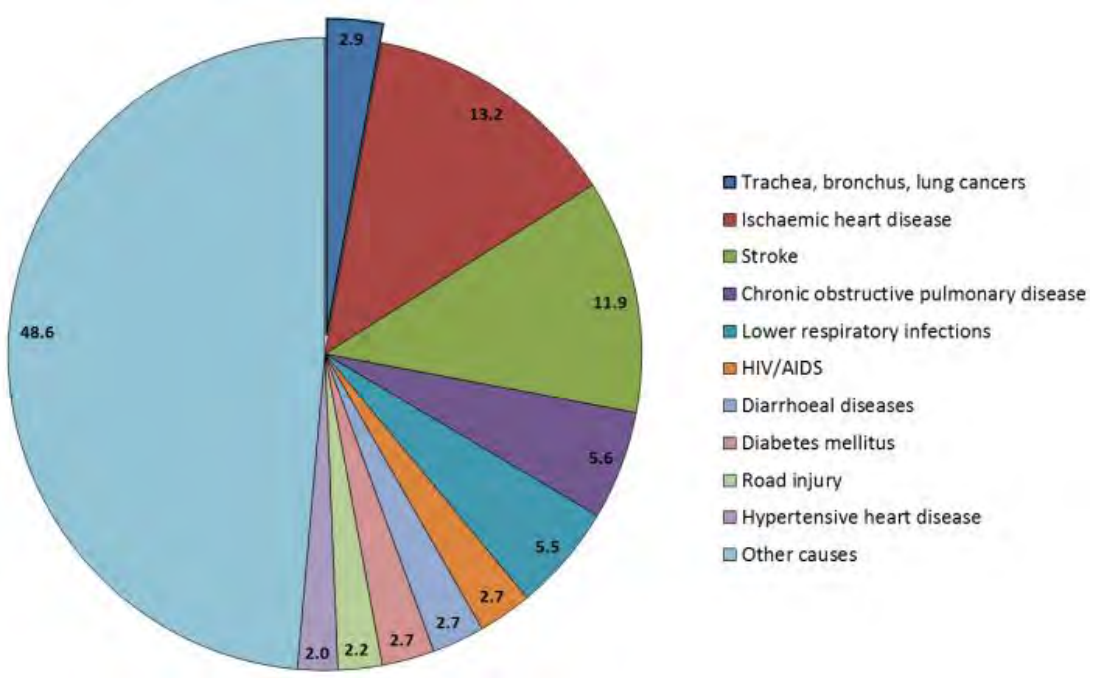

Although the top four leading causes of death have remained the same during the past decade, trachea, bronchus and lung cancer deaths have increased substantially, resulting in respiratory cancers becoming the 5th leading cause of death, a position previously occupied by diarrhoeal diseases. However, these values only consider the highest mortality-associated cancer type. When assessing the mortality contribution of all cancers combined, malignant neoplasms are responsible for 14.7%, with an estimated 8.2 million deaths in 2012. When assessing overall contribution to all-cause mortality, malignant neoplasms are ranked 2nd, following only cardiovascular diseases that have an estimated 17.5 million deaths. These statistics clearly indicate that the majority (68%) of the 56 million global deaths recorded in 2012 were caused by non-communicable diseases, such as cardiovascular disease, cancers, diabetes and chronic lung disease.

When considering cancer statistics specifically, the latest data from the most relevant, informative and up-to-date source (GLOBOCAN database, IARC) (Bray et al. 2013; Ferlay et al. 2015) indicate that it is essential to develop strategies aimed at reducing the global cancer burden. As a means of understanding how these mortality rates are distributed across each continent, a global mortality map based on ASR rates (weighted mean of the age-specific rates) across all cancer types, excluding non-melanoma skin cancers, for both genders is illustrated in Fig. 1.2.

Figure 1.2: Global mortality ASR for all cancers. This figure indicates the global mortality map represented in weighted mean of the age-specific rates (ASR) across all cancer types, with exception of non-melanoma skin cancers. A red colour gradient indicates increasing rates, from less to more intense, respectively, while grey indicates lack of data.

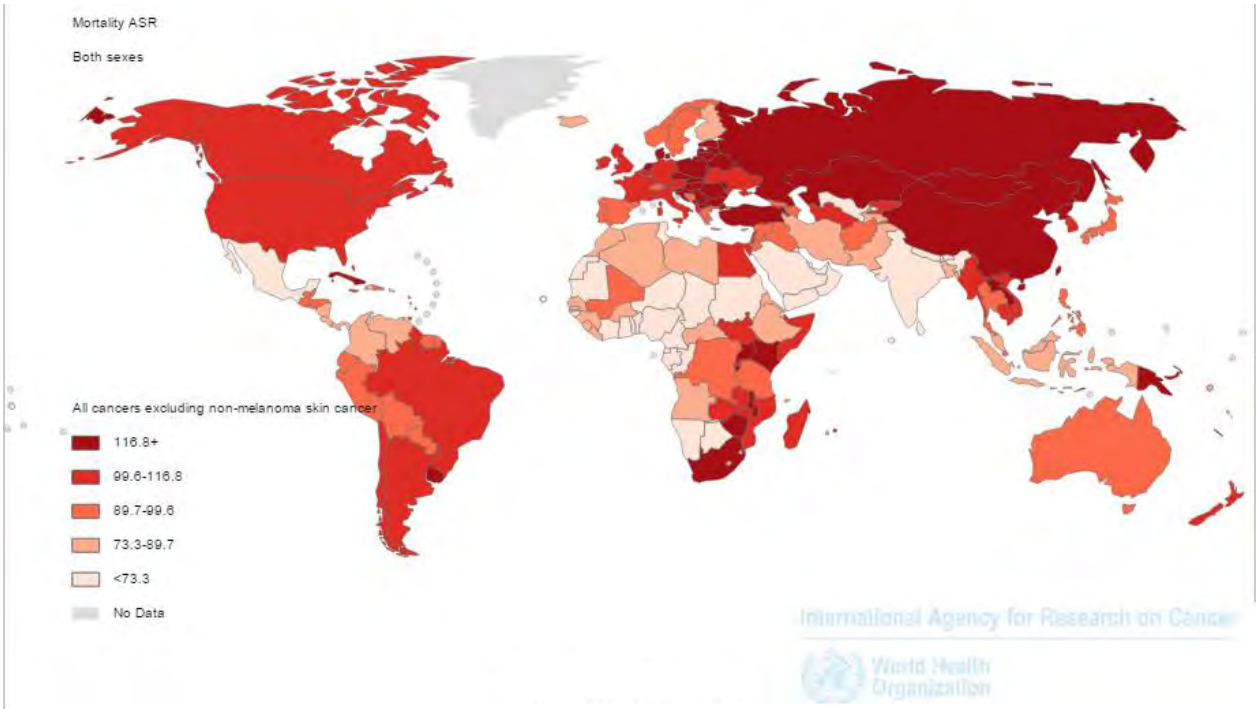

The darkest red areas indicate the regions of highest mortality (≥116.8), which appear to cluster mainly within the Asian, European (mainly Eurasia) and African continents. Interestingly, this includes Southern Africa, with a mortality ASR of 117.88, due largely to cancers of the lung, oesophagus, colorectal, liver and pancreas. This indicates that, although most research attention in Southern Africa is focused on infectious diseases, cancer accounts for concerning high mortality rates (1426 per 100000 population, overall age-standardized rates), relative to global statistics.

Additionally, in 2012 there were 14.1 million new cancer cases reported globally, with 32.6 million people living with cancer within 5 years of diagnosis. As a means of understanding whether regions with the highest cancer mortality rates were also those with the highest incidence, a global incidence map based on ASR rates across all cancer types, excluding non-melanoma skin cancers, including both genders is illustrated in Fig. 1.3.

Figure 1.3: Global incidence ASR for all cancers. This figure indicates the global incidence map represented in weighted mean of the age-specific rates (ASR) across all cancer types, with exception of non-melanoma skin cancers. A blue colour gradient indicates increasing rates, from less to more intense, respectively, while grey indicates lack of data.

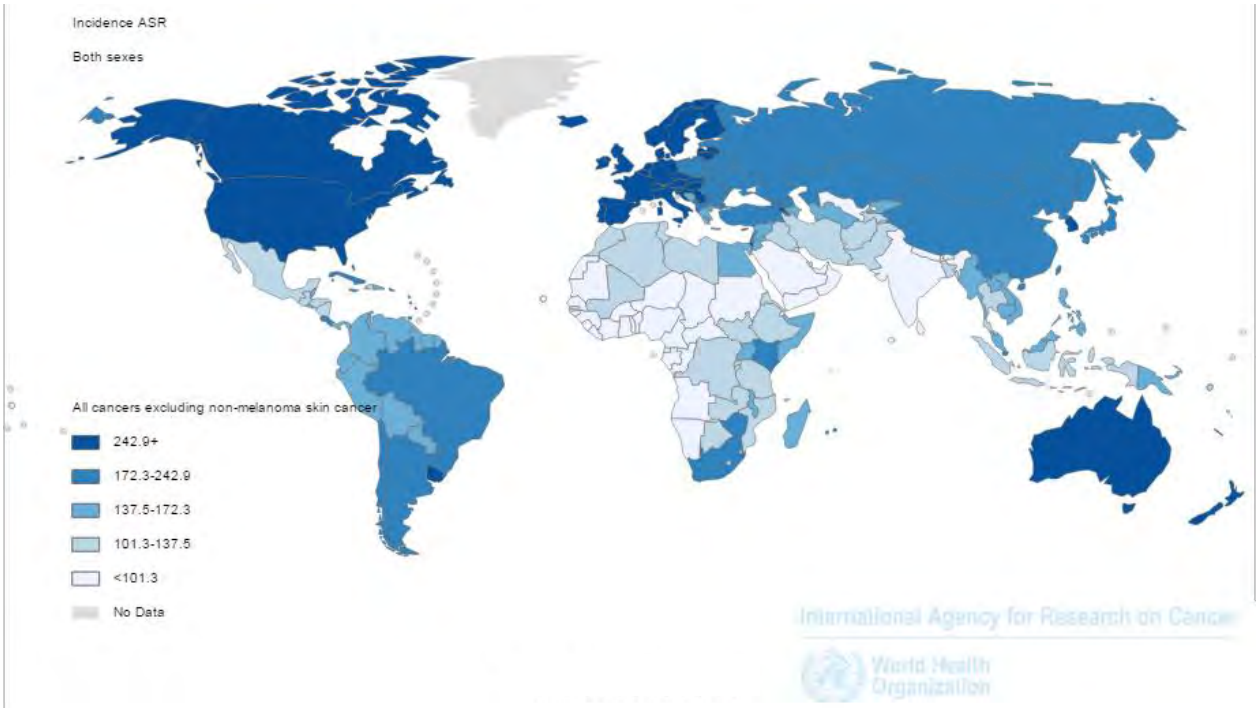

When comparing the mortality (Fig. 1.2) and incidence (Fig. 1.3) global maps, it is evident that the highest mortality and incidence regions do not overlap, with the highest incidence regions (darkest blue, ≥242.9) clustering mainly within the American (mainly North America), European and Australian continents: all more developed regions. These global disparities in cancer mortality and incidence are most likely due to differential presence of risk factors (modifiable and non-modifiable), screening practices, and/or the availability and use of treatment services (Jemal et al. 2011).

Regarding gender, incidence rates are almost 25% higher in men, with incidence rates of 205 per 100000 population compared to 165 per 100000 in women. Male rates vary by almost 5-fold across different regions globally. Southern Africa specifically, although a high mortality region, was not a high incidence one (incidence ASR of 187.09), with cancers of the lung, colorectal, oesophagus, Kaposi sarcoma and stomach dominating. These findings indicate that South African mortality rates should be lower, but are perhaps elevated as a function of South Africa's status as a developing country. Hence, it is of interest to verify whether mortality and incidence rates vary greatly between developed and developing countries. For this purpose, the mortality and incidence rates across the top 25 cancers for both genders were

assessed and grouped by more or less developed regions. The resulting dual multi-bar chart is indicated below in Fig. 1.4.

Figure 1.4: Cancer incidence and mortality rates (thousands) by region development. This figure indicates a dual multi-bar chart with the incidence and mortality rates represented in thousands across the top 25 cancer types for both genders, grouped by more or less developed regions. Blue bars indicate incidence rates, whilst red bars indicate mortality rates.

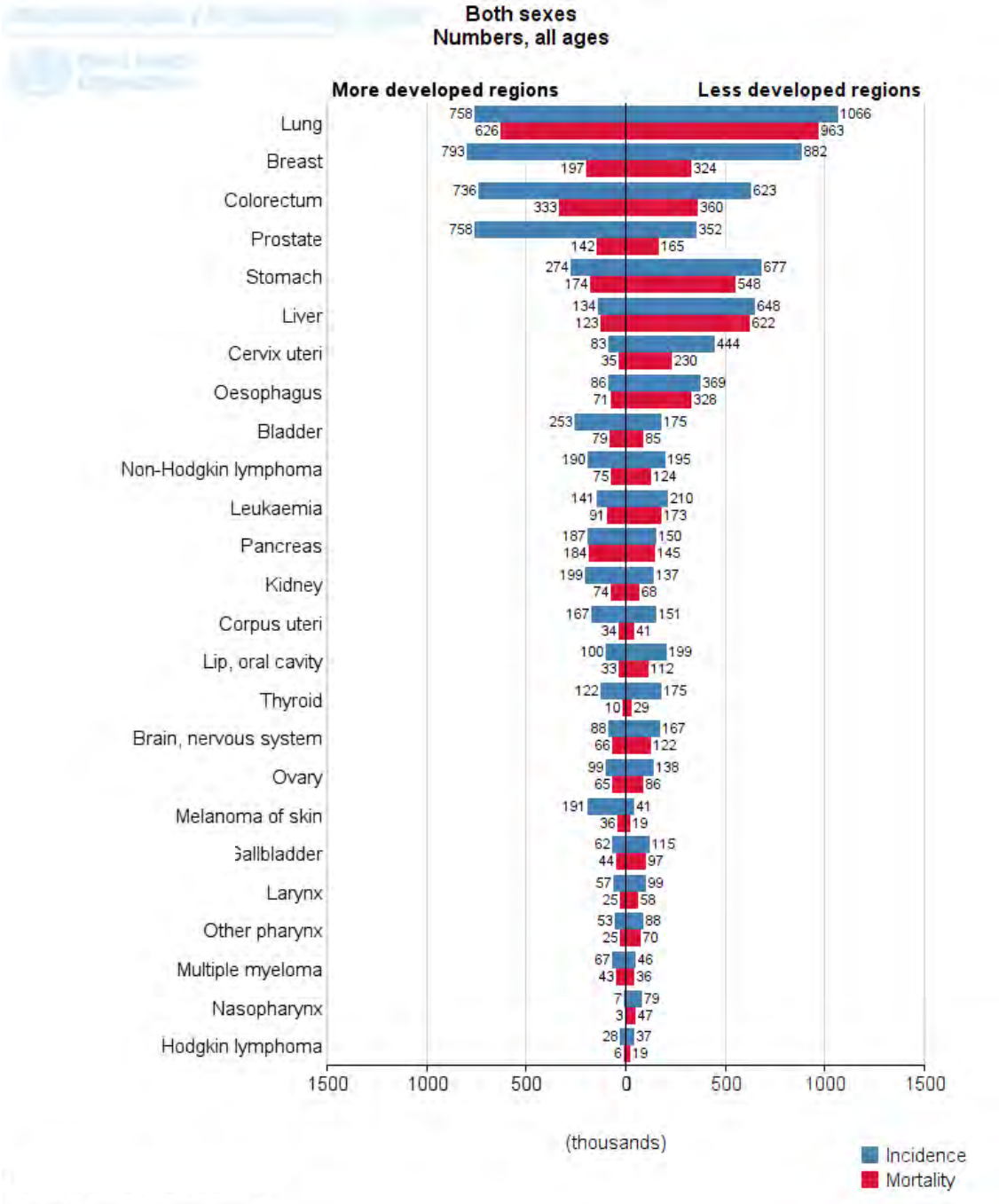

Differences amongst both incidence and mortality rates between more and less developed regions are evident, with 57% of all new cancer cases and 65% of all cancer deaths occurring in less developed regions. When considering gender, less regional variability is seen for mortality rates, with higher rates estimated in men (15%) relative to women (8%) in more developed regions. The global cancer predictions for 2015 estimate 15.2 million new cases of cancer, with 8.1 million in men and 7.1 million in women. Additionally, an estimated 8.9 million cancer deaths are expected in 2015, compared to 8.2 million deaths in 2012, with 5.1 million of those predicted in men and 3.8 million in women. Predictions estimate continued increases in the years to come, more so in low income countries. This further highlights the need for cancer research as a means to reducing the cancer burden in such areas and worldwide. Intervention measures may include generating awareness of cancer-associated modifiable risk factors, such as tobacco use, alcohol consumption, obesity, and lack of physical activity, as well as appropriate vaccination (infections agent-related cancers) and vaccine development, treatment, and screening programmes, especially in less developed regions (Ferlay et al. 2015).

1.2 The hallmarks of cancer

The six hallmarks of cancer describe the biological capabilities that human tumour cells sequentially develop during a multistep process (Hanahan & Weinberg 2000; Hanahan & Weinberg 2011). The early established hallmarks include 1) sustaining proliferative signalling, 2) evading growth suppressors, 3) resisting cell death, 4) enabling replicative immortality, 5) inducing angiogenesis, and 6) activating invasion and metastasis, as indicated below in Fig. 1.5.

Figure 1.5: An illustration of the originally proposed hallmarks of cancer. This illustration indicates the originally proposed hallmarks of cancer which include sustaining proliferative signalling, evading growth suppressors, resisting cell death, enabling replicative immortality, inducing angiogenesis and activating invasion and metastasis. [Adapted from (Hanahan & Weinberg 2011).]

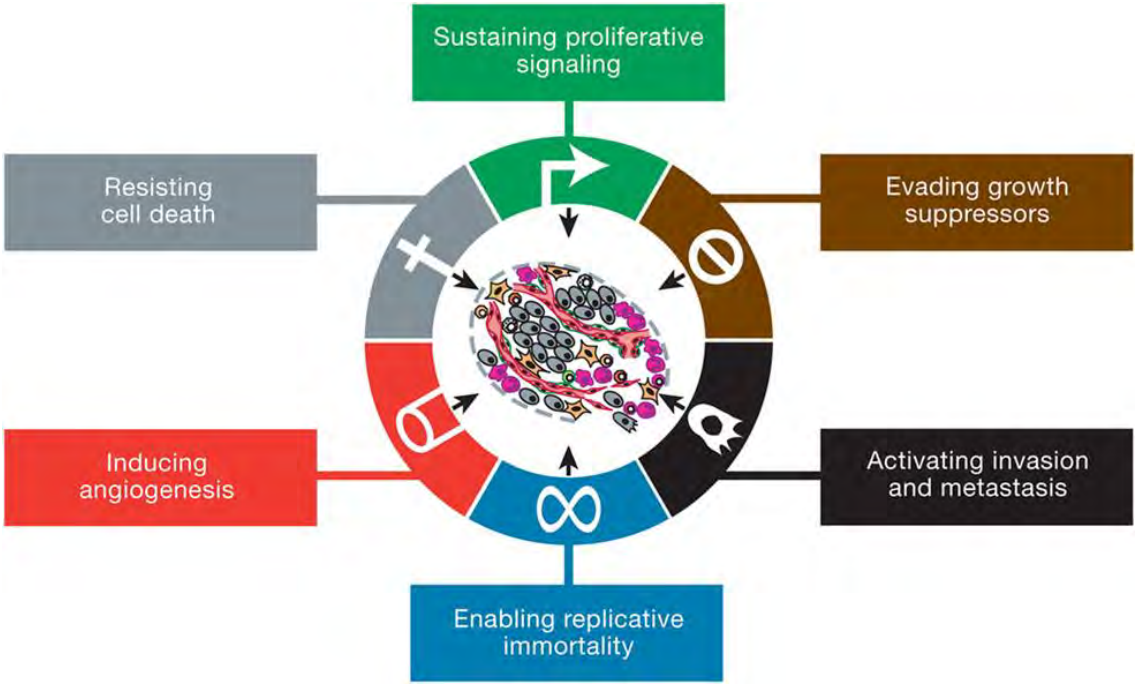

Cancer cells are able to sustain proliferative signalling, indicating the ability to induce and sustain chronic proliferation, by deregulating the previously controlled production and release of growth-promoting signals, transported mainly by cell-surface receptor binding growth factors, that usually control cell number homeostasis to allow normal function and tissue architecture. These growth factors usually contain intracellular tyrosine kinase domains, which produce signals that regulate cell cycle related progression and cell growth, potentially influencing additional properties like cell survival and energy metabolism.

The ability to evade growth suppressors is another ability of cancer cells, as growth suppressors are responsible for negatively regulating cell proliferation, via tumour suppressor genes. These encode for example the retinoblastoma-associated and the p53 proteins, which subsequently direct cellular proliferation, or activate senescence (a non-proliferative but viable state) or apoptosis (cell death).

Resisting cell death is perhaps one of the most interesting abilities, as cancer cells are able to achieve a multiplicity of apoptosis-avoiding mechanisms, the most common strategy being the loss of p53 tumour suppressor function. This acquired ability is said to reflect all apoptosis-inducing signals encountered by these cells during their evolution to malignancy. Most normal cells are only able to undergo a limited

number of cell growth and cell division cycles, limitation of which is usually associated with senescence and subsequent apoptosis.

Rarely, cells emerge from a population in apoptosis which exhibit a replicative immortality, another characteristic required by cancer cells. This ability has been linked to the up-regulation of telomerase expression or to telomerase maintenance mechanisms, both of which permit cells to maintain telomerase DNA length sufficiently to avoid triggering senescence or apoptosis.

The induction of angiogenesis – the ingrowth of new blood vessels – is a means by which fast-growing tumours acquire access to sustenance and waste evacuation. Although angiogenesis is usually only ordinarily active during processes such as embryogenesis, wound healing and uterine lining cycling, this process becomes abnormally activated during tumour progression.

Finally, cancer cells are able to activate invasion and metastasis pathways, the least comprehended and complex hallmark. This commences with local invasion, followed by transit through the lymphatic or haematogenous systems, leading to the formation and growth of micrometastatic lesions into macroscopic tumours, a term usually known as colonization (Hanahan & Weinberg 2000; Hanahan & Weinberg 2011).

In addition to the six classical hallmarks described above, recent progress has identified two additional emerging ones, 7) reprogramming energy metabolism, and 8) evading immune destruction, as well as two enabling characteristics, a) genomic instability and mutation, and b) tumour promoting inflammation, as indicated below in Fig. 1.6.

Figure 1.6: An illustration of the emerging and enabling hallmarks of cancer. This illustration indicates the most recently updated version of the hallmarks of cancer, which now include the emerging and enabling hallmarks. [Adapted from (Hanahan & Weinberg 2011).]

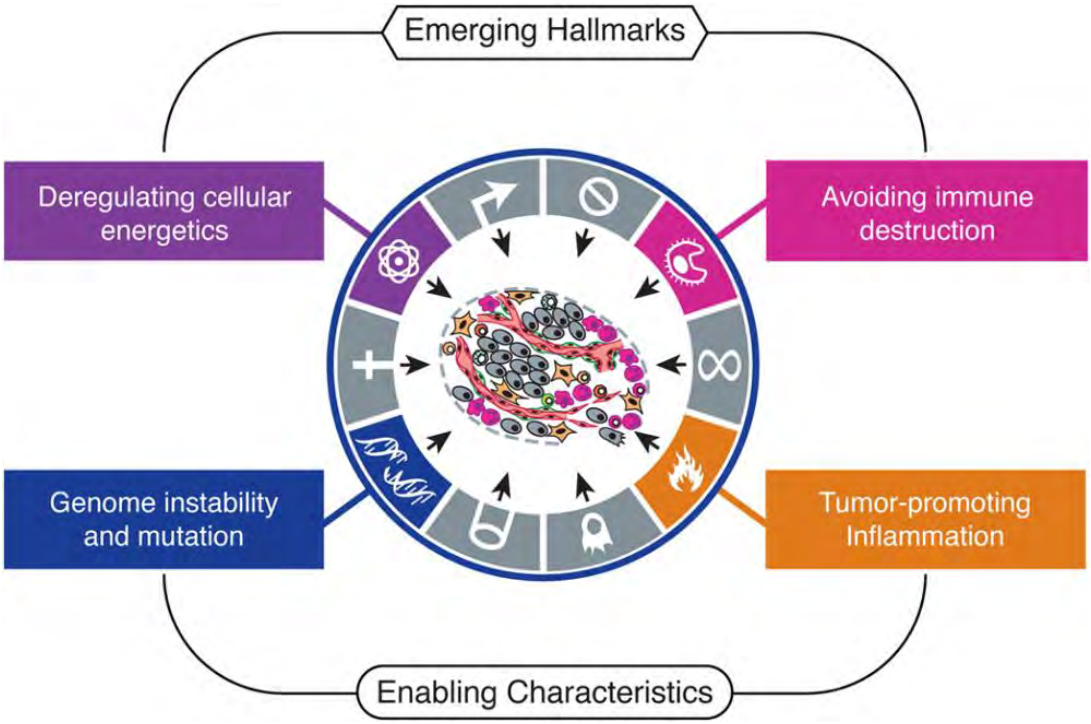

The acquisition of the classical hallmarks is believed to be dependent on enabling characteristics, such as genome instability and mutation. Genome maintenance and repair defects are selectively beneficial for tumour progression, accelerating the rate at which developing premalignant cells are able to accumulate useful genotypes, thus enabling cancer. Tumour-promoting inflammation is able to enhance tumourigenesis and progression, and thus permit the acquisition of hallmark capabilities. In regards to emerging hallmarks, reprogramming energy metabolism has shown to be present in cancer cells to the equivalent degree of many other cancer-associated traits. The ability of cancer cells to make adjustments in energy metabolism is a function of the deregulated control of cell proliferation which requires additional energy to fuel cell growth and division. Additionally, evading immune destruction appears to be another emerging hallmark and whilst demonstrations of anti-tumour immunity as a barrier to tumour formation and progression are still underdeveloped, there are several well-known anti-cancer and cancer-permissive mechanisms (Hanahan & Weinberg 2011).

Hopefully, the full molecular understanding of these key hallmarks will enable a more specific focus on the discovery of novel cancer therapeutics to assist in the eradication of the global burden that is cancer.

1.3 Cancer diagnosis and treatment

Cancer may be found early either through regular screening of asymptomatic individuals, process facilitated by the existence of cancer type-specific tests (e.g. clinical breast examination and mammography for breast cancer screening) and access to the appropriate facilities, or through early detection of symptomatic individuals, that is aided by increased awareness of typical cancer signs and symptoms (e.g. significant rapid growth of a new mole above 5 mm for suspected melanoma or non-melanoma skin cancers). Although early detection of cancer is advantageous, because these precursor stages when treatment are most successful, this only holds true when linked to effective treatment. It is essential that an accurate diagnosis is made, and this may be attained by use of clinical assessment and diagnostic testing, such as imaging, histopathology and cytology. When a suspicious lesion is found, a tissue biopsy (core, excisional or subtotal) is commonly performed to assess malignancy. Only once a malignant diagnosis is confirmed, can the extent of cancer spread (staging) be investigated, which will facilitate treatment planning and the determination of a prognosis (World Health Organization 2002). The tumour, node, metastasis staging system (TNM), is one of the most commonly used staging systems, and classifies cancer by the size of the primary tumour (T), the absence or presence and extent of regional lymph node metastasis (N) and the absence or presence of distant metastasis (M). The use of numerical subsets of the TNM components indicates the progressive extent of the malignant disease (Edge & Byrd 2010).

Once an accurate cancer diagnosis and staging is obtained, therapeutic planning can occur with the aim to cure, prolong life or improve quality of life of these individuals, depending on the extent of disease. There are different types of treatment for patients with cancer, including some that are currently in use and are considered to be standard, and others that are in the process of being tested in clinical trials. The primary treatment for most cancers at all clinical stages is surgery, when possible, which usually includes either partial to total resection of the malignant lesion(s). Additional treatment options include chemotherapy and radiotherapy. Chemotherapy aims to stop cancer cell growth, either by inducing apoptosis or by inhibiting cell division, whilst radiotherapy uses high-energy x-rays or other types of radiation to kill cancer cells or to prevent tumours from spreading. Chemotherapy can be administered systemically or regionally, and radiotherapy can be administered externally or internally, depending on the type and stage of cancer being treated. Systemic chemotherapy (e.g. dacarbazine for the treatment of malignant melanoma) is administered orally or is injected into a vein or muscle, and the drugs enter the bloodstream and reach cancer cells throughout the body (Blank et al. 2011). On the other hand, regional chemotherapy (e.g. intrathecal administration of cytotoxic chemotherapy for the treatment of meningeal leukaemia) is directed solely at the organ or body cavity where the cancer is present, which limits negative effects on healthy cells and tissue (Kufe et al. 2003). External radiotherapy (e.g. intensity

modulated radiation therapy (IMRT) for the treatment of colorectal cancer) consists of localising radiation toward the cancer location, whilst internal radiotherapy (e.g. microspheres containing the β-emitter yttreium-90 for the treatment of metastatic non-resectable liver tumours) uses radioactive substances which are injected directly into or near the cancer (Stubbs et al. 2001) (www.ncbi.nlm.nih.gov/pubmedhealth).

Additional and more recently developed treatment options include biological and targeted therapies. Biological therapy, also known as immunotherapy, focuses on the patient's immune system to fight the cancer, utilising naturally occurring endogenous and exogenous substances, as well as chemically synthesized substances, which boost, direct or restore the body's natural defences against cancer. This therapy is one of the main focal points of our study, as we will assess the effects of immunotherapy on the immune system, amongst other experimental treatments. Targeted therapy, on the other hand, uses drugs or other substances to identify and attack specific cancer cells without harming normal cells (www.ncbi.nlm.nih.gov/pubmedhealth). Several immunotherapies in use and in development consist of attempts to manipulate the patient's immune system, as a means to activate anti-tumour immunity, with the objective of improving currently available cancer treatments by increasing their efficacy and reducing their toxicity (Dougan & Dranoff 2009). The most commonly used and researched form of targeted therapy is monoclonal antibody therapy, which consists of antibodies which identify and attach to cell-surface markers on cancer cells (e.g. cetuximab (targets epidermal growth factor receptor - EGFR), for the treatment of colorectal cancer; ipilimumab (targets cytotoxic T-lymphocyte-associated protein 4 - CTLA-4) and pembrolizumab/nivolumab (targets programmed death-1 receptor - PD-1) for the treatment of malignant melanoma) and therefore either kill cancer cells, or inhibit their growth and prevent spreading (www.ncbi.nlm.nih.gov/pubmedhealth) (Scott et al. 2012).

1.4 Cancer immunology

Both the innate and more specific adaptive immune responses are involved in targeting cancer. Components of the innate immune response relative to cancer include soluble factors, such as complement proteins, and cellular effectors, such as natural killer (NK) cells, dendritic cells (DCs), macrophages, mast cells and granulocytes (neutrophils, eosinophils, and basophils); whilst those of the adaptive immune response include B lymphocytes (B-cells) and T lymphocytes (T-cells), which include cytotoxic T-cells (CTLs), helper T-cells (Th), suppressor T-cells (Tsupp) or regulatory T-cells (Tregs), and natural killer T-cells (NKTs), amongst others (see Fig. 1.7). Specific steps in an immune response include antigen presentation and lymphocyte activation, as well as various soluble effector molecules, e.g. cytokines such as interleukins (ILs), interferons (IFNs), tumour necrosis factors (TNFs), transforming growth factor-β (TGFβ), and colony stimulating factors (CSFs). Immune responses have both humoral

and cell-mediated components, for example via antibodies or direct lymphocyte contact, respectively (Kufe et al. 2003).

Figure 1.7: Illustration of the main components of the immune response. This illustration indicates the main components of the innate and adaptive immune response, and includes visual representations of each of these. [Adapted from (Dranoff 2004).]

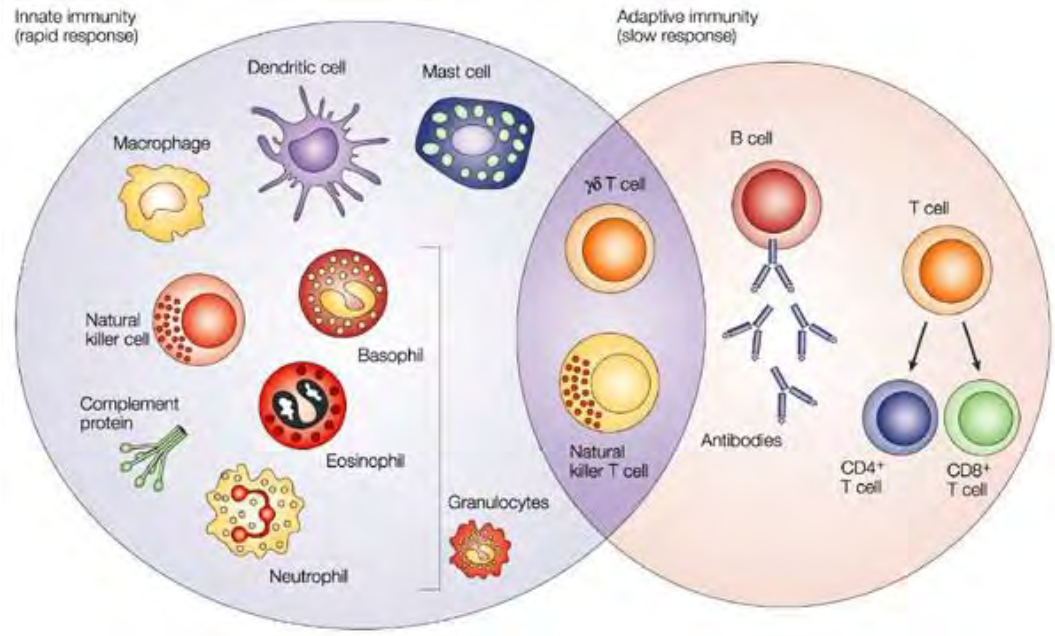

NK cells, particularly important in anti-tumour responses, express two major classes of inhibitory receptors for major histocompatibility complex (MHC, or 'self') molecules and can recognize cells that fail to express MHC class I molecules as abnormal. NK cells are then activated in response to these tumour cells, a process which is known as 'missing-self' triggering of NK cell activation (see Fig. 1.8) (Vivier et al. 2012). They use a number of surface receptors to identify their targets – including tumour cells – which they then lyse largely via the perforins/granzymes pathway or via apoptosis-inducing ligands. More specifically, NK cells secrete IFN-γ, which aid the killing of tumour cells by 1) inhibiting tumour-cell proliferation, 2) enhancing tumour-cell apoptosis, 3) improving tumour antigen presentation, and 4) inhibiting angiogenesis (Dranoff 2004).

Figure 1.8: Immune recognition of tumour cells by NK cells. This illustration indicates a visual representation of NK activation commonly referred to a 'missing-self' triggering, indicating immune recognition of a tumour cell and subsequent release of cytokines and cytotoxic mediators. [Adapted from (Vivier et al. 2012).]

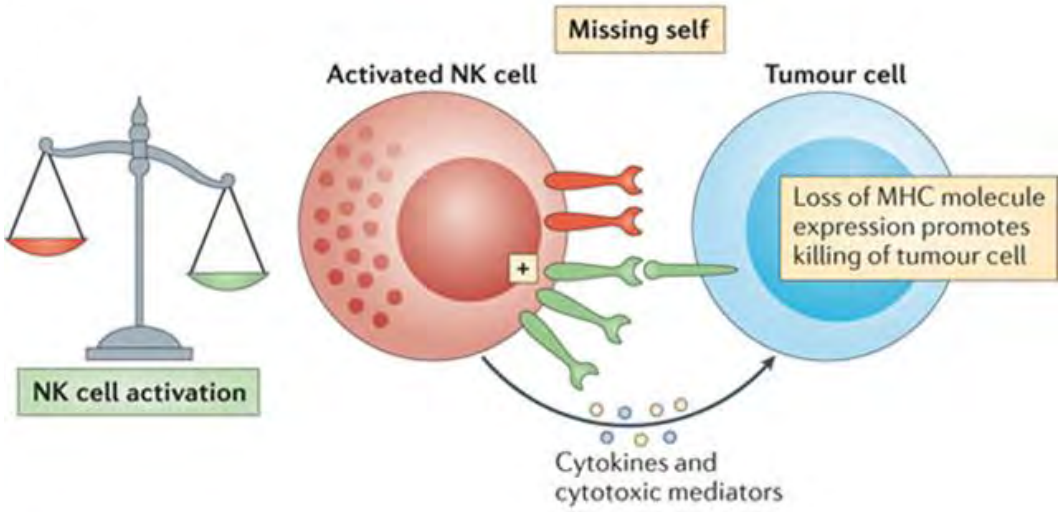

DCs, on the other hand, are antigen-presenting cells (APCs), whose role is to take up, process and present antigenic peptides to cognate T-cells in the regional lymph nodes in order to activate them (see Fig. 1.9). Therefore, APCs play a pivotal role in the induction of functional activity of helper T-cells, and are seen as the interface between the innate and adaptive branches of the immune response. Macrophages – which are phagocytic cells – remove particulate antigens, participate in the inflammatory and healing response, and can lyse tumours by producing nitric oxide and reactive oxygen species.

Figure 1.9: Immune recognition of tumour cells by DC-activated T-cells. This illustration indicates a visual representation of the immune recognition of tumour cells by DC-activated T-cells, indicating specifically each step of how the adaptive immune system responds to tumour antigens inside cells. [Adapted from (Tindle 2002).]

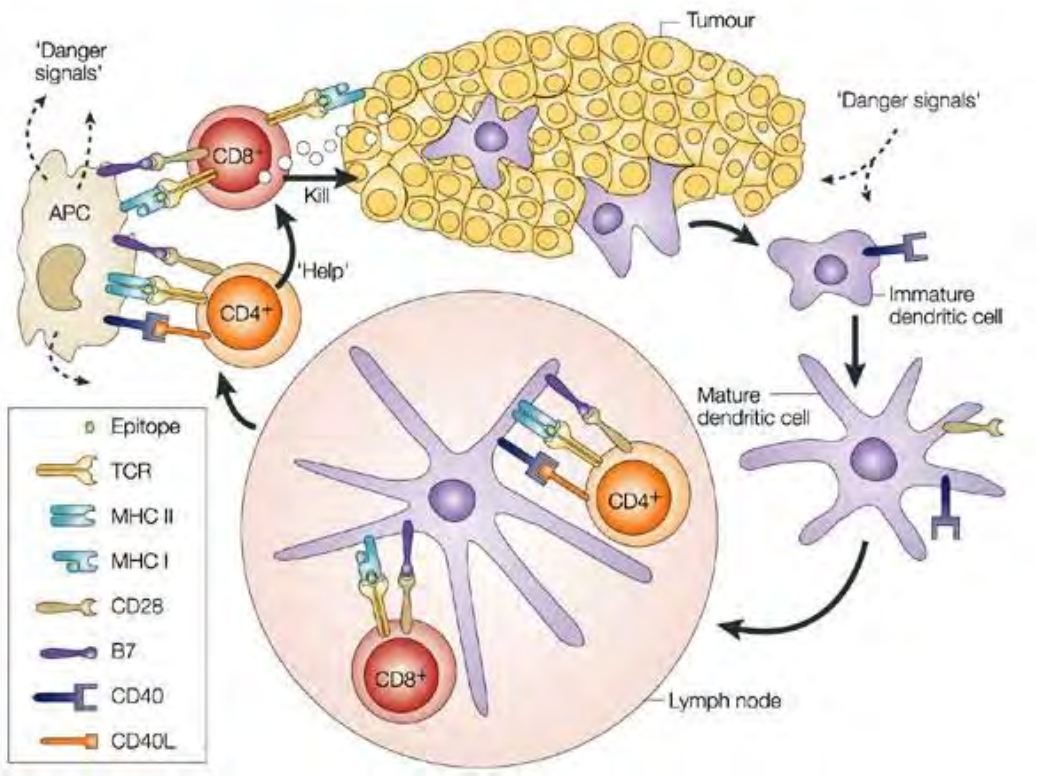

Lymphocytes are responsible for the specific immune recognition of pathogens, and thus for adaptive immune responses. All lymphocytes are derived from bone-marrow stem cells, as are cells of the innate system, but whilst T-cells then mature in the thymus, B-cells continue to develop in the bone marrow. Both B- and T-cells encode surface receptors specific to particular cognate antigens. Having recognized this antigen presented by an APC, the B-cell clonally multiplies and differentiates into plasma cells, which produce large amounts of the receptor molecule in a soluble form (antibodies) that can be secreted and bind to the original activating antigen. There are several different lineages of T-cell, and each has a variety of functions. Helper T-cells, for instance, interact with mononuclear phagocytes and help destroy intracellular pathogens, while cytotoxic T-cells are responsible for the destruction of host cells infected by intracellular pathogens. Although T-cells recognize antigens via their T-cell antigen receptors (TCR), this can only occur when these receptors are presented on the surface of MHC molecules, i.e. by APCs. T-cells generate their effects either by releasing cytokines that signal other cells, or by direct cell-cell interaction (Roitt et al. 2001). More specifically, antibodies are generally known as immunoglobulins (Ig), and are one of the most abundant protein constituents present in the blood.

These are composed of five different classes - IgA, IgD, IgE, IgG and IgM – which differ in biological features, structure, target specificity and distribution. Amongst these, IgG is the major class produced in large amounts during secondary immune responses. Numerous forms of antibodies are produced exclusively by B-cells, each with a distinct antigen-binding site and associated amino acid sequence. Immunoglobulins may be characterized as either soluble antibodies or as membrane-bound antibodies, with the production of secreted antibodies and surface-bound B-cell receptors being regulated via alternative splicing. An antibody molecule is usually Y-shaped, with two identical antigen-binding sites at the upper ends of the Y with the ability to cross-link antigens and form antibody-antigen complexes, and with binding sites for complement components and cell-surface receptors on the lower end of the Y (Fig. 1.10) (Alberts et al. 2002).

Figure 1.10: A schematic diagram representing a typical antibody molecule composed of four polypeptide chains - two identical heavy chains and two identical light chains. The two identical antigen-binding sites are each formed by a N-terminal region of a light chain and a N-terminal region of a heavy chain. The tail (Fc) and hinge sites are formed by two heavy chains. [Adapted from (Alberts et al. 2002).]

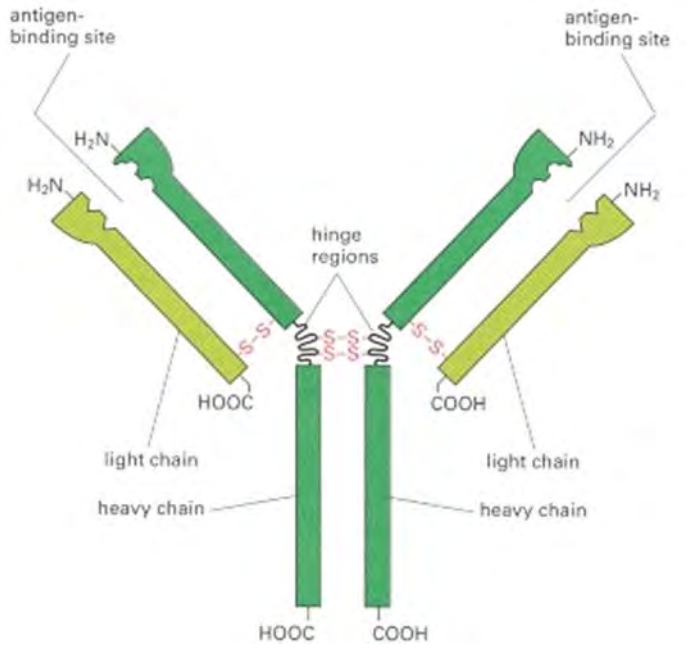

General antibody functions may include neutralisation, agglutination, complement activation, opsonisation, and antibody-dependent NK-mediated cytotoxicity. Additionally, the release of early soluble inflammatory mediators, such as eicosanoids and histamine, is mediated by activating Fc receptor signalling. Furthermore, optimal helper T-cell memory responses require Fc receptor-mediated

antibody function for T-cell activation, as there is a decreased memory response in the absence of a functional antibody response. B-cells are able to impact T-cell activity by functioning as APCs, secreting cytokines such as IFN-γ and IL-10, and thus influencing the cytokine production of other cells (such as Tregs). Conversely, B-cells require the aid of helper T-cells activated by the same cognate antigen to become adequately activated. When a naive B-cell receives an initial activating signal, its surface receptor cross-links with an antigen, which results in antigen ingestion, processing and display by the B-cell, as well as a migration towards an adjacent T-cell area. However when receiving an additional activating signal, the immobilised antigen on its surface binds with a helper T-cell, which results in B-cell activation and proliferation, thus forming plasma cells (also known as effector B-cells) for antibody production (Roitt et al. 2001). Intuitively, the regulation of antibody production depends on the production and maintenance of these plasma cells, which are the long-lived mediators of lasting humoral immunity. Plasmablasts (immature rapidly produced plasma cells) on the other hand correspond to the short-lived effector cells of the early antibody response. Numerous cellular and molecular regulatory mechanisms control this subset of the immune response. Nonetheless, the process of B-cell differentiation is controlled by a central gene-regulatory network, and can be modified by potential environmental stimuli (Nutt et al. 2015).

In regards to cancer, there are many mechanisms of tumour cell killing by antibodies, the majority of which can be grouped into direct tumour cell killing, immune-mediated tumour cell killing, and vascular and stromal cell ablation, which are outlined in Fig. 1.11. Direct tumour cell killing can occur in numerous ways, such as 1) Elicited by receptor agonist activity - antibody binding to the tumour cell surface receptor, which results in activation and apoptosis, 2) Mediated by receptor antagonist activity - antibody binding to a cell surface receptor and as a result blocking dimerization, kinase activation and downstream signalling, leading to reduced proliferation and apoptosis, 3) Triggered by antibody binding to a specific enzyme, which can lead to neutralization, signalling abrogation and eventually cell death, and 4) Drug delivery to tumour cells using conjugated antibodies. Immune-mediated tumour cell killing can also occur in a variety of ways, such as 1) Induction of phagocytosis, 2) Complement activation, 3) Antibody-dependent cellular cytotoxicity (ADCC), 4) Tumour targeting by single-chain variable fragment (scFv) using genetically modified T-cells, 5) T-cell activation via antibody-mediated cross-presentation of antigen to DCs, and 6) Inhibition of T-cell inhibitory receptors, such as CTLA-4. Finally, vascular and stromal cell ablation can occur via 1) Induction by vasculature receptor antagonism or ligand trapping, 2) Inhibition of stromal cells, 3) Toxin delivery to stromal cells, and 4) Toxin delivery to the vasculature (Scott et al. 2012).

Figure 1.11: Mechanisms of tumour cell killing by antibodies. These illustrations indicate a) Direct tumour cell killing; b) Immune-mediated tumour cell killing; and c) Vascular and stromal cell ablation. MAC: membrane attack complex; MHC: major histocompatibility complex; NK: natural killer. [Adapted from (Scott et al. 2012)]

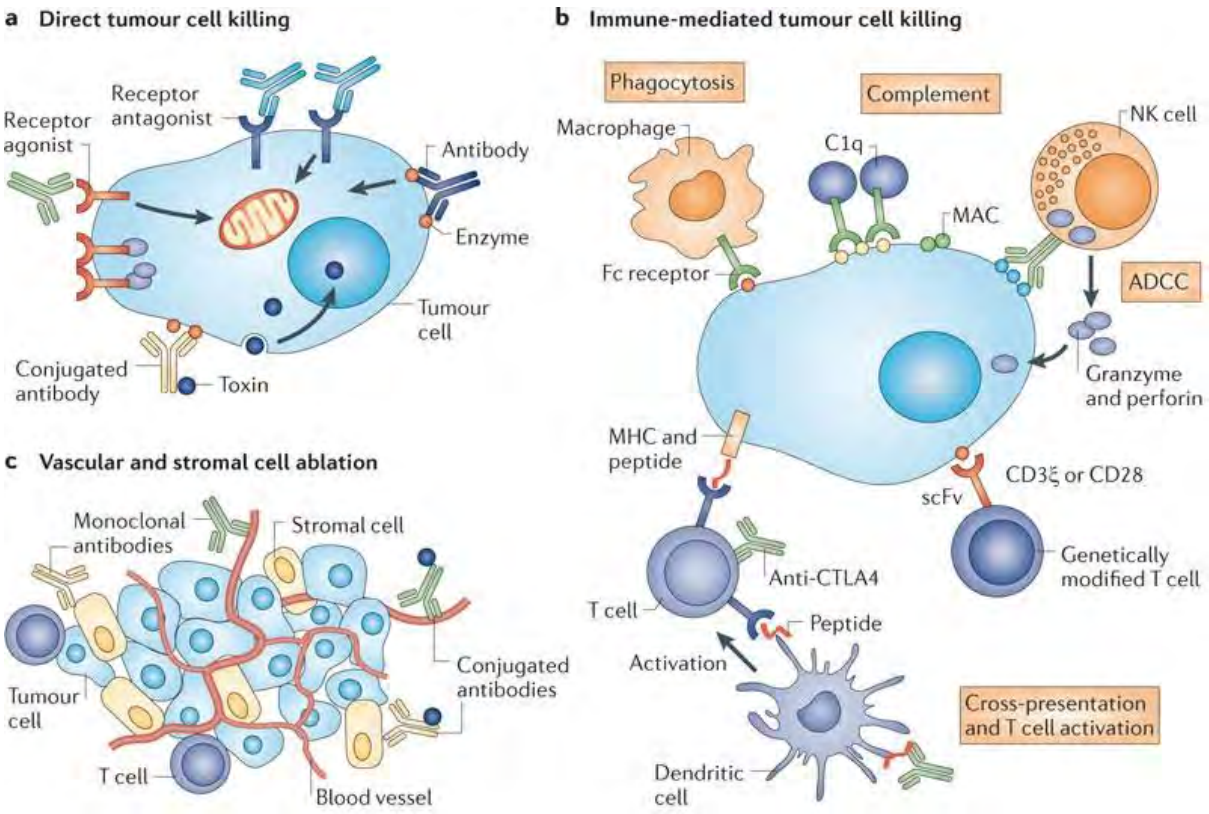

Because cancer cells resemble normal host cells in that they display self-MHC, they tend not to be very immunogenic. Several factors make it challenging for the immune system to target growing cancers for destruction. The literature describes a range of tumour antigens, including tumour-specific antigens (TSAs) and tumour-associated antigens (TAAs), but these are typically poorly immunogenic. TSAs (see Table 1.1) are unique antigens not found in normal cells that usually result from point mutations in genes that are expressed ubiquitously, while TAAs (see Table 1.2) are antigens similar to those found in normal cells, but are either modified or produced in greater quantities. Recently, TAAs have been further divided into three categories: 1) shared tumour-specific antigens that are expressed in many tumours and only in limited normal tissues, 2) differentiation antigens that are expressed in the normal tissue of origin of the malignancy, and 3) overexpressed antigens that are expressed across a wide variety of normal tissues and overexpressed in tumours (Vigneron et al. 2013). Common examples of these tumour antigens are indicated in Tables 1.1 and 1.2, based on the Cancer Immunity Peptide Database (www.cancerimmunity.org/peptide).

Table 1.1 List of common tumour–specific antigens. This table indicates a selection of common tumour-specific antigens, and the respective tumour type where they are present [Adapted from the cancer immunity peptide database (www.cancerimmunity.org/peptide).]

Tumour-specific antigens	
Antigen	Tumour
Beta-catenin	Melanoma
BRAF	Melanoma
CDK4	Melanoma
Elongation factor 2	Lung squamous cell carcinoma
HLA-A2	Renal cell carcinoma
K-ras	Pancreatic adenocarcinoma
ME1	Non-small cell lung carcinoma
Myosin class I	Melanoma
N-ras	Melanoma
p53	Head and neck squamous cell carcinoma

Table 1.2 List of common tumour-associated antigens subdivided into shared tumour-specific antigens, differentiation antigens and overexpressed antigens. This table indicates a selection of common tumour-associated antigens, and the respective tumour type or normal tissue where they are present. [Adapted from the cancer immunity peptide database (www.cancerimmunity.org/peptide).]

Tumour-associated antigens		
Shared tumour-specific antigens	Differentiation antigens	
Antigen	Antigen	Tumour
BAGE-1	CEA	Gut carcinoma
Cyclin-A1	MART-1/Melan-A	Melanoma
GAGE-1,2,3,4,5,6,7,8	PSA	Prostate carcinoma
LAGE-1/CTAG2	SILV/gp100	Melanoma
MAGE-A1,A2,A3,A4,A6,A9,A10,A12	Tyrosinase	Melanoma
MAGE-C1,C2	Overexpressed antigens	
Mucin	Antigen	Normal tissue expression
NY-ESO-1/LAGE-2	HER-2/neu	Ubiquitous (low level)
SSX-2,4	Cyclin D1	Ubiquitous (low level)
TAG-1,2	p53	Ubiquitous (low level)
TRAG-3	Survivin	Ubiquitous
XAGE-1b/GAGED2a	VEGF	Ubiquitous (low level)

Immune evasion of tumours may occur due to the dysfunction of the immune system, immune suppression, cell deletion and immune ignorance, and/or poor immune surveillance. Dysfunction of the immune system induced by cancer cells may lead to various immune defects, such as poor DC function including antigen presentation, T-cell defects leading to T-cell anergy and resulting in immune evasion and loss of T-cell function. Immune suppression occurs when certain enzymes produced by cancer cells decrease or increase levels of various cytokines. Cell deletion takes place when developing T-cells specific to a tumour antigen are destroyed, thereby preventing an anti-tumour immune response to that antigen. Immune ignorance implies that because most cancer cells lack co-stimulatory molecules which are present on functional APCs, such as DCs, these cannot activate naive T-cells, either at the site of tumourigenesis or via cancer cells/antigens circulating in the spleen (Houghton & Guevara-Patiño 2004). Although the immune system may recognize and eliminate the vast majority of emerging cancer lesions

via immune surveillance, tumour formation and progression still occurs, indicating that solid tumours have either managed to avoid immune detection or have limited the extent of immunological destruction, and thus evading eradication (Kufe et al. 2003; Tabi 2009; Perales et al. 2002; Hanahan & Weinberg 2011). In addition to these mechanisms of immune evasion, changes in the expression of MHC class I molecules on solid tumours may also affect the recognition of tumour antigen peptides by T-cells, which will interfere with the regulation NK cell function, as described above (Garcia-lora et al. 2003). Hence, the role of the immune system in resisting or eradicating the formation and progression of cancer, from emerging lesions to metastases, is still unknown, with immunoevasion being considered as an emerging hallmark, as mentioned above in Section 1.2 (Hanahan & Weinberg 2011).

Alternatively, tumours may also evade immune responses due to immune tolerance. Immune tolerance consists of the failure to generate an immune response towards an antigen, usually due to a lack of antigen recognition, and can be subdivided into either 'self' tolerance or induced tolerance. 'Self' tolerance prevents the immune system from attacking its own antigens, and when dysfunctional may lead to autoimmune diseases. Alternatively, induced tolerance prevents an immune response against external antigens, due to intentional immune manipulation. Immune tolerance may occur towards both T-cells and B-cells, and can either be central (within the thymus or bone marrow, respectively) or peripheral (outside of the thymus or bone marrow, respectively) (Kimball 1994).

Central T-cell tolerance occurs before the maturation and circulation of T-cells within the thymus, when its receptor is formed, expressed and rearranged on the cell surface. On the other hand, peripheral T-cell tolerance occurs when mature circulating T-cells are restrained in numbers or in function by external antigens that are not present in the thymus. T-cell clonal deletion (negative selection) and clonal diversion (Treg differentiation) are the two central tolerance mechanisms, whilst T-cell receptor editing or anergy are the two peripheral tolerance mechanisms, which jointly limit the self-reactivity of the T-cell repertoire. (Xing & Hogquist 2012). Contrary to T-cells, B-cell tolerance is not as acute, as these cannot respond to most antigens without the aid of helper T-cells. Nonetheless, these may also become tolerant towards there 'self' components during maturation. Central B-cell tolerance occurs before the formation and maturation of B-cells within the bone marrow, when its receptor is formed, expressed and rearranged on the cell surface. On the other hand, peripheral B-cell tolerance occurs when self-reactive B-cells are mediated by the absence of helper T-cells. (Kimball 1994).Of particular interest to this Thesis, autoantibodies – potential serum biomarkers in cancer – have the ability to target specific TAAs (Shiku et al. 1977; Tan et al. 2009). It is thought that the production of autoantibodies as a result of immune surveillance may serve as an early reporter of tumourigenesis, with potential impact on disease outcome (Tan 2001; Anderson & LaBaer 2005b). These may be identified or analysed using a wide variety of techniques, such as protein microarrays – a high-throughput tool used for the screening of immune responses in cancer patients - to identify autoantibody signatures, novel cancer biomarkers

for early diagnosis, monitoring of disease progression and response to treatments, and development of novel therapeutics (Balboni et al. 2006; Madoz-Gúrpide et al. 2008).

1.5 Cancer-testis antigens

The cancer-testis (CT) antigen family are a group of > 90 structurally and functionally unrelated antigens usually only expressed in the germ cells in the adult testis or ovary and in the trophoblast of the placenta (Scanlan et al. 2002), but which are aberrantly expressed in various cancers in adult somatic tissues as a result of disrupted gene regulation. As the testis is an immune-privileged site, aberrant expression of these antigens in somatic tissues typically triggers a spontaneous immune response to the relevant CT antigen. CT antigens have therefore been exploited as therapeutic tumour vaccines, as well as potential prognostic markers in a variety of tumour types (Hunder et al. 2008; Beeton-Kempen et al. 2014).

Increasing numbers of clinical trials are evaluating therapeutic cancer vaccines that either target specific tumour-associated antigens, such as the CT antigens NY-ESO-1 or MAGEA3, or aim to transiently inhibit critical immune check points such as those mediating peripheral tolerance (Ueda et al. 2003). However, in many cases, the chronic nature of the disease makes it difficult to gain an early assessment of whether an individual patient is generating a therapeutically useful response following vaccination (Beeton-Kempen et al. 2014).

The expression of different CT antigens is known to be associated with many different types of cancer (Simpson et al. 2005), but the absence or presence of expression of any one CT antigen is not in itself exclusively indicative of any specific cancer (Scanlan et al. 2002). It remains plausible though that patterns of CT antigen expression or anti-CT antigen autoantibody titres may prove useful as diagnostic markers of specific cancer types or as correlates of disease progression and response to therapy. However, to be viable as cancer biomarkers, these signatures should preferably be quantifiable in peripheral fluids to avoid unnecessarily invasive treatments and should be highly accurate for diagnostic and/or prognostic purposes to allow improved clinical management of patients (Berrade et al. 2011; Frank & Hargreaves 2003; Rifai et al. 2006). One way in which this may be achieved, and the particular method used in this Thesis, is through the quantitative measurement of correlated anti-CT antigen autoantibody signatures – B-cell responses – in serum of cancer patients using protein microarrays (Beeton-Kempen et al. 2014).

1.6 Cancer immunotherapeutics

Cancer vaccines belong to a class of substances known as biological response modifiers which work by stimulating, restoring or beneficially exploiting the immune system's ability to fight infections and

disease. There are two types of cancer vaccines: preventive vaccines, which are intended to prevent cancer from developing in healthy people; and therapeutic vaccines, which are intended to treat an existing cancer by strengthening the body's natural defences against the cancer (www.ncbi.nlm.nih.gov/pubmedhealth). The ideal therapeutic cancer vaccine should induce a strong anti-tumour adaptive immune response (mainly T-cell), and a subsequent clinical response (e.g. solid tumour size reduction measured by the response evaluation criteria in solid tumours (RECIST) post-treatment) in the host, while sparing normal tissue. The two essential factors of a cancer vaccine are specificity, such as recognition of a tumour antigen by the T-cell receptor or antibody, and strength of the immune response, which is achieved by non-specific or general immunostimulators. The two types of molecules that usually boost immunity non-specifically are adjuvants, which are potent but poorly understood immunostimulatory agents, and cytokines, which are soluble factors used for signalling by immune cells and are often used in conjunction with other treatments (Kufe et al. 2003).

The different types of therapeutic cancer vaccines include 1) tumour antigen-based vaccines, such as tumour antigen DNA vaccines and tumour antigen synthetic peptide vaccines; 2) monoclonal antibody-based vaccines, such as idiotype vaccines; and 3) cell-based immunotherapy, such as tumour cell-based vaccines, DC-based vaccines, T-cell-based vaccines and NK cell-based therapy (www.ncbi.nlm.nih.gov/pubmedhealth/)(Kufe et al. 2003).

Although many DNA vaccines (e.g. transcription factor Fos-related antigen-1 (Fra-1) DNA vaccine (Xiang et al. 2008)) initially showed potential in animal models by suppressing tumour growth and metastasis through the induction of cell-mediated immune responses, early clinical trials have been disappointing with low magnitudes of response (Liu 2011; Schlom 2012). Similarly to DNA vaccines, clinical trials assessing idiotype vaccines (e.g. clonal immunoglobulin idiotype, (Bendandi 2009)) have not achieved the desired outcomes, although initially showing clinical benefit.

Tumour antigen synthetic peptide vaccines (e.g. SILV/gp100 (Schwartzentruber et al. 2011), and HER2/neu (Disis et al. 2009) peptide vaccines), on the other hand, have shown high magnitudes of response upon reaching the clinical trial setting. The SILV/gp100 modified peptide vaccine in particular, in combination with IL-2, has shown improved overall clinical responses and increased survival rates across a vast majority of advanced melanoma patients (Schwartzentruber et al. 2011).

Although the above-mentioned peptide vaccines have several advantages, when considering tumour cell-based vaccines, a large meta-analysis across 173 clinical trials has reported that the latter have higher response rates (Neller et al. 2008). This increase is most likely related to tumour cells providing a broad pool of antigens that may potentially trigger T-cell ($CD4^+$ and $CD8^+$) responses, as well as tumour-reactive antibodies. However, even though this vaccine type has shown higher response rates, these are

still relatively low, and current studies are attempting to increase overall tumour cell vaccine efficacy (Andersen & Ohlfest 2012).

The remaining cell-based vaccines include three distinct cell types – DCs, T-cells and NK cells – all crucial players in the immune response towards tumours. DC-based vaccines (e.g. monocyte-derived DC vaccine, (Lesterhuis et al. 2011)) have shown to be safe and immune-response inducing across a substantial number of cancer patients, although with limited clinical efficacy, an issue that is currently being researched by attempts to optimize DC-specific vaccine parameters. T-cell-based vaccines may consist in adoptively transferring patient-derived natural occurring or engineered T-cells – after a selective *in vitro* isolation, expansion and activation – back into patients, to effectively eradicate tumours by targeting expressed tumour antigens and associated vasculature (Restifo et al. 2012). Finally, NK-cell based therapy functions similarly to that described of T-cells, where patient-derived NK cells may be isolated from a healthy donor, activated and expanded *in vitro*, and then infused into the cancer patient, as a means of promoting anti-tumour function (Vivier et al. 2012). The possibility of editing a cancer patient's immune system to confer it the ability of triggering a desired substantial anti-tumour response is one of great interest and relevance, highlighting the true potential of these therapeutic cancer vaccines.

Recent studies indicate that current challenges in designing effective cancer therapeutics targeted at the immune system are as follows: antigens need to be specifically selected based on ideal characteristics (e.g. restricted tissue distribution to tumours and relevant to tumour progression based on the timing of their cell surface display); selected antigens should to be combined with adjuvants that may potentially enhance their immunogenicity and yield strong immune responses; vaccination should be timed to anticipate the development of regulatory suppressive immune mechanisms; and specific antagonists may be required to enhance immune outcomes, in the advent of suppressive regulatory mechanisms arising (Cebon 2010).

CT antigens are therefore intuitively attractive targets for antigen-specific immunotherapy since they are distributed across cancers of many histological types, are immunogenic and show restricted expression profiles. As mentioned above (Section 1.5), increasing numbers of clinical trials are evaluating tumour-associated CT antigens – such as NY-ESO-1 and MAGEA3 – as potential therapeutic vaccines across a variety of different cancer types (Whitehurst 2014).

In regards to the most commonly reported NY-ESO-1 vaccine, full-length recombinant NY-ESO-1 protein formulated with ISCOMATRIX adjuvant, clinical trials have reported the generation of immune responses, both humoral and T-cell mediated, as well as reduced risk of disease relapse in melanoma patients. However, although clinical responses are obtained in patients with residual disease, this is not the case for advanced melanoma patients, which may be due to an overall tumour-induced systemic

immune suppression, with a clear correlation between disease progression and an elevated proportion of Tregs in the blood (Nicholaou et al. 2009). Tregs – a T-cell subtype that releases suppressive cytokines and serves to silence immune responses – have recently been reported to play a key role in the suppression of anti-tumour T-cell immunity, with animal studies showing that when inhibiting or removing Tregs an increase in tumour clearance and survival is seen, thus showing that tumours may have the ability to create a local immunosuppressive environment by selective recruitment and/or expansion of Tregs (Zou 2006; Beyer & Schultze 2006). Hence, clinical trials targeting advanced cancers with known well established immunosuppressive networks in place have recently been adapted to include a Treg specific cytotoxic agent, as a means of depleting Tregs and bypassing this issue. However, these findings also indicate that future vaccine development efforts should rather be directed towards early stages of disease, as patient's with lower tumour volume and extent of immune suppression are most likely to receive treatment benefit (Nicholaou et al. 2009).

MAGEA3-based vaccines, recombinant MAGEA3 protein (RecMAGE A3, MAGRIT trial), have been mainly aimed towards melanoma (Kruit et al. 2008) and non-small cell lung cancer (Vansteenkiste et al. 2007). In regards to melanoma, MAGEA3 trials have shown T-cell and antibody responses, as well as clinical responses (tumour regressions) with correlative gene expression signatures (Ulloa-Montoya et al. 2013). Hence, current related trials are being conducted in advanced melanomas (Drake et al. 2014). In non-small cell lung cancer, the largest phase III trial in this cancer type is currently ongoing and investigating the efficacy of relapse prevention of a MAGEA3-based vaccine (Peled et al. 2009). Although results of this trial are not yet available, initial trials have demonstrated induction of specific T-cell responses and tumour growth inhibition.

Hence, although current CT antigen vaccines can induce strong immune responses (usually cellular, but ideally humoral responses too), conclusive evidence of clinical benefit has been somewhat elusive to date. The correlation between an elicited immune response and a succeeding clinical one may assist in comprehending the causes of tumour responses and the several mechanisms of tumour escape. Hence, patient stratification prior to vaccination based on disease stage, antigen expression or immune profiles have been suggested as a means to improve clinical outcomes (Cebon 2010). Additionally, a large number of studies continue to investigate the therapeutic applicability of additional CT antigens across distinct cancer types, whilst others explore different avenues including agents that may block immune checkpoints, such as CTLA-4 and PD-1 (programmed death-1) (Drake et al. 2014).

To be introduced as a new cancer treatment option and to be approved by the U.S. Food and Drug Administration body (FDA), a vaccine must fundamentally be effective (Roitt et al. 2001). Patient stratification strategies might be essential to improve the potential effectiveness of a therapeutic vaccine, which could lead in turn to an increased probability of gaining regulatory approval in due course. Furthermore, recent studies have shown that to obtain improved clinical outcomes during

cancer treatment, effective combination therapies should be used (Vanneman & Dranoff 2012). Potential combinations may include surgery, chemotherapy or targeted therapies with immunotherapy. This finding is supported by evidence that anti-tumour immunity is essential to assure clinical response to conventional cancer treatments. For example, a dense amount of tumour infiltrating lymphocytes (TILs) within colorectal cancer tumours revealed a strong correlation with improved chemotherapy efficacy and a better prognosis, when compared to patients with smaller infiltrates (Halama et al. 2011). It has further been reported that surgical resection of primary tumours has shown to reverse in tumour-derived immunosuppression, indicating that for maximal efficacy immunotherapy should only be administered post-operatively (Danna et al. 2004). In regards to the combination of chemotherapy and immunotherapy, combining CTLA-4 blockade (ipilimumab) with standard chemotherapy in melanoma patients, in a phase II clinical trial setting, resulted in an increase in overall survival rates (Hodi et al. 2010). Additionally, combining IL-2 and mucin 1 (MUC1) immunotherapy with chemotherapy in metastatic non-small cell lung cancer resulted in an increased progression-free survival (Quoix et al. 2011). When considering the combination of targeted therapies and immunotherapy, a phase I/II clinical trial assessed the combination of BRAF inhibitor (vemurafenib) with CTLA-4 (ipilimumab) in patients with metastatic melanoma, with the intent of achieving long-lasting responses through immune memory induction. This treatment has been shown to affect the immune system by increasing antigen expression, such as SILV/gp100 and MART-1/Melan-A, and decreasing tumour secretion of immunosuppressive cytokines, resulting in an expected boost in T-cell responses (Boni et al. 2010; Sumimoto et al. 2006). Therefore, the promising benefits of combining different cancer therapeutics is one of great relevance, indicating that a greater understanding of tumour suppressive mechanisms, cancer pathogenesis and protective anti-tumour immunity facilitate the ability to target key molecular pathways, and thus increase the likelihood of prolonging patient survival (Vanneman & Dranoff 2012).

1.7 Cancer biomarkers

Ideally, a cancer biomarker should have the following characteristics: 1) easy and inexpensive to measure to allow easy accessibility in developing countries, 2) measureable in peripheral fluids – such as serum – to avoid unnecessarily invasive treatments, and 3) highly accurate for diagnostic and/or prognostic purposes to allow improved clinical management of patients (Berrade et al. 2011; Frank & Hargreaves 2003; Rifai et al. 2006). However, currently used cancer biomarkers, such as PSA in prostate cancer (Prensner et al. 2012) and CEA in colorectal cancer (Nicholson et al. 2014), are not well suited for an accurate diagnosis, due to several reported limitations in sensitivity and specificity.

When considering serum as a target peripheral fluid for cancer diagnosis, the first approach in this search would be the identification through serology of a set of candidate serum biomarkers that might correlate with disease status. Serological analysis of cancer patient samples could identify and quantify

either circulating tumour antigens or autoantibodies to tumour antigens that are aberrantly expressed in cancer.

Of particular interest to this Thesis, the study of autoantibody profiles in cancer patients could lead to the discovery of novel biomarkers for early detection of tumours, patient stratification, personalised patient treatment, development of improved therapies, and monitoring therapeutic response and disease progression (Duarte et al. 2013). This Thesis thus intends to explore the potential of identifying novel cancer biomarkers, which could aid in the detection and management of cancer. With use of a newly developed proteomic technique, a cancer antigen microarray platform, we aim to comprehend and shed light on the interplay between the immune system and tumour responses to treatment, including chemotherapy, radiotherapy and immunotherapy.

1.8 Aims

1.8.1 Hypothesis

The underlying hypothesis of this study is that there are measurable differences in autoantibody repertoires towards tumour-specific and –associated antigens between pre- and post-treated cancer patient samples (using various trial therapies), potentially augmented by prior chemo- or radiotherapy, which correlate with likelihood of response of individual patients to a given therapeutic treatment – including those treatments that aim to generate T-cell responses – and which would also correlate with the nature and extent of individual patient responses to treatment.

1.8.2 Objectives

We developed and used novel protein microarrays that contain over 100 cancer antigens to quantify broad cancer-related autoantibody profiles in cancer patient serum samples collected pre- and/or post-chemotherapy, radiotherapy or immunotherapy, the aims being:

(i) To identify novel biomarkers that could be used in patient stratification prior to chemotherapy/radiotherapy/immunotherapy;

(ii) To identify novel biomarkers that could be used in monitoring therapeutic responses in patients undergoing chemotherapy/radiotherapy/immunotherapy;

(iii) To identify novel diagnostic and/or prognostic biomarkers that could be used in detection and management of disease;

(iv) To discover whether prior chemo- or radiotherapy significantly altered the pattern of CT antigen autoimmune titres , thereby potentially influencing the outcome of any subsequent treatment program;

(v) To validate our protein microarray data by conducting sample reproducibility studies;

(vi) To correlate our data with patient responder phenotypes;

(vii) To correlate our findings to available patient clinical data, with the intent of revealing the biological significance and feasibility of our protein microarray platform and generated data.

1.8.3 Study design

We carried out a retrospective serological study of primary and secondary autoimmune responses of various cohorts of cancer patients prior to and/or following a variety of distinct treatments (chemotherapy, radiotherapy and immunotherapy), using a large number of archived human serum samples previously collected by the Blackburn Laboratory, our collaborators at the Ludwig institute for Cancer Research (LICR, Melbourne, Australia), and our collaborators at the University of Zurich Hospital (UZH, Zurich, Switzerland). Our goals were to develop and validate a novel cancer antigen microarray platform and to then explore its utility and general applicability in the cancer immunology field. In addition, we sought to cross-correlate our protein microarray data from specific cohorts with *in vitro* T-cell re-stimulation assays for a selected subset of patients. Furthermore, as a means of determining the biological significance of our protein microarray data, we also collected clinical patient data where possible.

This research, which is summarized in a flowchart indicated below in Fig. 1.12, took place in the Blackburn Laboratory located in the Division of Medical Biochemistry of the University of Cape Town (UCT), the Centre for Proteomic and Genomic Research (CPGR) facilities, the Groote Schuur Hospital (GSH), and the Cancer Immunobiology Laboratory (CIBL), located at the LICR.

Figure 1.12: Flowchart of study design.

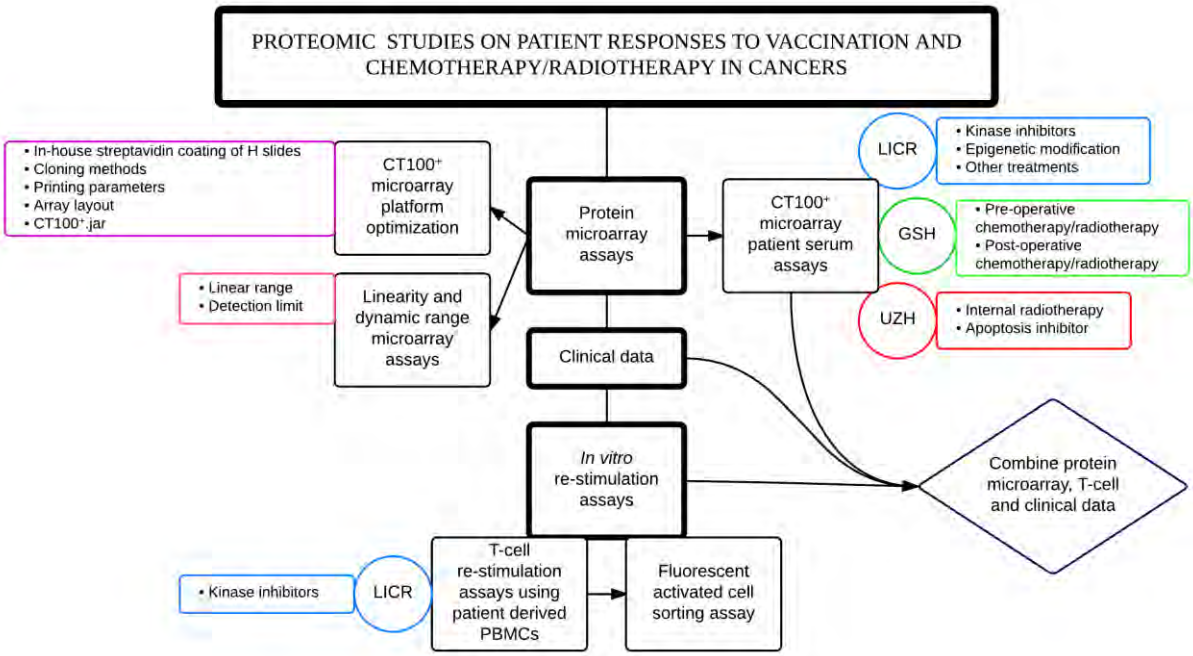

2 CLINICAL COHORTS

2.1 Introduction

This study included several distinct treatment cohorts, each with a different, unique set of patients in either a clinical trial or a standard treatment setting. These cancer treatments include 1) Kinase inhibitors (BRAF, BRAF+MEK, BRAF+/-MEK, BRAF/MEK), 2) Pre- or post-operative chemotherapy/radiotherapy, 3) Epigenetic modifiers (panobinostat and azacitidine), 4) Apoptosis inhibitor (survivin), 5) Internal Radiotherapy (SIRT), and 6) Others. Informed consent was obtained for each treatment cohort according to standard clinical trial practice, and our study was conducted after review and approval by the Human Research Ethics Committees (UCT HREC 240/2011, UCT HREC 269/2011).

The collection of patient clinical information and its addition to experimental data may aid in the process of data analysis and interpretation. Demographic information, such as gender and age, could provide relevant incidence or prevalence rates, in a disease specific context. Clinical information, such as cancer type, stage, treatment undergone and responses thereof, could provide useful details which permit grouping of patients into distinct categories and allow for more focused analyses. In conjunction, this detailed demographic and clinical information could indicate how homogenous or heterogeneous a cohort may be. Consequently, patient cohorts with a great deal of variety amongst them provide numerous limitations in the potential data translation.

For the ability to determine the statistical power of the potential findings of each treatment cohort, i.e. the likelihood that a study will detect an effect when there is an effect there to be detected, we estimated the need for a minimal sample size of 54 patients. This estimate was generated *a priori* using a size-power calculation (G*Power 3.1.9.2 program, T-test, difference between two dependent means

(matched pairs)) with a given probability of error ($\alpha = 0.05$), power ($1 - \beta = 0.95$) and effect size ($dz = 0.5$) (Faul et al. 2007; Faul et al. 2009).

2.2 Methodology

2.2.1 Kinase Inhibitor cohorts

The kinase inhibitor treatment cohort included 36 malignant melanoma patients undergoing 1) BRAF (dabrafenib, GSK2118436: Study ID 112680; Clinicaltrials.gov Identifier: NCT00880321), 2) Alternative BRAF (vemurafenib, RO5185426, Study ID BRIM2/3; Clinicaltrials.gov Identifier: NCT01006980), 3) MEK (trametinib, GSK1120212: study ID: MEK113583, Clinicaltrials.gov Identifier: NCT01037127), 4) BRAF + MEK (dabrafenib and trametinib, GSK2118436 + GSK1120212: Study ID 113220; Clinicaltrials.gov Identifier: NCT01072175), 5) BRAF +/- MEK (dabrafenib and/or trametinib, GSK2118436 +/- GSK1120212: Study ID 115306; Clinicaltrials.gov Identifier: NCT01584648) inhibitor treatments. Due to limited patient numbers within each four distinct variations of this treatment cohort in regards to treatment with BRAF alone (using two distinct BRAF drugs, dabrafenib and vemurafenib), BRAF in combination with MEK, or MEK alone, and as a means of obtaining statistically significant data, these treatments were joined and treated as a unique cohort of malignant melanoma patients undergoing kinase inhibition.

Serum or plasma was obtained for these patients before (Baseline/D0) and after treatment (D*n*), with at least one time point post-treatment per patient. This serum or plasma was collected under the supervision of our collaborators, Prof. Jonathan Cebon at the Austin Health in Melbourne, and Prof. Georgina Long, at the Westmead Hospital in Sydney.

As part of our ongoing collaboration, a 3-month long research visit was planned and took place at the LICR. One of the main objectives of this visit was to obtain access and collect the complete clinical profile of the patients included in our cohort from individual patient records. This was possible for all 16 patients undergoing treatment at the Austin Health, and for all 20 patients being treated at the Westmead Hospital.

2.2.2 Pre- or Post-operative chemotherapy/radiotherapy cohort

The pre- or post-operative chemotherapy/radiotherapy treatment cohort included 62 colorectal cancer patients undergoing chemotherapy/radiotherapy prior- or post-surgical resection of their primary tumours.

Blood samples were previously collected prior to surgical resection of the main tumour(s) by our laboratory at the GSH, as part of a local collaboration, and buffy coats with added plasma were

prepared. Patients were divided into those who received or did not receive pre-operative chemotherapy/radiotherapy. These samples were collected under the supervision of our collaborators, Dr. Paul Goldberg at the GSH, and Prof. Raj Ramesar at the Division of Human Genetics, UCT.

As part of this ongoing collaboration, complete access and collection of clinical profiles of these patients was possible.

2.2.3 Epigenetic Modifier cohort

The epigenetic modifier treatment cohort included 12 myelodysplasia patients undergoing a combination of panobinostat (histone deacetylase (HDAC) inhibitor) with azacitidine treatment (LBH589 + 5-AC; Australian and New Zealand Clinical Trial ID: ACTRN12610000924055).

Serum was obtained for these patients before (Screening) and after treatment (Cycle *n*), with at least one time point post-treatment per patient. This serum was collected under the supervision of our collaborator, Prof. Andrew Spencer, at the Alfred Hospital in Melbourne.

This clinical trial's progress has been recently published (Tan et al. 2014), and therefore public access and collection of the clinical profile of the patients included in our cohort was possible.

2.2.4 Apoptosis Inhibitor cohorts

The apoptosis inhibitor treatment cohort included 48 varied cancer (urothelial cancer, colorectal cancer, sarcoma, renal cancer, ovarian cancer, adenoid cystic cancer, breast cancer, mesothelioma, melanoma, head and neck cancer, non-small cell lung carcinoma (NSCLC), testicular cancer, thymoma, neuroendocrine tumour) patients with solid tumours undergoing survivin treatment (EMD640744; ClinicalTrials.gov Identifier: NCT01012102).

Serum was obtained for these patients before (Baseline) and after treatment (Week *n*), with at least one time point post-treatment per patient. This serum was collected under the supervision of our collaborator, Prof. Alexander Knuth, at the UZH.

This clinical trial's progress has also been recently published (Lennerz et al. 2014), and therefore public access and collection of the clinical profile of the patients included in our cohort was possible.

2.2.5 Internal Radiotherapy cohort

The internal radiotherapy treatment cohort included 11 primary colorectal cancer patients with metastatic non-resectable liver tumours undergoing selective internal radiotherapy treatment (SIRT) (ClinicalTrials.gov Identifier: NCT00724503).

Serum was obtained for these patients before (D0) and after treatment (Cycle *n*), with at least one time point post-treatment per patient. This serum was also collected under the supervision of our collaborator, Prof. Alexander Knuth, at the UZH.

Access and collection of the complete clinical profile of the patients included in our cohort was not possible.

2.2.6 Other treatment cohorts

The other treatments cohort included 89 malignant melanoma patients undergoing several distinct treatments. Due to the majority of these patients contributing samples at a single time point only, post-treatment analysis was not possible, and therefore these patients were grouped together as a means of conducting a cancer-specific group analysis, focusing on typically expressed antigens and possible correlations with disease stage.

Serum was obtained for these patients at a random time point during their treatment course. This serum or plasma was collected under the supervision of our collaborator, Prof. Jonathan Cebon at the Austin Health in Melbourne.

As part of our ongoing collaboration, access and collection of the complete clinical profile of the patients included in our cohort was possible.

2.3 Results and Discussion

The following Section contains all clinical information that could be collected, such as patient IDs, gender, age, diagnosis/tumour, karyotype/HLA type, treatment dosage, best response, cycles of treatment, overall survival, etc., as well as all treatment-specific information for each cohort analysed in this Thesis.

2.3.1 Kinase Inhibitor cohorts

The kinase inhibitor treatment cohort included 36 malignant melanoma patients undergoing 1) BRAF, 2) Alternative BRAF (aBRAF), 3) MEK, 4) BRAF + MEK, 5) BRAF +/- MEK treatments. Of these, clinical and treatment-specific information was available for all 36 patients undergoing treatment.

Melanoma is a form of skin cancer that originates in melanocytes, cells that produce the skin pigment called melanin that is responsible for skin and hair colour. Melanomas can form at any skin site and the four major types are: radial spreading (superficial spreading), nodular, lentigo maligna (Hutchinsons's freckle) and acral lentiginous. The development of melanoma is related to sun exposure or ultraviolet

radiation and can spread very rapidly, being the leading cause of death from skin disease (www.ncbi.nlm.nih.gov/pubmedhealth).

Metastatic melanoma is known to have a very poor prognosis, with a median overall survival between 9 to 11 months, or, if brain metastasis are present, between 4 to 5 months instead (Balch et al. 2009; Davies et al. 2011). As these tumours are usually unresponsive to standard treatment options, viable alternatives are required. As a result, many researchers are currently investigating the potential of kinase inhibitors in treating melanoma. The basis of this selection is that the RAF–MEK–ERK kinase pathway is responsible for mediating cellular responses to growth signals, and BRAF, a known serine/threonine kinase, is usually activated by somatic point mutation in cancers (Chapman et al. 2011; Curtin et al. 2005; Davies et al. 2002; Peyssonnaux & Eychène 2001). Therefore, several distinct kinase inhibitor drugs have and are currently still being tested in a clinical trial setting, due to their potential as anti-tumour therapeutics, and associated ability to prolong progression-free survival rates for metastatic melanoma patients with limited or no alternative treatment options (www.clinicaltrials.gov).

This treatment cohort in our study includes patients from five distinct kinase inhibition clinical trials, each of which will be briefly explained as a means to facilitate data interpretation and analysis.

The first clinical trial (NCT00880321) consisted of a completed phase I study that investigated the safety, pharmacokinetics, and pharmacodynamics of a BRAF inhibitor (dabrafenib, GSK2118436) in subjects with BRAF mutated-positive solid tumours that were unresponsive to standard therapies. The study's summarized results found this drug to be safe in patients, and cases of complete and partial tumour responses were seen across melanoma, although resistance was noted in the majority of the metastatic cases (Falchook et al. 2012).

The second clinical trial (NCT01006980) consisted of a randomized, open-label, controlled, multicentre, global study on progression-free and overall survival in previously untreated patients with unresectable metastatic melanoma with the V600E BRAF mutation-positive receiving an alternative BRAF inhibitor (vemurafenib, RO5185426) or dacarbazine (chemotherapeutic drug). This study indicated beneficial overall results, with improved rates of progression-free survival across patients, and response rates of up to 48%, when compared to standard dacarbazine treatment (Chapman et al. 2011; McArthur et al. 2014).

The third clinical trial (NCT01037127) consisted of a completed phase II open-label, multicentre study that determined the effectiveness of a MEK inhibitor (trametinib, GSK1120212) in BRAF mutation-positive melanoma previously treated with or without a BRAF inhibitor. This study reported a good drug tolerance, and a significant clinical activity in BRAF inhibitor-naïve patients, but a minimal one in those previously treated with chemotherapy and/or immunotherapy (Kim et al. 2013).

The fourth clinical trial (NCT01072175) consisted of a currently active open-label, dose-escalation, phase I/II study that investigated the safety, pharmacokinetics, pharmacodynamics and clinical activity of a BRAF inhibitor (dabrafenib, GSK2118436) in combination with a MEK inhibitor (trametinib, GSK1120212) in subjects with BRAF mutant metastatic melanoma. This study has already reported a good tolerance of the combined drugs, and a significantly improved progression-free survival when comparing monotherapy to combination therapy (Flaherty et al. 2012).

The fifth and final clinical trial (NCT01584648) consisted of a currently ongoing phase III, randomized, double-blinded study comparing the combination of a BRAF inhibitor (dabrafenib, GSK2118436) and a MEK inhibitor (trametinib, GSK1120212) to dabrafenib and placebo, as first-line therapy in patients with unresectable metastatic BRAF V600E/K mutation-positive cutaneous melanoma. This study has reported that the combination of these two drugs, when compared with BRAF inhibitor only, improved the overall response rates and progression-free survival in these patients (Long et al. 2014).

The patients included in this treatment cohort were selected from the large number of patients included in these five treatment trials, due to all of them displaying interesting responses, ranging from complete responses to gaining apparent resistance to treatment. Although this pre-selection enabled the analysis of a wide variety of different responses amongst malignant melanoma patients undergoing kinase inhibitor treatment, it is essential to note that this introduced significant diversity within this cohort. Furthermore, all analyses should take into account this diversity when interpreting any posterior findings. Nonetheless, it may be possible to make preliminary assumptions with regards to the benefits of treating patients with either BRAF alone or in combination with MEK, although, due to the limited number of patients and the heterogeneity amongst them, these may not be of significant statistical relevance.

For the above-mentioned patients, the clinical information that was found most relevant for this analysis included patient ID, gender (M: male, F: female), age when treated, treatment undergone, best overall response to treatment (SD: stable disease, CR: complete response, PR: partial response, PD: progressive disease), and overall survival time in months, as indicated in Tables 2.1 and 2.2. Besides from the information included in this Table, the RECIST measurements across time points were collected, when available, as a means of further defining a more detailed response status per time point.

Table 2.1 Patient demographics of the BRAF, aBRAF and MEK (single inhibitor) cohorts. This table includes the complete accessed patient information for the BRAF, aBRAF and MEK (single inhibitor) cohorts. M: male; F: female; OS: overall survival; mo: months; SD: stable disease; CR: complete response; PR: partial response; PD: progressive disease; +: still ongoing. Dark grey shaded areas indicated outstanding clinical information.

Patient ID	Gender	Age	Treatment	Best response	OS (mo)
KI001: RR	M	69	BRAF	SD	18
KI002: TL	M	46	BRAF	CR	12+
KI003: BH	M	50	BRAF	PR	15
KI004: DD	M	69	BRAF	PR	6
KI005: DBr	M	52	BRAF	SD	15+
KI006: AB	M	66	BRAF	SD	5
WMD-006	F	38	BRAF		29
WMD-007	M	31	BRAF	SD	7
WMD-008	F	61	BRAF	PR	62+
WMD-009	F	58	BRAF	PR	31
WMD-010	M	31	BRAF	SD	6
WMD-011	M	67	BRAF	PR	15
WMD-012	M	59	BRAF	SD	9
WMD-016	M	62	BRAF	PR	10
WMD-017	F	55	BRAF	PR	56+
WMD-018	F	29	BRAF	PD	3
WMD-020	M	28	BRAF	PR	10
WMD-021	F	33	BRAF	PR	29
WMD-019	M	69	aBRAF	PR	14
WMD-014	M	29	MEK		5

Table 2.2 Patient demographics of the BRAF + MEK and BRAF +/- MEK (dual inhibitor) cohorts. This table includes the complete accessed patient information for the BRAF + MEK and BRAF +/- MEK (dual inhibitor) cohorts. M: male; F: female; OS: overall survival; mo: months; SD: stable disease; CR: complete response; PR: partial response; PD: progressive disease; +: still ongoing.

Patient ID	Gender	Age	Treatment	Best response	OS (mo)
KI007: DR	M	26	BRAF + MEK	PR	5
KI008: MC	M	44	BRAF + MEK	SD	28+
KI009: Dbe	M	49	BRAF + MEK	PD	12
KI010: NH	M	26	BRAF + MEK	PR	7
KI011: GD	M	52	BRAF + MEK	PR	27+
KI012: KM	M	59	BRAF + MEK	PR	14
KI013: EB	F	31	BRAF + MEK	SD	26
WMD-005	M	37	BRAF + MEK	SD	28
WMD-022	M	41	BRAF + MEK	SD	3
WMD-023	M	39	BRAF + MEK	PR	48+
WMD-024	M	62	BRAF + MEK	CR	46+
WMD-015	F	24	BRAF + MEK	PR	10
WMD-013	M	71	aBRAF + BRAF + MEK	SD	22
KI014: KD	F	53	BRAF +/- MEK	PR	14+
KI015: EL	F	78	BRAF +/- MEK	PR	11
KI016: DM	M	74	BRAF +/- MEK	PR	14

The characteristics of these 36 patients included quite an unevenly weighed population, with more males (*n* = 26/36, 72%) than females (*n* = 10/36, 28%), and a median patient age of 51 years (mean = 49 years), with ages ranging widely from 24 to 78 years. This population included 20 patients (*n* = 20/36, 56%) undergoing single inhibitor treatment (BRAF, aBRAF or MEK), and 16 patients (*n* = 16/36, 44%) undergoing dual inhibitor (BRAF + MEK, aBRAF + BRAF + MEK, or BRAF +/- MEK) treatment. Amongst the 18 patients with an available overall disease status undergoing single inhibitor treatment subset, one achieved a complete response (6%) and ten achieved a partial response (55%), for an overall response rate of 61%, while the remaining patients were either stable (*n* = 6/18, 33%) or had progressive disease

(*n* = 1/18, 6%). For this subset, the median overall survival was 13 months (mean = 18 months). However, amongst the 16 dual inhibitor treatment subset, one achieved a complete response (6%), and nine achieved a partial response (57%), for an overall response rate of 63%, while the remaining patients were either stable (*n* = 5/16, 31%) or had progressive disease (*n* = 1/16, 6%). For this subset, the median overall survival was 14 months (mean = 20 months). When comparing these two treatment subsets, the overall response rates and disease status distributions were very similar, 61% vs 63%, as well as the overall survival in months, with only a slightly higher benefit (an additional 2% overall response rate, and 1 month median survival) for those patients undergoing dual inhibitor treatment. When considering these subsets as a one, the overall distribution by disease status included two complete responses (*n* = 2/34, 6%), and nineteen partial responses (*n* = 19/34, 56%), for an overall response rate of 62%, while the remaining patients were either stable (*n* = 11/34, 32%) or had progressive disease (*n* = 2/34, 6%). The median overall survival was 14 months (mean = 19 months) for these patients.

In regards to the statistical power of these descriptive findings, the number of patients (n = 36) was below the a priori estimate (n = 54), indicating that any potential findings would be obtained with lower sensitivity than ideally required. Nonetheless, a post hoc estimate was generated to compute the achieved statistical power of this cohort (G*Power 3.1.9.2 program, T-test, difference between two dependent means (matched pairs), 2-tailed) with a given probability of error (α=0.05), sample size (n = 36) and effect size (dz=0.5) (Faul et al. 2007; Faul et al. 2009). This calculation indicated an estimated power (1-β) of 0.83 (noncentrality parameter σ = 3.00, critical t = 2.03, degrees of freedom = 35), which was above the generally recommended and accepted minimum power of 0.8 (Cohen 1988). Therefore, when treating the two distinct treatment subtypes (single vs. dual inhibitor treatment) as a whole, the probability of this cohort detecting a statistically relevant finding may be acceptable. However, comparing findings between the two treatment subtypes does not hold statistical significant relevance. Furthermore, although patient selection for each clinical trial was conducted following the necessary pre-stipulated statistical design, the patients that were posteriorly included in this analysis cohort were not selected based on a pre-determined study design, but rather on a variety of distinct clinical responses, as a means to aid in comprehending why malignant melanoma patient responses to the same treatment differ substantially. As a consequence, this cohort was quite heterogeneous regarding patient demographics, namely age and gender, which may further limit the achieved statistical power of potential findings.

2.3.2 Pre- or Post-operative chemotherapy/radiotherapy cohort

The pre- or post-operative chemotherapy/radiotherapy treatment cohort included 62 colorectal cancer patients undergoing chemotherapy/radiotherapy prior- or post-surgical resection of their primary tumours.

Colorectal cancer originates in the large intestine (colon) or the rectum (end of the colon), and usually begins as a noncancerous polyp, which develops in the lining of the colon or rectum. There are several types of colon and rectal cancers, but adenocarcinomas account for more than 95% of all colorectal cancer, whilst other less common types include carcinoid tumours, gastrointestinal stromal tumours, lymphomas and sarcomas. As with most cancers, an early diagnosis is critical to obtain as successful treatment outcome and reduced chance of recurrence (www.ncbi.nlm.nih.gov/pubmedhealth).

When possible, the primary treatment for colorectal cancer is surgery, and the additional treatment options include chemotherapy and radiotherapy. In this specific treatment cohort, systemic chemotherapy, usually 5-fluorouracil (5FU) and leucovorin (LV), was administered orally or via injection, and external radiotherapy was administered localised toward the cancer location. Several studies have researched the effects of pre- or post-operative chemotherapy/radiotherapy in rectal cancer, and whilst some studies show that pre-operative therapy is beneficial in regards to the reduction of local re-occurrences, others state that this beneficial effect is obtained whether the therapy is administered pre- or post-operatively (Sauer et al. 2004; Kapiteijn et al. 2001; Bosset et al. 2006).

The 62 patients included in this treatment cohort were selected based solely on sample availability (single time point per patient), emerging from a previous sample collection effort within our group, without following a pre-established patient selection or study design. These patients were undergoing standard cancer treatments (surgery, chemotherapy and radiotherapy) based on an individually defined personal treatment plan by their oncologist, as well as personal preference to undergo treatment. It is essential to note that these patients were not involved in a particular clinical trial, and that these samples were analysed here with the intent of conducting a retrospective analysis on whether pre- or post-operative therapy was most beneficial, and on how this therapy significantly altered the pattern of cancer-associated antigen autoimmune titres in these patients, thereby potentially influencing the outcome of any subsequent treatment. Whether or not potential findings may be of significant statistical relevance would depend on the heterogeneity of the resulting cohort. For these patients, the clinical information that was found most relevant for this analysis included patient ID, gender, age at diagnosis, colorectal cancer type (sporadic or HNPCC: hereditary non-polyposis colorectal cancer), stage, location and site (rectum, RSJ: recto-sigmoid junction, DC: descending colon, TC: transverse colon, SC: sigmoid colon, AC: ascending colon, PDC: proximal descending colon, HF: hepatic flexure), presence or absence of pre-operative chemotherapy or radiotherapy, risk factors (HT: hypertension, S: smoking history, fCRC: familial history of CRC, AC: alcohol consumption, O: Obesity), and recurrence information, as indicated in Table 2.3.

Table 2.3 Patient demographics of the pre- or post-operative chemotherapy/radiotherapy cohort. This table includes the complete accessed patient information for the pre- or post-operative chemotherapy/radiotherapy cohort. CRC: colorectal cancer; Pre-op CT/RT: pre-operative chemotherapy/radiotherapy; M: male; F: female; HNPCC: hereditary non-polyposis colorectal cancer; -: none; RSJ: recto-sigmoid junction; DC: descending colon; TC: transverse colon; SC: sigmoid colon; AC: ascending colon; PDC: proximal descending colon; HF: hepatic flexure; Y: yes; N: no; HT: hypertension; S: smoking history; fCRC: familial history of CRC; AC: alcohol consumption; O: Obesity. Dark grey shaded areas indicated outstanding clinical information.

Patient ID	Gender	Age	CRC type	Stage	Location	Site	Pre-op RT/CT	Risk factors	Recurrence
CRC002	M	67	Sporadic	II	Distal	Rectum	Y	-	N
CRC003	M	70	Sporadic	III	Distal	RSJ	N	HT	Y
CRC004	F	44	HNPCC	III	Proximal	Caecum	N	S, fCRC	N
CRC005	M								
CRC006	F	23	Sporadic	III	Distal	Rectum	Y	-	N
CRC007	M	52	Sporadic	III	Distal	Rectum	N	HT, AC	Y
CRC008	M	61	Sporadic	III	Distal	Rectum	N	HT, S, AC	N
CRC009	F	64	Sporadic	III	Distal	Rectum	N		N
CRC010	M	63	Sporadic	III	Distal	DC	N	-	Y
CRC011	M	84	Sporadic	I	Proximal	TC	N	S	N
CRC012	M								
CRC013	F	46	HNPCC	II	Proximal	Caecum	N	-	N
CRC014	M	80	Sporadic	IV	Distal	SC	N	-	N
CRC015	M	74	Sporadic	II	Distal	Rectum	N	S, AC	N
CRC016	M	76	Sporadic	I	Proximal	AC	N	-	Y
CRC017	M	79	Sporadic	III	Distal	SC	N	-	N
CRC019	F	62	Sporadic	I	Distal	Rectum	Y	-	N
CRC020	F	26	HNPCC		Proximal	Caecum	N	-	
CRC021	F	61	Sporadic	III	Distal	Rectum	N	HT, O	N
CRC022	M	49	Sporadic	III	Distal	Rectum	Y	-	N

Patient ID	Gender	Age	CRC type	Stage	Location	Site	Pre-op RT/CT	Risk factors	Recurrence
CRC024	M	42	Sporadic	III	Distal	Rectum	Y	-	N
CRC025	F	67	Sporadic	I	Distal	Rectum	Y	-	N
CRC026	F	73	Sporadic	I	Distal	Rectum	Y	HT, S, fCRC	Y
CRC028	M	79	Sporadic	II	Distal	Rectum	Y	-	N
CRC029	M	73	Sporadic	III	Distal	Rectum	Y	HT	N
CRC031	F	54	Sporadic	I	Distal	Rectum	Y	-	N
CRC032	F	52	Sporadic	III	Proximal	Caecum	N		N
CRC033	F	69	Sporadic	III	Distal	Rectum	N	HT, S	N
CRC034	F	70	Sporadic	III	Distal	Rectum	N	-	Y
CRC035	M	68	Sporadic	II	Distal	Rectum	Y	-	Y
CRC036	F	67	Sporadic	III	Distal	Rectum	Y		N
CRC037	M	49	Sporadic	III	Distal	PDC	N	-	N
CRC038	M	49	Sporadic	I	Distal	Rectum	Y		N
CRC039	F	51	Sporadic	II	Distal	Rectum	Y	O	
CRC040	F	47	Sporadic	II	Distal	Rectum	Y	-	N
CRC041	F	71	Sporadic	II	Distal	Rectum	N	HT, O	N
CRC042	M	37	Sporadic	II	Distal	Rectum	Y		Y
CRC043	F	67	Sporadic	II	Distal	Rectum	Y	-	N
CRC044	M	36	Sporadic	III	Proximal	Caecum	N	-	N
CRC045	F	36	Sporadic	II	Distal	Rectum	Y	-	Y
CRC046	F								
CRC047	M	25	HNPCC	III	Distal	DC	Y	S, fCRC	N
CRC048	M	37	Sporadic	IV	Distal	Rectum	N	O	N
CRC049	F	50	Sporadic		Distal	RSJ	Y		N
CRC050	F	60	Sporadic	I	Distal	Rectum	Y		Y
CRC051	M	47	Sporadic	II	Distal	Rectum	Y	-	Y
CRC052	F	42	Sporadic	II	Distal	Rectum	Y		N

Patient ID	Gender	Age	CRC type	Stage	Location	Site	Pre-op RT/CT	Risk factors	Recurrence
CRC053									
CRC054	M	60	Sporadic				N	-	
CRC055	M	64	Sporadic	III	Distal	DC	N	-	Y
CRC056	F	54	Sporadic	III	Distal	RSJ	N	fCRC	N
CRC057	M	45	Sporadic	III	Distal	RSJ	N	S	N
CRC058		71	Sporadic	II	Distal	Rectum	Y	-	N
CRC059	F	79	Sporadic	II	Distal	Rectum	Y	-	Y
CRC060	M	65	Sporadic	II	Distal	RSJ	N	fCRC	N
CRC062	F	40	Sporadic	II	Distal	Rectum	Y	-	N
CRC063	F	78	Sporadic	II	Proximal	HF	N	fCRC	N
CRC064	F	69	Sporadic	II	Distal	Rectum	Y	-	N
CRC065	M	73	Sporadic	III	Distal	Rectum	Y	-	N
CRC066	F	59	Sporadic	III	Distal	Rectum	Y	-	N
CRC067	M	64	Sporadic	III	Distal	Rectum	N	-	N
CRC068	F	76		II	Proximal	Caecum	N		N

The available characteristics of these 62 patients included quite an equally weighed population, with an equal number of males (*n* = 30/60, 50%) and females, and a median patient age of 62 years (mean = 59 years), with ages ranging widely from 23 to 84 years. The majority of these patients presented with sporadic colorectal cancer (*n* = 53/57, 93%), whilst only a few types were HNPCC (hereditary non-polyposis colorectal cancer, *n* = 4/57, 7%). Amongst this population, a great deal of patients presented with stage III (*n* = 25/55, 45%), followed by stages II (*n* = 20/55, 36%), I (*n* = 8/55, 15%) and IV (*n* = 2/55, 4%). In regards to tumour location, most cancers occurred in a distal location (*n* = 48/57, 84%), with only a few cases located proximally (*n* = 9/57, 16%). Interestingly, the three most common cancer sites amongst the nine were in the rectum (*n* = 37/57, 65%), caecum (*n* = 6/57, 11%) and recto-sigmoid junction (*n* = 5/57, 9%). Of the 58 patients for which pre-operative chemotherapy/radiotherapy information was available, exactly half (*n* = 29/58, 50%) underwent pre-operative therapy, and the other half did not. However, when considering disease recurrence, the majority of these patients did not have recurrent disease (*n* = 42/55, 76%), whilst a small subset did (*n* = 13/55, 24%). Amongst the patients that

did not have disease recurrence, exactly half underwent pre-operative therapy (*n* = 21/42, 50%), and the other half did not. When assessing the recurring patients (*n* =13/55, 24%) in regards to presence or absence of pre-operative therapy, patient numbers were limited, thus preventing further analysis.

In regards to the statistical power of these findings, the number of patients (*n* = 62) was above the *a priori* estimate (*n* = 54), indicating that any potential findings would be obtained with higher sensitivity than ideally required. A *post hoc* estimate was generated to compute the achieved statistical power of this cohort (G*Power 3.1.9.2 program, T-test, difference between two dependent means (matched pairs), 2-tailed) with a given probability of error ($\alpha = 0.05$), sample size (*n = 62*) and effect size ($dz = 0.5$) (Faul et al. 2007; Faul et al. 2009). This calculation indicated an estimated power ($1 - \beta$) of 0.97 (noncentrality parameter σ = 3.94, critical t = 2.00, degrees of freedom = 61), and therefore the probability of this cohort detecting a statistically relevant finding surpassed the initial ideal estimate. Thus, when conducting analysis within this treatment cohort, findings are of statistical relevance, whereas when dividing this cohort into those that received pre-operative chemotherapy/radiotherapy and those who did not, patient numbers are limited and do not permit statistically worthy considerations to be made. Furthermore, although the inclusion of patients in this study cohort was not according to a pre-established study design, this cohort was homogenous and equally weighed regarding demographics such as gender. However, a wide age range was obtained, which may reduce the estimated sample number-based power, although not significantly.

2.3.3 Epigenetic Modifiers cohort

The epigenetic modification treatment cohort included 12 myelodysplasia patients undergoing a combination of panobinostat (HDAC inhibitor) with azacitidine treatment, of which clinical and treatment-specific information was available (Tan et al. 2014).

Epigenetics, one of the most promising and expanding fields in cancer research, is currently defined as the study of heritable changes in gene expression, that are not due to any DNA sequence alterations (Holliday 1987; Esteller 2008). Cancer is known to have aberrant epigenetic regulation and, due to the possibility of reversing these alterations, unlike with mutations, epigenetic therapies showed great potential as a cancer therapy (Esteller 2008). This aberrant regulation is usually characterized by global changes in DNA methylation and altered histone modification patterns, both which are being targeted by the epigenetic therapies used in this cohort, which could lead to epigenetic silencing of tumour supressing genes (Jones & Laird 1999; Rodríguez-Paredes & Esteller 2011). This epigenetic inactivation, which is associated with dense CpG-island promoter hypermethylation and the appearance of repressive histone markers, can be partially modified using epigenetic drugs, by way of removing inactivation markers (DNA methylation) and inducing the presence of active markers (Histone

acetylation), which explains the rationale of using this dual epigenetic targeting as a potential cancer therapeutic (Esteller 2008).

Myelodysplastic syndrome (MDS) is a type of cancer where blood stem cells, immature cells resulting from the bone marrow, do not become healthy red blood cells, white blood cells or platelets, dying instead either in the bone marrow or shortly after reaching the blood (www.ncbi.nlm.nih.gov/pubmedhealth). MDS can evolve into acute myeloid leukaemia (AML), depending on the associated risk-based categorical cytogenetic subgroups (Good: normal, del(5q) only, del(20q) only, -Y only; Intermediate: +8, single miscellaneous, double abnormalities; Poor: complex with $\geq$3 anomalies or chromosome 7 abnormalities). Additionally, MDS can be scored using the International Prognostic Scoring System (IPSS), which provides relevant survival and AML evolution predictions based on an aggregate prognostic score of bone marrow blasts (%), karyotype (normal, complex or intermediate) and cytopenias (Greenberg et al. 1997). The resulting scores for each risk group are low (0), Int1 (0.5 – 1.0), Int2 (1.5 – 2.0) and high ($\geq$2), which is usually represented as part of the MDS diagnosis, such as MDS-low, for example.

Azacitidine, a hypomethylating agent, was the first FDA-approved drug (5-azacytadine, Vidaza) for the treatment of MDSs that showed improvement of overall survival rates and delayed progression to AML (Vigil et al. 2010). Panobinostat, a potent HDAC inhibitor, has shown great promise as an anti-proliferative and cytotoxic clinically efficient therapeutic in hematologic and solid tumours (Atadja 2009). Both therapeutic options are categorized as epigenetic modifiers, and are widely studied in the epigenetics field.

This clinical trial in particular, an open-label phase Ib/II study, conducted at the Alfred, Princess Alexandra and Austin hospitals in Australia, aimed to clinically evaluate the safety and efficacy of combining panobinostat with azacitidine in patients with high-risk MDS or AML that were unsuitable for standard induction chemotherapy (ACTRN12610000924055). Usually, limited therapeutic options and poor treatment outcomes are common for older patients with AML, mainly due to the high treatment-related mortality risk. Therefore, this potential treatment alternative was investigated with the intent of prolonging their median survival and quality of life. To assess the clinical efficacy of this treatment, patients were given an injection with azacitidine (75 mg/m^2) on days 1-5, followed by an oral dose of panobinostat (10, 20, 30 and 40 mg) three times a week on days 5-28 for seven doses of each 28-day cycle. Clinical responses to treatment were measured using bone marrow assessments after cycles 1, 3 and 6, and patients were classified accordingly as having a complete response (CR), a partial response (PR), progressive disease (PD) or being resistant (R) to treatment (Tan et al. 2014).

The 12 patients included in this treatment cohort were selected by our collaborators amongst the 39 patients treated in this clinical trial, as a means of assuring the provision of a full range of observed

responses to treatment. Although this pre-selection enabled the analysis of a wide variety of different responses amongst myelodysplasia patients undergoing dual epigenetic modification treatment, it is essential to note that this resulted in a very limited number of patients. Furthermore, all analyses should take this limitation into account when interpreting any posterior findings.

For these patients, the clinical information that was found most relevant for this analysis included patient ID, gender, age when treated, attributed diagnosis and karyotype, baseline white blood cell (WBC) levels, treatment dosage, best overall response to treatment, cycles of treatment undergone and overall survival time in months, as indicated in Table 2.4. Besides from the information included in this Table, time point-specific patient assessments were collected based on clinician's patient notes, as a means of further defining a more detailed response status per time point.

Table 2.4 Patient demographics of the epigenetic modification cohort. This table includes the complete accessed patient information for the epigenetic modification cohort. M: male; F: female; WBC: white blood cell count; Pano: panobinostat; OS: overall survival; mo: months; MDS: myelodysplastic syndrome; AML: acute myeloid leukaemia; MRC: myelodysplasia-related changes; HI-E: major hematologic improvement with erythroid response; HI-N: major hematologic improvement with neutrophil response; HI-P: major hematologic improvement with platelet response; CR: complete response; PR: partial response; PD: progressive disease; #co-existent severe co-morbidities; 1prior MDS; 2prior myelofibrosis (MF); 3prior chronic myelomonocytic leukaemia (CMML).

Patient ID	Gender	Age	Diagnosis	Karyotype	Baseline WBC (10^9/L)	Pano dose (mg)	Best response	Cycles	OS (mo)
001-0001	M	68	MDS- Int2	Complex	4.4	10	CR, HI-E	16	16
001-0002	M	70	AML MRC[1]	Normal	4.3	10	PR	7	8
001-0003	F	72	MDS- Int2	Normal	3.3	10	CR	30	34+
001-0004	M	61	MDS- high	del(20q)	10.8	10	PD	5	6
001-0006	F	43	MDS- Int2	t(3;3)	3.2	20	CR, HI-E	18	32
001-0007	F	73	AML MRC[1]	Normal	27.5	20	Resistant	7	7
001-0008[#]	M	58	AML MRC[2]	Normal	37.1	20	Resistant	7	7
001-0011	M	65	AML MRC[1]	7-	2.8	20	Resistant	12	16
001-0012	M	73	AML MRC[3]	Normal	1.9	20	PR	14	13
001-0013	F	67	MDS- Int2	Complex	3.6	30	SD, HI-N	6	12
001-0016	M	36	MDS- Int2	7-	4.6	30	PD	6	11
001-0018	F	60	MDS- high	Normal	38.8	30	PR, HI-E,P	23	23+

The characteristics of these 12 patients included quite an equally weighed population, with slightly more males (58%) than females (42%), and a median patient age of 66 years (mean = 62 years), with ages ranging widely from 36 to 73 years. This population included 7 patients with high-risk MDS and 5 patients with acute myeloid leukaemia (AML), with half of the population (*n* = 6/12, 50%) displaying a normal karyotype. Amongst the 7 patients with MDS, three achieved a complete response (43%) and one achieved a partial response (14%), for an overall response rate of 57%, while the remaining patients were either stable (*n* = 1/7, 14%) or had progressive disease (*n* = 2/7, 29%). However, amongst the 5 patients with AML, two achieved a partial response (40%), for a lower overall response rate of 40%,

while three became resistant to treatment (60%), with no patient exhibiting a complete response or remaining stable. The median overall survival (OS) was 16 months for patients with MDS, and 8 months for patients with AML.

In regards to the statistical power of this treatment cohort, the number of patients (n = 12) was well below the a priori estimate (n = 54), indicating that any potential findings would be obtained with much lower sensitivity than ideally required. Nonetheless, a post hoc estimate was generated to compute the achieved statistical power of this cohort (G*Power 3.1.9.2 program, T-test, difference between two dependent means (matched pairs), 2-tailed) with a given probability of error (α=0.05), sample size (n = 12) and effect size (dz=0.5) (Faul et al. 2007; Faul et al. 2009). This calculation indicated an estimated power (1-β) of 0.35 (noncentrality parameter σ = 1.73, critical t = 2.20, degrees of freedom = 11), which was well below the generally recommended minimum power of 0.8 (Cohen 1988). Therefore, the probability of this cohort detecting a statistically relevant finding was not acceptable. Furthermore, although patient selection for this clinical trial was conducted following the necessary pre-stipulated statistical design, the patients that were posteriorly included in this analysis cohort were not selected based on a pre-determined study design, but rather on a variety of distinct clinical responses, and as a result very limited patients sample numbers were obtained, thus limiting our analysis substantially. Nonetheless, it may be possible to make very preliminary assumptions regarding comprehending why AML and high-risk MDS patients respond differently to dual epigenetic modification, which could provide insight into patient stratification or even likelihood of a desired response.

2.3.4 Apoptosis Inhibitor cohorts

The apoptosis inhibitor treatment cohort included 48 varied cancer (urothelial cancer, colorectal cancer, sarcoma, renal cancer, ovarian cancer, adenoid cystic cancer, breast cancer, mesothelioma, melanoma, head and neck cancer, non-small cell lung carcinoma (NSCLC), testicular cancer, thymoma, neuroendocrine tumour) patients with advanced solid tumours undergoing survivin treatment, of which clinical and treatment-specific information was available (Lennerz et al. 2014).

Several cancer types were included in this treatment cohort, as solely a metastatic or locally advanced survivin-expressing solid tumour was required, rather than a specific cancer type.

Survivin, also known as baculoviral IAP repeat containing protein 5 (BIRC5), is a unique member of the inhibitor of apoptosis (IAP) family, and is critically required for the suppression of apoptosis and to ensure normal cell division, being a key apoptosis inhibitor/cell cycle regulator (Ambrosini et al. 1997; Tamm et al. 1998; Li et al. 1998; Shin et al. 2001)(www.uniprot.org). Although survivin expression is developmentally regulated in normal tissues, it has found to be aberrantly overexpressed across a variety of cancers, from premalignant to metastatic lesions, which is most likely related to the

suppression of apoptosis that contributes to carcinogenesis (Ambrosini et al. 1997; Thompson 1995). In cancer, the evasion of cell cycle checkpoints that would normally induce apoptosis may contribute towards aberrantly prolonging the cell life span, which could potentially facilitate the accumulation of harmful gene mutations and a growth factor-independent cell survival, which could promote patient resistance towards immune-based cytotoxicity (Thompson 1995; Tamm et al. 1998). These features, along with the reported association with increased tumour recurrence and poor prognosis, make this protein a very attractive anti-cancer immunotherapy target (Islam et al. 2000; Swana et al. 1999; Altieri 2003). Therefore, several studies have assessed whether the disruption of survivin activity in cancer cells could sensitize them to subsequent therapeutic interventions, and have found decreased cell proliferation and increased apoptosis without any apparent toxicity to healthy tissues (Fukuda & Pelus 2006).

This cohort in particular is derived from a randomized first-in-man phase I study with a cocktail of survivin-derived and 5 partially modified HLA class I-restricted peptides in the oil adjuvant, montanide ISA (EMD640744), conducted at 5 medical centres in Switzerland, that aimed to compare three dosages with respect to immunologic efficacy, safety, tolerability, and clinical activity in patients with different types of metastatic or locally advanced solid tumours (NCT01012102). Although multiple HLA class I-binding peptides of survivin have been identified, previous trials have only tested single survivin peptides associated with a restricted number of common HLA alleles (clinicaltrial.gov). The therapeutic cocktail of this study included five multiepitope short peptides, based on the amino acid sequence of different regions of the survivin protein, shown to bind HLA-A01/A02/A03/A24/B07 peptides, due to a wider HLA type distribution and T-cell stimulatory activity. Therefore, this treatment was investigated with the intent of maximizing the number of patients with survivin-expressing tumours that could benefit from receiving this vaccine. To assess the immunological efficacy of this treatment, patients were given an injection with EMD640744 (30 μg, 100 μg or 300 μg) reconstituted and emulsified with montanide ISA for an 11-week initiation therapy (8 treatments), followed by 13-week maintenance therapy (4 weekly treatments). Clinical benefit (complete response, partial response, or stable disease) was assessed by imaging, physical examination, nuclear scanning, and/or serum tumour markers established for the given tumour entity. Immunologic efficacy was assessed by ELISpot and pHLA-multimer staining before and until week 17 after vaccination, until tumour progression or unacceptable toxicity was seen (Lennerz et al. 2014).

The 48 patients included in this treatment cohort were selected by our collaborators amongst the 53 patients treated in this clinical trial, based on sample availability. Although this pre-selection enabled the analysis of a large amount of patient responses undergoing apoptosis inhibitor treatment, it is essential to note that these included a variety of tumour types, which introduces a substantial amount of clinical diversity amongst this cohort. Furthermore, all analyses should take into account this diversity

when interpreting any posterior findings. Nonetheless, it should still be possible to make preliminary assumptions with regards to the benefits of treating patients with apoptosis inhibitors, although, due to the broad range of cancer types, these may not be of large significant statistical relevance.

For these, the clinical information that was found most relevant amongst what was available for this analysis included patient ID, gender, age, tumour type, HLA type, treatment dosage, best overall tumour response to treatment (PD: progressive disease, SD: stable disease) and presence of a post-vaccination immunological response. This data was grouped according to each medical centre of treatment (C01, C02, C03, C04 and C05), and is indicated in Tables 2.5, 2.6, 2.7, 2.8 and 2.9. The above-mentioned clinical data was available for all but two patients, C01P005 and C02P008.

Table 2.5 Patient demographics of the apoptosis inhibition cohort C01. This table includes the complete accessed patient information for the apoptosis inhibition cohort C01. M: male; F: female; PD: progressive disease; SD: stable disease; Y: yes; N: no; Dark grey shaded areas indicated outstanding clinical information.

Patient ID	Gender	Age	Tumour	HLA type	Dose (µg)	Best response	T-cell response
C01P002	M	56	Urothelial cancer	A01, A03, B07	30	PD	Y
C01P005							
C01P007	F	67	Colorectal cancer	A03	100	PD	Y
C01P009	F	67	Colorectal cancer	A01, A02	30	SD	Y
C01P012	M	62	Colorectal cancer	A02	300	SD	Y
C01P013	M	36	Sarcoma	A02	100	PD	Y
C01P015	M	51	Renal cancer	B07	30	PD	N
C01P016	F	28	Ovarian cancer	A02	300	PD	Y
C01P017	F	63	Adenoid cystic cancer	A01	30	SD	N
C01P018	F	55	Breast cancer	A01, A02	100	PD	N
C01P024	M	79	Colorectal cancer	A01	300	SD	N
C01P027	M	60	Mesothelioma	A03	300	SD	Y
C01P028	F	44	Ovarian cancer	A01, A03, B07	30	PD	Y
C01P029	F	67	Ovarian cancer	A02, A03	100	PD	N
C01P032	F	69	Ovarian cancer	A02	30	PD	Y
C01P033	F	51	Melanoma	A02	100	SD	N
C01P035	M	58	Head and neck cancer	A02, A24	30	PD	Y
C01P037	F	58	Ovarian cancer	A02	300	PD	Y
C01P040	M	45	Mesothelioma	A02	30	PD	N

Table 2.6 Patient demographics of the apoptosis inhibition cohort C02. This table includes the complete accessed patient information for the apoptosis inhibition cohort C02. M: male; F: female; PD: progressive disease; Y: yes; N: no; Dark grey shaded areas indicated outstanding clinical information.

Patient ID	Gender	Age	Tumour	HLA type	Dose (µg)	Best response	T-cell response
C02P003	M	62	Melanoma	A01, A02	30	PD	N
C02P007	F	53	Melanoma	A03	300	PD	Y
C02P008							
C02P010	F	43	Melanoma	A02	30	PD	Y

Table 2.7 Patient demographics of the apoptosis inhibition cohort C03. This table includes the complete accessed patient information for the apoptosis inhibition cohort C03. M: male; F: female; SD: stable disease; PD: progressive disease; NE: not evaluable; Y: yes; N: no.

Patient ID	Gender	Age	Tumour	HLA type	Dose (µg)	Best response	T-cell response
C03P001	M	65	Sarcoma	A24, B07	100	SD	N
C03P002	F	49	NSCLC	A03	30	PD	Y
C03P005	M	51	NSCLC	A02, B07	30	SD	Y
C03P009	F	20	Melanoma	A02	300	PD	Y
C03P012	M	71	Colorectal cancer	A01, A24, B07	100	NE	N
C03P014	F	53	Breast cancer	A02	100	PD	Y
C03P015	M	65	Colorectal cancer	A02	100	SD	Y
C03P016	M	71	Colorectal cancer	A01, A02	30	NE	Y
C03P017	M	38	Testicular cancer	A01, A02	100	PD	Y
C03P019	M	34	Sarcoma	A02	300	SD	Y
C03P020	M	55	Melanoma	A01, A02	100	PD	N

Table 2.8 Patient demographics of the apoptosis inhibition cohort C04. This table includes the complete accessed patient information for the apoptosis inhibition cohort C04. F: female; M: male; PD: progressive disease; NE: not evaluable; SD: stable disease; Y: yes; N: no.

Patient ID	Gender	Age	Tumour	HLA type	Dose (µg)	Best response	T-cell response
C04P004	F	68	Mesothelioma	A02, B07	300	PD	N
C04P005	M	60	NSCLC	A02, A03, B07	100	PD	Y
C04P007	M	58	Mesothelioma	A03	100	PD	Y
C04P012	F	64	NSCLC	A02, A24	100	NE	N
C04P013	M	52	Melanoma	A01, A03	300	PD	N
C04P014	M	68	Thymoma	A02, A03, B07	30	SD	Y
C04P015	M	80	Adenoid cystic tumour	A02	100	SD	Y
C04P016	F	59	Colorectal cancer	A02	300	PD	N

Table 2.9 Patient demographics of the apoptosis inhibition cohort C05. This table includes the complete accessed patient information for the apoptosis inhibition cohort C05. F: female; M: male; NE: not evaluable; SD: stable disease, PD: progressive disease; Y: yes; N: no.

Patient ID	Gender	Age	Tumour	HLA type	Dose (µg)	Best response	T-cell response
C05P002	F	61	Ovarian cancer	A01, A03	100	NE	N
C05P005	F	63	Ovarian cancer	A01	300	NE	N
C05P011	M	51	Neuroendocrine tumour	A24	300	SD	Y
C05P012	M	61	Melanoma	A01, A24, B07	300	PD	Y
C05P014	M	47	Melanoma	A01, A02	300	PD	Y
C05P017	M	63	Neuroendocrine tumour	A01, A02	300	SD	Y

The characteristics of these 46 patients included quite an equally weighed population, with slightly more males (57%) than females (43%), and a median patient age of 59 years (mean = 57 years), with ages ranging widely from 20 to 80 years. This population included patients with a wide range of advanced

solid tumours, the most frequent tumours being melanoma (*n* = 9/46, 20%), colorectal cancer (*n* = 8/46, 17%), and ovarian cancer (*n* = 7/46, 15%). Patients expressed one to three of the alleles HLA-A01, HLA-A02, HLA-A03, HLA-A24 and HLA-B07, with the most commonly expressed allele being HLA-A02 (*n* = 29/46, 63%), followed by HLA-A01 (*n* = 17/46, 37%), HLA-A03 (*n* = 12/46, 26%), HLA-B07 (*n* = 10/46, 22%), and lastly HLA-A24 (*n* = 6/46, 13%). Amongst the 46 patients and in regards to best overall tumour responses, the majority had progressive disease (*n* = 27/46, 59%), or remained stable (*n* = 14/46, 30%), whilst five patients were not evaluable due to safety concerns (11%). Hence, as progressive disease was not an inclusion criterion, stable disease as best response cannot be considered a clinical benefit. Immunological benefit, T-cell responses against survivin peptides measured by *ex vivo* and/or *in vitro* ELISpot and/or pHLA-multimer staining, was detected post-vaccination in 29/46 (63%) patients, the majority of which were not present at baseline, providing evidence for *de novo* induction. No dose-dependent effects of the treatment were observed.

In regards to the statistical power of this treatment cohort, the number of patients (*n* = 48) was below the *a priori* estimate (*n* = 54), indicating that any potential findings would be obtained with lower sensitivity than ideally required. Nonetheless, a *post hoc* estimate was generated to compute the achieved statistical power of this cohort (G*Power 3.1.9.2 program, T-test, difference between two dependent means (matched pairs), 2-tailed) with a given probability of error ($\alpha = 0.05$), sample size (*n = 48*) and effect size ($dz = 0.5$) (Faul et al. 2007; Faul et al. 2009). This calculation indicated an estimated power ($1 - \beta$) of 0.92 (noncentrality parameter σ = 3.46, critical t = 2.01, degrees of freedom = 47), which was well above the generally recommended minimum power of 0.8 (Cohen 1988). Therefore, the probability of this cohort detecting a statistically relevant finding was acceptable. Furthermore, although patient selection for each clinical trial was conducted following the necessary pre-stipulated statistical design, the patients that were posteriorly included in this analysis cohort were selected based on sample availability, which excluded 5 patients from the original clinical trial. When considering the demographic and clinical characteristics of this cohort, the diversity amongst patient ages and tumour types may limit the achieved statistical power of potential findings. Nonetheless, this cohort may aid in comprehending how patient responses to the same treatment differ amongst distinct cancer types.

2.3.5 Internal Radiotherapy cohort

The internal radiotherapy treatment cohort included 11 primary colorectal cancer patients with metastatic non-resectable liver tumours undergoing selective internal radiotherapy treatment (SIRT).

Secondary or metastatic liver tumours – metastasis resulting from an alternative primary site (most likely colon cancer) – are much more common rather than primary liver tumours, and are usually

treated as a means of either increasing survival or removing metastasis-related blockages or discomfort, when possible (www.ncbi.nlm.nih.gov/pubmedhealth). Selective internal radiotherapy is a very attractive and effective therapy used in these circumstances, as it permits a high-dose internal radiotherapy delivery with little damage to healthy liver tissue, through use of microspheres containing radioactive yttrium (Stubbs & Wickremesekera 2004). These microspheres are delivered via a trans-femoral hepatic artery catheter, lodging in the blood vessels supplying tumours, as a means of impeding blood flow and therefore oxygen and nutrient supply to the tumours, a technique known as radioembolisation.

This clinical trial in particular, a randomised multi-centre comparative study of standard systemic chemotherapy regimen of FOLFOX - combination of 5-fluorouracil, leucovorin and oxaliplatin – in combination with SIR-spheres microspheres containing the β-emitter yttrium-90 (FDA approved) versus chemotherapy alone, as first line treatment in patients with non-resectable liver metastases from primary colorectal carcinoma (NCT00724503). Although this therapy is used often, its efficacy is yet to be tested on a large scale, which will hopefully be done by this trial (Gibbs et al. 2014). However, these results are yet to be officially reported.

The patients included in this treatment cohort were selected by our collaborators from the large number of patients included in this clinical trial, based only on sample availability. It is essential to note that this resulted in a very limited number of patient samples. Furthermore, all analyses should take this limitation into account when interpreting any posterior findings. Unfortunately, patient clinical information was not available for this treatment cohort, and therefore only the treatment and cancer type, as well as the patient and corresponding samples distribution before and after treatment were available.

The lack of accessible clinical information for these patients limited the possible data analysis, as the clinical relevance of our findings could not be assessed. Hence, solely the presence or absence of an immune response as a result of selective radiotherapy treatment could be analysed here.

In regards to the statistical power of this treatment cohort, the number of patients (n = 11) was well below the *a priori* estimate (n = 54), indicating that any potential findings would be obtained with much lower sensitivity than ideally required. Nonetheless, a *post hoc* estimate was generated to compute the achieved statistical power of this cohort (G*Power 3.1.9.2 program, T-test, difference between two dependent means (matched pairs), 2-tailed) with a given probability of error ($\alpha = 0.05$), sample size (n = *11*) and effect size ($dz = 0.5$) (Faul et al. 2007; Faul et al. 2009). This calculation indicated an estimated power ($1 - \beta$) of 0.32 (noncentrality parameter σ = 1.66, critical t = 2.23, degrees of freedom = 10), which was well below the generally recommended minimum power of 0.8 (Cohen 1988). Therefore, the probability of this cohort detecting a statistically relevant finding was not acceptable.

Furthermore, although patient selection for this clinical trial was conducted following the necessary pre-stipulated statistical design, the patients that were posteriorly included in this analysis cohort were not selected based on a pre-determined study design, but rather on sample availability, which resulted in very limited patient sample numbers, thus limiting our analysis substantially. Nonetheless, it may be possible to make very preliminary assumptions regarding comprehending how colorectal cancer patients with non-resectable liver metastasis respond to selective internal radiotherapy, which could provide insight into patient stratification or even likelihood of a desired response.

2.3.6 Other treatment cohorts

The other treatment cohort included 88 malignant melanoma patients undergoing either no treatment or one of several distinct treatments. Due to the majority of these patients contributing samples at a single time point only, post-treatment analysis was not possible, and therefore these patients were grouped together as a means of conducting a cancer-specific group analysis, focusing on typically expressed antigens and possible correlations with disease stage.

The primary treatment for melanoma, cancer type described above in Section 2.3.1, is surgery when possible, and the additional treatment options include chemotherapy and radiotherapy. In this specific treatment cohort, three distinct chemotherapeutic drugs are administered, and these include gemcitabine, vinorelbine and dacarbazine. Immunotherapy, also known as biological therapy, focuses on the patient's immune system and utilises naturally occurring endogenous and exogenous substances, as well as chemically synthesized substances, which boost, direct or restore the body's natural defences against cancer (www.ncbi.nlm.nih.gov/pubmedhealth). Also in this specific treatment cohort, five distinct immunotherapeutic drugs are administered in a clinical trial setting, and these include NY-ESO-1/ISCOM, BRAF + MEK, ipilimumab, vaccinia melanoma oncolysate, and A2/IL-12. These treatments will not be discussed in detail, as we were not assessing responses to treatment, as done in previous cohorts, due to sole access to single time point samples across the majority of these patients.

The 88 patients of this treatment cohort were selected based solely on sample availability (mainly single time points per patient, collected by the LICR), and these patients were undergoing a variety of distinct cancer treatments (surgery, chemotherapy, radiotherapy, immunotherapy or none), either in a clinical trial setting or not, based on an individually defined personal treatment plan by their oncologist, as well as personal preference to undergo treatment. Although this selection enabled the analysis of a large malignant melanoma cohort, it is essential to note that this introduced significant diversity within this cohort. Furthermore, all analyses should take into account this diversity when interpreting any posterior findings. Nonetheless, it may be possible to conduct a retrospective analysis, as a means of verifying

potential diagnostic or prognostic biomarkers with significant statistical relevance, as well as to assess whether and how different therapies significantly alter autoimmune titres.

For these patients, the clinical information that was found most relevant for this analysis included patient ID and number of samples, gender, age at the time of sample collection, disease stage, date at which samples were collected and matching treatment at the time, as well as deceased information, as indicated in Table 2.10.

Table 2.10 Patient demographics of the melanoma cohort undergoing other treatments. This table includes the complete accessed patient information for the melanoma cohort undergoing other treatments. -: none; NY-ESO-1/ISCOM, BRAF + MEK, Ipilimumab, VMO (vaccinia melanoma oncolysate), A2/IL-12: immunotherapeutic drugs; Gemcitabine, Vinorelbine and DTIC (Dacarbazine): chemotherapeutic drugs; RXT: radiotherapy. Dark grey shaded areas indicated outstanding clinical information.

Patient ID	Gender	Age	Stage	Sample date	Treatment	Deceased
581576	M	54	III	10/Feb/2000	Surgery	N
		59		17/Mar/2005	NY-ESO-1/ISCOM follow on-study (2003)	
578172	M	58	II	04/Nov/1999	Surgery	N
		64		20/Oct/2005	-	
579634	M	69	III	24/Nov/2005	NY-ESO-1/ISCOM follow on-study (2004)	N
		70		16/Feb/2006		
825325	F	33	IV	20/Jul/2006	-	Y
		37		02/Sep/2010		
				21/Oct/2010	Ipilimumab	
756870	M	77	IV	22/Sep/2000	VMO, NY-ESO-1/ISCOM	Y
		83		26/Oct/2006	NY-ESO-1/ISCOM follow on-study (2003)	
773298	F	60	III	04/Jul/2002	Surgery	Y
		68		16/Mar/2010	-	
				30/Sep/2010	Ipilimumab	
707903	F	45	IV	10/Jun/1998	-	Y
		46		01/Nov/1999	A2/IL-12	

Patient ID	Gender	Age	Stage	Sample date	Treatment	Deceased
2044549	M	26	IV	28/Mar/2011 22/Jul/2011	BRAF + MEK	Y
811116	F	71	III	21/Jun/2005	Surgery	Y
806076	M	47	III	20/Oct/2005	-	Y
819515	M	75	II	03/Mar/2006	-	N
827874	M	47	IV	12/Oct/2006	-	Y
532958	F	81	IV	09/Nov/2006	Surgery	N
045723	F	87	IV	08/Nov/2007	Surgery	Y
018615	M	78	I	12/Jun/2008	-	Y
859616	F	48	III	31/Jul/2008	-	Y
189526	F	64	IV	07/Aug/2008	-	Y
115092	M	48	III	18/Mar/2010	-	Y
556868	F	62	IV	22/Apr/1998	-	Y
558959	M	66		02/Jun/1998	Gemcitabine, Vinorelbine	Y
555751	M	48	IV	06/Jun/1998		Y
540994	F	37	IV	06/Jul/1998	-	Y
068526	F	54		15/Dec/1998		N
568788	F	32	II	18/Feb/1999	-	N
570397	F	39	II	08/Apr/1999	-	N
560261	F	39		10/May/1999		Y
574156	F	51	III	15/Jul/1999	Surgery	Y
318133	F	74	III	29/Jul/1999	Surgery, VMO	Y
570369	M	21	III	01/Apr/1999	-	Y
228343	F	48	III	24/Jun/1999		Y
577323	F	55	III	30/Sep/1999	Surgery	Y
X228302	M	77		03/Dec/1999		N
574184	F	50	IV	22/Jul/1999	-	

Patient ID	Gender	Age	Stage	Sample date	Treatment	Deceased
574971	F	64	IV	05/Aug/1999	-	Y
576503	F	63	III	02/Sep/1999	DTIC	Y
735678	F	40	III	25/Nov/1999	-	Y
579655	F	59	IV	09/Dec/1999	-	Y
081308	M	30	IV	16/Dec/1999	RXT	N
581512	F	55	III	27/Jan/2000	-	
739201	M	25	III	18/Jan/2001	-	N
739649	M	72	IV	30/Jan/2001	Surgery	Y
739648	M	72	III	30/Jan/2001	Surgery	Y
760422	M	39	IV	08/Mar/2001	-	Y
588383	F	45	III	15/Mar/2001	-	N
739555	M	60	IV	29/Mar/2001	-	Y
739586	F	59	II	21/Jun/2001	-	Y
766755	M	62	IV	04/Oct/2001	DTIC	Y
557856	M	42	IV	08/Jun/2000	DTIC	Y
567297	M	63	III	29/Jun/2000	-	Y
739492	F	45	III	30/Nov/2000	-	Y
592455	M	49	IV	14/Dec/2000	-	Y
760600	M	31	III	24/May/2001	-	Y
766181	M	54	III	09/Aug/2001	-	N
767120	F	36	III	01/Nov/2001	-	N
739657	F	44	III	15/Mar/2002	-	N
h310975	F	54	III	31/May/2002	Surgery	Y
773301	M	55	III	04/Jul/2002	-	N
790406	M	39	III	28/Nov/2002	-	Y
175175	M	66	III	05/Dec/2002	Surgery	N
783776	F	44	IV	06/Mar/2003	Surgery	Y

Patient ID	Gender	Age	Stage	Sample date	Treatment	Deceased
792319	F	58	II	17/Apr/2003	-	Y
793139	M	55	III	22/May/2003	-	Y
785265	M	68	II	22/May/2003	-	Y
793393	M	76	II	26/Jun/2003	Surgery	Y
788768	F	71	IV	14/Oct/2003	-	Y
584653	M	51	IV	23/Oct/2003	Surgery, RXT	Y
584655	M	54	IV	22/Apr/2004	Surgery	N
733506	M	45	III	02/Jun/2004	Surgery	Y
539105	F	69	I	24/Jun/2004		N
802701	F	67	III	14/Oct/2004	-	N
163149	M	77	II	18/Nov/2004	-	Y
642244	M	42	III	25/Nov/2004	Surgery	Y
702850	M	62	IV	11/Dec/2004	-	Y
566332	F	58	IV	10/Feb/2005	Surgery, RXT (CR)	N
583239	M	40	III	16/Mar/2000	-	N
773823	M	72	III	01/Aug/2002	-	Y
541666	F	31	IV	13/May/2004	-	N
801733	M	32	IV	19/Aug/2004	-	Y
694790	M	76	IV	30/Sep/2010	Ipilimumab	
775519	M	55	IV	21/May/2010	Ipilimumab	Y
386412	M	76	III	15/Mar/2005	NY-ESO-1/ISCOM	N
535907	M	57		06/May/1997		
AP 28/09/2007	M	50	IV	28/Sep/2007	Ipilimumab	Y
C 6/3/1996				06/Mar/1996		
CIBL1	M					
2052357	M	49	IV	04/Oct/2011	BRAF + MEK	Y
2052508	M	26	IV	19/Oct/2011	BRAF + MEK	Y

Patient ID	Gender	Age	Stage	Sample date	Treatment	Deceased
2050349	M	38	IV	21/Sep/2011	BRAF + MEK	Y

The characteristics of these 88 patients, for which clinical information was available, included an unevenly weighed population, with more males (*n* = 50/87, 57%) than females (*n* = 37/87, 43%), and a matching median and mean patient sample age of 54 years, with ages ranging widely from 21 to 87 years. Amongst this population, the majority of these patients presented with stage III (*n* = 35/81, 43%) and IV (*n* = 35/81, 43%), and then the remaining stages II (*n* = 9/81, 11%) and I (*n* = 2/81, 3%). In regards to the treatment undergone, the majority of these patients, for whom treatment information was available, received no treatment (*n* = 47/89, 53%), followed by immunotherapy (*n* = 18/89, 20%), surgery only (*n* = 17/89, 19%), chemotherapy (*n* = 4/89, 5%) and radiotherapy (*n* = 3/89, 3%). Based on the available deceased information, the majority of these patients were deceased (*n* = 58/82, 71%), whilst a smaller subset was still alive (*n* = 24/82, 29%), which was in agreement with the larger number of patients with a more advanced stage of disease.

In regards to the statistical power of this treatment cohort, the number of patients (*n* = 88) was well above the *a priori* estimate (*n* = 54), indicating that any potential findings would be obtained with higher sensitivity than ideally required. A *post hoc* estimate was generated to compute the achieved statistical power of this cohort (G*Power 3.1.9.2 program, T-test, difference between two dependent means (matched pairs), 2-tailed) with a given probability of error ($\alpha = 0.05$), sample size (*n = 88*) and effect size ($dz = 0.5$) (Faul et al. 2007; Faul et al. 2009). This calculation indicated an estimated power ($1 - \beta$) of 0.996 (noncentrality parameter σ = 4.69, critical t = 1.99, degrees of freedom = 87), and therefore the probability of this cohort detecting a statistically relevant finding surpassed the initial ideal estimate. However, as sample collection was based only on availability, a very heterogeneous cohort undergoing a variety of different or no treatments was obtained, which may substantially and differentially alter patient antibody repertoires, thus limiting the achieved statistical power of potential findings. Nonetheless, this is the treatment cohort with the largest number of patient samples, which is of great use when attempting to verify potential diagnostic or prognostic biomarkers with significant statistical relevance.

3 PROTEIN MICROARRAY DEVELOPMENT

3.1 Introduction

The following Section will discuss in detail our protein microarray assays, from prototypical protein microarray principles to our patient sera assays, covering all relevant topics which will enable a complete understanding of this topic.

Protein microarrays have many potential applications in biomarker discovery and the systematic, quantitative analysis of protein function. This technology addresses several biological questions via the high-throughput analysis of biochemical and/or biological interactions between the arrayed proteins and other biomolecules contained in complex sample solutions, thereby generating significant volumes of proteomic information for analysis (Hardiman 2003; Duarte et al. 2013).

Fundamentally, protein microarray technology is based on the immobilisation of multiple proteins onto a surface (typically glass, gold or plastic) in a spatially defined array for use as capture probes. The techniques of immobilisation are important both for effective concentration and orientation of immobilised proteins on the surface and also to preserve their folded conformations. There are two categories of protein immobilisation methods, covalent and non-covalent. The covalent immobilisation method is based on a covalent coupling to a cross-linker attached to the surface. By contrast, the biotin–streptavidin methodology used by our group is a non-covalent immobilisation method based on the high affinity of the biotin and streptavidin interaction. This method links biotinylated macromolecules to a

surface that was previously derivitised with streptavidin via a single point of attachment (see Fig. 3.1) (MacBeath & Schreiber 2000; Büssow et al. 2001; Duarte et al. 2013).

Figure 3.1: Schematic of single-step immobilisation/purification route to array fabrication. The array surface is intrinsically 'nonstick' with respect to proteinaceous material but has a high affinity and specificity for biotinylated proteins. Crude cellular lysates containing the recombinant biotinylated proteins can then be printed onto the surface in a defined array pattern (step a) and all non-biotinylated proteins removed by washing (step b), leaving the recombinant proteins purified and specifically immobilised via the affinity tag in a single step. [Adapted from (Duarte et al. 2013).]

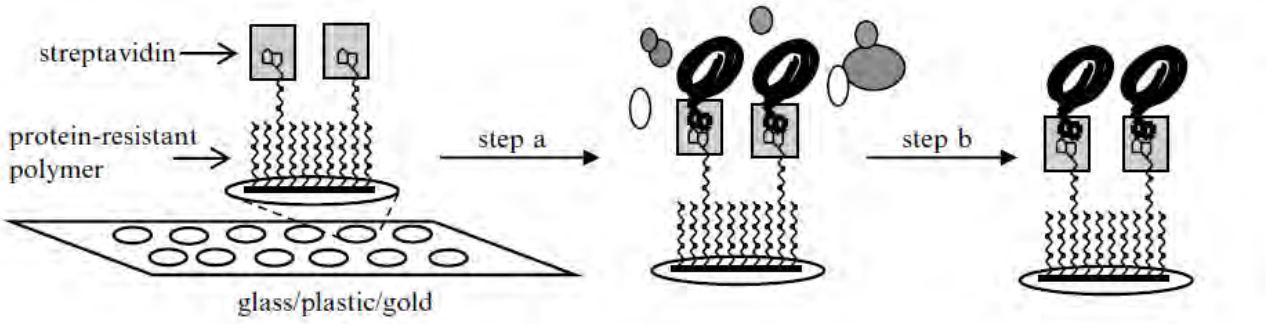

One of the main goals in protein microarray experiments is the quantitation of interactions between the probes immobilised on the slide surface and target analytes contained in the sample solution. To permit detection of this typically bimolecular interaction, molecules with specific interaction properties are labelled with either fluorescent, photochemical or radioisotope tags. The choice of one detection method over another depends on the need to reach a low signal-to-noise ratio at an affordable cost for the specific assay in question. Since the vast majority of target analytes are not naturally coloured, fluorescent, bioluminescent or radioactive, detection of the molecular interaction on a protein microarray usually requires that some detectable molecule (a 'label') be included in the assay, either by direct conjugation to the analyte molecule itself or by conjugation to some secondary detection agent (e.g. an antibody) that can also bind to the analyte once it is specifically captured onto the array surface. Label-free biosensors (e.g. surface plasmon resonance- and quartz crystal microbalance-based biosensors) circumvent this problem, but in most manifestations are not yet truly compatible with medium- to high-density protein microarrays, plus they struggle to match label-based methods in terms of assay sensitivity (i.e. limit of detection). The choice of potential labels is wide: Chemiluminescence is a highly sensitive label-based detection method, but it has a relatively limited dynamic range; radioactivity-based methods are much less frequently used today because of safety concerns;

fluorescent labelling is still therefore currently the most widely used detection method for protein microarray experiments since it is highly sensitive, stable, safe and effective and can be archived for future imaging. However, the direct labelling of analyte molecules might affect their ability to interact with their respective binding partners (Klein & Thongboonkerd 2004; Hall et al. 2007; Schweitzer et al. 2003). In the context of antigen microarray-based assays to measure human autoantibody profiles, the simplest mode of detection is thus via use of a fluorescently labelled antihuman IgG as a secondary detecting agent, since this will bind with high affinity to all human autoantibodies captured onto the antigen array surface, removing the need to label each target analyte in every biological sample (Duarte et al. 2013).

This technology thus enables the high throughput, parallel analysis of a number of different molecular interactions under uniform assay conditions (Wolf-Yadlin et al. 2009; Boutell et al. 2004; Kodadek 2001; Predki 2004; Zhu et al. 2000; Zhu et al. 2001; Michaud et al. 2003; Fang et al. 2003), albeit not typically yielding robustly quantitative data, and in principle therefore enables identification of novel disease-specific serological markers that are not readily accessible by other proteomic technologies (Matarraz et al. 2011; Sanchez-Carbayo 2011; O'Kane et al. 2011).

Upon commencement of this study, the initial prototype of the CT antigen array platform (CT100) had been assessed and defined as poorly reproducible, with non-workable intra-array CVs, and rudimentary data analysis software. Additionally, no data was available regarding limits of detection or linearity of response. Therefore, the first goal of this Thesis was to systematically develop and validate a robust, quantitative CT antigen array platform with expanded content. This process is thoroughly described in this protein microarray development Chapter.

3.2 Methodology

3.2.1 In-house streptavidin coated surfaces

In-house streptavidin-coated array surfaces were developed, based initially on a protocol published by our group (Blackburn et al. 2012), with a focus on significantly improving uniformity and reproducibility of surface coatings.

A vial containing 100 mg of streptavidin lyophilisate (Prospec, 100 mg, #PRO-283) was equilibrated to RT, and then dissolved in 10 mL of 1x spotting buffer (100 mM KCl, 0.01% Triton X-100, 25 mM HEPES, pH 8.5 in dH_2O), with constant vortexing for 30 min. A 10 mL streptavidin solution at a final concentration of 1 mg/mL was prepared in the 1x spotting buffer. Nexterion H slides (Schott, 25 slides, #1070936) were removed from -20 °C storage and equilibrated to RT for 1 h to avoid condensation. A processing chamber was put together to allow for the assay steps to occur fluidly, as indicated in Fig.

3.2. The following steps took place in a plastic chamber wrapped in foil placed on an orbital shaker at RT with gentle shaking (20-40 rpm). Each slide was immersed in the sequential chambers as follows: 1) Derivitising in streptavidin solution for 1 h, 2) Blocking in blocking buffer (50 mM Ethanolamine in 0.1 M Potassium phosphate buffer (PPB) pH 8.0) for 1 h, 3) three washes in wash buffer (0.1 M PPB pH 8.0) for 5 min each, 4) one final wash in dH_2O, 5) drying in a falcon tube using the centrifuge at 483 x *g* at RT. This process was repeated until obtaining a pre-determined amount of streptavidin coated H slides. Slides were then stored in an appropriate light blocking container, labelled with batch details, and stored at -20 °C.

Figure 3.2: Flowchart of in-house streptavidin coating of Nexterion H slides.

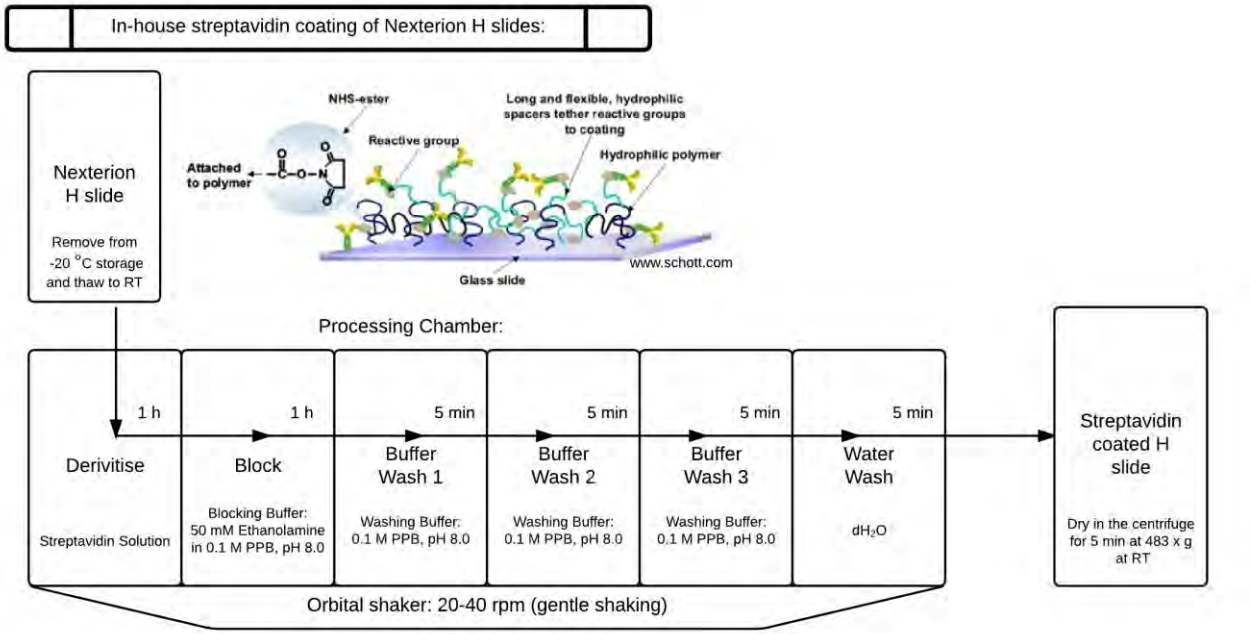

QC tests were performed for each batch to determine whether the coating across the slide surface was homogenous. For this purpose, the last slide of the batch was immersed in a 5 ng/µL concentration of Cy5-biotin-BSA (provided by the CPGR) for 30 min at RT in a container wrapped in foil placed on an orbital shaker with gentle shaking. The slide was then washed three times in PBST (1x phosphate buffered saline (PBS), 0.1% Tween-20) for 5 min each, and once in dH_20 for 5 min. After drying, the slide was scanned using a Tecan LS Reloaded fluorescence microarray scanner (Tecan Group, Mäannedorf, Switzerland). Using the ArrayPro data extraction and analysis software (Media Cybernetics, Rockville, MD), the CVs were calculated using spots, blocks and whole slide area overlaid grid settings. The main intent was to obtain a homogeneity measure of solely the printing/assay area, as the whole slide area CV could be misleading. Finally, a QC report was prepared, as a means of being able to refer back to

these details after performing assays. A CV of < 5% for the slide assay area was required, to ensure good quality coating for subsequent assays.

3.2.2 Cloning cancer-testis antigen genes

The following cloning was carried out by Dr. Aubrey Shoko from the CPGR.

A parental insect cell expression vector was constructed essentially according to previously published methods (Blackburn & Shoko 2011). The *E. coli* biotin carboxyl carrier protein (BCCP) domain, amino acids 74–156 of the *E. coli* accB gene (Athappilly & Hendrickson 1995; Chapman-Smith & Cronan 1999) was cloned 5' to a c-Myc epitope in an *E. coli* transfer vector, pAS1, derived from pTriEx-1.1 (Novagen, Merck Millipore, Johannesburg, South Africa). cDNA clones for each CT antigen of interest were obtained from Origene (Rockville, MD, USA), Open Biosystems (Thermo Scientific, Waltham, MA, USA) or GeneService (Source BioScience, Nottingham, UK). PCR primers were designed from the coding sequence of each cDNA such that the stop codon would be removed, enabling cloning into the pAS1 transfer vector 5' to and in-frame with the 3'-BCCP tag via ligation-independent cloning methods (all primers were synthesized by IDT, Glasgow, UK) (Yang et al. 1993). Each resulting recombinant transfer vector thus encoded an individual CT antigen fused to a C-terminal c-Myc-BCCP tag. Successful PCR amplification of each antigen was confirmed by gel electrophoresis, while successful cloning was determined by Sanger sequencing. All sequences were verified against the RefSeq database (www.ncbi.nlm.nih.gov/refseq). Recombinant baculoviral vectors were prepared for each cDNA clone and these were then transfected into Sf21 cells, using a system we previously adapted from the work of Prof Ian Jones (Reading University, UK) (Blackburn & Shoko 2011; Zhao et al. 2003). Based on the intended array layout, size restrictions and necessary spot spacing, a total of 123 full length antigens were cloned and expressed in insect cells as N-terminal fusions to the *Escherichia coli* BCCP protein domain (Athappilly & Hendrickson 1995; Chapman-Smith & Cronan 1999) for printing on the $CT100^{+}$ array. These were compiled based on a broad literature search of relevant cancer-related antigens, some of which have been previously described as potential biomarkers or therapeutic targets (CT antigen database: www.cta.lncc.br; Cancer Immunity Peptide Database: www.cancerimmunity.org/peptide; Protein database: www.uniprot.com). It was intended that these were not specific to a single cancer type, as a means of assuring potential applicability across a variety of cancers, and that these included TAAs and TSAs. Of the 123, 79 were CT antigens, which were thoroughly described in Section 1.5, while the remaining 44 were other cancer-associated antigens, such as protein kinases, p53s, cytochrome P450s and oncoproteins (see Table 3.1).

Table 3.1 List of the 123 antigens included on the CT100^{+} array.

ID	Name	ID	Name	ID	Name	ID	Name	ID	Name
001	BAGE2	026	LEMD1	051	SGY-1	076	CDK7	101	5T4/TPBG
002	BAGE3	027	LIP1	052	SILV	077	FES	102	XAGE1B
003	BAGE4	028	MAGEA1	053	SPAG9	078	FGFR2	103	SOX2
004	BAGE5	029	MAGEA10	054	SPANXA1	079	MAPK1	104	ACVR2A
005	CCDC33	030	MAGEA11	055	SPANXB1	080	MAPK3	105	ACVR2B
006	CEP290	031	MAGEA2	056	SPANXC	081	PRKCZ	106	ITGB1
007	COL6A1	032	MAGEA3	057	SPANXD	082	RAF	107	MAP9
008	COX6B2	033	MAGEA4v2	058	SPO11	083	SRC	108	PIM1
009	CSAG2	034	MAGEA4v3	059	SSX1	084	CALM1	109	TKTL1
010	CT47.11	035	MAGEA4v4	060	SSX2A	085	CDC25A	110	SPATS1
011	CT62	036	MAGEA5	061	SSX4	086	CREB1	111	DPPA2
012	CTAG2	037	MAGEB1	062	SYCE1	087	CTNNB1	112	SOX1
013	CXorf48.1	038	MAGEB5	063	SYCP1	088	p53 S6A	113	ROPN1A
014	DDX53	039	MAGEB6	064	THEG	089	p53 C141Y	114	CEACAM 1
015	DSCR8	040	MART-1	065	TPTE	090	p53 S15A	115	POU5F1
016	FTHL17	041	MICA	066	TSGA10	091	P53 T18A	116	NANOG
017	GAGE1	042	NLRP4	067	TSSK6	092	p53 Q136X	117	BORIS B0
018	GAGE2A	043	NXF2	068	TYR	093	p53 S46A	118	DPPA4
019	GAGE4	044	NY-CO-45	069	XAGE-2	094	p53 K382R	119	DPPA3
020	GAGE5	045	NY-ESO-1	070	XAGE3av1	095	p53 S392A	120	GDF3
021	GAGE6	046	OIP5	071	XAGE3av2	096	p53 M133T	121	LAGE-1b
022	GAGE7	047	p53	072	ZNF165	097	p53 L344P	122	CAMEL
023	GRWD1	048	PBK	073	AKT1	098	CYP450 3A4	123	NY-ESO-1 ORF2
024	HORMAD1	049	RELT	074	CDK2	099	CYP450 red		
025	LDHC	050	ROPN1	075	CDK4	100	EGFR		

3.2.3 Expression of cancer-testis antigens

The following protein expression was carried out by Dr. Aubrey Shoko from the CPGR.

Recombinant CT antigens were expressed in Sf9 insect cells using a previously published protocol (Blackburn & Shoko 2011). The soluble, crude protein extracts were collected, the protein concentrations were determined by Bradford assay (Bradford 1976) and the extracts were stored at -80 °C before array printing. Expression of each antigen was assessed by western blot using a 1:5000 dilution of monoclonal anti-c-Myc antibody produced in mouse (Sigma-Aldrich, 2 mL, #M5546) followed by a 1:25000 dilution of anti-mouse IgG (H+L) horseradish peroxidase (HRP) conjugate produced in goat (KPL, 1 mg, #074-1806). Biotinylation of each antigen was assessed by western blot using a 1:40000 dilution of streptavidin-HRP conjugate probe (KPL, 0.5 mg, #14-30-00).

3.2.4 Fabrication and optimization of the cancer-testis antigen ($CT100^+$) microarray

Crude lysates of each antigen were diluted 1:1 in printing buffer (1x PBS, 20% sucrose) and 40 µL of the diluted crude protein extract for each BCCP-tagged protein was transferred to individual wells of a 384-well V-bottom plate. The plate was centrifuged at 1000 x *g* for 2 min at 4 °C to pellet any residual cell debris and then kept at 4 °C before and during the microarray print run. Each $CT100^+$ array was printed on a previously thawed streptavidin-coated microarray slide using a QArray2 robotic arrayer equipped with 8 x 300 µm flat-tipped solid pins. Each array was printed in eight grids of 8 x 8 spots (i.e., 480 discrete protein spots per array) with a spot-to-spot spacing of 562 µm. In principle, this format enables up to 170 individual protein types, including controls, to be printed in triplicate in each array field. The printing procedures were performed at RT, while the source plate was kept at 4 °C and the print chamber humidity was maintained at ~50%. The arrays were printed using the settings indicated in Table 3.2.

Table 3.2 CT100$^+$ microarray printing settings used for each print run.

Arraying pattern	8 rows x 8 columns of spots per grid
Maximum stamps per ink	1
Number of stamps per spot	1
Stamp time	0ms
Inking time	500 ms
Print depth adjustment	150 microns
Number of touch offs	0
Water washes	60 s wash and 0 s dry
Ethanol wash	10 s wash and 1 s dry

Replica CT100$^+$ arrays were printed in a four-plex format (i.e., four replica arrays per slide) using the previously loaded samples. Each of the 123 CT antigens and cancer-associated antigens was printed in triplicate within each array. The positive controls consisted of 10 ng/µL of biotinylated human IgG (Rockland Immunochemicals, 1 mg, #009-0602), which serves as a confirmation that detection antibody was added to the assay and was able to bind to the antigen under the assay conditions; 100 ng/µL of biotinylated anti-human IgG antibody produced in goat (Sigma-Aldrich, 1 mL, #I5260), which bind to IgG present in patient sera and thus serves as a confirmation that sera was added to the assay and was able to interact with the antibody under the assay conditions. In addition, three concentrations of biotinylated Cy5-BSA (5, 10 and 15 ng/µL) were included in each sub-array for slide orientation and signal normalization purposes, which also serve as a confirmation that the protein microarray print run was successful. The negative controls comprised of control buffer only; BCCP-myc tag only; and insect cell "empty vector" lysate, to ascertain any background fluorescence or non-specific immunochemical interactions. The array design is shown in Fig. 3.3. These printing parameters and the array layout, including the location of individual antigens, were recorded in a .gal file output from the arrayer. After printing had concluded, each slide was kept in the microarrayer for at least 30 min, as a means of assuring a humid environment to prevent evaporation and facilitate protein-surface interactions. Each slide was then stored in an upright light-protected container at 4 °C until use.

Figure 3.3: CT100^{+} array design printed four times (4-plex) across each slide. This image indicates a single slide with 4 replica arrays, with focus on the complete representation and localisation of the printed antigens across a single CT100^{+} array, with antigens indicated by their ID number, and controls indicated by name. Positive controls are indicated in red across the array.

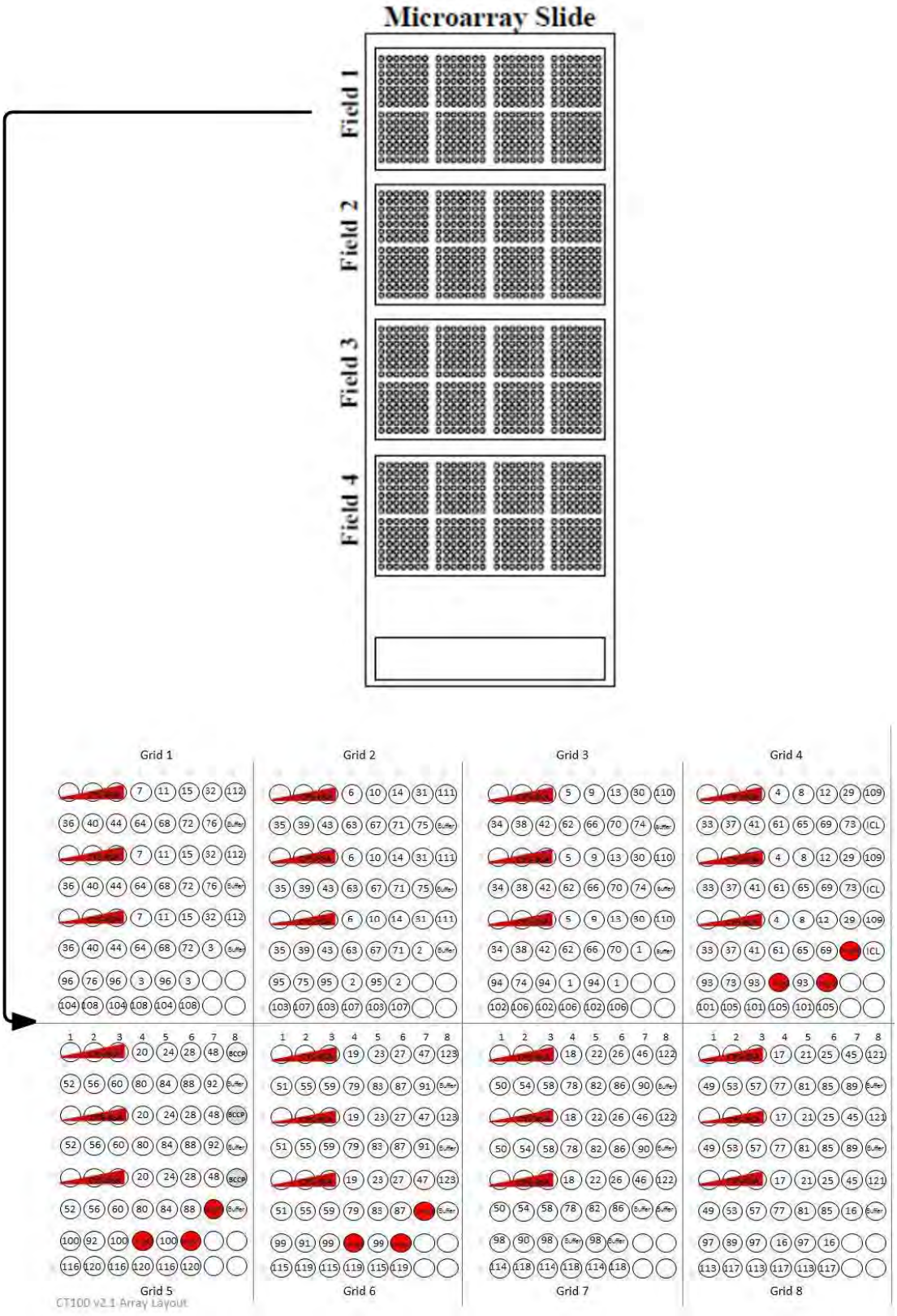

3.2.5 Development of the CT100^{+}.jar bioinformatic tool

We developed a bioinformatic pipeline for pre-processing and quality control of custom protein microarray data, which was automated in Java. A prototype version of this program suitable for the first version of our platform (CT100 array) was created previously by a previous student in the Blackburn Laboratory, Mr. Jean-Michel Serufuri (Safari Serufuri 2010). The following processing steps were included in this original bioinformatic tool:

1) the local background signal – mean intensity of local corners – for each spot was replaced by its neighbourhood background (i.e. median value of the mean background intensities of the surrounding 8 (3 x 3 window) neighbourhood spots, see Fig. 3.4) (Zhu et al. 2006);
2) The net intensity for each spot was calculated by subtracting its neighbourhood background from its foreground signal;
3) All spots containing a net intensity of less than two standard deviations of the background (noise threshold) thereof were removed from analysis;
4) The mean net intensities for each set of replicates were calculated, and replicates containing a CV of > 20% (user-defined) were removed;
5) Whole arrays were filtered to remove any exhibiting a CV > 20% (user-defined) across the array for a chosen control (we used 5, 10 or 15 ng/µL Cy5-biotin-BSA). Any resulting whole arrays with unsatisfactory CV values were discarded and indicated as a required repeat;
6) Sub-arrays within each array were normalized with respect to each other to minimize any effects of pin-to-pin variation;
7) Whole arrays were then normalized with respect to each other to minimize any effects of slide-to-slide variation.

Figure 3.4: Visual illustration of the local background correction method. The local background of the centre spot is replaced by a median of the local backgrounds of surrounding neighbourhood spots (3 x 3 spot window), as a means of avoiding skewed background intensities due to artefacts or dust particles. The corrected net intensity is measured by the centre spot's raw intensity minus corrected background intensity. Green spot: neighbourhood spot: Red spot: centre spot; Brown diamond: local background [Adapted from (Zhu et al. 2006).].

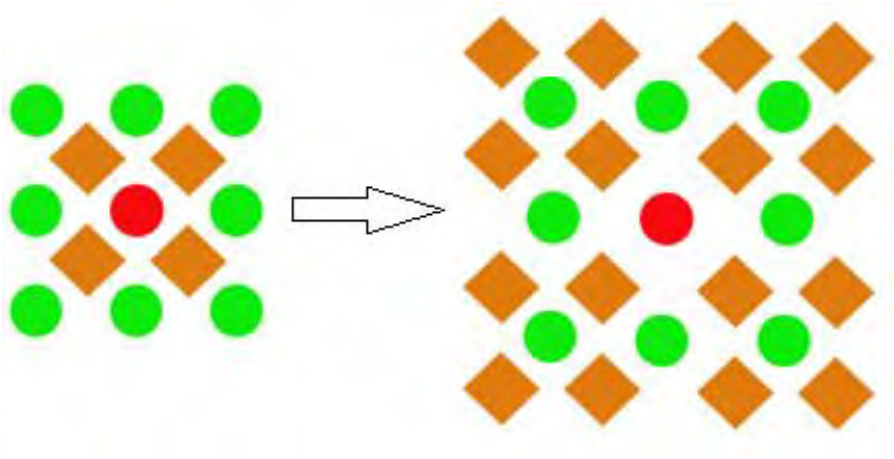

In regards to the normalization of the pin-to-pin and array-to-array variation, a novel composite normalization method combining both quantile and total intensity normalization modules was used (Duarte et al. 2013). This method aimed to make more efficient, effective and robust usage of a relatively small number of positive controls to correct for systematic bias in pin-to-pin and array-to-array variations. Robustness is the ability of the method to cope with the flagging of some positive controls, while still being based on sound biological principles. The normalisation assumption was that our positive control spots shared a common underlying distribution across the chips (block, arrays, etc.) on which they were printed. This perspective provided greater flexibility than assuming that the individual positive control spots maintained the same intensities across the chips. Thereafter, our composite normalisation method corrects for systematic bias among the chips, while providing more robustness when dealing with flagged positive control spots (Causton et al. 2004)(Bolstad et al. 2003). These modules are thus described below in detail.

i) Quantile-Based Module

Since the positive control spots (Cy5-biotin-BSA) are replica spots across different arrays, it seemed reasonable to assume that they share an underlying distribution across arrays, and the quantile approach can be used to identify the corresponding housekeeping spot intensities based on their intensity distributions.

Bolstad et al. described an algorithm to carry out spot identification within the same quantile according to the following steps, where S_{ij} is the intensity of a positive control spot i on chip j: a) load the positive control spot intensities S_{ij} into an $I \times J$ matrix X, b) sort the spot intensities in each column j of X to get X_{sort} and c) Take the means across each row i of X_{sort} and get $\bar{X}_i$.

$\bar{X}_i$ is considered the underlying distribution of the positive control spot intensities across chips (Bolstad et al. 2003). This reorganisation enabled more flexibility in handling outliers or flagged spots within the positive control data set.

ii) Total Intensity-Based Module

This module assumed that post-normalisation, all arrays had a common total intensity value of their positive control spots (i.e. the sum of all the positive control spot intensities on each array should be constant), given by $\sum_{i=1}^{N_{spots}} \bar{X}_i$. The normalisation factor α_k to normalise array k is then given by

$$\alpha_k = \frac{\sum_{i=1}^{N_{spots}} \bar{X}_i}{\sum_{i=1}^{N_{spots}} \bar{X}_{ik}}$$

where $\sum_{i=1}^{N_{spots}} \bar{X}_{ik}$ is the total intensity of all the positive control spots on array k prior to normalisation (Causton et al. 2004; Quackenbush 2001). This scaling normalisation method assumes that different arrays share a common total intensity of their housekeeping spots, while taking into account the potential existence of flagged spots within the housekeeping spots. Importantly, if a given positive control spot is identified as an outlier on one array (i.e. it is flagged for some reason), the corresponding positive control spots across all arrays are identified in the quantile module above and are then also flagged across all arrays prior to normalisation; the net consequence of this is to ensure that the same number of positive control spots are considered across all arrays during normalisation.

This prototype program was rigidly designed for the CT100 array exact antigen layout, which initially comprised only 100 cancer-associated antigens and original controls. Therefore, if any additional antigen was added to this layout, this tool was not able to function correctly, which accentuated the need for a dynamic version of this program, that could function with any antigen layout (read from the .gal file) that was provided. Additionally, when interpreting the program's code itself, several bugs were identified, which required immediate attention. For example, when saturated spots were observed, these were flagged, and set to zero, which led to the loss of data from our highest detected autoantibody titres. A solution to this issue would be to scan each slide using an automatic gain control (AGC) mode, which would automatically adjust the scanning gain setting to a level where no saturation was observed. As our program includes normalization steps, these values would later be adjusted, and no signals would be lost. An additional error included averaging the mean net intensities of triplicate spots for a given antigen. When one of the replica spots was discarded based on a previous filtering

condition, the program automatically set that titre to zero. This led to the loss of real autoantibody titres for certain antigens, which was not ideal. A solution to this issue would be when only two out of the three autoantibody titre replicas for a given antigen are available and similar (i.e. where the duplicate means have low CV values), a mean should still be calculated and utilised in the final consolidated data file. Therefore, together with the assistance of a current colleague, Mr. Ryan Goosen, we adapted and improved this prototype tool to accommodate the numerous changes our protein microarray platform has undergone since then ($CT100^{+}$ array).

Besides from the above-mentioned adaptations, the following parameters were also included:

1) A user-defined adjustable noise threshold;
2) A more descriptive program output, which includes CV information per antigen and array, as a means of allowing the user to verify why an array has been discarded from analysis;
3) Whole array CV discarding automatically calculated for each Cy5-biotin-BSA control, but all processing that follows conducted using the user-selected control. This addition would permit the user to verify which control is best used for this purpose, without having to conduct three separate program runs;
4) Autoantibody titre replicates should only be considered if two or three of the replicates were available and similar, which would assure that skewed means were not calculated if one of the three replicas was either too high or too low, and that titres towards an antigen were not flagged as high CV and unnecessarily set to zero due to one unusable replicate. This addition would avoid us from obtaining skewed means and from losing relevant autoantibody signals;
5) A less cluttered output file, which only includes the consolidated files, before and after averaging, the user-defined settings and processing steps used, the whole array discarded lists per Cy5-biotin-BSA control, user-friendly program interface (see Fig. 3.5 and 3.6) and understandable output.

Figure 3.5: CT100^{+}.jar program interface settings selection. After selection of the raw data, this user-friendly interface allows the user to indicate which settings should be used for analysis, such as mean or median intensity, whole array filtering control selection and CV threshold, replica CV threshold and noise filter threshold.

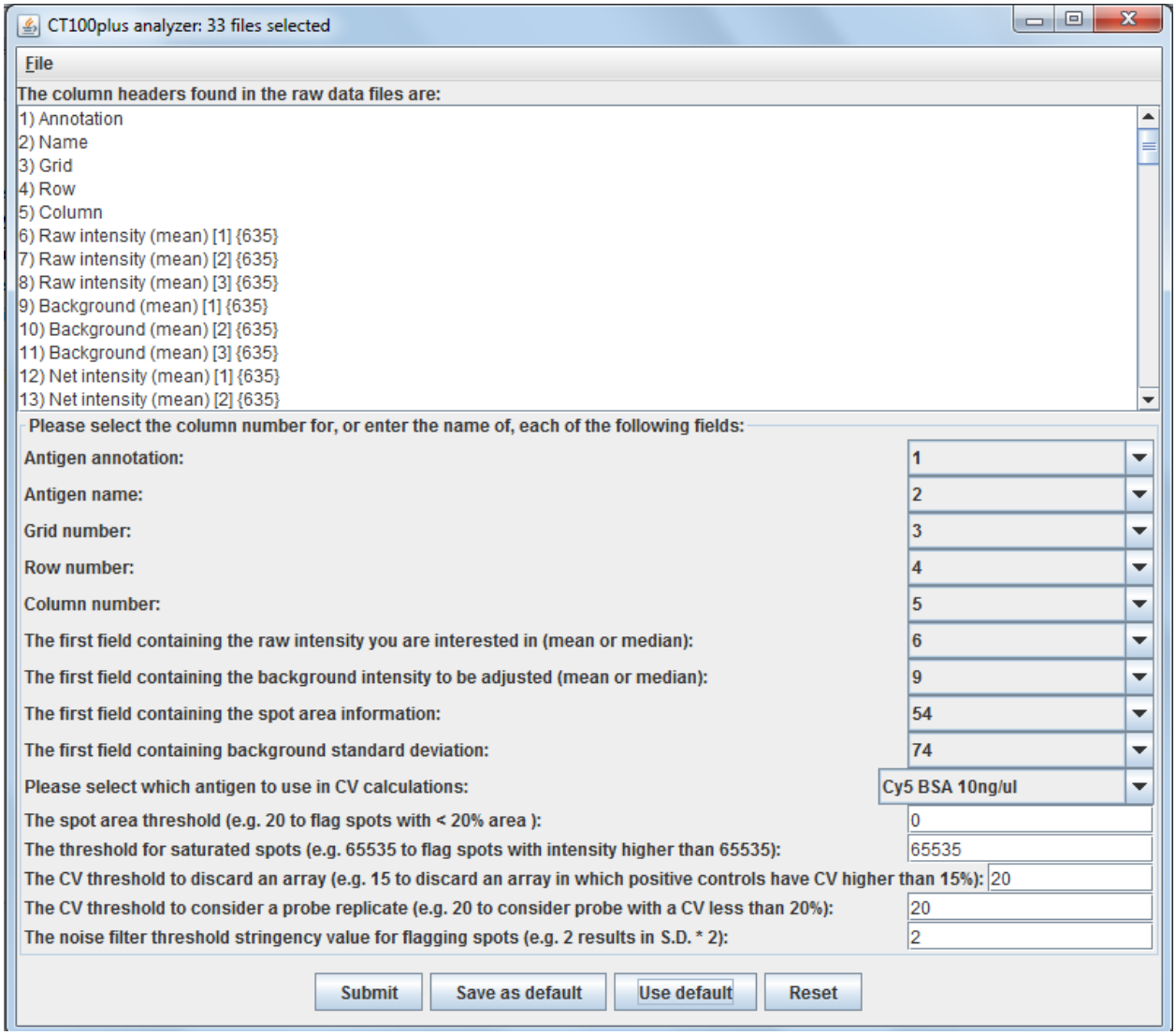

Figure 3.6: CT100^{+}.jar program interface processing steps selection. After the selection of analysis settings, this interface allows the user to select which methods should be used for processing.

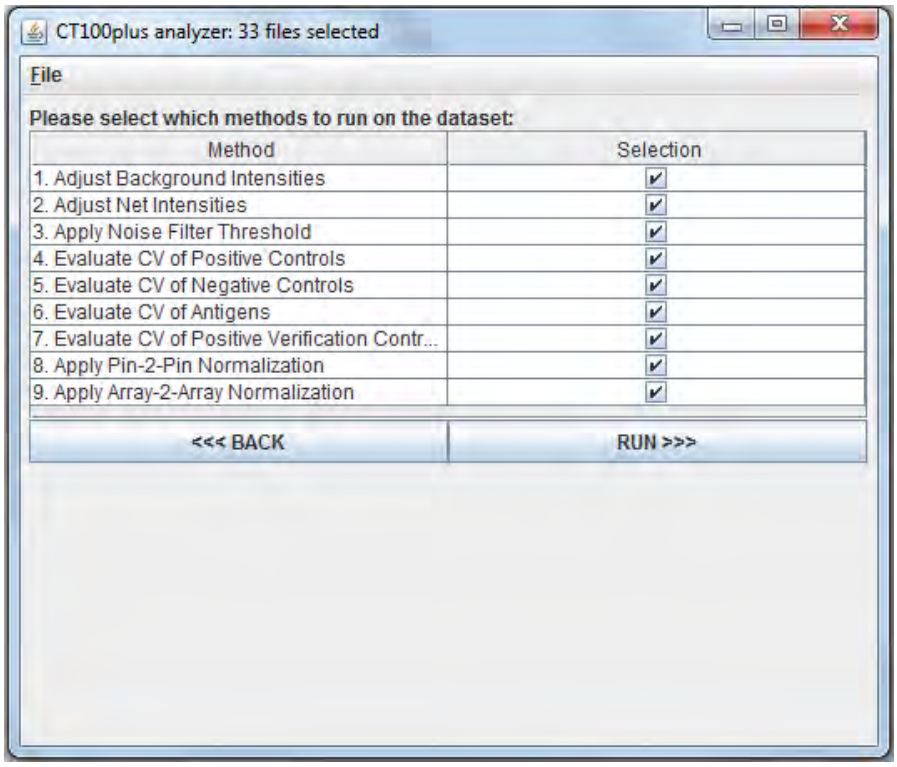

Additionally, to account for issues such as spot running, missing spots (pin sticking), washing artefacts, dust particles, and faded arrays, a visual assessment and discarding of each array image was essential (Duarte et al. 2013). When evaluating the quality of an array image, there are many considerations that should be taken into account, such as:

1) Spot-to-spot variation – when looking at the signal of triplicate spots, one should expect a similar signal across all replicas, as well as uniform spots across the whole slide. Variations which may occur include a) spot running (2 or more spots run into each other due to close proximity between spots or inappropriate spotting buffer, compromising the signal of all affected spots); b) pin sticking or erroneous pin calibration (inadequate cleaning of the arrayer pins and printhead between print runs could lead to the failure to print some or all intended spots, as well as non-reproducible printed spots); and c) washing artefacts and speckles (inadequate washing steps throughout the assay could lead to large washing artefacts which appear as negative spots or random additional smaller spots across the slide) on the array surface;
2) Spot homogeneity – when looking at the signal of an individual spot, one should expect a homogenous signal across all pixels within that spot. Variations which may occur include a) the 'doughnut' effect (inadequate pin height during print run and liquid residues on the pin body when immersing pin head in source plate could lead to uneven spot distribution); b) dust

particles (inadequate storage and handling of slides during assays could lead to the presence of dust particles on spots of interest, which appear as high-intensity pixels and skews the real signal) on the array surface; and c) temperature and humidity conditions (increased temperature/decreased humidity may lead to the evaporation of printed spots, and humidity above 75% may lead to condensation, which would account for an uneven intensity within spots). The homogeneity between replica spots can be measured by calculating the coefficient of variation (CV), which is the ratio between the standard deviation (SD) of all pixel intensities within a spot and the mean intensity as a percentage;

3) Background variation – when looking at several spots across an array, one should expect low variation of the background between the neighbourhood spots. Variations which may occur include dust particles (inadequate storage and handling of slides during assays could lead to the presence of dust particles around spots of interest, which results in high local background for a specific spot and difficulty distinguishing between real signal) on the array surface;
4) Signal-to-noise ratio – when looking at several spots across an array, one should expect the spot intensity to be greatly above its local or neighbourhood background. Variations which may occur include washing artefacts and speckles (inadequate washing steps throughout the assay could lead to large washing artefacts which appear as negative spots or random additional smaller spots across the slide) and dust particles (inadequate storage and handling of slides during assays could lead to the presence of dust particles around spots of interest, which results in high local background for a specific spot and difficulty distinguishing between real signal) across the array surface. To be confident that the net spot intensity (i.e. foreground intensity minus background intensity) is significantly above background, a signal-to-noise ratio of at least 2 is used for quality assurance, with 'noise' defined as the standard deviation of the background pixels.

Therefore, a list of all computationally or visually discarded arrays was compiled, and the respective sera samples re-assayed. These adaptations increase the possibility of obtaining more robust resulting data and associated conclusions in a rapid automated setting, which removes chances of human error and time-consuming processing when dealing with large amounts of data.

3.2.6 Linearity and dynamic range microarray assays

Prior to commencing the array experiments, robust linearity and dynamic range experiments were carried out to determine the optimal serum and anti-human IgG antibody dilutions for detection of antibody-antigen binding.

3.2.6.1 Linearity and dynamic range microarray fabrication

A single NY-ESO-1 crude lysate was diluted 1:2 in lysis buffer (25 mM HEPES, 50 mM KCl, 20% glycerol, 0.1% Triton X-100, 1 mM DTT in dH_20), and 30 µL was transferred to an individual well of a 384-well V-bottom plate (Separations, #MD-X7022), along with 30 µL of lysis buffer only (negative control), and 30 µL of Cy5-bioitn-BSA (16 ng/mL, positive control). On each array, a 6 x 6 grid was printed on a previously thawed streptavidin-coated microarray slide using a QArray2 robotic arrayer (Genetix, Berkshire, UK)) equipped with a single 300 µm flat-tipped solid pin. The printing procedures were performed at RT, while the source plate was kept at 4 °C and the print chamber humidity was maintained at ~50%. The arrays were printed using the settings indicated in Table 3.3.

Table 3.3 Linearity and dynamic range microarray printing settings used for each print run.

Arraying pattern	6 rows x 6 columns of spots per grid
Maximum stamps per ink	1
Number of stamps per spot	1
Stamp time	0 ms
Inking time	500 ms
Print depth adjustment	150 microns
Number of touch offs	0
Water washes	60 s wash and 0 s dry
Ethanol wash	10 s wash and 10 s dry

Replica arrays were printed in a 16-plex format (i.e., 16 replica arrays per slide) using the previously loaded samples. Each antigen and control had six replica spots printed within each array. These printing parameters and the array layout, including the location of individual antigens, were recorded in a .gal file output from the arrayer. After printing had concluded, each slide was kept in the microarrayer for at least 30 min, as a means of assuring a humid environment. The printed slide was then stored in an upright light protected container at 4 °C until use.

3.2.6.2 Linearity and dynamic range assay

An initial linearity assay was performed in duplicate using serial dilutions of a single serum sample (P117, day 483) at 1:50, 1:100, 1:200, 1:400, 1:800, 1:1,600, 1:3200 and 1:6400 dilutions in PBST. A

previously printed slide was immersed in blocking buffer (50 µM biotin in lysis buffer) and incubated on ice for 1 h, in a plastic chamber wrapped in foil with gentle shaking. The slide was then washed three times for 5 min in lysis buffer, and then placed in a falcon tube and centrifuged at 483 x *g* for 5 min at RT to dry. A 16-chamber silicone gasket (Flexwell incubation chamber; Grace Bio-Labs, OR) and a 16-chamber metal gasket (ProPlate slide chamber system; Grace Bio-Labs) were assembled over the slide. A serum volume of 45 µL was added to each gasket chamber and incubated at RT for 1 h, after which each chamber was washed independently with PBST. Alexa Fluor 546 (Cy3 equivalent) Goat anti-Human IgG (H+L) (Invitrogen, Life Technologies, 2 mg/mL, #A21089; 1:100 dilution in PBST) was added to each chamber and incubated for 1 h at RT. The gasket was removed and the slide was washed in PBST, dried and scanned at various gain settings on an LS Reloaded fluorescence microarray scanner.

An additional linearity assay was performed using serum dilutions 1:200 and 1:2400 (P117, day 483), with each serum dilution (45 µL) added to a separate individual array on a previously blocked and washed slide. After incubation as above, each array was washed independently and Alexa Fluor 546 Goat anti-Human IgG (45 µL diluted in PBST to final concentrations of 1.25, 2.5, 5, 10, 15, 20, 30 and 40 µg/mL) was incubated on duplicate individual arrays for 1 h at RT. The slide was then washed, dried and scanned.

A dynamic range assay was similarly performed in duplicate using serial serum dilutions (1:1000, 1:2000, 1:4000, 1:8000, 1:16000, 1:32000, 1:64000 and 1:128000) and a fixed concentration of Alexa Fluor 546 goat anti-human IgG (20 µg/mL).

The complete assay design is summarized in the flowchart indicated below in Fig. 3.7.

Figure 3.7: Flowchart of the linearity and dynamic range assay design.

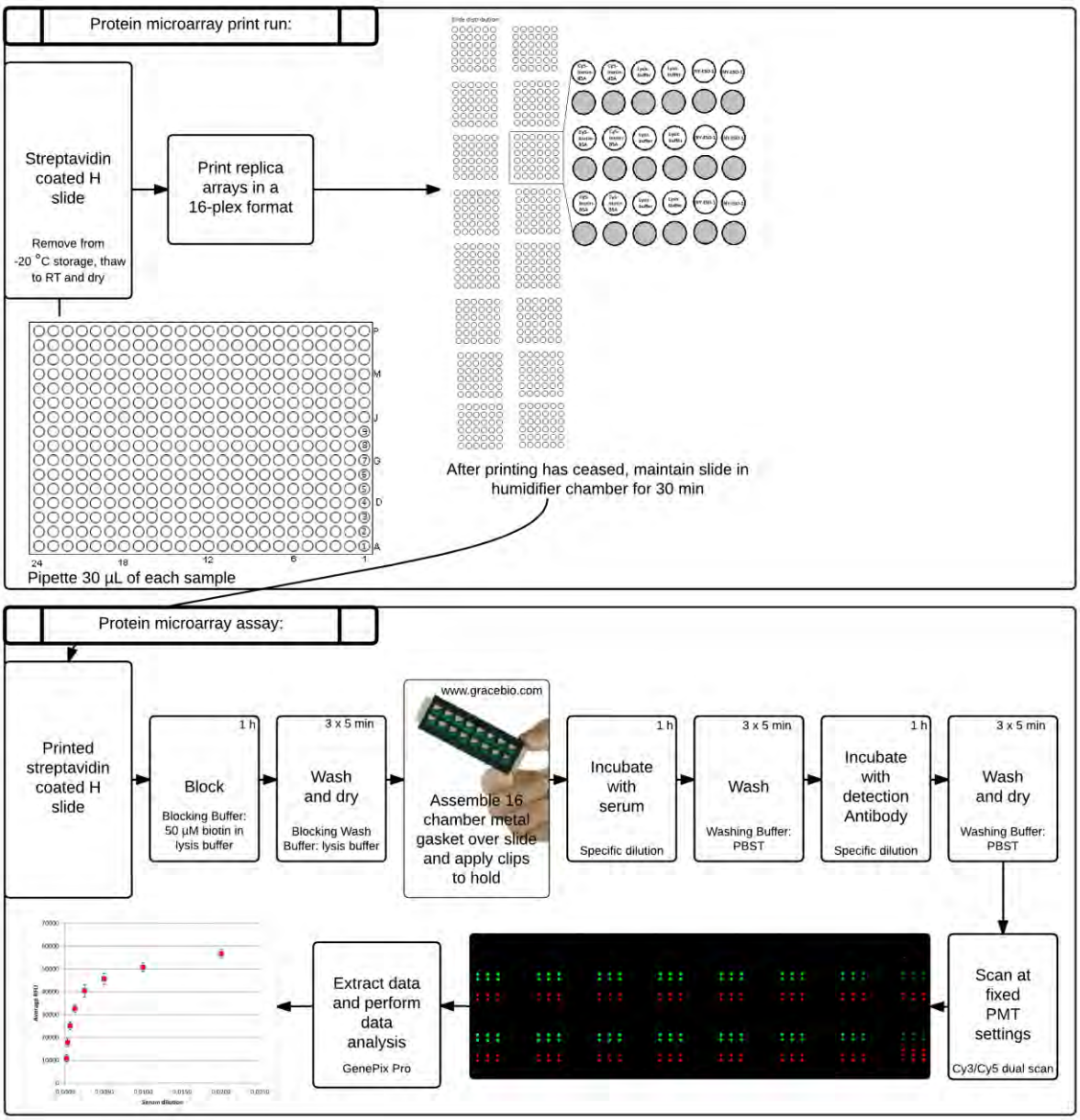

3.2.6.3 Linearity and dynamic range data extraction

Using GenePix Pro Acquisition and Analysis Microarray software (Molecular Devices Inc., USA), a grid was autoaligned over the individual spots on each scanned image file and manually configured across the whole array surface. The raw data of each feature on the array was then analysed and a report was generated containing the median fluorescence and background pixel intensities per sample spot. This data was then used for further processing and analysis.

3.2.6.4 Linearity and dynamic range data processing and analysis

A manual analysis of protein array raw data was carried out as follows: (1) Any spots which displayed saturation were removed from analysis; (2) The net intensity (RFU values) for each spot was calculated by subtracting its median background from its median fluorescent intensity; (3) All spots in each grid containing a net intensity of less than two median standard deviations of the background were removed from analysis; (4) The mean net intensities for each set of replica spots were calculated across the array, and replicates containing a CV of above 30% were removed from analysis. No pin-to-pin normalization was necessary as the printing design only used a single pin. No slide-to-slide normalization was necessary as each assay was contained within a single printed slide. GraphPad Prism software (GraphPad Software, Inc. – Version 4.0, Radioligand Binding Analysis) was used to generate saturation binding curves and Scatchard plots.

3.2.7 Quantification of the absolute array detection limit for cancer-testis antigens

To estimate the absolute detection limit of our CT antigen microarray platform, three further assays were performed using the same serum sample used for the linearity assays: a Bradford assay, a Sodium dodecyl sulphate polyacrylamide gel electrophoresis (SDS-PAGE)-based densitometry assay, and a protein microarray assay.

Firstly, the absolute total protein concentration of the serum sample was determined by extrapolation of a standard curve obtained by conducting a typical Bradford protein assay, using BSA standards (Bradford 1976).

Secondly, a 7.5 % SDS-PAGE gel was prepared and analysed according to standard methodology (Ausubel et al. 1999). The protein molecular weight marker used was the PageRuler prestained protein ladder (Thermo Scientific, # 26616). The SDS-PAGE gel was then stained using AcquaStain (Vacutec) for 10min and rinsed in dH_2O, as no destaining was required. A densitometry analysis (Gene Tools; Syngene, Cambridge, UK) was then performed to determine the proportion of total protein corresponding to total IgG.

Thirdly, a protein microarray assay was performed to determine the proportion of total IgG corresponding to anti-NY-ESO-1. This last assay was performed in quadruplicate as follows: replica 16-plex arrays of the serum sample (1:800 dilution in 1 M PPB pH 8.0 containing 15% glycerol) were printed on an un-derivitised Nexterion H slide using a single 300 µm flat-tipped solid pin, unreacted NHS esters were blocked for 1 h in blocking buffer (50 mM ethanolamine in chilled 50 mM PPB), and 45 µL anti-human IgG (100 ng/mL), NY-ESO-1-BCCP crude insect cell lysate (1:20 dilution), insect cell “empty

vector" lysate (ICL) (1:20 dilution), or buffer-only control were incubated on discrete replica arrays for 1 h at RT. Each array was washed independently with PPB, and Cy5-labelled streptavidin (GE Healthcare, 0.5 mg/mL, # PA45001; 1:500 dilution in PBST) was incubated on each replica array for 1 h at RT, after which the slide was washed, dried, scanned and analysed as before.

3.2.8 Standard CT100$^+$ array quality controls

As a means of assessing whether each protein microarray print run met the defined robust quality standards, three distinct assays were performed routinely for each print run. These included verifying that the 123 printed antigens were bound successfully to the array, that a pooled cancer patients sample gave rise to a positive array with several autoantibody titres towards cancer-related antigens being detected, and that a pooled healthy patients sample gave rise to a negative array with no autoantibody titres towards cancer-related antigens being detected.

3.2.8.1 Verification of the immobilization of BCCP-tagged proteins to array surface

A c-Myc assay was conducted to verify that all antigens were immobilized on the array surface, following a successful microarray print run, as each protein contains both a BCCP-tag and a c-Myc tag. An individual array per print run was incubated with 100 µL of Monoclonal anti-c-Myc-Cy3 Clone 9E10 (Sigma, 1.3 mg/mL, #C6594; 1:50 dilution in PBST) for 30 min at RT. This assay differs from that indicated previously in Section 3.2.5.2 only in regards to adding c-Myc antibody instead of detection antibody, and by not including a serum sample incubation step. Additionally, the array was scanned using both the Cy3 and the Cy5 laser (dual scan), as a means of detecting all Cy5-biotin-BSA control spots and all antigens which have a c-Myc tag. Both anti-human IgG and human IgG spots are not detected in this assay, as their signal is sera and detection antibody dependent. The resulting data was extracted and processed as indicated previously.

3.2.8.2 Verification of array specificity for cancer

As a means of verifying the array's specificity for cancer, two control groups, cancer and healthy patients, were defined. All sera samples gathered for each group were later pooled together, creating a cancer control pool and a healthy control pool, respectively. Two individual arrays were incubated with either control pool per print run, and the assay proceeded as a typical CT100$^+$ patient assay. It is expected that the array incubated with the cancer control pool would display several cancer-specific antibody signals, and that the healthy control pool would display solely the standard positive controls, with no cancer-associated antibody signals. The resulting data was extracted and processed as indicated above.

3.2.9 Reproducibility studies

As a means of validating the resulting array data, a number of different assays and parameters were considered, such as the linearity and dynamic range assays, the standard quality control assays, the biotinylated Cy5-BSA controls, the replicate spots, and the pre- and post- optimized CT100$^+$ runs. These assays would inform us on how reproducible and consistent our resulting data was.

3.3 Results and Discussion

This Section presents and discusses the complete set of results obtained whilst optimizing the CT100$^+$ array, as well as the resulting data.

3.3.1 In-house streptavidin coated slides

In order to determine optimal conditions for uniform coating of microarray slides with streptavidin, several methods were tested ranging from no shaking to gentle or vigorous shaking. QC tests using each of these shaking methods were conducted, and spots, blocks and whole slide area CVs were obtained using median raw intensity/RFU and SD values, as a measure of coating homogeneity. When comparing whole slide area CVs, it was found that a gentle shaking method was best (13.3%) versus the no shaking (14.6%) and vigorous shaking (27.0%) methods. As mentioned in Section 3.2.1, the CV for the printing/assay area of the slide, i.e. the spots and blocks CVs, provides a more useful measure of slide coating homogeneity, as our quantifiable signals are located there, and should therefore be considered instead. When comparing blocks and spots CVs, it was also found that a gentle shaking method was best (blocks: 2.1%, spots: 2.2%) versus the vigorous (blocks: 4.4%, spots: 3.0%) and no shaking (blocks: 7.6%, spots: 7.4%) methods. Additionally, when visually inspecting the resulting QC slides, it was apparent that gentle shaking was certainly the preferred method, as seen indicated below in Fig. 3.8.

Figure 3.8: Comparison of QC slides testing distinct shaking methods. This figure includes the resulting scanned images of three distinct slides, each testing a distinct shaking method: left: vigorous shaking; middle: gentle shaking; right: no shaking. Fluorescent intensity is indicated in red.

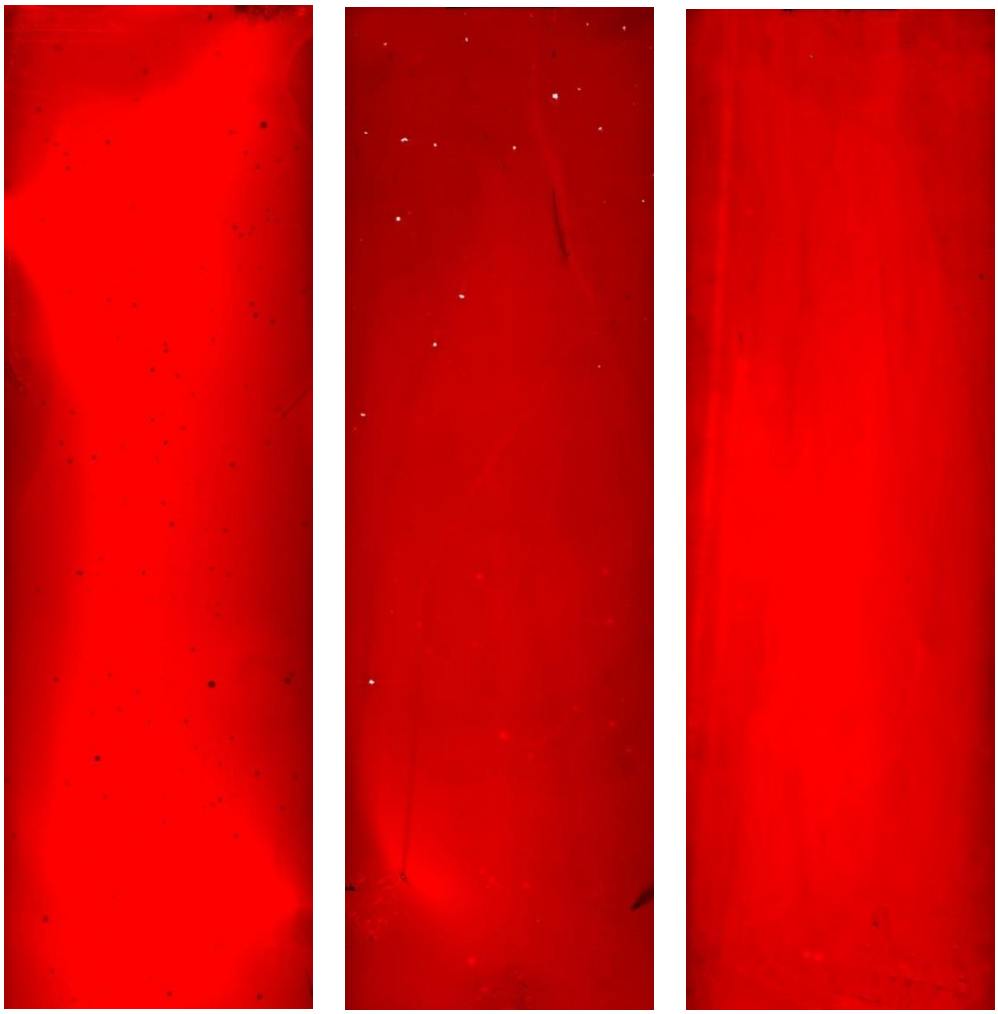

Vigorous shaking led to the appearance of several bubbles in the streptavidin solution during the coating procedure, which was also apparent in the resulting QC slide (Fig. 3.8 on left) as several black spots are visible across the slide. A swirl pattern is also seen across this slide, as a result of the rapid movement of the coating solution. No shaking led to non-optimal washing of the slide, as a distinct washing artefact is apparent on the resulting QC slide (Fig. 3.8 on right). Hence, based on both CV and visual data, the gentle shaking method was the most optimal one, and was therefore used for all subsequent coating procedures. Furthermore, when comparing the initial and improved coating procedures, as indicated below in Fig. 3.9, it was very evident that an improved coating procedure was obtained.

Figure 3.9: Comparison of QC slides testing initial and improved method. This figure includes the resulting scanned images of two distinct slides, each testing a distinct coating method: left: initial procedure; right: improved procedure. Fluorescent intensity is indicated in red.

When comparing whole area CVs, a decrease in CV from 27.6% (initial procedure) to 13.3% (improved procedure), and therefore an increase in slide coating homogeneity, was evident. Visually, saturation due to lifterslip-associated uneven coating (Fig. 3.9 on left) was completely eliminated with the immersion technique (Fig. 3.9 on right), and a more homogenous coating was obtained. Furthermore, it was shown that the streptavidin solution was reusable, as no change in overall coated intensity was apparent after multiple re-use.

3.3.2 Cloning and expression of cancer-testis antigens

The following cloning expression results were obtained by Dr. Aubrey Shoko from the CPGR.

Recombinant gene cloning methods were used to insert a total of 79 CT antigen and 44 non-CT antigen genes into a baculoviral expression vector as N-terminal fusions to an *E.coli*-derived biotin-carboxyl

carrier protein (BCCP) tag carrying a c-Myc tag (see Table 3.1 for the full list of antigens). The BCCP-tag is biotinylated in vivo, enabling single-step immobilization and purification of folded, BCCP-tagged recombinant proteins by printing crude lysates directly onto streptavidin-coated, PEG-derivitised microarray surfaces under native conditions; the very high affinity (K_d ~10^{-15} M) (Boutell et al. 2004) and specificity of the streptavidin-biotin interaction combined with the intrinsic resistance of PEG surfaces to non-specific protein adsorption (Zheng et al. 2005) enabled avoidance of laborious pre-purification of each recombinant protein under denaturing conditions (O'Kane et al. 2011).

In the absence of any pre-purification step, it might be expected that host cell proteins that are endogenously biotinylated and observed in western blots would compete with the biotinylated recombinant proteins for available streptavidin-binding sites on the array surface. However, under native conditions we have observed that these endogenous biotinylated proteins do not compete efficiently with biotinylated recombinant proteins for binding (Koopmann & Blackburn 2003), probably because in such endogenous proteins the biotin moiety is typically buried (Choi-Rhee & Cronan 2003) and therefore not physically available to bind streptavidin under native conditions.

Western blotting using a monoclonal anti-c-Myc antibody was used to confirm expression of each antigen, and a representative image for a subset of 12 antigens is indicated in Fig. 3.10, courtesy of Dr. Aubrey Shoko. These antigens include GAGE1, GAGE2A, GAGE4, GRWD1, HORMAD1, LDHC, LIPI, MAGEA1, MAGEA10, MAGEA11, MAGEA3, MAGEA4, and adequate control. In this western blot, good levels of expression were obtained for all antigens across a range of unrelated proteins, with the exception of HORMAD1, LIPI and MAGEA11. Similarly, the expression of all of the remaining antigens, 123 in total, was also confirmed. The recombinant insect cell expression used approach was found to give a > 95% success rate from cloned, sequence-verified transfer vector to expressed, folded and biotinylated proteins suitable for array fabrication; this compares favourably with the lower success rates observed when attempting to express mammalian proteins in *E. coli* (Terwilliger et al. 2009). Any antigen that was not initially produced (< 5%) was repeated until successful. Western blotting using a streptavidin-HRP conjugate probe was used to confirm biotinylation of the expressed recombinant proteins, and a representative image for the same subset of 12 antigens is indicated in Fig. 3.11, courtesy of Dr. Aubrey Shoko. The addition of free biotin to the growth medium was observed to increase the extent of biotinylation of the recombinant BCCP fusion proteins despite the absence of a co-expressed *E. coli* biotin ligase. Antigen expression was further confirmed by assaying printed arrays for the c-Myc tag using a c-Myc assay, which will be discussed below in Section 3.3.7.2.

Figure 3.10: Western blot confirming the expression of a subset of 12 antigens. 1-GAGE1, 2-GAGE2A, 3-GAGE4, 4-GRWD1, 5-HORMAD1, 6-LDHC, 7-LIPI, 8-MAGEA1, 9-MAGEA10, 10-MAGEA11, 11-MAGEA3, 12-MAGEA4, 13-control. Molecular weight marker is indicated on left. Western blot was done using crude insect cell lysates and developed using a monoclonal anti-c-Myc antibody. Good expression levels were observed across a range of unrelated proteins, with the exception of HORMAD1, LIPI and MAGEA11.

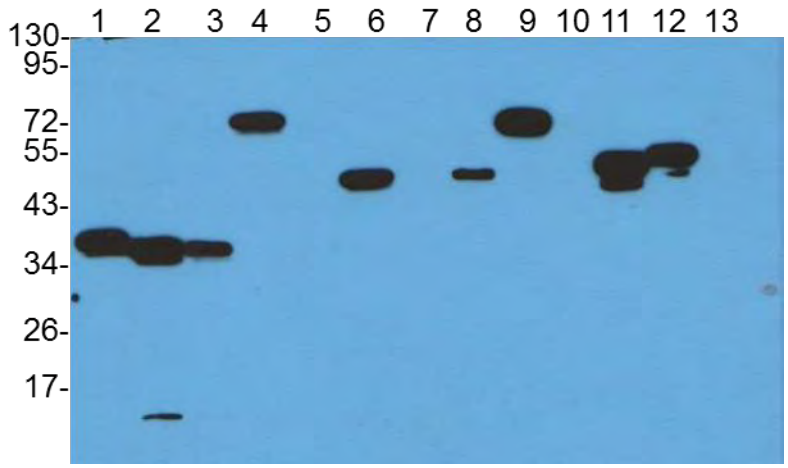

Figure 3.11: Western blot confirming the biotinylation of a subset of 12 antigens. 1-GAGE1, 2-GAGE2A, 3-GAGE4, 4-GRWD1, 5-HORMAD1, 6-LDHC, 7-LIPI, 8-MAGEA1, 9-MAGEA10, 10-MAGEA11, 11-MAGEA3, 12-MAGEA4, 13-control. Molecular weight marker is indicated on left. Western blot was done using crude insect cell lysates and developed using a streptavidin–HRP conjugate probe. Good biotinylation levels were observed across a range of unrelated proteins, with the exception of HORMAD1, LIPI and MAGEA11.

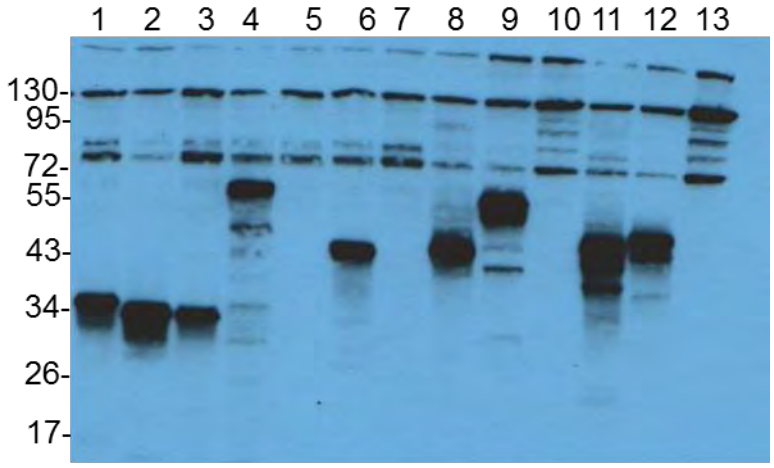

All recombinant proteins were expressed under the same conditions, with no attempt made to maximize expression levels. We estimated there to be a limiting number of available biotin-binding sites on the streptavidin-coated microarray surface, and the high affinity of the streptavidin-biotin interaction means that the surfaces saturate with antigen even at low antigen expression levels. This provides a crude normalization of protein loading without the need to pre-adjust the concentrations of the individual crude lysates to compensate for differences in expression levels before array fabrication (Boutell et al. 2004).

3.3.3 Fabrication and optimization of the cancer-testis antigen (CT100+) microarray

In the process of improving the first version of our platform (CT100), which contained 100 cancer-associated antigens, to the current augmented version ($CT100^{+}$), which contains 123 cancer-associated antigens, several issues arose, resulting in a relatively high assay repeat rate of ~40%, even when using a relatively high CV threshold (40%). These included spot running and associated carryover, as a result of reduced spacing between spots on each array, and variable spot size, as a result of differences in buffer composition between antigens of interest and positive controls (Cy5-biotin-BSA), as seen below in Fig. 3.12. These indicated that additional development was required, as a means of assuring data reproducibility.

Figure 3.12: Array printing settings comparison. This figure includes the resulting scanned $CT100^+$ array images of two distinct arrays, each utilising distinct printing settings and assay conditions: above: $CT100^+$ array using previous settings; below: $CT100^+$ array using improved settings. The array below indicates red and green spots, due to the uses of two distinct fluorescent tags – Cy3 and Cy5 – solely with the intent of verifying if spot carry-over was occurring.

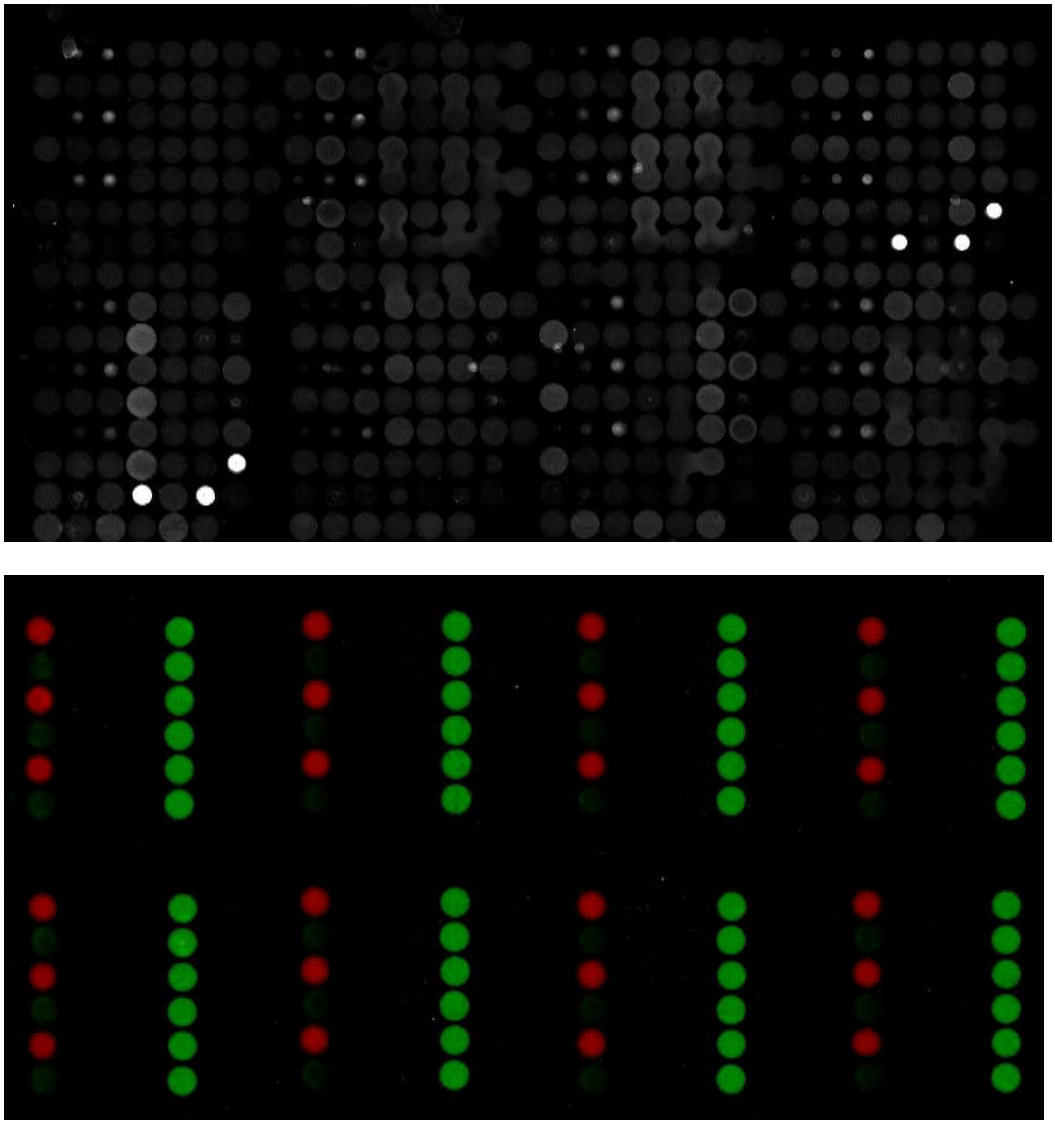

As a means to resolve these, several printing settings and buffer compositions were tested, and the most advantageous ones were implemented. Namely, the number of pin stamps onto the slide per spot was reduced from 2 to 1, which reduced spot size and thereby increased spacing between spots to an acceptable level, and a standard printing buffer was stipulated for all samples, which now included sucrose to increase surface tension and thereby allow for an increased spot consistency. As seen in Fig. 3.12, these alterations eliminated the issues stated above, resulting in well-defined consistently sized spots, with no spot running or carry-over, exemplified by use of two distinct fluorophores, Cy3 and Cy5

equivalents, amongst samples. When re-running these samples, a drastic reduction in repeat rate to ~6% was obtained, even when using a more stringent CV threshold (20%).

Additionally, as a means of resolving previous issues related to *E. coli* expression vector-based non-specific signal, all antigens were now expressed using insect cells, which removed all unwanted non-patient-specific signals, which was confirmed by a consistent lack of signal in our "empty lysate" negative control across assays.

Each print run was cohort size-dependent, with each run including all patient samples along with 3 arrays reserved for quality control assays (c-Myc assay, cancer pool and health pool assay). On each slide, 4 replica $CT100^{+}$ protein microarrays were printed in a 4-plex format, with each spotting event delivering ~10 nL sample, allowing for 4 patient samples to be assayed per slide. Due to the very small volumes required, each 50 µL aliquot of harvested expression cells provided enough recombinant protein to print 25 replica slides in four-plex format, with each protein printed in triplicate in each array. Therefore, one 3 mL baculovirus culture yielded sufficient expressed protein to fabricate 700 replica arrays, or >2000 replica spots of each protein, thereby aiding reproducibility.

3.3.4 Development of the CT100+.jar bioinformatic tool

As a means of demonstrating the usefulness of the CT100+.jar bioinformatic tool, the background correction and the normalization methods were tested for a selected print run.

As described above in Section 3.2.5, the background correction method smooths the local background by reducing the effect of artefacts and noise in the background, thus enabling calculation of more accurate net intensities by subtracting the corrected neighbourhood background value from the median local foreground pixel intensity. As a means of exemplifying this correction, the net intensities (RFU values) of Cy5-biotin-BSA control spots at 5, 10 and 15 ng/µL of a selected array were plotted before and after background selection, as is indicated below in Fig. 3.13.

Figure 3.13: Quantitative illustration of the local background correction method. The local background of each Cy5-biotin-BSA spot is replaced by a median of the local backgrounds of surrounding neighbourhood spots (3 x 3 spot window). The corrected net intensity is measured by each spot's raw intensity minus corrected background intensity. Red line: mean net intensities before background correction; Blue line: mean net intensities after background correction.

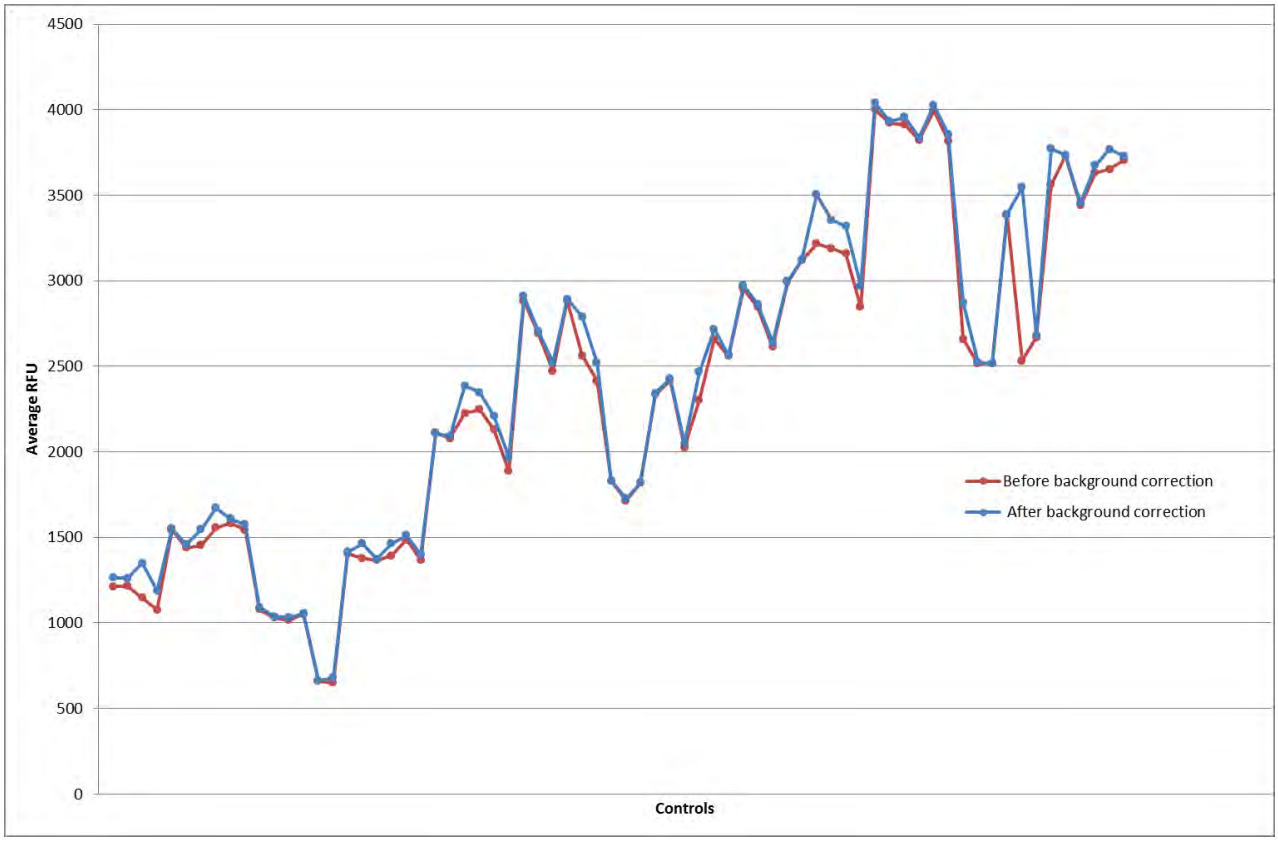

It was evident that there were differences between the pre- and post-corrected net intensities, accentuated at some times more than others. As expected, net intensities before background correction appear to be slightly skewed due to noisy local background signals. Once this background was replaced by neighbourhood local backgrounds, the net intensities increased slightly to a more representative intensity, without local background bias. Hence, it was apparent that this method is most relevant, as it permits a larger amount of confidence in the generated array data.

In regards to the pin-to-pin and array-to-array normalization methods, the novel composite normalization method combining both quantile and total intensity normalization modules was used, as described above in Section 3.2.5, enabling more flexibility in the presence of outliers of flagged spots and ensuring that an adequate number of positive controls are available for normalization. As a means of exemplifying this normalization, the net intensities (RFU values) of Cy5-biotin-BSA control spots of a

selected slide – four distinct arrays – were plotted before (see Fig. 3.14) and after (see Fig. 3.15) normalization, as is indicated below.

Figure 3.14: Quantitative illustration pre-composite normalization method. This graph indicates the Cy5-biotin-BSA average net intensities across four distinct arrays of a single slide prior to conducting pin-to-pin and array-to-array normalization.

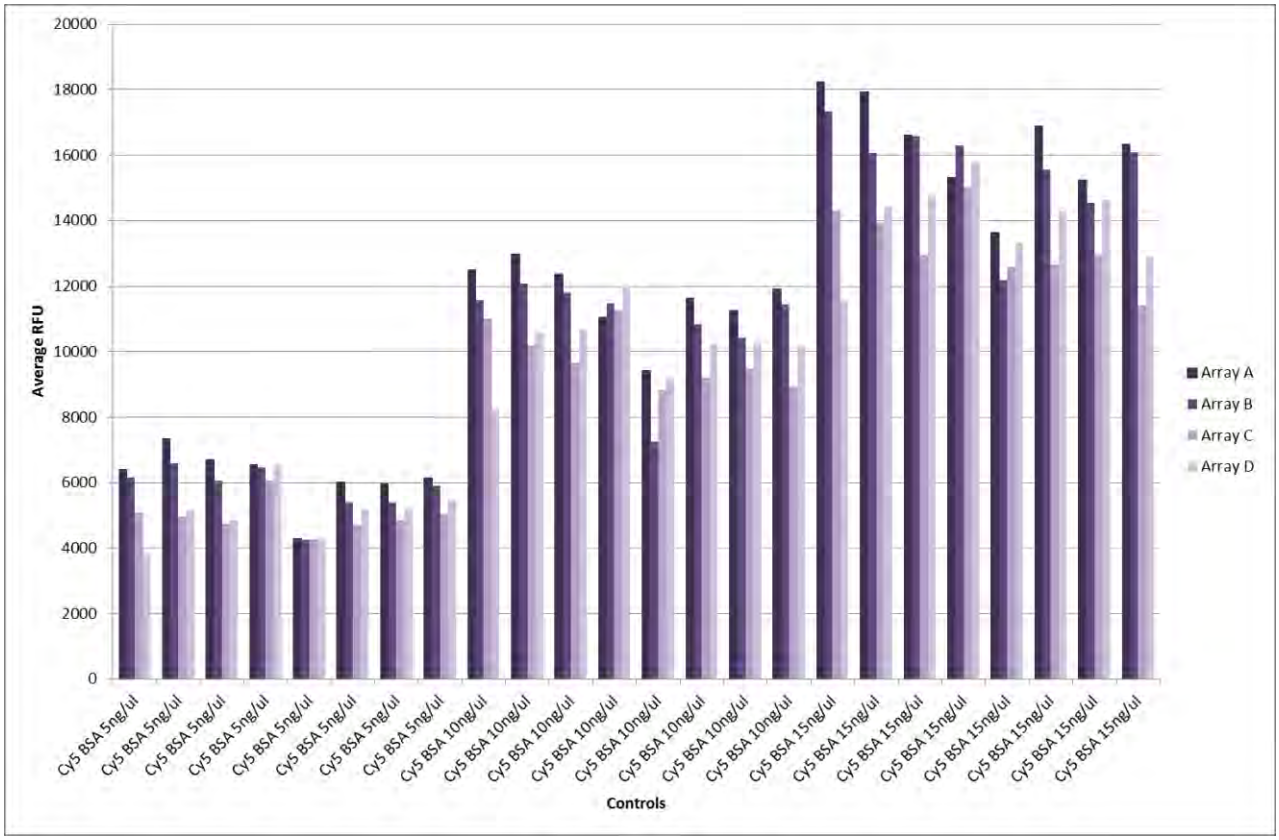

Figure 3.15: Quantitative illustration post-composite normalization method. This normalization method combines both quantile and total intensity normalization modules to account for inter- and intra-array variability. This graph indicates the Cy5-biotin-BSA average net intensities across four distinct arrays of a single slide after conducting pin-to-pin and array-to-array normalization.

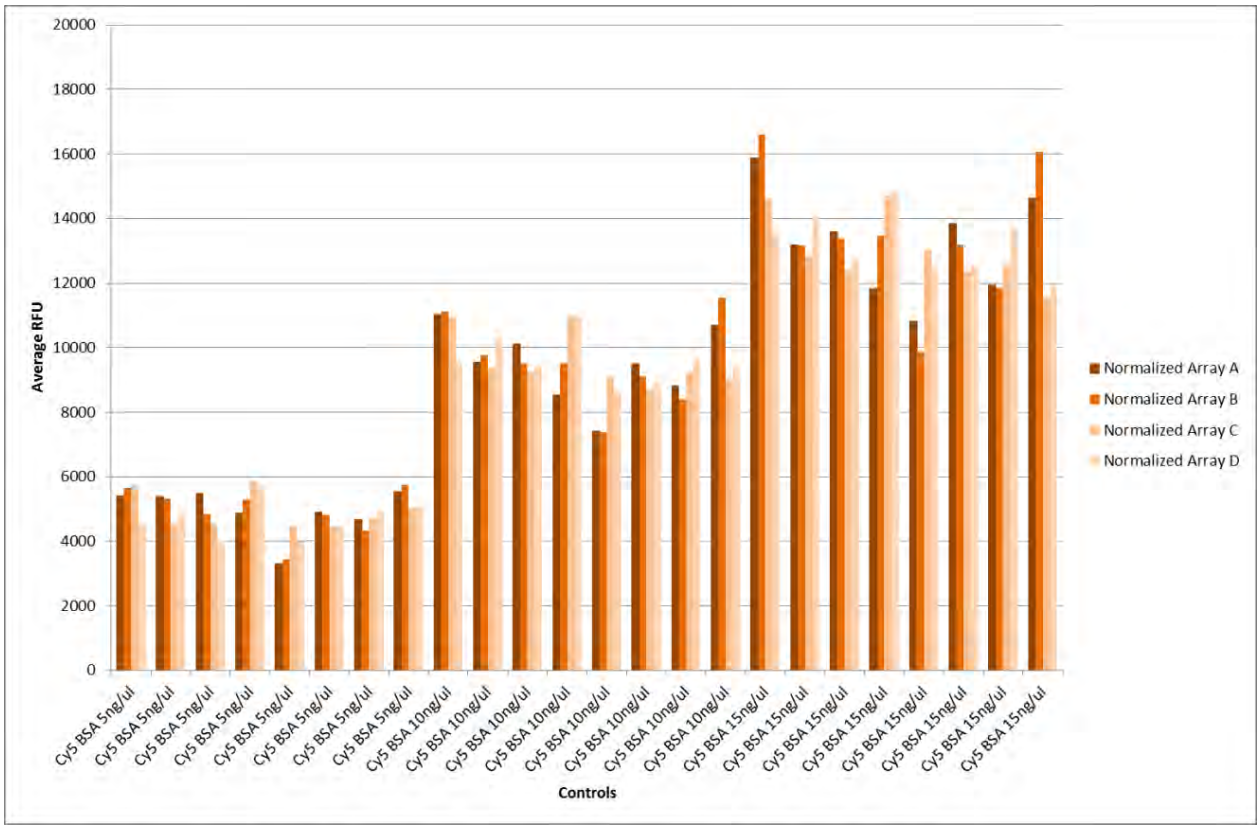

By comparing the average RFU values of the positive controls across four arrays – one single slide – before and after inter- and intra-array normalization, it was evident that there were differences between the pre- and post-normalized net intensities across the whole graph, although these may not be visible at first glance. The most evident difference seen was that for each control post-normalization, the range of values across the four arrays is smaller when compared to the same control pre-normalization. For example, in Fig. 3.14, the first set of Cy5-biotin BSA controls at 5 ng/µL ranges from ~3800 RFU to ~6200 RFU (2400 RFU variation), whilst the same set after normalization in Fig. 3.15 ranges instead from ~4600 RFU to ~5800 RFU (1200 RFU variation), thus indicating that the variability for that set of controls across all arrays was halved. Additionally, it was also evident that the average RFU values appear slightly lower after normalization, with the maximum intensity lowering from ~18200 RFU to ~16600 RFU (1600 RFU difference).

Hence, this normalization method proved highly beneficial, guaranteeing to reduce bias caused by problematic spots or arrays amongst the obtained data. Furthermore, by normalizing results between

arrays, it is possible to compare different time points for a single patient with confidence, thus enabling autoimmune comparisons between time points.

3.3.5 Linearity and dynamic range microarray assays

Robust linearity and dynamic range experiments were performed to determine the optimal serum and anti-human IgG antibody dilutions for the detection of antibody-antigen binding. All data generated by the protein arrays for these assays were pre-processed and analysed as described in Methodology. No data points were excluded by the data filtering steps, indicating that the arrays were of good quality.

An initial linearity assay was performed using a range of serial dilutions (1:50, 1:100, 1:200, 1:400, 1:800, 1:1,600, 1:3200 and 1:6400) of a randomly chosen serum sample (P117, Day 483) using a fixed secondary Ab concentration (20 μg/mL) (Fig. 3.16). After analysing the resulting array image, a classic saturation binding curve was obtained (Fig. 3.17) which indicated that at serum dilutions of ~1:50 of a randomly chosen serum sample demonstrating a high response to NY-ESO-1 (P117, day 483), the available NYESO-1 binding sites on the microarray were saturated (maximum number of binding sites (Bmax) = 55370 RFU), with half-maximal binding occurring at ~1:1250 dilution. This corresponds with the known high immunogenicity of NY-ESO-1 (Nicholaou et al. 2006). Therefore, an optimal serum dilution was selected at 1:800 and used in all further assays.

Figure 3.16: Array image (16-plex) obtained from the Initial linearity assay using a series of serum dilutions of a randomly chosen patient sample (P117, Day 483) to measure saturation binding of patient autoantibodies to the NYESO-1 antigen on the array surface, using 20 µg/mL secondary Ab for detection. This figure includes the resulting overlapped array images of a dual-scanned (Cy3 and Cy5 lasers) single slide. Positive control spots consisting of Cy5-biotin-BSA (10 ug/mL) are indicated in red on image. Negative control spots consisting of lysis buffer only did not display any non-specific fluorescence. NY-ESO-1 autoantibody signals obtained are in green on image, across a range of serum dilutions (1:50, 1:100, 1:200, 1:400, 1:800, 1:1600, 1:3200 and 1:6400) from top to bottom and a fixed detection antibody concentration . Fluorescent intensity is indicated in red (Cy5) or green (Cy3).

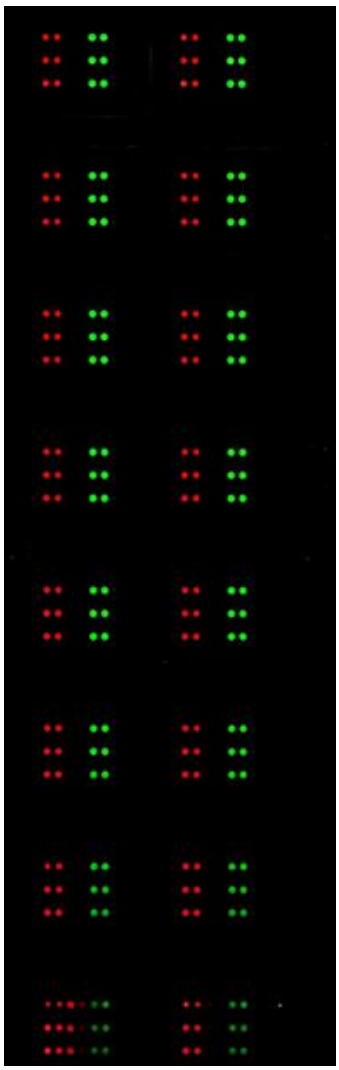

Figure 3.17: Saturated binding curve obtained for the initial linearity assay using a series of serum dilutions of a randomly chosen patient sample (P117, Day 483) to measure saturation binding of patient autoantibodies to the NYESO-1 antigen on the array surface, using 20 µg/mL secondary Ab for detection. Insert: Scatchard plot of the same data.

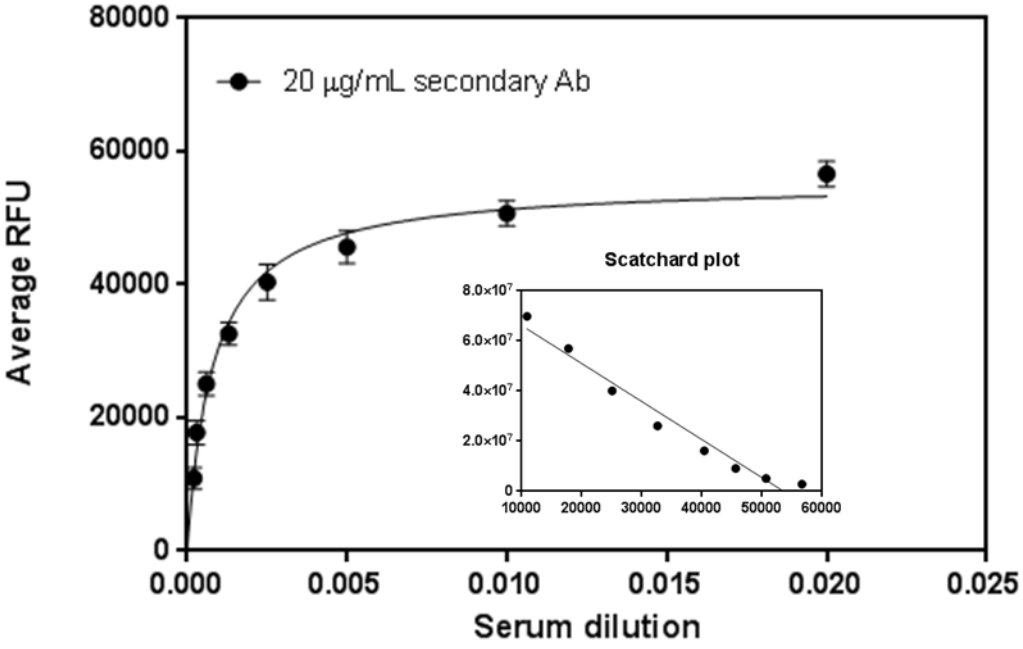

To exclude the possibility that the observed saturation binding occurred due to limiting secondary antibody availability, an assay was performed using two different serum dilutions (1:200 and 1:2400) and a range of secondary antibody concentrations (Fig. 3.18). After analysing the resulting array images at both serum dilutions, saturation of secondary antibody binding was obtained at ~10 µg/mL (Bmax = 58936 RFU; Fig. 3.19), with a calculated binding affinity (K_d) of the primary–secondary antibody interaction on the array surface of ~2 µg/mL. This confirmed that the data in Fig. 3.17 reflected the saturation binding of the serum autoantibodies to the immobilized antigens, rather than a limiting quantity of secondary antibody. Therefore, 20 µg/mL of secondary antibody was used in all further assays.

Figure 3.18: Array images (16-plex) obtained from the second linearity assay using two serum dilutions (1:200 and 1:2400) of the same patient sample and a range of secondary Ab concentrations to determine the dynamic range of secondary Ab binding. This figure includes the resulting scanned images of a single slide scanned twice, using the Cy5 (image on left) and the Cy3 (image on right) lasers. Array on left: Positive control spots consisting of Cy5-biotin-BSA (10 ug/mL) indicated in red on image. Negative control spots consisting of lysis buffer only did not display any non-specific fluorescence. Array on right: NY-ESO-1 autoantibody signals obtained in green on image, across a 1:200 (left panel of image) and 1:2400 (right panel of image) dilutions. Detection antibody concentrations of 40, 30, 20, 15, 10, 5, 2.5, 1.25 ug/mL were used for both dilutions from top to bottom, respectively. Fluorescent intensity is indicated in red (Cy5) or green (Cy3).

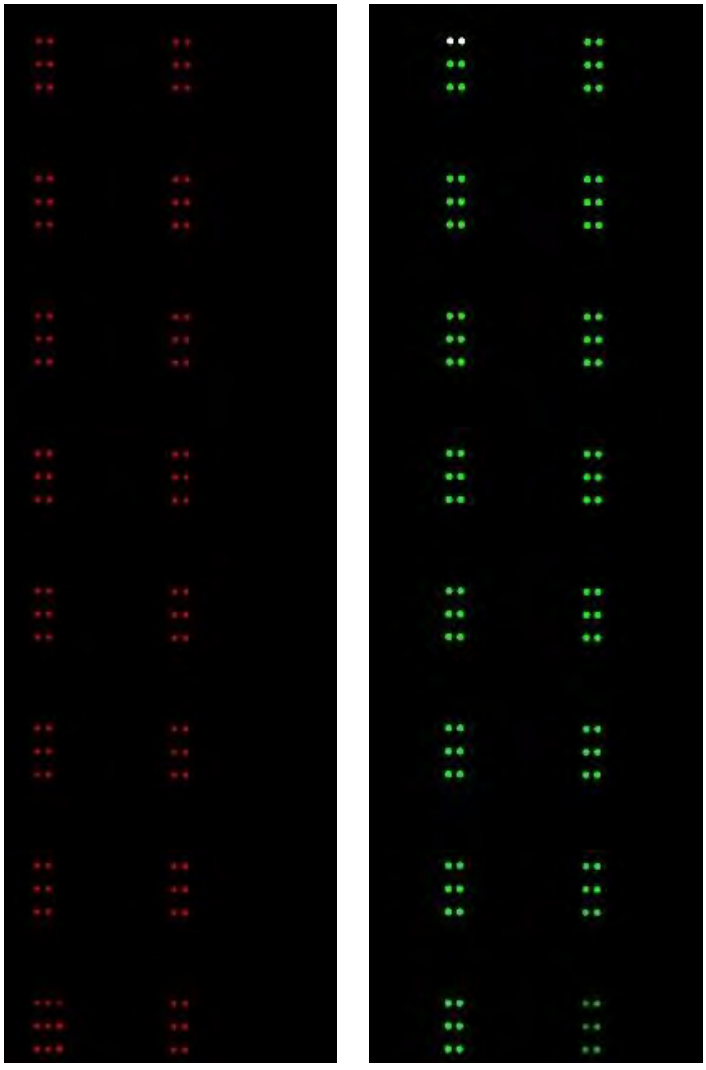

Figure 3.19: Saturation binding curves of the second linearity assay using two serum dilutions (1:200 and 1:2400) of the same patient sample and a range of secondary Ab concentrations to determine the dynamic range of secondary Ab binding.

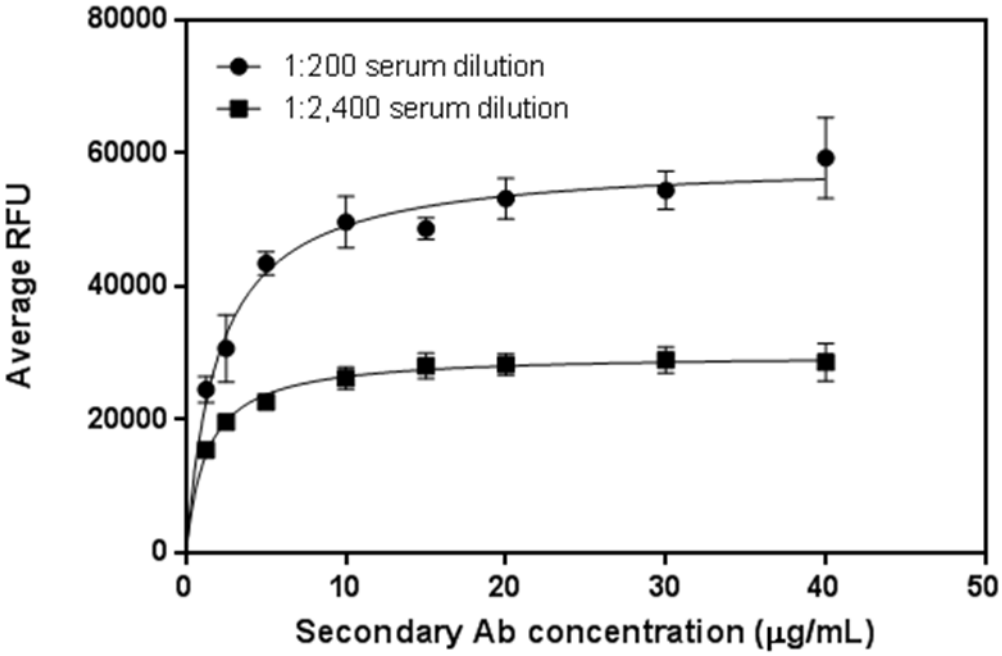

To assess the linear range of this platform, a dynamic range assay was performed using serial serum dilutions (1:1000, 1:2000, 1:4000, 1:8000, 1:16000, 1:32000, 1:64000 and 1:128000) and a fixed secondary Ab concentration (20 µg/mL) (Fig. 3.20). This assay revealed a linear response over greater than three orders of magnitude (Fig. 3.21) and no evidence of signal limitation was observed at the serum dilutions tested. Even at the highest tested dilution (1:128000), a measurable signal was still detectable well above the median background values.

Figure 3.20: Array images (16-plex) obtained from the dynamic range assay indicating the linear range of the platform. This figure includes the resulting scanned images of a single slide scanned twice, using the Cy5 (image on left) and the Cy3 (image on right) lasers. Array on left: Positive control spots consisting of Cy5-biotin-BSA (10 ug/mL) indicated in red on image. Negative control spots consisting of lysis buffer only did not display any non-specific fluorescence. Array on right: NY-ESO-1 autoantibody signals obtained in green on image, across a range of serum dilutions (1:1000, 1:2000, 1:4000, 1:8000, 1:16000, 1:32000, 1:64000 and 1:128000) from top to bottom and a fixed detection antibody concentration (20 ug/mL). Fluorescent intensity is indicated in red (Cy5) or green (Cy3).

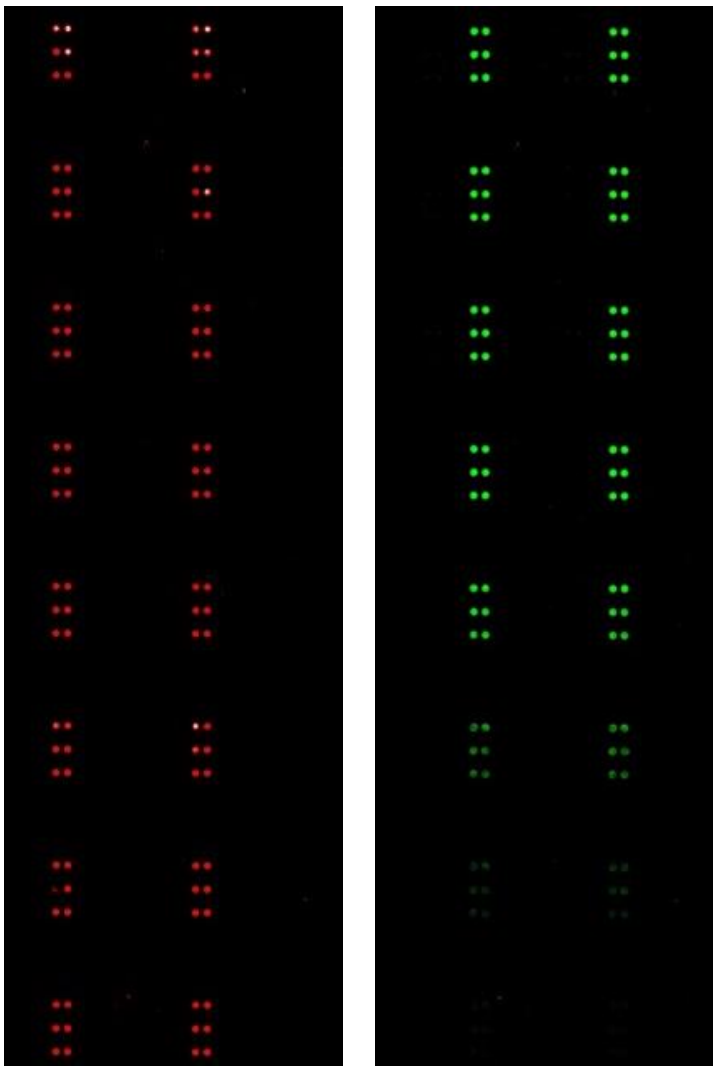

Figure 3.21: A dynamic range assay indicating the linear range of the platform. The limit of detection (1:1000000 serum dilution) is where the data intersects with the signal cut-off level (two standard deviations of the background; indicated here as the dashed line).

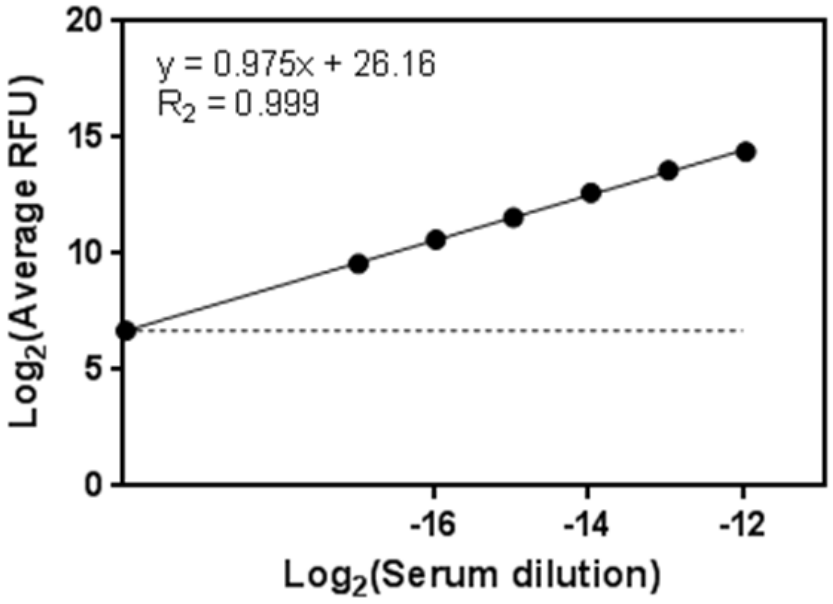

By extrapolation of the linear range to the lower limit and assuming a noise threshold of two standard deviations (SD) of the background, the detection limit was estimated to be ~1:1000000 serum dilution.

3.3.6 Quantification of the absolute array detection limit for cancer-testis antigens

To estimate the absolute detection limit of our CT antigen microarray platform, three assays were performed using the same serum sample used for the linearity assay.

Firstly, a Bradford protein assay was successfully conducted using BSA standards, with the intent of obtaining an absolute total protein concentration of the serum sample. By extrapolation of the standard curve ($y = 0.3372x + 0.37350, R^2 = 0.99$), a concentration of 63.7 mg/mL was obtained, which is in agreement with the reported total protein range in serum of 60-80 mg/mL (Merrell et al. 2004).

Secondly, a SDS-PAGE densitometry analysis was conducted on the same sample, as a means of determining what proportion of total proteins corresponded to total IgG. A 7.5% polyacrylamide gel was prepared, and 1.0, 1.5 and 2.0 µg of serum were loaded in triplicate, along with a protein molecular weight marker. The SDS-PAGE gel was electrophoresed accordingly, and the gel obtained is indicated in Fig. 3.22. Increasing band intensities were seen with increasing loaded amounts of serum, with several bands appearing from 25 to 170 kDa. Serum albumin (66.5 kDa) was present as expected and was

consistently the most abundant protein, as well as the anticipated IgG heavy (55 kDa) and light (25 kDa) chains.

Figure 3.22: SDS-PAGE protein gel of serum (1.0, 1.5 and 2.0 µg) using AcquaStain. This image indicates the resulting stained gel with indications on left of molecular weights, and on right of relevant protein band identification.

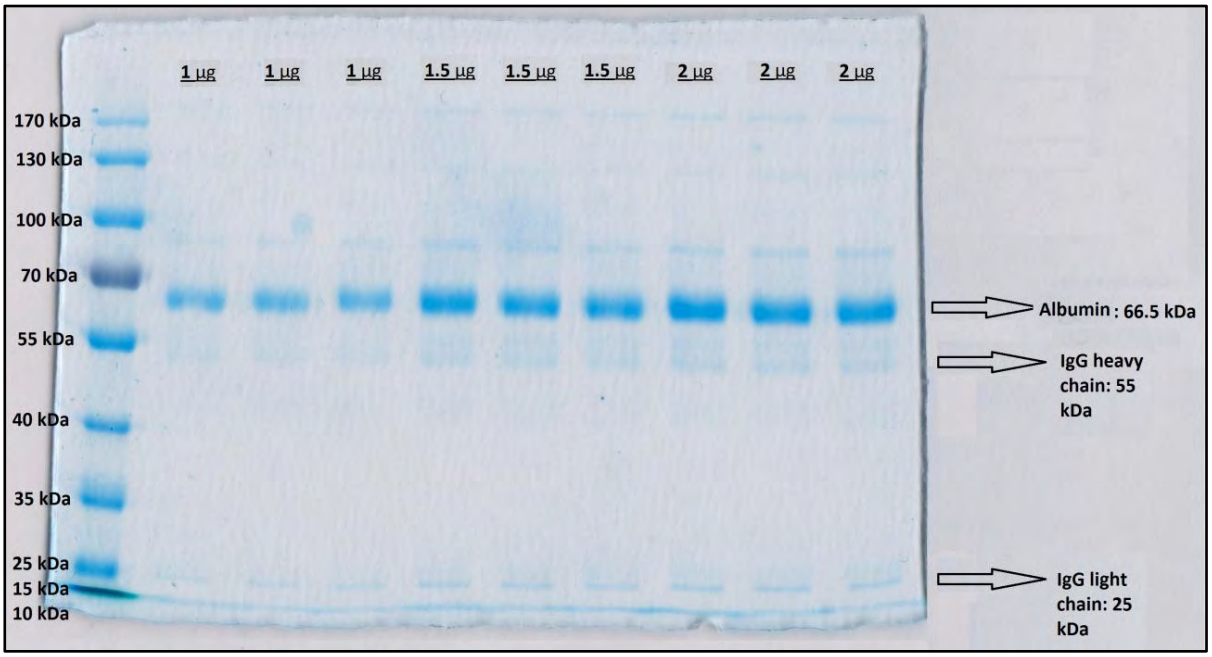

A densitometry analysis was performed on this gel using Gene Tools, and all existing bands were identified automatically. Each band was attributed an automated molecular weight, after indicating the protein ladder used, and each band was assigned a raw volume. Using the three lanes loaded with 2.0 µg of serum, a proportion of each band was indicated in the form of a percentage, utilising the sum of all bands as the total proportion and removing the background volume. After adding the IgG heavy and light chains, the IgG proportion corresponded to 5.7% of the total serum, slightly below the normal IgG regular range (7.5 – 22 mg/mL). This difference is most likely due to the fact that the serum used was collected from a potentially immunosuppressed advanced melanoma patient, and therefore, IgG levels were not within the usually reported healthy range. The proportion of serum albumin, on the other hand, was 64.3%, well within the reported range (57-71%), validating these results (Merrell et al. 2004). Considering that the sum of all bands equated to the absolute total protein concentration of 63.7 mg/mL (measured above via Bradford assay), a rough concentration of IgG was determined, obtaining 3.63 mg/mL.

Thirdly, a protein microarray assay was performed to determine the proportion of total IgG corresponding to anti-NY-ESO-1. The assay was performed as indicated above in Section 3.2.6, and the resulting data was analysed accordingly. When incubating anti-human IgG, NY-ESO-1-BCCP crude insect cell lysate, ICL and buffer-only control on the previously printed serum spots, and after adding detecting antibody (Cy5-labelled streptavidin) on this inverted array format, the intensities obtained corresponded to levels of total IgG, anti-NY-ESO-1, non-specific binding to the insect cell vector, and non-specific binding to the assay buffer, respectively. Non-specific binding to the assay buffer was not detected, indicating that solely the ICL values should be deducted from the anti-NY-ESO-1 levels, as the NY-ESO-1-BCCP crude lysate was expressed in this vector. The 48 replicas of each of these were averaged, and a single median net intensity value was obtained, as indicated in Table 3.4.

Table 3.4 Average net intensity values of IgG, anti-NY-ESO-1, ICL and buffer only measured by a protein microarray assay.

	Average Net intensity
IgG	22346.94
anti-NYESO1	1418.25
ICL	266.10

Assuming that each anti-human IgG molecule had one biotin attached to it, and knowing that each NY-ESO-1-BCCP crude lysate was also attached to one biotin, IgG and anti-NY-ESO-1 were at a 1:1 ratio. Hence, the proportion of anti-NY-ESO-1 in IgG was of 5.6%. Considering that the rough concentration of IgG was 3.63 mg/mL, as determined above via densitometry analysis, the concentration of anti-NY-ES0-1 was therefore 0.19 mg/mL in the neat serum sample. Based on the estimated detection limit of ~1:1000000 serum dilution by extrapolation of the linear range graph indicated in Fig. 3.21 using the same serum sample, the detection limit could thus be quantified, obtaining an autoantibody titre of ~190 pg/mL.

Herein, we have shown that our CT antigen microarray platform can detect and quantify specific human autoantibodies in serum with a detection limit in the pg/mL range—equating to a million-fold serum dilution, and with linearity over at least three orders of magnitude, representing a significant advance in the field compared to ELISA or other protein microarray platforms.

3.3.7 Standard CT100^{+} array quality controls

3.3.7.1 Verification of the immobilization of controls to array surface

As part of each standard microarray print run, great attention was given towards assuring that a robust quality was obtained. All positive, negative and assay controls were plotted per print run, as seen below in Fig. 3.23, for a selected print run.

Figure 3.23: Positive, negative and assay controls for a selected print run. This graph indicates the complete set of negative (buffer, ICL, BCCP-myc) and positive (Cy5-biotin-BSA at 5, 10 and 15 ng/µl, biotin-hIgG 10ng/ul and biotin-αhIgG) controls included on the CT antigen array for a selected print run with associated average RFU values.

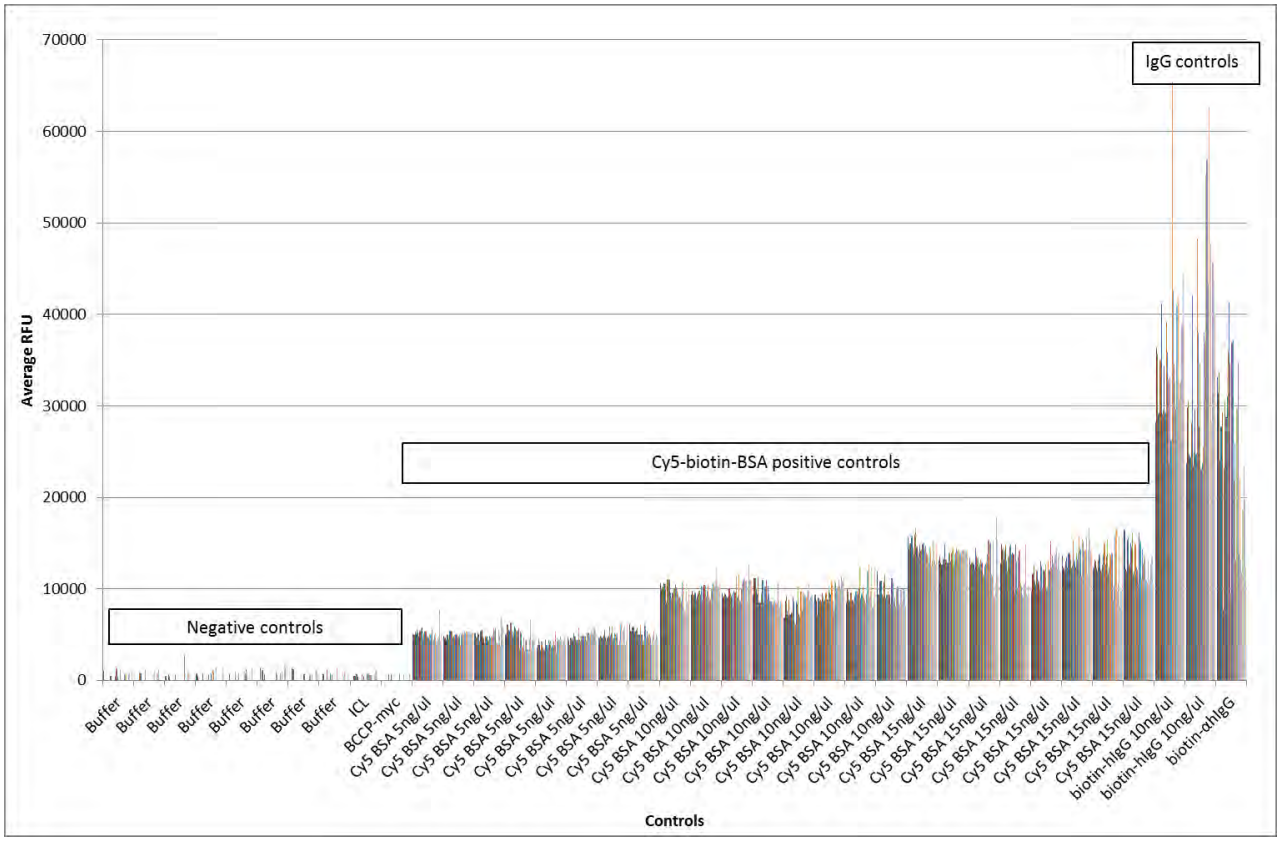

Based on the plot indicated above, all negative controls which included buffer only ("Buffer"), insect cell "empty vector" lysate ("ICL") and BCCP-myc tag only ("BCCP-myc") displayed either very low or no intensities, which indicated that all signals arising from these were negligible, and therefore non-specific binding and associated fluorescence did not occur. Additionally, besides from the standard noise threshold – two standard deviations (SD) of the background – an additional threshold stipulated as the median of all negative controls per array (usually below 1000 RFU) was measured for each assay, and

autoantibody intensities were only considered if above this value. The biotinylated Cy5-BSA controls ("Cy5 BSA 5ng/ul", "Cy5 BSA 10ng/ul", "Cy5 BSA 15ng/ul") displayed a gradual increase in intensity as a function of an increasing concentration, with relatively stable signals amongst each, which indicated that the print run was successful, and that all slides used had a satisfactory homogeneous streptavidin coating. It is also important to note that these controls would still be present and available for use, independent of a successful subsequent assay. The biotinylated human IgG controls ("biotin-hIgG 10ng/ul") displayed relatively high intensities across all arrays, which indicated that detection antibody was added to all, and that these antibodies were able to bind to the serum autoantibodies. Lastly, the biotinylated anti-human IgG controls ("biotin-αhIgG") also displayed high, but quite variable, intensities, which indicated that serum was added to all arrays, and that the available autoantibodies were able to bind to respective antigens on the array. Furthermore, this parameter displays the high variability of total IgG levels amongst patients, which are most likely true fluctuations as a result of treatment, rather than varying overall serum concentrations. Each print run conducted per treatment cohort roughly matched this expected pattern, which indicated successful print and assay runs, eliminating the need for any high-scale repeats.

3.3.7.2 Verification of the immobilization of BCCP-tagged proteins to array surface

Since all arrayed antigens should also carry a c-Myc tag, an anti-c-Myc assay was conducted per print run, as a means of reconfirming that all antigens were successfully expressed, and that all spotted antigens had successfully bound to the array, as seen below in Fig. 3.24, for a selected print run.

Figure 3.24: c-Myc assay for a selected print run. This image indicates a dual scanned array of a c-Myc assay, with Cy5-biotin BSA controls indicated with red fluorescence (independent of c-Myc assay) and antigens indicated with green fluorescence.

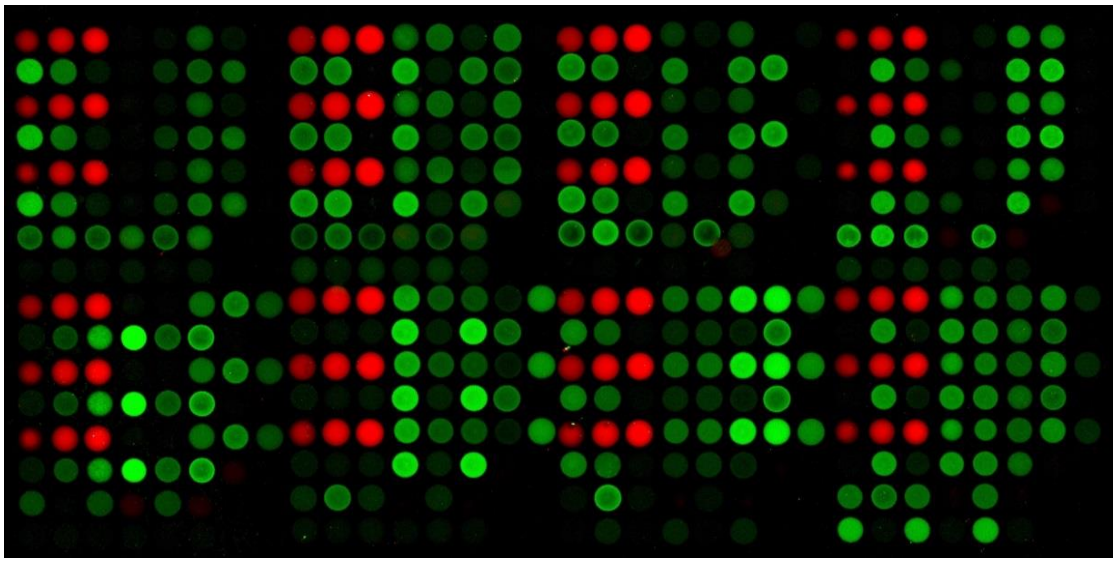

Based on the image indicated above, it was apparent that all spotted recombinant proteins of interest (green spots) were indeed successfully expressed and bound to the array. Due to the higher sensitivity achieved with protein microarrays when compared to western blot assays, we verified that for the very few antigens where expression could not be confirmed via western blot, expression was in fact verified via this c-Myc assay. Furthermore, it also confirms that the printing and assaying conditions and parameters were optimal, as no spot running, variable spot size, carry-over or even washing artefacts were seen on the array. These findings provide great assurance that the obtained data derived from robust quality arrays. These results were obtained consistently across all print runs, serving as a clear indication of the high reproducibility of the array.

3.3.7.3 Verification of array specificity for cancer

Array specificity was tested using the cancer and healthy patient pools on the array. For a selected print run, the resulting scanned array for the pooled cancer patient samples is displayed below in Fig. 3.25.

Figure 3.25: Cancer control pool scanned array for a selected print run. This image indicates a scanned array assaying the cancer pooled sample, and thus indicating the presence of multiple cancer-specific autoantibody responses besides from the positive controls. Red boxes highlight triplicate CTAG2 (above) and NY-ESO-1 (below) positive signals.

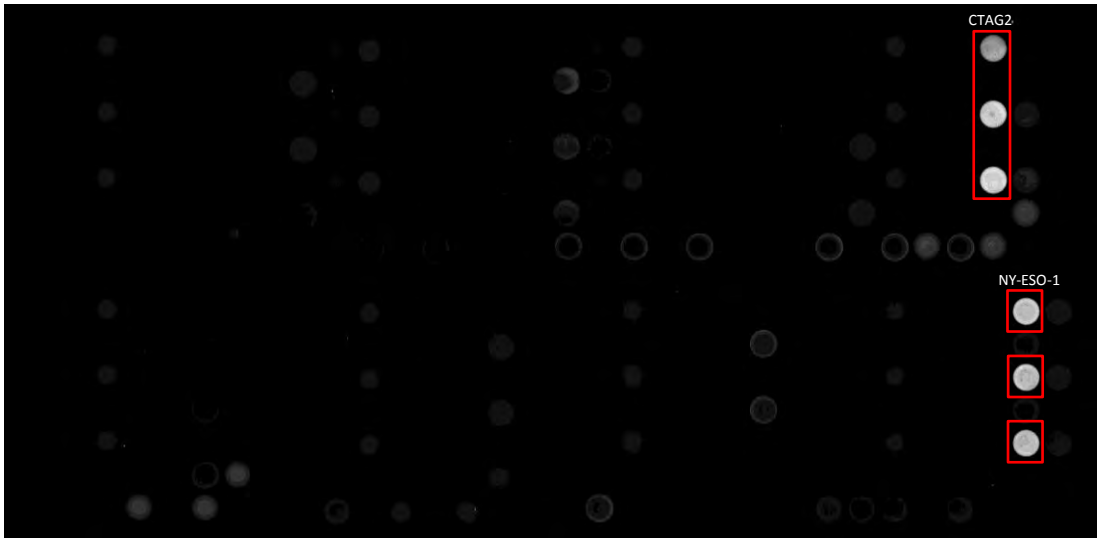

This resulting array image clearly indicated that many cancer-specific autoantibodies were abundant amongst these patients, resulting in a positive array with several above noise quantifiable signals. This was certainly expected as a result of pooling a variety of different cancer patients, due to the well-known patient-specific autoimmune diversity. As a means of facilitating interpretation of the visual array, this data was plotted in Fig. 3.26, indicated below.

Figure 3.26: Cancer control pool plotted data for a selected print run. This graph indicates the resulting quantitative data when assaying the cancer control pool for a selected print run with associated average RFU values.

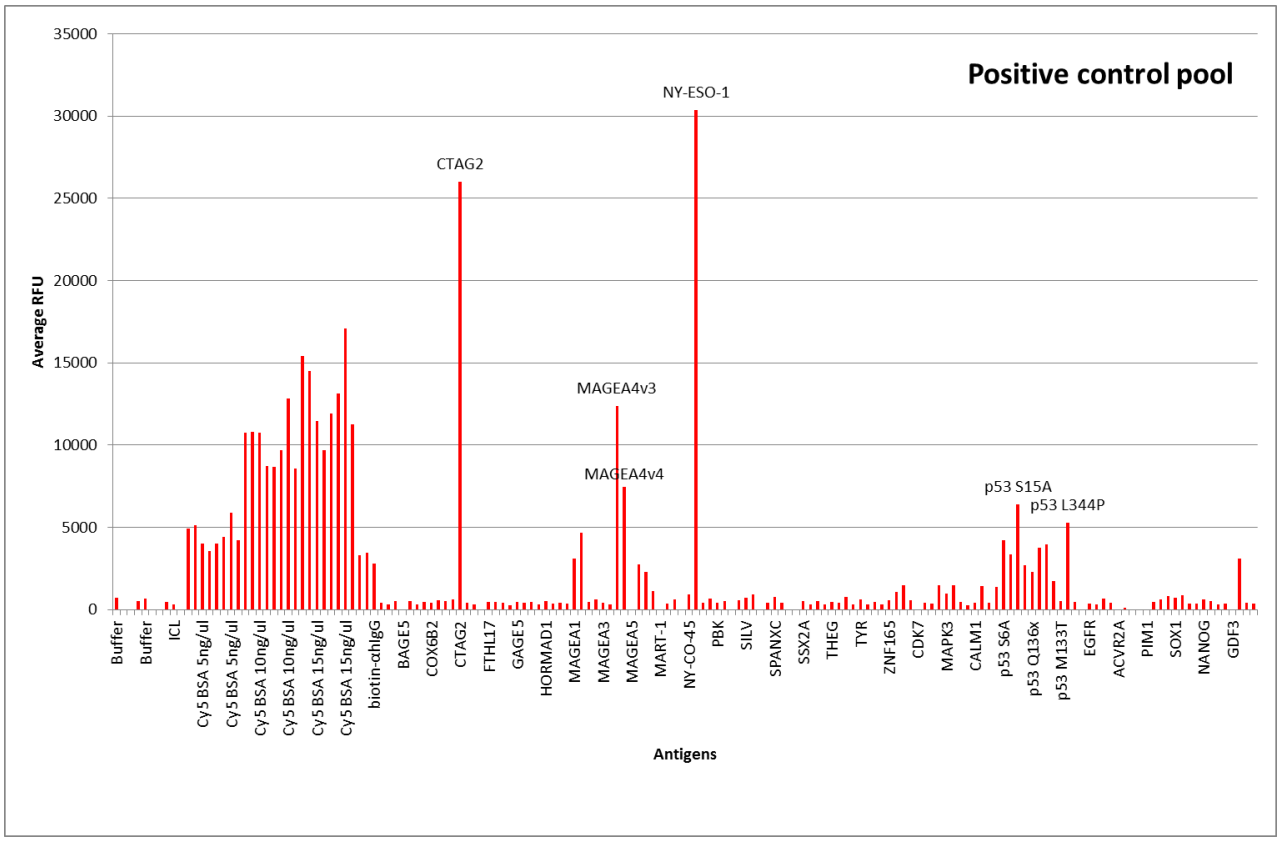

This graph indicated signals according to the controls mentioned above, along with several autoantibody titres to antigens of interest, including NY-ESO1, CTAG2 and MAGEA4, amongst others. This assay was deemed successful, and suggested that all existing autoantibody signals should be effectively detectable and quantifiable. Additionally, healthy patient pooled samples were also assayed per print run, and a resulting scanned array is shown in Fig. 3.27 for a selected print run.

Figure 3.27: Healthy control pool scanned array for a selected print run. This image indicates a scanned array assaying the healthy pooled sample, and thus indicates the absence of cancer-specific autoantibody responses, besides from the positive controls.

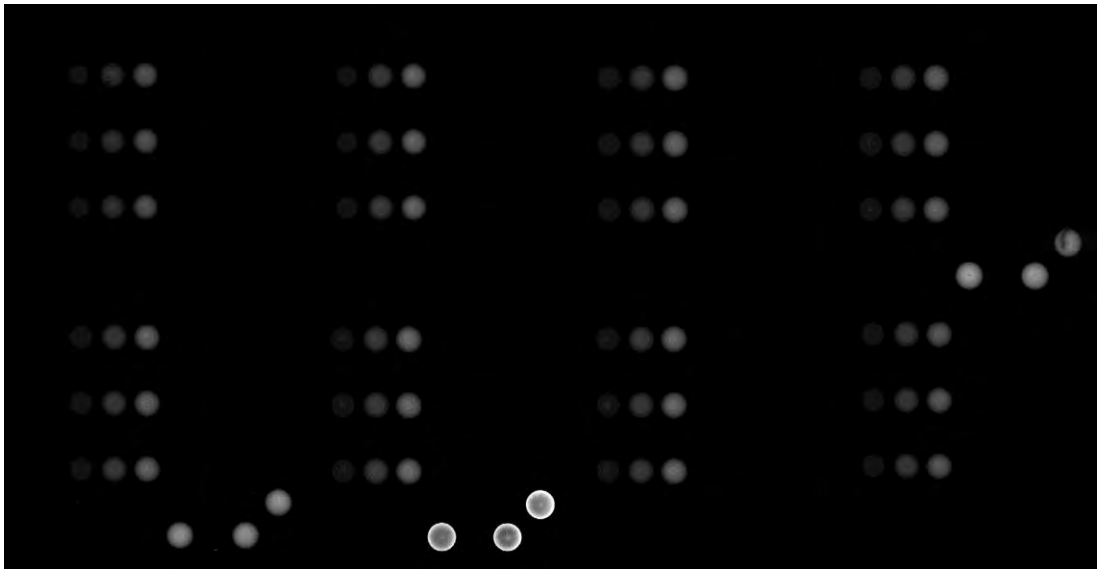

This resulting array image clearly indicated that, aside from the expected positive controls, no cancer-specific autoantibodies were present amongst these patients, resulting in a negative array with no quantifiable signals. This was certainly expected, as healthy patients should certainly not display any cancer-specific signals. As a means of further deciphering all signals on this array, the data was plotted in Fig. 3.28, indicated below.

Figure 3.28: Healthy control pool plotted data for a selected print run. This graph indicates the resulting quantitative data when assaying the healthy control pool for a selected print run with associated average RFU values.

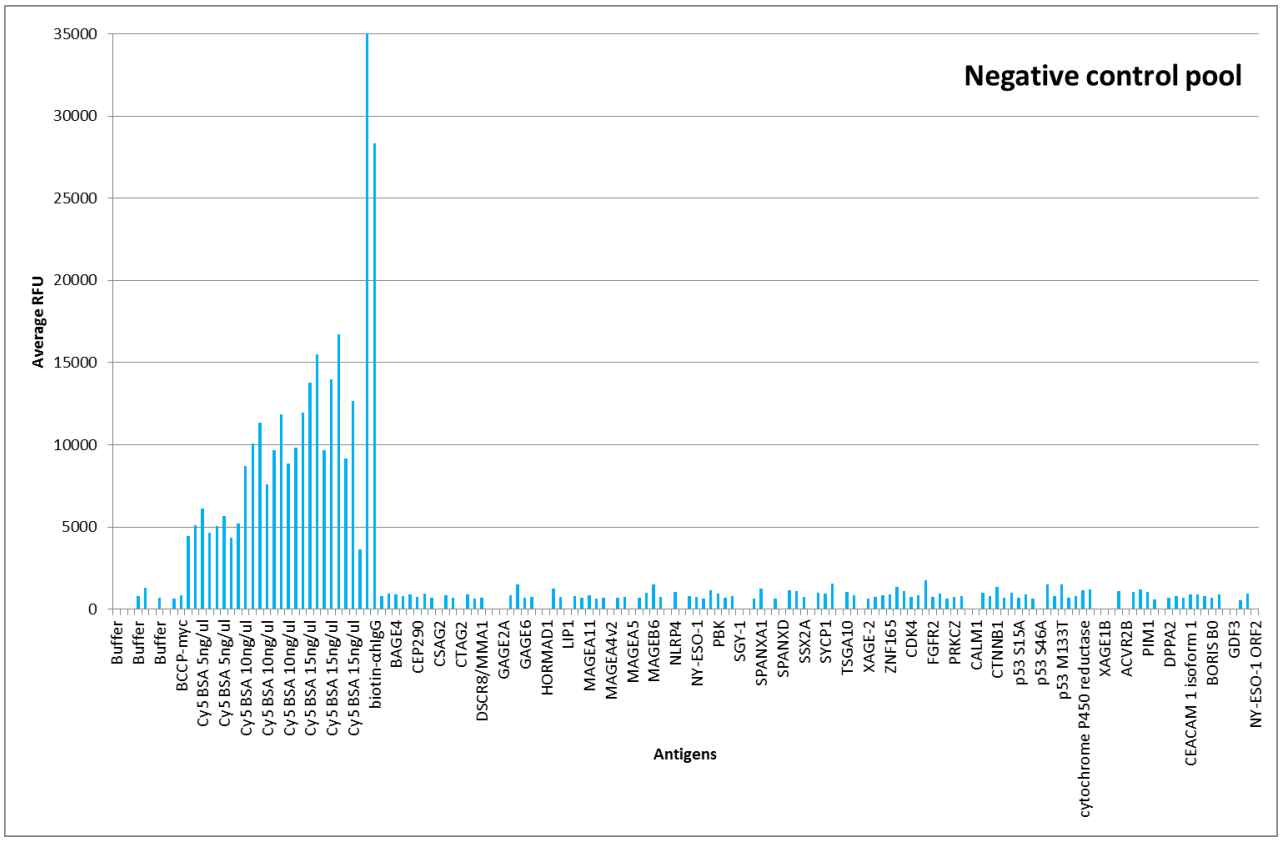

This graph confirmed that solely the positive controls were detected, with all cancer-specific signals falling below the noise threshold, with low non-specific binding to the arrayed antigens in healthy controls. This assay was also therefore deemed successful, emphasizing that all detected autoantibody signals are indeed cancer-specific. Both these cancer and healthy pooled samples were assayed per print run, with consistently satisfactory results, similar to those indicated above. Therefore, all resulting patient data was obtained with high confidence and quality, which was according to our pre-established necessary standards.

3.3.8 Reproducibility studies

During the linearity and dynamic range assays, it was evident that given the ability to produce the above-mentioned data (Section 3.3.5) using the same randomly selected sera sample, our CT100^{+} protein microarray platform was a means to repeatedly obtain consistent data.

Whilst performing the standard array quality controls assays (Section 3.3.7), it was evident that lack of data reproducibility was not a concern, as the routinely conducted c-Myc, cancer control and healthy

control pools assays gave rise to highly constant results, even amongst arrays from distinct print runs. Moreover, the biotinylated Cy5-BSA controls repeatedly gave rise to stable signals within and across arrays. This was guaranteed with the low CV requirement of 20% amongst replicates within each array, which discarded any array that did not display steady signals across replicates.

Additionally, when considering inter-array reproducibility, such as reproducibility amongst replicate spots, it was evident that the majority of all signals showed consistent signals across all replicates, which was apparent visually, amongst those relatively high signals, and quantifiably, across the majority of all signals above the noise threshold. Furthermore, as a means of assuring that only highly reproducible data was obtained for each protein of interest, a robustly low replicate CV threshold of 20% was also defined. Thus, thereafter, if any three protein-specific replicates varied more than 20%, these were excluded from analysis. Even though this strict threshold was applied, the majority of all signals were retained, indicating that only a small number of protein-specific replicates had been discarded due to lack of signal reproducibility.

Also, when comparing our pre- and post-optimized CT100^{+} array runs, although the initial runs resulted in a high repeat rate, when visually analysing the same sample it was very evident that the same relatively high signals were present in both runs, which is indicated in Fig. 3.29. This finding further implies uniformity amongst our data.

Figure 3.29: Pre- and Post-optimized arrays for a selected patient. This figure contains two scanned array images of a selected patient sample assayed on two different occasions, demonstrating consistent results: above: pre-optimized patient CT100+ array; below: post-optimized patient CT100+ array. Red boxes highlight triplicate CTAG2 (above) and NY-ESO-1 (below) positive signals.

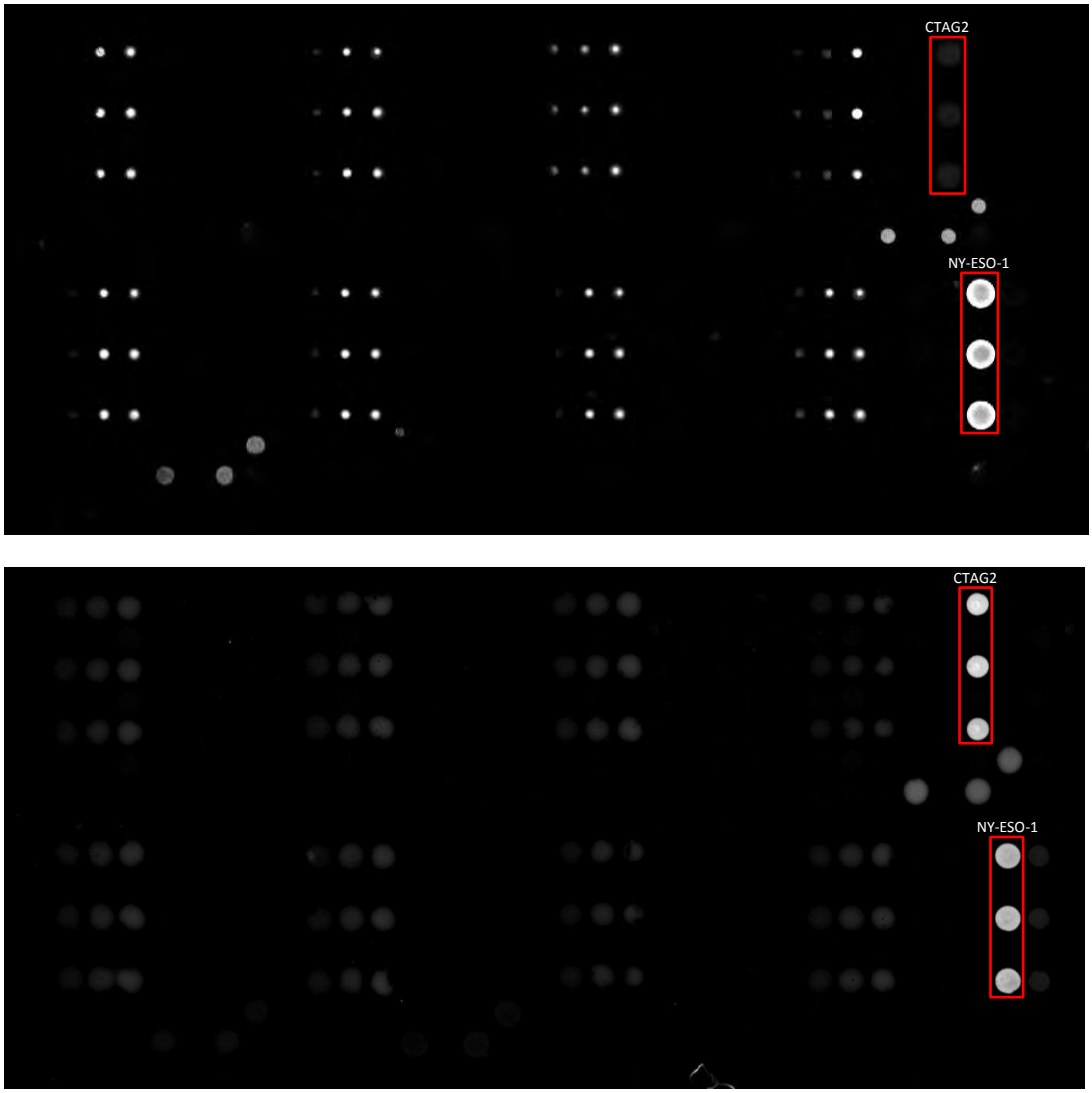

Hence, these studies verified that our array data is highly reproducible, with the ability to generate consistently robust ad high quality data. The ability to obtain high inter- and intra-assay reproducibility highlights the feasibility and applicability of our protein microarray platform, a high-throughput tool used for the screening of immune responses in cancer patients. The protein microarray approach described here has the advantage of providing data on cancer-associated antigen expression through direct quantitation of autoantibody titres in serum, which are elicited relatively early in tumourigenesis and bind to their target autoantigens with high affinities and specificities (Anderson & LaBaer 2005b). Hence, the detection of cancer-specific autoantibodies is possible in principle at significantly lower serum concentrations than is routinely possible for detection of the cancer antigens themselves,

thereby leading to the potential for pre-symptomatic cancer diagnosis. Furthermore, when this array was originally created (CT100), ELISAs were performed as a means of validating the obtained antibody responses. These data suggested that our microarray platform was more sensitive than the ELISA (currently the gold standard for measuring antibody-antigen interactions), with an even higher capacity of multiplexing.

4 PROFILING PATIENT AUTOIMMUNE RESPONSES

4.1 Introduction

This Section intends to explore the potential of our CT100+ protein microarray platform identifying novel cancer biomarkers, which could aid in the detection and management of cancer. The main objective of this Chapter is to attempt to comprehend and shed light on the interplay between chemotherapy, radiotherapy or immunotherapy and anti-cancer autoimmune responses.

The quantitative study of antibodies that recognize cancer antigens in patients could in principle enable early detection of tumours, patient stratification, personalized patient treatment, development of improved therapies, and more efficient monitoring of therapeutic response and disease progression (Tan et al. 2009; Anderson & LaBaer 2005a).

Although much progress has been made regarding comprehending the key hallmarks of cancer, effective diagnostic, predictive and therapeutic strategies are still yet to be discovered and implemented in a clinical setting. Profiling autoimmune patient responses towards tumour-specific and –associated antigens across several cancer types and treatments holds great promise and potential regarding the discovery of potential novel biomarkers. Similar assays have been performed by others, with promising results. For instance, (Wang et al. 2005) assessed autoantibody levels of prostate cancer patients and obtained evidence of a potential novel screening test, whilst more recently (Xu et al. 2014) assessed these levels across esophageal squamous cell carcinoma patients and obtained evidence of a potential

biomarker for early detection of disease. Furthermore, the latter study reported that these autoantibody titres were found to precede manifestations of symptomatic cancers, which further highlights the clinical applicability of this tool.

4.2 Methodology

4.2.1 CT100^{+} protein microarrays with patient sera

4.2.1.1 CT100^{+} assay

Following printing, slides were immersed in blocking buffer (50 µM biotin in PBST) and incubated on ice for 1 h, in a plastic chamber wrapped in foil. Slides were then washed three times for 5 min in PBST, and placed in slide holders and centrifuged at 240 x *g* for 2 min at RT to dry. Individual arrays were each incubated with a unique serum sample (100 µL at 1:800 dilution, dilution based on the results obtained for the initial linearity assay indicated in Section 3.3.5) for 1 h at RT, washed in PBST and dH_20, and incubated with 100 µL of 20 µg/mL (concentration based in the results obtained for the additional linearity assay also indicated in Section 3.3.5) of Alexa Fluor 647 (Cy5 equivalent) Goat anti-Human IgG (H+L) (Invitrogen, Life Technologies, 2 mg/mL, #A21445; 1:100 dilution in PBST) for 30 min at RT. The individual arrays were then washed, dried and scanned using a Tecan LS Reloaded fluorescence microarray scanner in automatic gain control (AGC) mode. All liquid handling steps were performed on a Tecan HS4800 Pro automated hybridization station (Tecan Group Ltd., Switzerland), using QuadChambers. These chambers permitted each slide to have four separate segments, which eliminated the risk of cross-contamination between subarrays per slide. The complete assay design is summarized in the flowchart indicated below in Fig. 4.1.

Figure 4.1: Flowchart of CT100^{+} assay design.

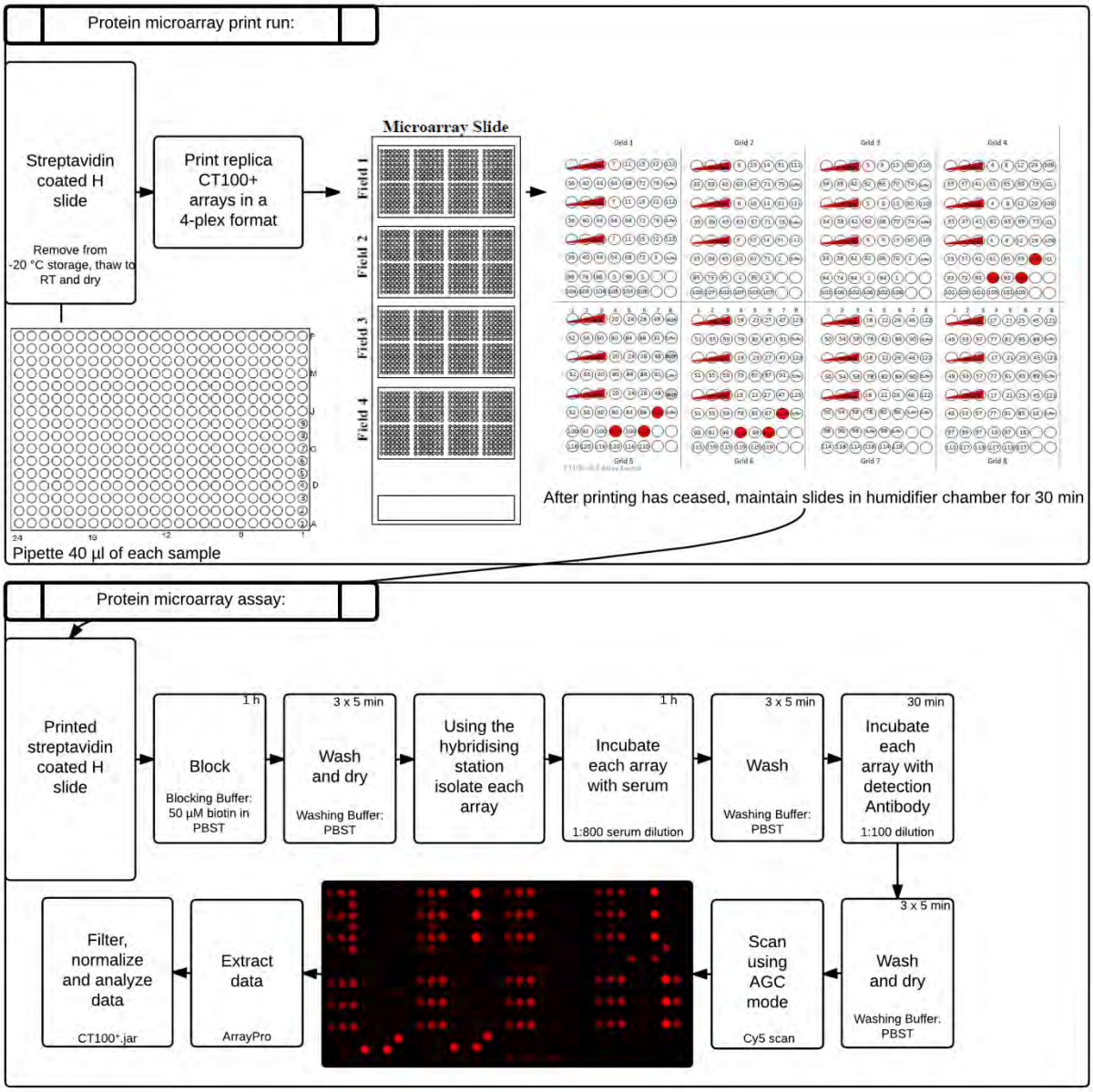

4.2.1.2 CT100^{+} data extraction

All raw image files were visually inspected to assess spot morphology and background signal. Any arrays showing high background, excessive speckling, the presence of interfering dust particles or fibres, or evidence of coalescing protein spots were re-assayed in a subsequent new print and assay run. Typically, < 10% of assays were repeated for these reasons. In ArrayPro Analyzer software, a grid was autoaligned over the individual spots on each scanned image file and a constant area feature finder was used across the array surface. Following automatic spot finding using a fixed spot size, manual curation of the grid alignment was performed. A .gal file containing information on the sample identity in each spot was read into ArrayPro and the raw data was extracted from each spot as well as the local background –

using the local corners approach (see Fig. 4.2) – in batch processing mode using a 200 RFU pixel threshold, yielding the median foreground and background pixel intensities per sample spot.

Figure 4.2: Local background setting used on ArrayPro Analyzer software. The mean intensity of the pixels located in the local corners of each spot was used as the local background, a setting commonly used in dense arrays. [Adapted from the ArrayPro Analyzer user guide.]

4.2.1.3 CT100^{+} data processing and analysis

The extracted data was then processed using a bioinformatic pipeline automated in a Java script for pre-processing and quality control of custom protein microarray data – the CT100+.jar bioinformatic tool – which is described in detail in Section 3.2.5. Briefly, the local background signal for each spot was replaced by its neighbourhood background. A corrected net intensity was then calculated for each spot by subtracting its neighbourhood background from its foreground signal. A user-defined noise threshold (*n*SD of Background) was applied, and all spots containing a net intensity below that threshold were removed from analysis. The mean net intensities for each set of replicates were calculated, and replicates above the user-defined CV were removed. Similarly, whole array CVs were calculated using a chosen Cy5-bioin-BSA control, and arrays above the user-defined CV were removed. Sub-arrays within each array were normalized with respect to each other to minimize any effects of pin-to-pin variation. Whole arrays were then normalized with respect to each other to minimize any effects of slide-to-slide variation. Both normalization steps were performed using all Cy5-biotin-BSA controls. A novel composite normalization method combining both quantile and total intensity normalization modules was used for these purposes, as described previously. Any resulting whole arrays with unsatisfactory CV values were discarded and repeated. The processed and normalised triplicate data for each control/antigen was averaged, and only the final average net intensity per control/antigen was used further. Finally, each resulting data file – corresponding to an array – was consolidated, generating a single file containing the average net intensity values of each analysed array across all antigens.

Hence, data and statistical analyses were performed utilising only good quality robust data. To facilitate data analysis and interpretation, data analysis was performed using Excel. Statistical analysis was performed using Excel and GraphPad Prism, such as non-parametric one-way ANOVA (Friedman) and t-tests (Mann-Whitney), to compare intensities of different time points for the same patient, and scatter plots (mean + 95% confidence intervals) to verify the distribution of signals across patients and antigens.

4.2.2 *In vitro T-cell* re-stimulation assays using patient derived PBMCs

As a means of validating our array results, secondary immune responses to treatment using a selected subset of patients was assessed. This was done with T-cell re-stimulation assays using patient derived peripheral blood mononuclear cells (PBMCs) at previously assayed matching time points, followed by fluorescent activated cell sorting (FACS). This work was conducted during a 3-month research visit to the CIBL.

4.2.2.1 T-cell re-stimulation assay design

PBMCs from protein microarray-tested matched patients and time points were collected from liquid nitrogen storage and thawed in a bead bath at 38 °C, along with T-cell-RPMI media (450 mL RPMI 1640 medium, 25 mM HEPES (Life Technologies, 500 mL, #22400-089), 60 mg/L penicillin, 12.5 mg/L streptomycin (Life Technologies, 10000 U/L, #15140-122), 2 mM GlutaMAX (L-glutamine) (Life Technologies, 100 mL, #35050-038), 100% human sera (Australian Red Cross, Melbourne), 1% MEM-NEAA (non-essential amino acids) (Life Technologies, 100 x, #11140-050) and 1 mM sodium pyruvate (Life Technologies, 100 mM, #11360070) stored at 4 °C). When thawed, the content of each vial was transferred to a respective 15 mL tube, and 10 mL of media was added to each tube. These tubes were centrifuged at 688 x *g* for 5 min at 4 °C, and supernatants were carefully aspirated, assuring that pellets were not lost. A 5 mL volume of media was added to each tube, followed by gentle but thorough mixing until the pellet had completely dissociated. The content of each tube was then transferred into a respective well in a 6-well plate. Each well was mixed further, as a means of breaking up any potential cell clusters. Each well was viewed using a standard microscope, to confirm the presence of cells, and the plate was stored in the incubator at 37 °C overnight. Selected peptide pools (NY-ESO-1, MART-1/Melan-A, ROPN, MAGEA3, MAGE4, GAGE1, and TYR) (Mimotopes) were prepared to a final concentration of 1 mg/mL in PBS, as details regarding epitope specificity were not relevant for this study, and stored until use at -30 °C. Each peptide pool consisted of overlapping 18mer peptides, which spanned the full amino acid sequence of the relevant antigen.

The following day, the 6-well plate was removed from the incubator, and cells were viewed. After gently mixing each well, 10 µL of each was transferred to a well in a 96-well plate. An equal amount of 10 µL of Trypan blue dye (Bio-Rad, 0.4% solution, #145-0013) was added to each well, and after gently mixing,

half of that volume was pipetted under the coverslip of a haemocytometer. Live translucent bright round cells were counted following the defined counting technique using a standard microscope. After gentle mixing, cells were transferred from each well in the 6-well plate to a respective 50 mL tube. A 10 mL volume of PBS was added to each empty well, as an additional washing step to capture any remaining cells, and after further mixing was also added to the previous 50 mL tubes. These were centrifuged as above and supernatants were carefully aspirated. Each tube was then resuspended with media to allow 10^6 cells per well, based on the previous cell counting calculations. A 1:4000 dilution (25 U/mL) of human IL-2 (Miltenyi biotech, 50 µg, #130-093-903) was added to each tube, and mixed gently. Each tube volume was then divided by the number of peptides tested, and this respective volume was added to respective wells of 12-well plates. According to the number of peptides in each antigen pool, a final volume of 1 µg/mL of each was added to the respective well, with gentle swirls (primary stimulation). After confirming the presence of cells in each well, the plates were stored in the incubator. Our intention was to stimulate cells for 10 days, after which secondary stimulation and FACS analysis could follow. Cells were checked daily, with IL-2 re-additions every second day and only up to day 8, to avoid interference with results. Media was changed and cells were passaged in the process, if needed.

On day 11 after stimulation, wells were mixed gently, and each well was transferred to their respective 15 mL falcon tube. Each well was washed out with an additional 1 mL of PBS, to assure that little to no cells were lost. Tubes were centrifuged as above and supernatants were aspirated. The assay 96-well plate layout was planned and the required sample volume, 100 µL per well, was calculated. Cell pellets were resuspended in 10% more volume than required of warmed media, with gentle mixing to allow complete dissociation. A 1:1000 dilution of GolgiPlug (BD Biosciences, 1 mL, #555029) was added to each tube, as a means of preventing cytokine release from the cell interior. After gentle mixing, cells were transferred according to planned layout to a 96-well U-bottom plate. Peptide pools were then re-added to the respective wells, with exception of the negative and positive control cells (secondary stimulation). A mix of EBV (Mimotopes, 1 mg/mL), Influenza (Mimotopes, 333 µg/mL) and Hep. B (Mimotopes, 333 µg/mL) peptides were added to the positive control wells (one for each patient time point) at final concentrations of 1 µg/ml. No peptides were added to the negative control wells (one for each patient time point). The assay plate was then stored in the incubator for 3 h. After this incubation period, 100 µL of PBS was added to each well, and the plate was centrifuged at 300 x *g* for 5 min at 4 °C. The plate was decanted with one swift movement to remove supernatants, but retain pellets, and mixed on a shaker at 500 rpm for approximately 15 s. Cells were then ready for FACS fluorescent antibody staining to occur, which required all work from this step onwards to be conducted in the dark. The anti-CD antibody cocktail was aimed to stain helper T-cells ($CD3^+$, $CD4^+$) and Cytotoxic T lymphocytes ($CD3^+$, $CD8^+$), and therefore consisted of a mix of APC mouse anti-human CD3 (BD Biosciences, 100 tests, #555335, 1:50 dilution), V450 mouse anti-human CD4 (BD Horizon, 300 tests, #561838, 1:150 dilution),

AmCyan mouse anti-human CD8 (BD Biosciences, 100 tests, #339188, 1:50 dilution) prepared in PBS, in the sufficient final volume required to add 30 µL per well. The anti-CD antibody cocktail was added to each well (surface staining), and the plate was incubated in a dark fridge at 4 °C for 15 min. Following this incubation step, 170 µL of PBS was added to each well, and the plate was centrifuged, decanted and shaken as indicated above. A 100 µL volume of 1 x fixation/permeabilization solution (BD Biosciences, 125 mL, #554722) was added to each well, as a means of opening the cell pores to allow entry of anti-cytokine antibodies, and plates were incubated in a dark fridge for 20 min. Next, 100 µL of 1 x permeabilization/wash buffer (BD Biosciences, 125 mL, #554722) was added to each sample well. The plate was centrifuged at 500 x *g* for 5 min at 4 °C, and then decanted and shaken as before. An anti-cytokine antibody cocktail was prepared in PBS, which consisted of a mix of FITC mouse anti-human IFN-γ (eBioscience, 100 µg, #11-7319-82, 1:50 dilution), PE-Cy-7 mouse anti-human TNF-α (eBioscience, 100 µg, #25-7349-82, 1:50 dilution), in the sufficient final volume required to add 30 µL per well. The anti-cytokine antibody cocktail was added to each well (intracellular staining), and the plate was incubated in a dark fridge for 25 min. The plate was then washed, centrifuged, decanted and shaken, as indicated in the previous step. Finally, pellets were resuspended in either 100 µL of PBS (if FACS analysis would occur within 3 h of staining) or 4% PFA (Science Supply Associates, 16%, #15710) ((if FACS analysis would only occur between 3 h and 3 days later), and the plate was wrapped in foil and stored in a dark fridge at 4 °C until the FACS assay.

This assay design is summarized in the flowchart indicated below in Fig. 4.3.

Figure 4.3: Flowchart of T-cell re-stimulation assay design.

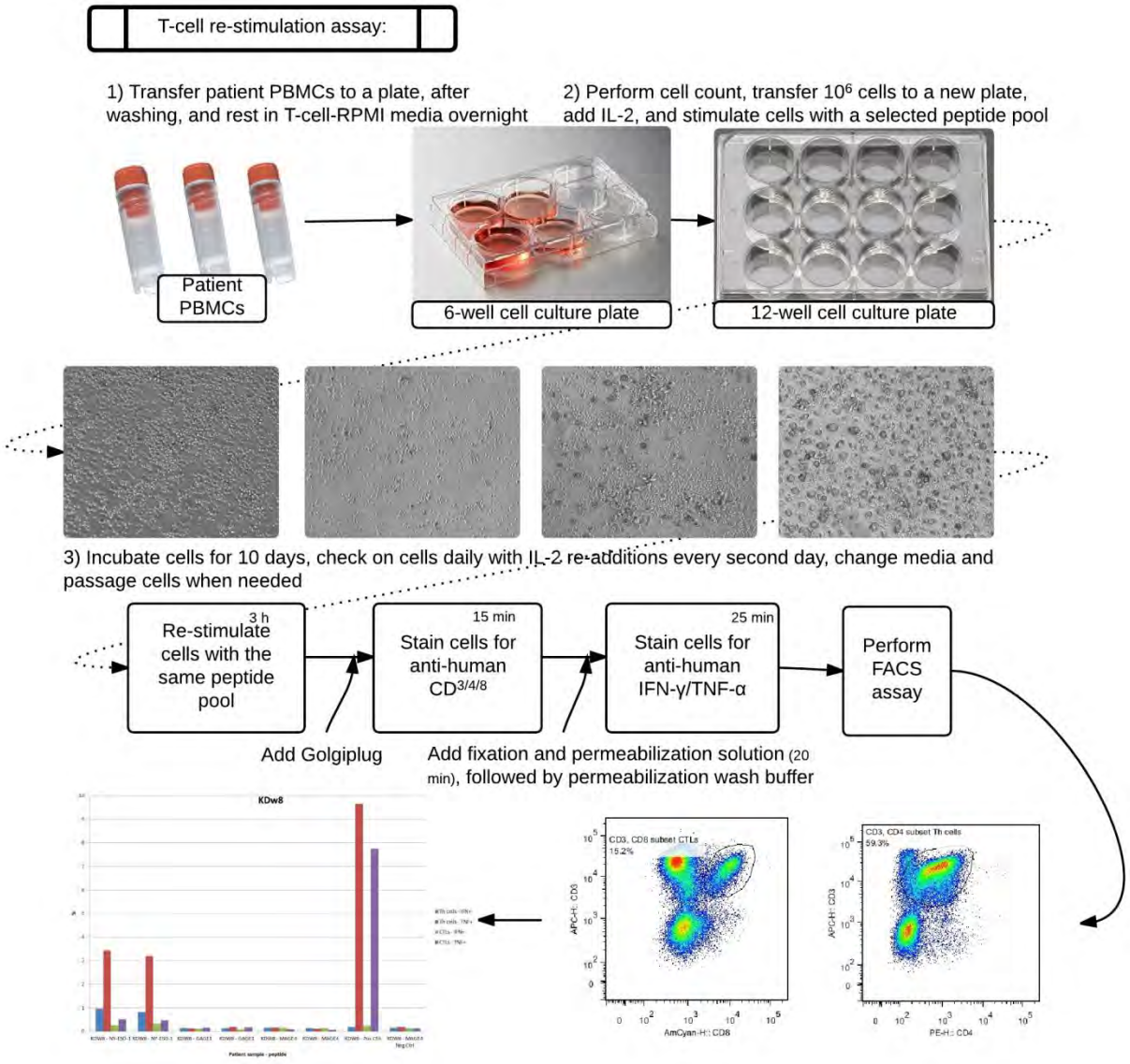

As a means of performing fluorophore calibration for FACS, a stain control plate was also prepared. 100 µL of stain control cells – unstimulated and unstained patient PBMCs – were added to respective wells (according to the number of individual stains that require calibration) in a 96-well U-bottom shaped plate, followed by 100 µL of PBS. This plate was then centrifuged at 500 x *g* for 5 min at 4 °C, decanted and shaken as mentioned above. 50 or 150 µL (depending on the antibody dilution) of PBS, followed by 1 µL of each stain, was added to each respective well (no stain, APC, V450, AmCyan, FITC, PE-Cy7), and the plate was incubated in a dark fridge for 15 min. 150 or 50 µL of PBS was added to each well, and the plate was then centrifuged, decanted and shaken, as indicated above. Finally, pellets were resuspended in either 100 µL of PBS or 4% PFA, and the plate was wrapped in foil and stored in a dark fridge at 4 °C until the FACS assay.

4.2.2.2 T-cell re-stimulation assay image capture

Throughout the T-cell re-stimulation assay, cell images were captured every second day using an Olympus IX81 Motorized Inverted Microscope. The objective here was to record the evolution of cell responses towards the specific stimulus, and to measure how these differ between and within patients and among stimuli.

4.2.2.3 Fluorescent activated cell sorting analysis

Prior to analysing our stimulated patient T-cells, instrument setup was required, which entailed fluorophore compensation and voltage optimization steps.

The previously prepared stain plate was assayed first using the BD FACSCanto II instrument and associated BD FACSDiva software, after the fluidics start-up was performed. This plate was collected from the fridge, shaken at 500 rpm for approximately 15 s, and placed on the plate holder after confirming that pellets had completely dissociated. The instrument's front and side doors were closed, and the experimental plan and plate layout was setup as required. The fluorophores used were specified and the corresponding antibody was indicated (APC: CD3, V450: CD4, AmCyan: CD8, FITC: IFN-γ, PE-Cy7: TNF-α) to allow for specific scatter plots to be constructed. The loading settings selected for the setup unstained control are indicated below in Table 4.1.

Table 4.1 FACS loading settings used for analysis of the setup unstained control.

Sample flow rate	0.5 µL/s
Sample volume	80 µL
Mixing volume	40 µL
Mixing speed	180 µL/s
Number of mixes	5
Wash volume	400 µL
Events to record	2500000
Throughput mode	standard

All other controls and sample wells were assayed using different settings, as indicated in Table 4.2.

Table 4.2 FACS loading settings used for analysis of each control and sample.

Sample flow rate	2.0 µL/s
Sample volume	80 µL
Mixing volume	40 µL
Mixing speed	200 µL/s
Number of mixes	5
Wash volume	200 µL
Events to record	2500000
Throughput mode	standard

On the global sheet, our intended scatter plots were constructed (SSC-A vs. FSC-A: population 1 of T-cells, CD3-APC-H vs. CD4-V450-H: population 2 of $CD3^+$ and $CD4^+$ helper T-cells, CD3-APC-H vs. CD8-AmCyan-H: population 3 of $CD3^+$ and $CD8^+$ cytotoxic T lymphocytes; IFN-γ-FITC-H vs. TNF-α-PE-Cy7-H: for both populations 2 and 3). The setup unstained control was run, and voltage optimization was carried out, which entailed adjusting each fluorophore's voltage until complete bell curves were seen below the 10^3 threshold. Next, the individual stained control wells were run, which would allow for compensation to be performed during data extraction and analysis.

The patient stimulated T-cells assay plate was collected and shaken, and a new experimental plan and plate layout was created indicating patient and peptide-specific relevant information. The fluorophore and loading settings were maintained, as well as the global sheet and scatter plots. The negative control wells, which did not undergo secondary stimulation, were assayed first for each patient sample, followed by the positive controls and all sample wells. Once the run was complete both plates were discarded, and the resulting data was exported as .fcs files to a selected destination folder. An HTS clean was performed using a cleaning plate containing a FACS clean solution (BD Biosciences, 5L, #340345) and Millipore water, followed by a fluidics shut down. Sheath fluid (BD Biosciences, 2L, #342003) was refilled and waste was emptied accordingly.

4.2.2.4 FACS data extraction, processing and analysis

FlowJo (version 7.6.5, LLC), the leading flow cytometry data viewer and analysis software, was used for the resulting data extraction, processing and analysis. The above-mentioned resulting data was dragged onto FlowJo, and the column heading was adjusted to include all relevant parameters, such as samples IDs. Before proceeding, fluorophore compensation was required, which entailed selecting each

individual stain, and creating two separate range gates for the negative and positive peaks. Once this was done for each stain, the compensation editor was opened, and the specific negative and positive subsets were selected, and this compensation was applied to all samples, to account for any possible peak overlap or proximity that might have occurred.

For each patient-specific negative control, a SSC-A vs. FSC-A graph was viewed and the T-cell population cluster was gated and defined. Within that population, a CD3-APC-H vs. CD4-V450-H graph was viewed, and the helper T-cell population located in the upper right quadrant ($CD3^+$ and $CD4^+$ cells) was selected, and within it both the CD4-V450-H vs. IFN-γ-FITC and the CD4-V450-H vs. TNF-α-PE-Cy7-H graphs were viewed. A gate was created close to the right of each viewed cluster, as a means of defining a baseline level prior to stimulation. This process was also conducted for the cytotoxic T lymphocyte population, a CD3-APC-H vs. CD8-AmCyan-H graph, located within the T-cell original population and also in the upper right quadrant ($CD3^+$ and $CD8^+$ cells). This gating was applied to all samples of this specific patient, and repeated accordingly for each distinct patient. Once this was done, it was then possible to visualize a percentage relative to baseline of increased T-cell response across all samples.

The resulting data could then be exported to Microsoft Excel for further analysis, using the table editor function while defining the relevant columns of interest, and the FlowJo worksheet was saved for potential re-analysis or storage purposes. Each resulting Excel spreadsheet per assay plate was further analysed and graphed using standard graphing and statistical tools.

4.3 Results and discussion

Serum or plasma samples from each treatment cohort, along with the 3 additional quality control standards (c-Myc, healthy control pool, cancer control pool), were assayed using the $CT100^+$ microarray platform as discussed in Section 4.2.1. The resulting arrays were scanned and extrapolated accordingly, after which the raw data was processed, filtered and normalized using our bioinformatic tool, the $CT100^+$.jar. The results presented in this Chapter have undergone a strict downstream analysis pipeline, thus permitting confidence when comparing autoantibody levels of a given patient towards a specific antigen at different time points.

In regards to the settings used, the selected specific whole array filtering control (5/10/15 ng/µL Cy5-biotin-BSA) might differ between cohorts, as well as the whole array CV threshold (between 20 and 25%), but consistent settings were used within any given cohort. Besides from the standard user-defined noise threshold (nSD of Background), an additional threshold stipulated as the median of all negative controls per array (usually below 1000 RFU) was measured for each assay, and autoantibody intensities were only considered if above this value. Repeats were conducted as needed, after which each

complete cohort was analysed, to allow for data interpretation to occur. The resulting data is indicated below for each treatment cohort. It is essential to note that as each treatment type, cohort size, sample numbers and clinical information availability is distinct, the data analysis process differed for each group.

Furthermore, when the term 'immune response' is used, it refers to either an autoantibody (protein array generated) or a T-cell (T-cell assays generated) response, without the implication of an associated clinical response. Similarly, the term 'clinical response' is only used when significant evidence indicates that clinical benefit was achieved, usually determined by RECIST measurements. Understanding antibody production in a cancer setting is extremely complex, and thus any preliminary evidence indicating that these titres may reflect immune responses that are important in controlling cancer progression or regression is merely speculative, warranting further larger focused studies. Patient titres may be affected by a large amount of variables, such as age, clinical interventions or treatment-related adverse events, which cannot be controlled in a retrospective analysis of this sort.

4.3.1 Malignant melanoma patients who underwent kinase inhibitor-based treatments

A total of 96 serum samples, corresponding to thirty-six malignant melanoma patients before and several time points after kinase inhibitor treatment, were assayed, processed and analysed according to our pre-established $CT100^+$ microarray pipeline. The following settings were used for the $CT100^+$.jar processing and filtering steps: mean or median values = mean, noise threshold = 2 standard deviations of the background, replicate CV threshold = 20%, whole array filtering control = 15 ng/µL Cy5-biotin-BSA and whole array CV threshold = 23%. The initial stipulated research question was whether the observed autoantibody responses correlated with the reported clinical responses, based on tumour size evolution for the kinase inhibitor treatment in question. For this cohort, data analysis was conducted according to the available clinical information, which permitted the attribution of a disease status per time point, allowing for an optimal direct comparison between the patient's clinical and immune responses towards treatment. Furthermore, based on sample number-based power calculations indicated in Chapter 2, this cohort includes sufficient patient and sample numbers to be able to report statistically relevant results (power = 0.83). A significant (> 1000 RFU) autoantibody response to treatment (increase in autoantibody titres above baseline) was present in all patients (*n* = 36/36, 100%), in at least one titre for at least one time point after treatment. However, when considering the overall complete array profile, it was evident that whilst some autoantibody responses were seen for some cases, others were not, with some profiles showing either a stable or decreasing response. Furthermore, within the same patient and across multiple time points, different responses were also seen over time, with many cases of patients

showing an initial response to treatment, but then a later lack of response. The strongest increase in autoimmune response (~120000 RFU) was seen for patient WMD-015 (see Fig. 4.4).

Figure 4.4: Strongest increase in autoimmune response of the kinase inhibition treatment cohort. This graph indicates the autoimmune profile of patient WMD-015 across four distinct time points (represented by different colours). As a means of clarifying the visualization of relevant titres, an insert of the magnified relevant data is indicated within this figure. *Statistically significant difference, $P < 0.05$ or **$P < 0.01$. D0: day 0; PR: partial response.

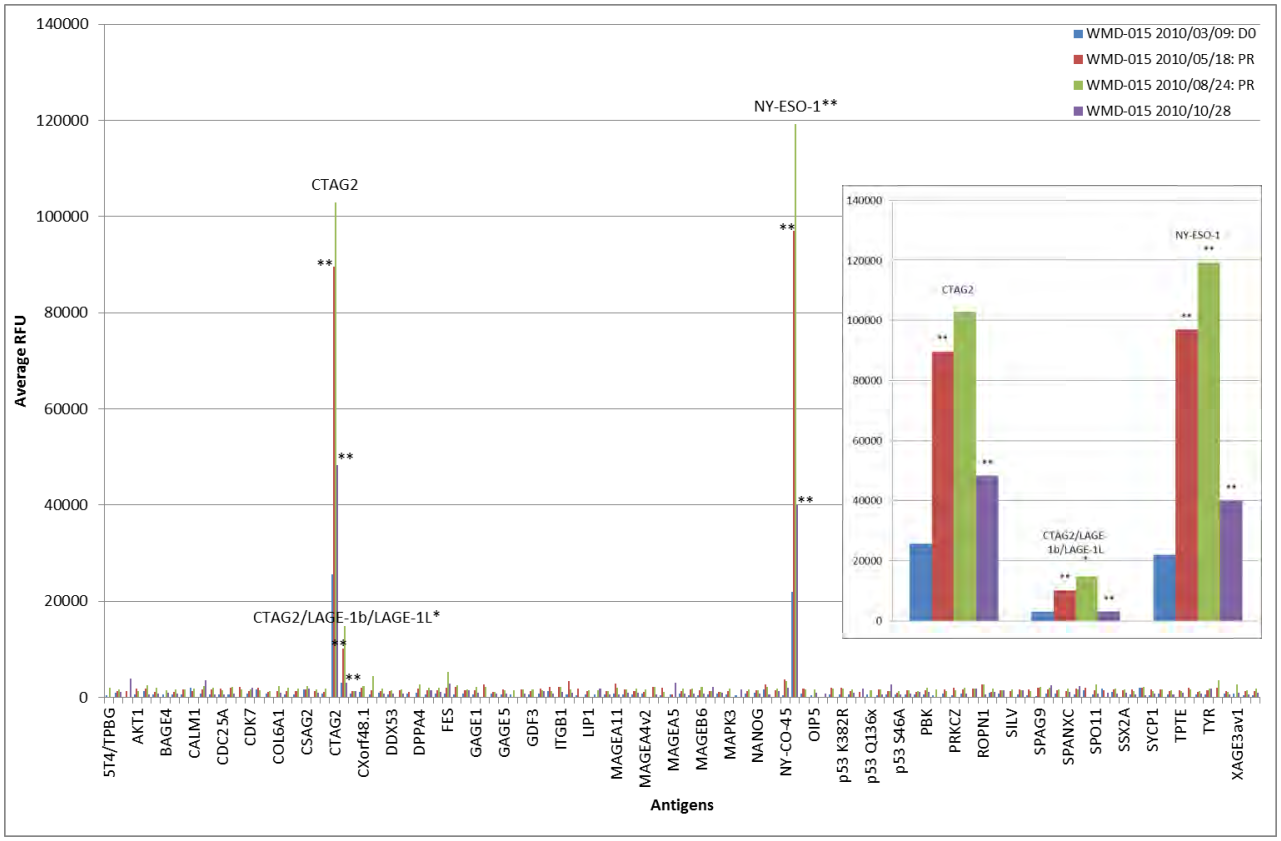

Patient WMD-015, a 24 year old female with malignant melanoma undergoing a combination of BRAF + MEK treatment, showed a statistically significant increase from baseline (D0) to the first post-treatment time point (2010/05/18) for CTAG2 (from ~26000 RFU to ~90000 RFU, $P < 0.01$), CTAG2/LAGE-1b/LAGE-1L (from ~3000 RFU to ~10000 RFU, $P < 0.01$) and NY-ESO-1 (from ~22000 RFU to ~97000 RFU, $P < 0.01$). An additional increase is also seen when comparing the latter time point to the second post-treatment time point (2010/08/24) for CTAG2/LAGE-1b/LAGE-1L (from ~10000 RFU to ~15000 RFU, $P < 0.05$) and NY-ESO-1 (from ~97000 RFU to ~119000 RFU, $P < 0.01$). Although autoantibody titres are also increasing for CTAG2 from ~90000 RFU to ~103000 RFU), this difference is not statistically significant. After these consistently gradual increases from time points 1 to 3, when comparing the latter with the third and

final post-treatment time point for this patient (2010/10/28), it was evident that CTAG2, its isoform, and NY-ESO-1 all showed a statistically significant ($P < 0.01$) decrease in immune response (B-cell responses). It is also worth mentioning that these three antigens, all members of the CT antigen family, are quite homologous, with NY-ESO-1 (also referred to as CTAG1) and CTAG2 sharing 77% of sequence homology, and CTAG2/LAGE-1b/LAGE-1L being an isoform of the latter. This indicates that a shared epitope amongst the three might be the potential location of the responsible antigen/antibody binding site.

By comparing the observed autoimmune profile for this patient with her matching temporal disease statuses, as a means of verifying if these responses were possibly indicative of temporal clinical responses (tumour size regression and patient clinical improvement), interpretation of this profile became possibly interesting. It appeared that in both instances where an immune response was present based on statistically significant increases in autoantibody titres, preliminary evidence of a clinical partial response was also seen. Specifically, from baseline to post-treatment time points 1 and 2, tumour size continuously decreased by 73%, which is certainly a very beneficial clinical response. When attempting to verify if disease progression occurred when this immune response was significantly decreasing, from post-treatment time point 2 to 3, this patient was indicated to have disease progression one day after the latter time point (2010/08/25), although no tumour size details were available. Therefore, once again, preliminary evidence of a matching decrease in immune response and lack of clinical response was seen. This patient was indicated to have an overall survival of ten months, having passed away three months after the last measured time point, potentially indicating that the drop in immune response may be as significant as the earlier increase and that disease progression may be correlated with this decline in immune response. These findings indicate that, for this particular patient, the time line of array measured immune responses show preliminary evidence of matching clinical responses, which may be of great importance. This early evidence suggests the possibility that our array data may serve as a rapid, non-invasive means to determine overall response, both immunological and clinical, as a result to treatment.

As a means to verify what was occurring in patients without positive immune responses to treatment, the strongest decrease in autoimmune response was assessed and seen for patient WMD-022 (see Fig. 4.5).

Figure 4.5: Strongest decrease in autoimmune response of the kinase inhibition treatment cohort. This graph indicates the autoimmune profile of patient WMD-022 across two distinct time points (represented by different colours). As a means of clarifying the visualization of relevant titres, an insert of the magnified relevant data is indicated within this figure. *Statistically significant difference, $P < 0.05$ or **$P < 0.01$. D0: day 0; PD: progressive disease.

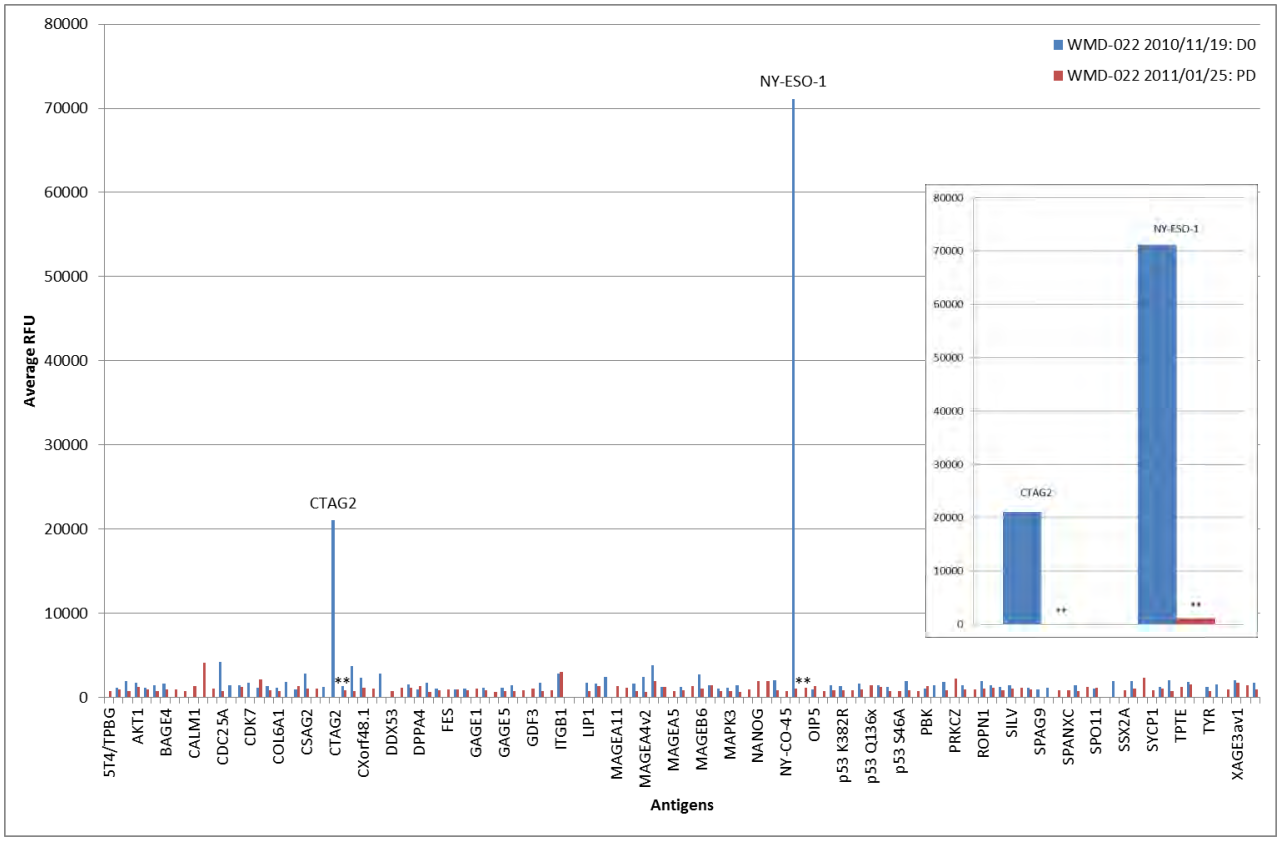

Patient WMD-022, a 41 year old male with malignant melanoma also undergoing a combination of BRAF + MEK treatment, showed a statistically significant decrease from baseline (D0) to the post-treatment time point (2011/01/25) for CTAG2 (from ~21000 RFU to 0 RFU, $P < 0.01$) and NY-ESO-1 (from ~71000 RFU to ~1100 RFU, $P < 0.01$).

When comparing the observed autoimmune profile for this patient with his matching temporal disease status, as a means of assessing whether there was preliminary evidence of a matching clinical response, it appeared that the lack of an immune response, statistically significant decrease in autoantibody titres, showed evidence of a matching clinical disease progression. Specifically, from baseline to post-treatment, tumour size increased by 10%, which may indicate no clinical efficacy of this treatment for this particular patient. This patient was indicated to have an overall survival of only three months, having passed away one month after the last measured time point, potentially indicating that the drop in immune response was gradual, and that disease progression may be correlated with this lack of an

immune response. Contrary to what occurred for patient WMD-015, this patient had no evident response to kinase inhibition treatment, with no signs of even an initial increase in autoantibody titres, potentially indicating some sort of immune suppression or resistance, warranting further investigation. Once again, patient WMD-022 showed preliminary evidence that the lack of an array measured immune response may indicate the lack of a clinical response, consistent with our initial early evidence mentioned above.

Of the 123 cancer-associated antigens present on our CT100^{+} array, the most prevalent significant autoantibody titres (above 1000 RFU) detected in this cohort were towards 19 leading antigens. These were detected in at least twenty-three or more instances across all patient time points (baseline or post-treatment) in this cohort, and most abundantly towards NY-ESO-1 and MAGEB1, as indicated below in Fig. 4.6.

Figure 4.6: Most prevalent autoantibody titres detected across the kinase inhibition treatment cohort. This graph indicates the summed number of times autoantibody levels were detected towards the 19 leading antigens at titres above 1000 RFU, with distinction between D0: day 0 and Dn: post-treatment (pooled post-treatment time points).

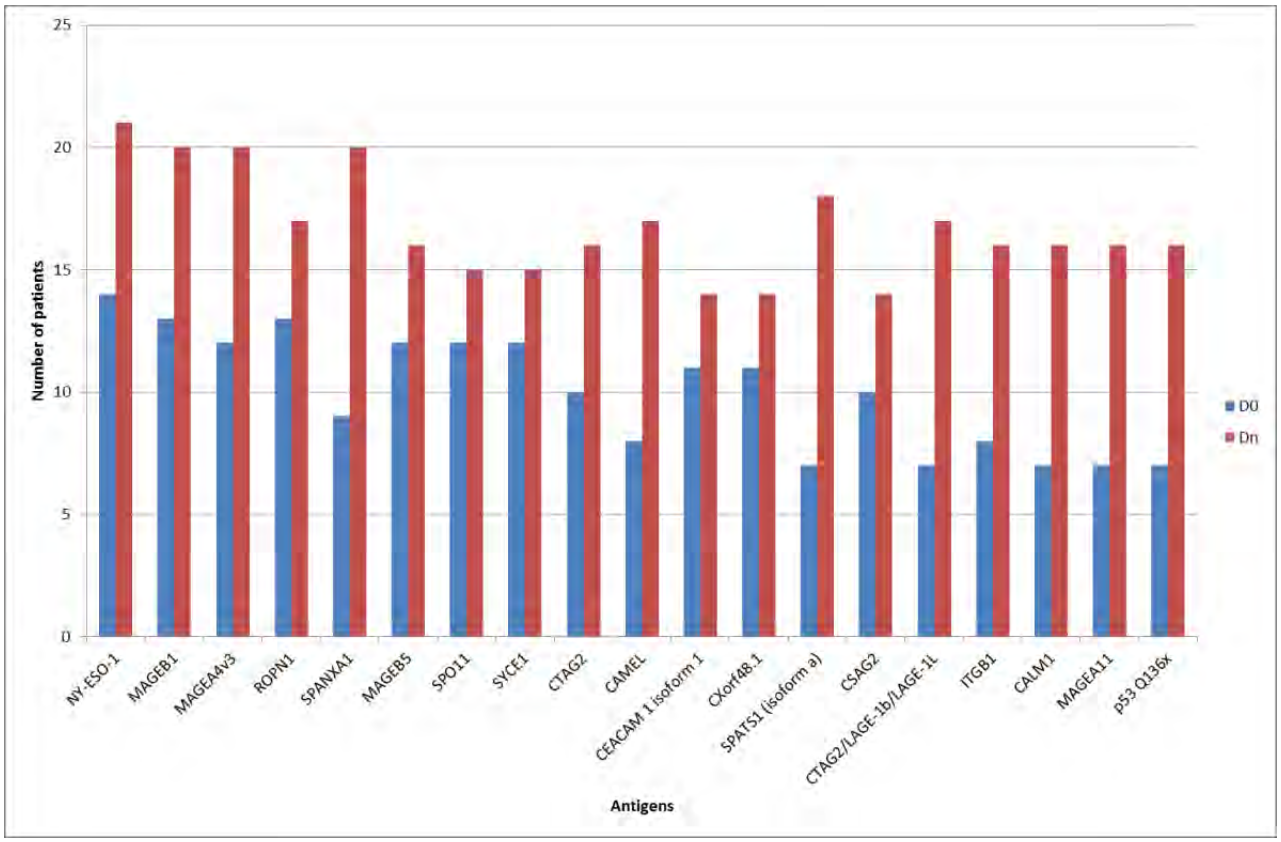

Based on this graph, it was evident that initially, when comparing baseline to post-treatment time points, all prevalent autoantibody responses towards these leading antigens were increasing (*n* = 19/19, 100%), suggesting that if preliminary evidence of matching clinical responses are seen, these antigens may somehow be involved in this response. Along with the most abundant autoantibody responses to the NY-ESO-1 antigen, fellow CT antigen members are amongst this set, including high sequence homologous CTAG antigens CTAG2, CTAG2/LAGE-1b/CTAG2-1L and CAMEL, melanoma (cancer type of this cohort) antigen (MAGE) family members, MAGEB1, MAGEA4v3, MAGEB5 and MAGEA11, as well as ROPN1, SPANXA1, SPO11, SYCE1 and CXorf48.1 (CTdatabase: www.cta.lncc.br). The remaining four antigens were either non-CT antigens, CEACAM 1 Isoform 1, SPATS1 (isoform a), CSAG2 and ITGB1, protein kinases, CALM1, or p53 mutants, p53 Q136X (www.uniprot.com).

NY-ESO-1, also known as CT antigen 1, is a member of the CT antigen family, antigens with restricted expression to cancer tissue and limited expression to normal tissue (placenta and testis), with potential uses as cancer immunotherapeutic targets (Simpson et al. 2005; Caballero & Chen 2009; Scanlan et al. 2002). Being an extremely attractive immunotherapeutic target overexpressed across a wide range of distinct cancers, NY-ESO-1 has been tested as a cancer therapeutic in a variety of clinical trials in a variety of cancer types, including melanoma (Scanlan et al. 2002; Cebon 2010; Nicholaou et al. 2006). Furthermore, studies have reported associations with clinicopathological parameters such as tumour thickness and metastasis (Scanlan et al. 2002; Li et al. 2005). When focussing on our research question, studies have shown that NY-ESO-1 expression has been associated with NY-ESO-1^{+} tumours and even disease evolution in malignant melanoma patients (Stockert et al. 1998; Jäger et al. 1999). With this in mind, the available data for NY-ESO-1 across all patients was inspected, and those patients exhibiting a relevant (> 1000 RFU) signal were as indicated below in Fig. 4.7. This data was isolated from the general array data, which included technical triplicates for each antigen and biological replicates for a subset of patients. However, it is essential to note that the latter were not true biological replicates, as patients differ genetically, and in disease status and progression.

Figure 4.7: Anti-NY-ESO-1 immunoglobulin titres across relevant patients in the kinase inhibition treatment cohort. This graph indicates anti-NY-ESO-1 immunoglobulin titres across all patients and time points, highlighting those with statistical significance. D0: day 0; PR: partial response. D0: day 0, PR: partial response, PD: progressive disease, SD: stable disease. *Statistically significant difference, $P < 0.05$ or **$P < 0.01$.

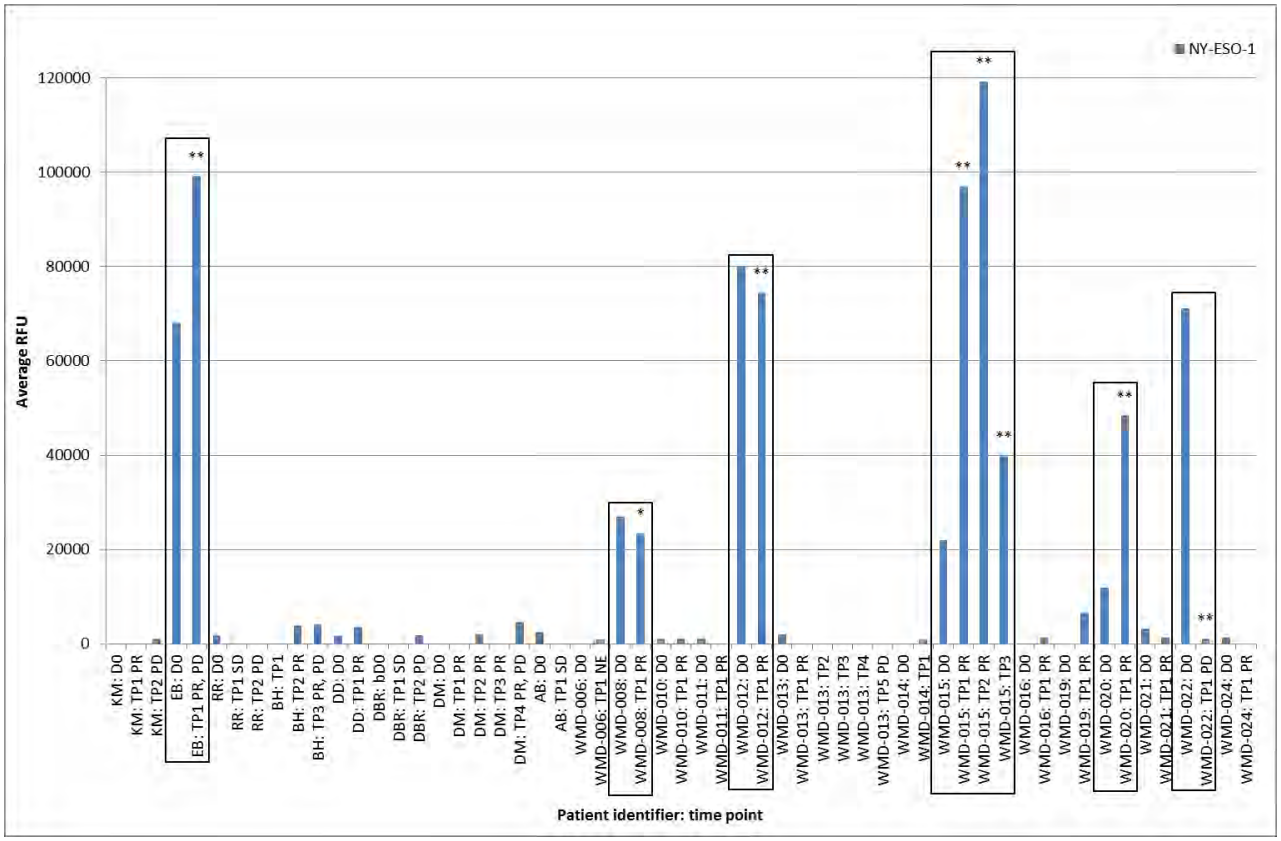

It was apparent that 22/36 (61%) patients showed relevant signals towards NY-ESO-1, without any particular exclusivity for a disease status (PR, PD and SD). Amongst these, six patients showed signals above 20000 RFU, and these were patients EB, WMD-008, WMD-012, WMD-015 and WMD-020. Patients EB, WMD-015 and WMD-020, all showed statistically significant increasing autoantibody titres with preliminary evidence of possible matching partial response temporal disease statuses, based on tumour size reductions of 16%, 73% and 35%, respectively, whilst patient WMD-022 showed a statistically significant decrease in autoantibody titres with equal evidence of possible matching progressive disease temporal status, based on a tumour size increase of 11%. However, although the remaining patients WMD-008 and WMD-012 showed a slight but still significant decrease in autoantibody titres, their partial response temporal disease statuses did not correlate, based on tumour size reductions of 22% and 14%, respectively. This might indicate that the autoantibody titres towards a single antigen may not be enough to possibly infer clinical efficacy of a specific treatment. Alternatively, it may indicate that slight increases or decreases in autoantibody titres may not be sufficient to

potentially infer matching clinical responses, but rather much larger significant difference are required, indicating a better estimation inference with smaller P-values.

MAGEB1, another member of the CT antigen family also known as melanoma-associated antigen B1, is a MAGE protein, as mentioned above, with known tumour antigen molecular function (www.uniprot.com). The MAGE antigens are known to bind to and activate RING E3 ubiquitin ligases, and studies have shown that MAGEB1 was expressed in a variety of cancer types, with evidence of spontaneous humoral responses (CT antigen database: www.cta.lncc.br). This cancer-specific expression has led to several studies which have identified MAGE family members as potential therapeutic targets and diagnostic markers, as well as prognosis markers (Scarcella et al. 1999; Germano et al. 2012). Therefore, similarly to NY-ESO-1, MAGE members have been highly considered as potential immunotherapeutic against melanoma, and several clinical trials have and continue to test its clinical efficiency, with many showing beneficial patient clinical responses (Marchand et al. 1999; Thurner et al. 1999). With this in mind, the available data for MAGEB1 across all patients was inspected, and those patients exhibiting a relevant (> 1000 RFU) signal were analysed as indicated below in Fig. 4.8.

Figure 4.8: Anti-MAGEB1 immunoglobulin titres across relevant patients in the kinase inhibition treatment cohort. This graph indicates anti-MAGEB1 immunoglobulin titres across all patients and time points, highlighting those with statistical significance. D0: day 0, SD: stable disease, PD: progressive disease, PR: partial response. **Statistically significant difference, P < 0.01.

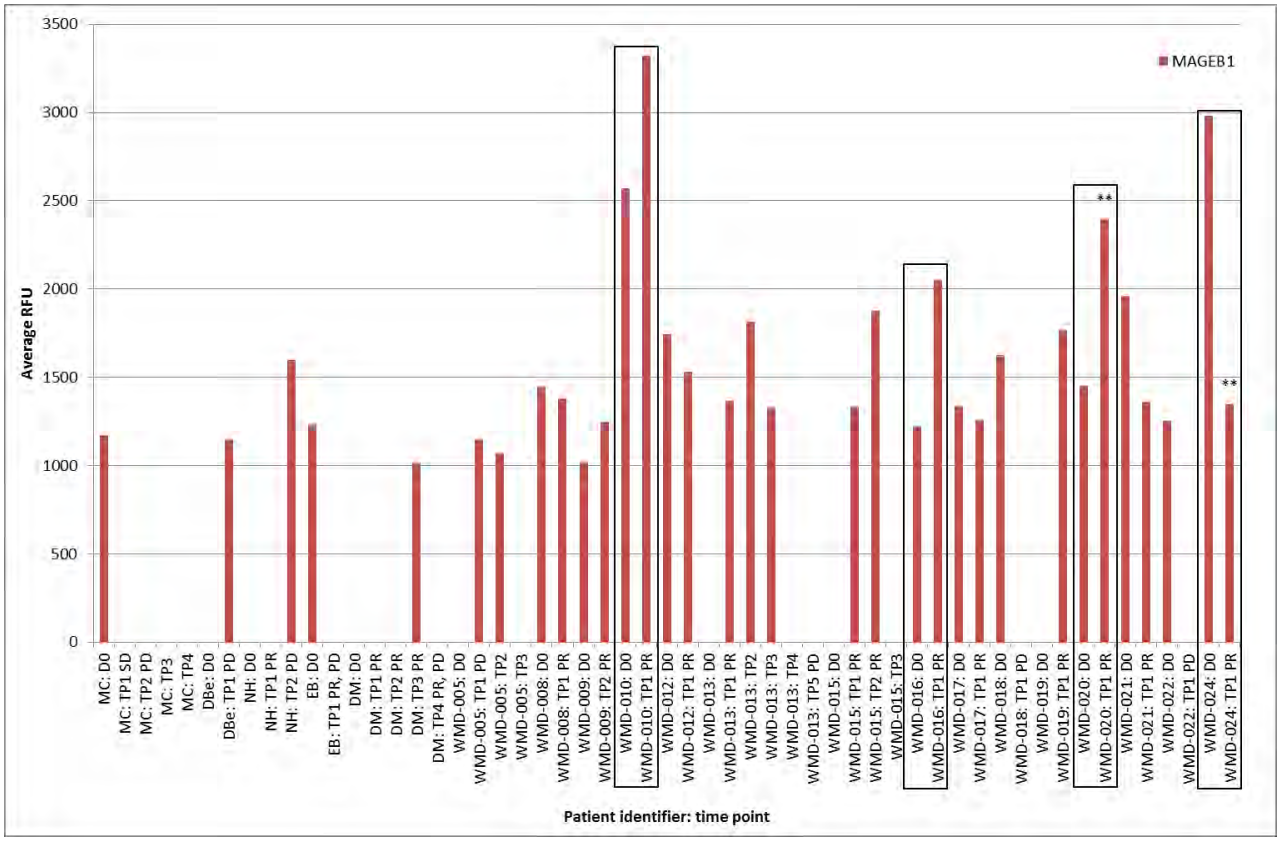

It was apparent that 20/36 (56%) patients showed relevant signals towards MAGEB1, without any particular exclusivity for a disease status (PR, PD and SD). Amongst these, four patients showed signals above 2000 RFU, and these were patients WMD-010, WMD-016, WMD-020 and WMD-024. Patient WMD-020 showed a statistically significant (P < 0.01) increasing autoantibody titre with preliminary evidence of possible matching partial response temporal disease statuses, based on a tumour size reduction of 35%, whilst patient WMD-024 showed a statistically significant (P < 0.01) decrease in autoantibody titres with evidence of a non-matching partial response temporal status, based on a tumour size decrease of 50%. In regards to patients WMD-010 and WMD-016, although both of these showed increasing autoantibody titres with early evidence of matching partial response temporal disease statuses, these differences were not statistically significant. Hence, we estimate that autoantibody titres towards multiple antigens may need to be taken into consideration when attempting to speculate about possible clinical inference, as some statistically significant increases or decreases in autoantibody titres may not necessarily show evidence of correlation with temporal clinical responses, whilst others may.

Both NY-ESO-1 and MAGEB1 have been highly cited in the literature, with both antigens currently being tested as potential cancer immunotherapeutics, implying the potential utility of our findings in this particular cohort for patient stratification in a new therapeutic trial. These findings further indicate that this array platform may be a useful new tool with which to identify novel cancer therapy targets across a variety of cancer types.

Based on these findings and the potential biological significance of our array platform, the complete cohort was assessed further to verify if potential clinical efficacy could be speculated across all patients. Formal statistics were conducted with GraphPad Prism (version 5.02), using a non-parametric 2-tailed T-test known as Mann-Whitney for patients with two time points, and a one way non-parametric ANOVA known as Friedman for patients with three or more time points. These tests, which were well suited for this data given a non-normal distribution and unequal variances, were done with the intent of assessing whether the observed patient time points were statistically significantly different from one another, as a means of allowing preliminary clinical assumptions to be made. In total, statically significant ($P < 0.05$) time points were present amongst twenty-nine patients (*n* = 29/36, 81%), with P-values varying between 0.0001 and 0.0230. When visually inspecting each patient's autoantibody profile and temporal disease statuses, eighteen patients (*n* = 18/34, 53%) showed evidence of a direct correlation between increase or decrease in autoantibody titres and presence or lack of clinical response, which indicated that for this subset clinical speculative inference could be made with basis on our immunological findings. Within the latter subset of possible visual correlation (*n* = 18/34, 53%), twelve of those patients (*n* = 12/18, 67%) had a corresponding statistical significance. For these twelve patients, the corresponding scatter plots across all antigens were combined and were indicated below in Fig. 4.9.

Figure 4.9: Scatter plots across relevant patients across the kinase inhibition treatment cohort. This figure indicates scatter plots for a selected subset of relevant patients, generated using GraphPad Prism, of the resulting statistical analysis using either a non-parametric 2-tailed T-test known as Mann-Whitney for patients with two time points, or a one way non-parametric ANOVA known as Friedman for patients with three or more time points. D0: day 0, SD: stable disease, PD: progressive disease, PR: partial response. Outliers have been removed to allow visual interpretation of this data.

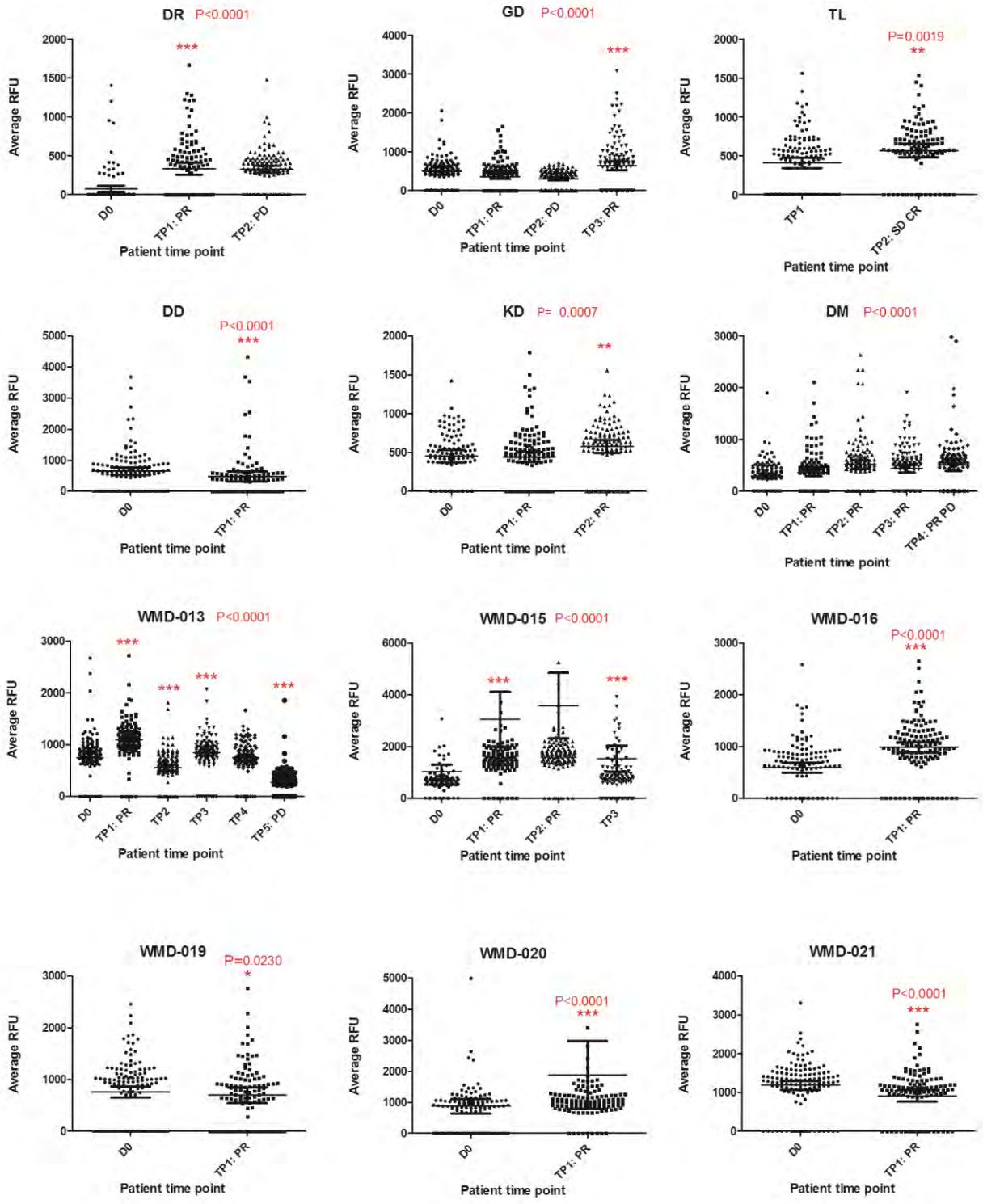

It is essential to note that the following 33 outliers have been automatically removed by the statistical method used to allow visual representation of the data: DR: MAGEA4v3 (2701 RFU, TP2); GD: MAGEA10 (4821 RFU, D0); TL: ACVR2B (2426 RFU, TP2), TKTL1 isoform a (2544 RFU, TP2), TSGA10 (2191 RFU, TP2); DD: CTAG2 (7000 RFU, TP1); KD: CT62 (2011 RFU, TP2), DDX53 (2735 RFU, D0), NXF2 (2692 RFU, TP2), p53Q136x (2331 RFU, TP2), SILV (2965 RFU, D0); DM: NY-ESO-1 (4716 RFU, TP4); WMD-013: cytochrome P450 3A4 (3885 RFU, TP1), TPTE (3252 RFU, TP1); WMD-015: CTAG2 (25628 RFU, D0; 89604 RFU, TP1; 102930 RFU, TP2; 48247 RFU, TP3), CTAG2/LAGE-1b/LAGE-1L (10109 RFU, TP1; 14771 RFU, TP2), NY-ESO-1 (22001 RFU, D0; 96965 RFU, TP1; 119280 RFU, TP2; 39954 RFU, TP3); WMD-016: ITGB1 (3209 RFU, D0); WMD-019: CTAG2 (4352 RFU, TP1), NY-ESO-1 (6578 RFU, TP1); WMD-020: CTAG2 (7181 RFU, D0; 50231 RFU, TP1), CTAG2/LAGE-1b/LAGE-1L (6116 RFU, TP1), NY-ESO-1 (11864 RFU, D0; 48442 RFU, TP1); WMD-021: TKTL1 isoform a (6445 RFU, TP1).

Based on the scatter plots indicated above, it was evident that across the majority of patients when a partial response is obtained, autoantibody titres are grouped above the previous time point, and when progressive disease is occurring, autoantibody titres are grouped below the previous time point, consistent with our preliminary observations described above. Furthermore, although 67% of the patients with evidence of a potential visual correlation had a statistically valid one, when comparing these to the complete patient cohort, only twelve out of thirty-four patients (two patients were lacking temporal disease statuses) (*n* = 12/34, 35%) presented with an autoimmune profile that could statistically significantly speculate a matching clinical response.

We have applied our CT antigen microarray platform to the investigation of autoantibody profiles in a cohort of metastatic malignant melanoma patients undergoing kinase inhibition, and observed a large number (81% of the cohort) of autoantibody responses – statistically significant changes in autoantibody titres – to treatment. The main intent of this study was to assess whether the induction of an autoantibody response may correlate with clinical improvements post-treatment amongst these patients, or whether other immunological features would provide preliminary evidence of correlation with a therapeutic response. In this regard, it is interesting that our CT antigen array data suggests preliminary evidence of a possible correlation between our observed autoantibody responses and the clinically reported ones across a subset of patients (35% of the cohort). The fact that this speculative finding is present across approximately a third of this complete cohort suggests that patient-specific autoantibody profiles may correlate with treatment responses. However, it appears plausible that other factors, which we have yet to determine, may be contributing towards this lack of suggested correlation amongst the remaining cohort. Such factors may include patient-specific differences amongst tumour-induced systemic immune suppression, common amongst patients presenting with advanced melanoma, as well as undesirable suppression of anti-tumour T-cell immunity by Tregs, amongst other common immune evasion mechanisms (Nicholaou et al. 2009). Additionally, it is plausible that several

melanoma-specific subtypes are present amongst these patients, and that the above-mentioned possible correlation may only be present across a given subtype, warranting additional genomic studies. This data also suggests preliminary evidence of immune suppression or resistance to therapy in individual patients post-treatment, evident by a drastic decrease in autoantibody titres after an initial evident increase in response to the first dosage of treatment. The possibility of detecting immune suppression or therapeutic resistance is of great interest in the therapeutic management of disease, and thus warrants further investigation.

In this kinase inhibition treatment cohort, we have successfully demonstrated that there are measurable differences in the autoantibody repertoires towards tumour-specific and –associated antigens between pre- and post-treated malignant melanoma patients, with preliminary evidence of possible correlation to the likelihood of clinical response. Furthermore, we have successfully identified well-established therapeutic targets – NY-ESO-1 and MAGEB1 – which were the two antigens towards which the most abundant autoantibody titres were detected amongst those tested, present across 61% and 56% patients, respectively. When considering patient sample numbers and relevant power calculations, although this cohort is quite diverse regarding patient demographics (age and gender) and treatments undergone (single vs. dual kinase inhibition treatment), the achieved statistical power is above recommended (power > 0.8), supporting the findings obtained in this cohort.

We therefore anticipate that our novel, quantitative, customizable CT antigen microarray platform may find usage in future cancer research in monitoring patient responses to treatment, identifying immune suppression and/or therapy resistance, and identifying novel therapeutic targets, warranting confirmation using a pre-stipulated specifically focussed study and homogeneous cohort design using sufficient patient numbers according to an *a priori* power calculation estimate.

As a means of verifying how well the above-mentioned autoantibody profiles correlate with T-cell responses in these same patients, T-cell assays were conducted amongst a subset of eight patients of this treatment cohort, across a matching timeline. These time points were temporally matched with the samples used for the array data, to allow for a direct comparison between temporal B- and T-cell data. Furthermore, the T-cell assay investigated IFN-γ and TNF-α cytokine release of helper T-cells and cytotoxic T-cells against NY-ESO-1 and MART-1/Melan-A.

For a selected T-cell assay which included patients AB and DM, images were captured microscopically across the 10-day cell re-stimulation, as a means of verifying morphologically visual changes towards treatment. It was rapidly evident that visual changes were quite evident amongst wells, which generally correlated to quantifiable T-cell responses to re-stimulation. Two distinct visual responses were seen, the first been a lack of visually evident morphological changes, as indicated below in Fig. 4.10.

Figure 4.10: Representative images depicting visually non-responding wells. This figure indicates four distinct microscope images captured after T-cell re-stimulation, showing no visual evidence of response defined by the lack of morphological changes after stimulation**.**

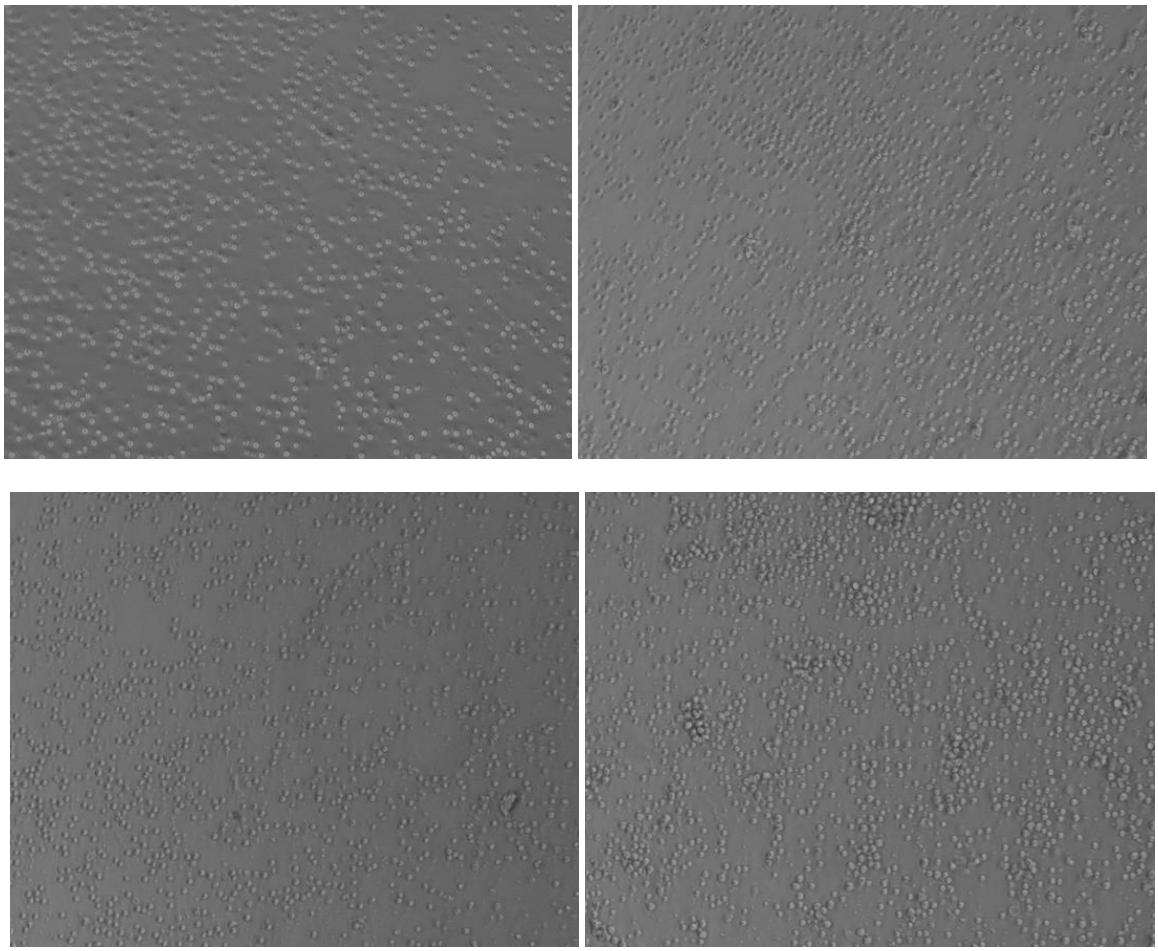

In the images indicated above, it was clear that the majority of the cells maintained a round healthy appearance throughout the 10-days of re-stimulation. These images were consistent with what was seen for each patient time point at day 0, prior to T-cell stimulation, indicating that a T-cell response was unlikely. On the contrary, the second type of visual responses seen was the clear presence of visually evident morphological changes, as indicated below in Fig. 4.11.

Figure 4.11: Representative images depicting visually responding wells. This figure indicates four distinct microscope images captured after T-cell re-stimulation, showing visual evidence of response defined by the presence morphological changes after stimulation. Red arrow: example of immature DC; Green arrow: example of maturing DC; Blue arrow: example of fibroblast.

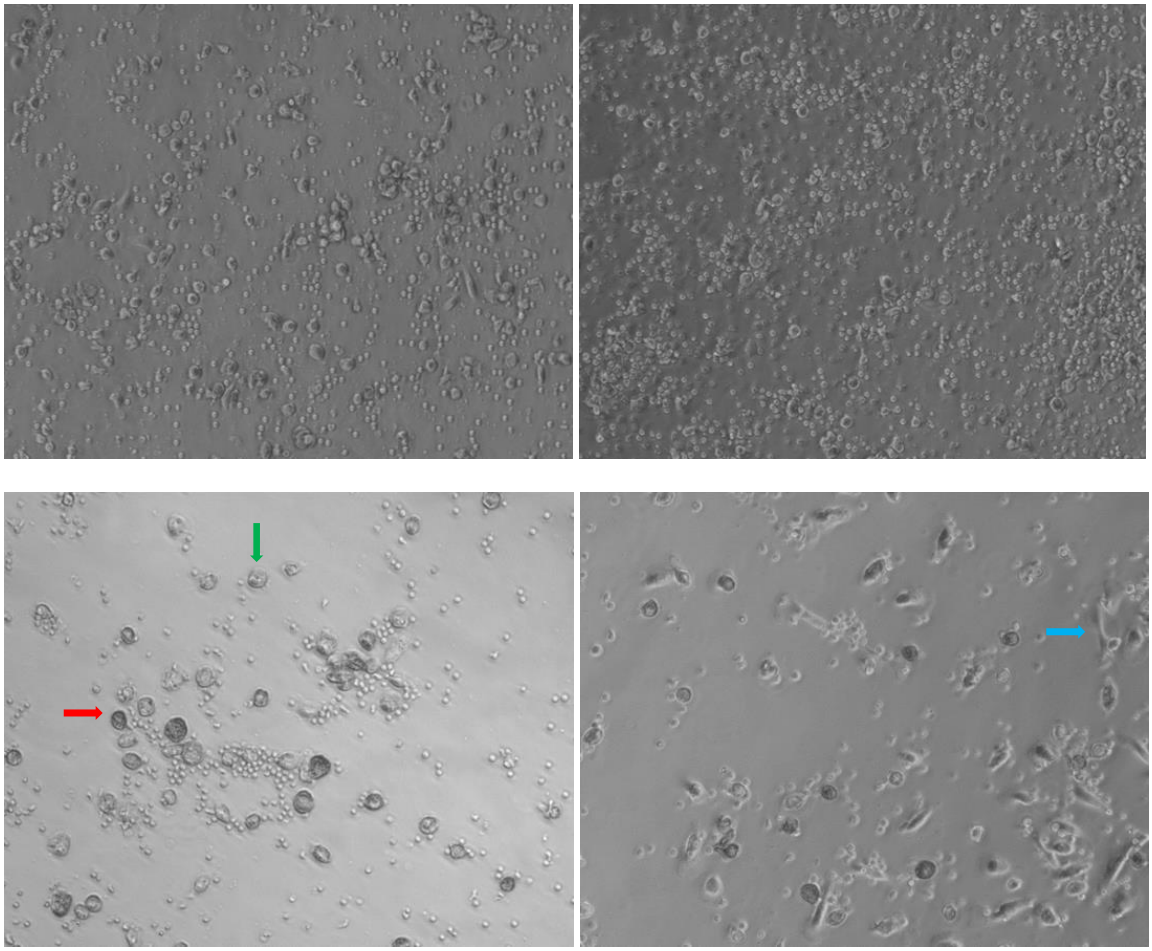

Amongst these images, it was evident that although healthy round cells were seen in high numbers, other cell types were also evident. These included the presence of DCs, immature and mature, and fibroblasts. These morphological changes were very distinct from the matching day pre-stimulation wells, and were generally indicative of a quantifiable T-cell response.

T-cell assays with NY-ESO-1 and MART-1/Melan-A were conducted across time lines for patients GD, TL, AB, DM, DD, EL, DBr and KD, using matching array tested temporal samples. The majority of the resulting FACS data was negligible, with patients TL, GD, DD and EL all showing T-cell responses below 1%. Of the remaining four patients showing responses above 1%, AB, DM, EL and KD, half of those (DM and KD) were amongst the statistically significant array profiles with preliminary evidence of clinical efficacy, and therefore, those data will be shown. Patient DM, a male malignant melanoma patient

undergoing BRAF +/- MEK, was assayed across three time points, day 0, week 28 (27/02/2013) and week 52 (17/07/2013), and the resulting data is indicated below in Fig. 4.12.

Figure 4.12: T-cell responses towards NY-ES0-1 and MART-1/Melan-A for patient DM at three distinct time points. Above: graph for NY-ESO-1; Below: graph for MART-1/Melan-A. Th cells: helper T-cells; CTLs: cytotoxic T-cells.

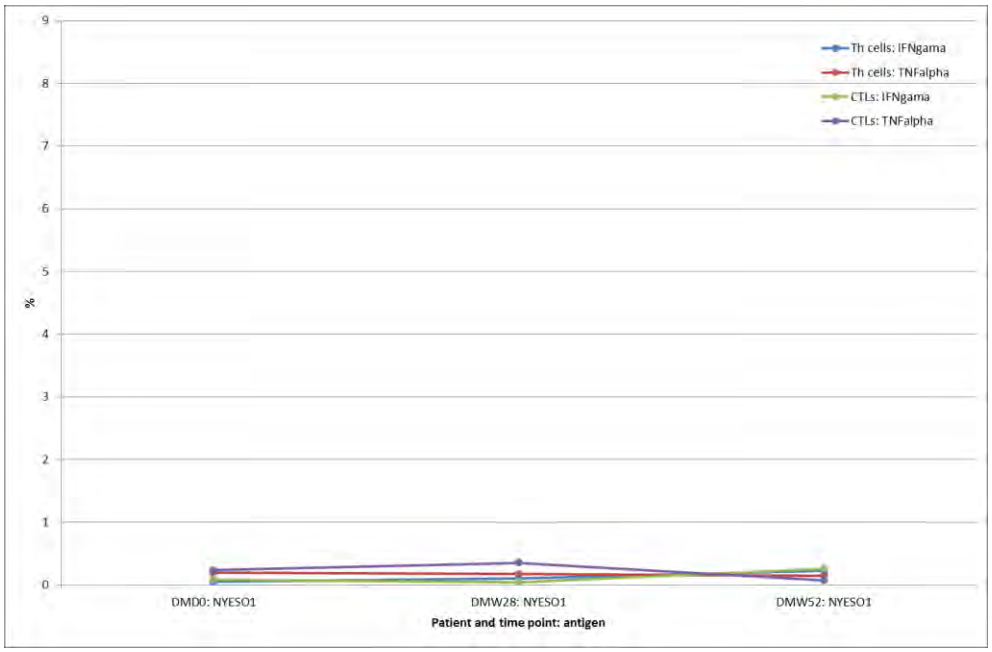

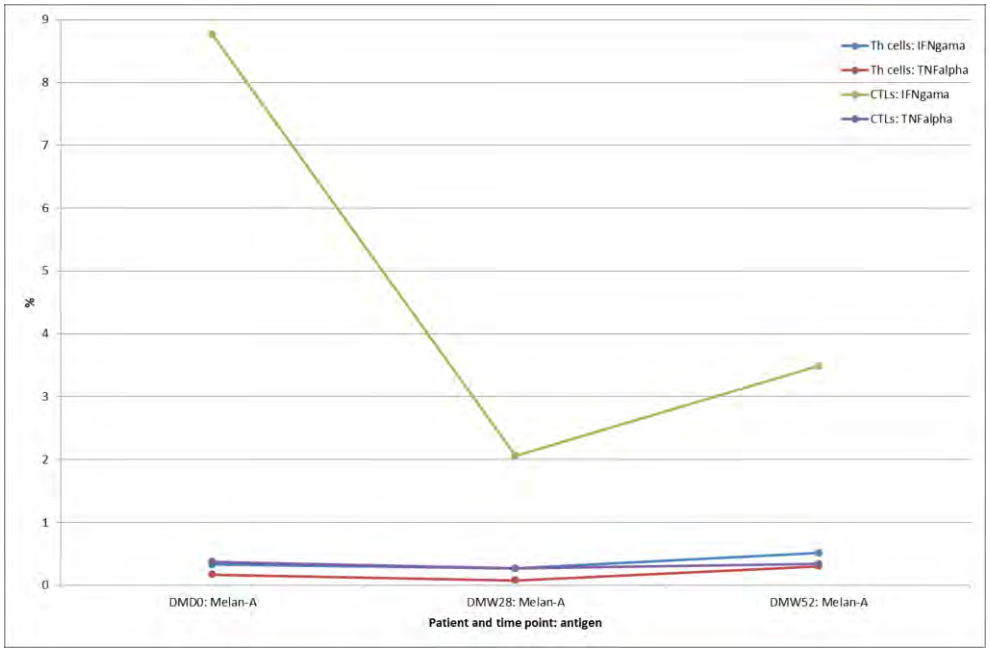

It was evident that all but one time point responses, IFN-γ^+ cytotoxic T-cells towards MART-1/Melan-A, were below 1%. This particular response initially declined from day 0 to week 28, and then increased

from week 28 to week 52. To further comprehend how these cells were responding, the relevant corresponding scatter plots and gating are indicated below in Fig. 4.13.

Figure 4.13: IFN-γ^{+} cytotoxic T-cells scatter plots and gating towards MART-1/Melan-A for patient DM at three distinct time points. Left: graph for day 0; Middle: graph for week 28; Right: graph for week 52. CTLs: cytotoxic T-cells.

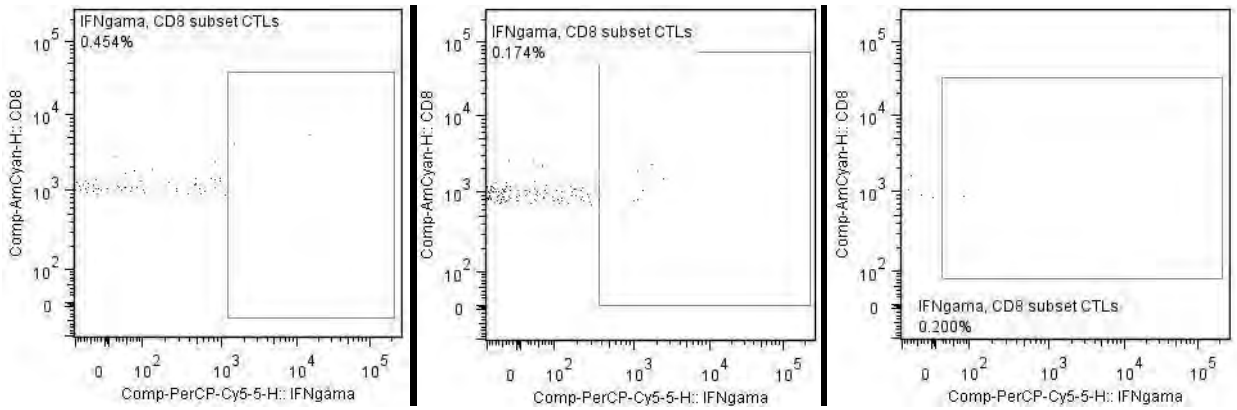

Based on the scatter plots indicated above, it was evident that very few cells were in fact responsible for the observed responses. When consulting the total percentage of cytotoxic T-cells relative to the complete T-cell population across this patient's time points, the obtained proportions were 6.71% at day 0, 7.01% at week 28, and 8.28% at week 52. As a means of verifying if this T-cell response correlated to an array generated B-cell response, the matching MART-1/Melan-A responses were assessed. This data showed baseline titres of ~400 RFU, below our significantly expressed threshold, which maintained stable at week 28, and then decreased to zero at week 52. When comparing these findings to the graph indicated above right in green, these did not match, indicating that in this instance a B-cell response was not indicative of a T-cell one. Moreover, when including the temporal disease status of a partial response at week 28, and progressive disease at week 52, the cytotoxic T-cells appeared to respond in a completely opposite manner, showing evidence of decreasing titres during a clinical response, and increasing titres during progressive disease. Therefore, specifically for patient DM, no preliminary evidence of a correlation was found between the generated B-cell, T-cell and clinical efficiency data.

Additionally, patient KD, a female malignant melanoma patient also undergoing BRAF +/- MEK, was assayed across three time points, day 0, week 8 (06/02/2013) and week 32 (23/07/2013), and the resulting data is indicated below in Fig. 4.14.

Figure 4.14: T-cell responses towards NY-ES0-1 and MART-1/Melan-A for patient KD at three distinct time points. Above: graph for NY-ESO-1; Below: graph for MART-1/Melan-A. Th cells: helper T-cells; CTLs: cytotoxic T-cells.

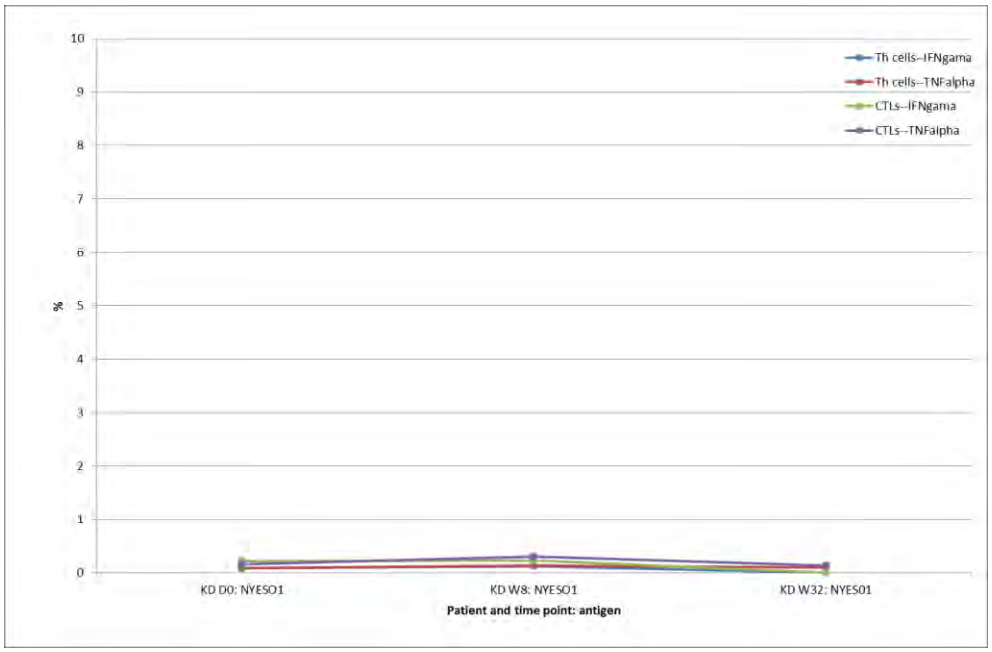

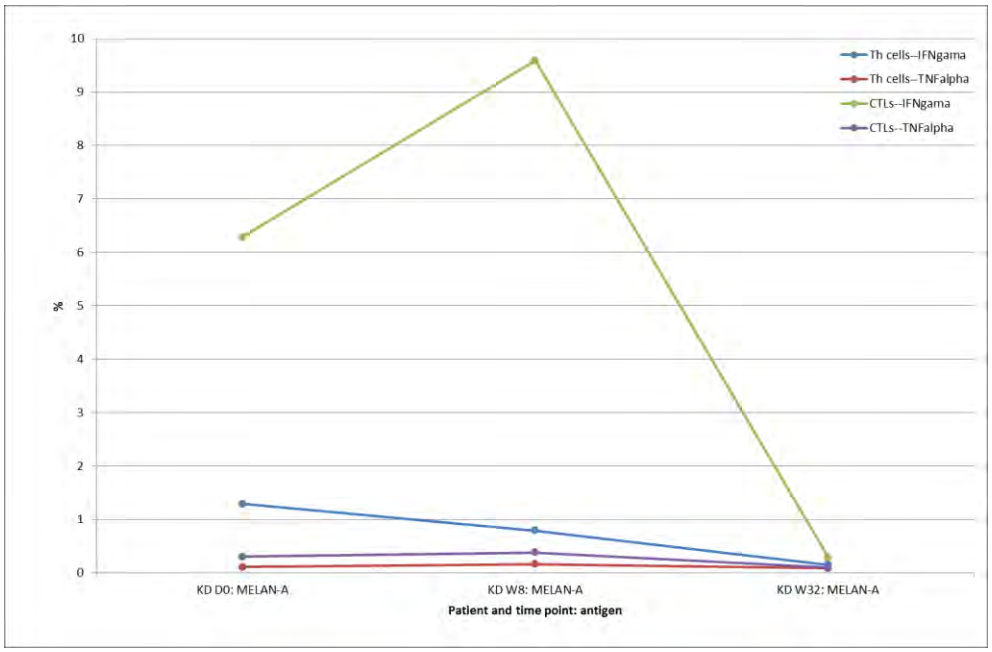

It was evident that all but two time point responses, IFN-γ^+ helper T-cells and cytotoxic T-cells towards MART-1/Melan-A, were below 1%. The helper T-cells steadily declined from day 0 to week 8 and to week 32, whilst the cytotoxic T-cells initially increased from day 0 to week 8, and then decreased from week 8 to week 32. To further comprehend how these cells were responding, the relevant corresponding scatter plots and gating are indicated below in Fig. 4.15.

Figure 4.15: IFN-γ^{+} helper and cytotoxic T-cells scatter plots and gating towards MART-1/Melan-A for patient KD at three distinct time points. Above: helper T-cells; Below: cytotoxic T-cells Left: graph for day 0; Middle: graph for week 8; Right: graph for week 32.

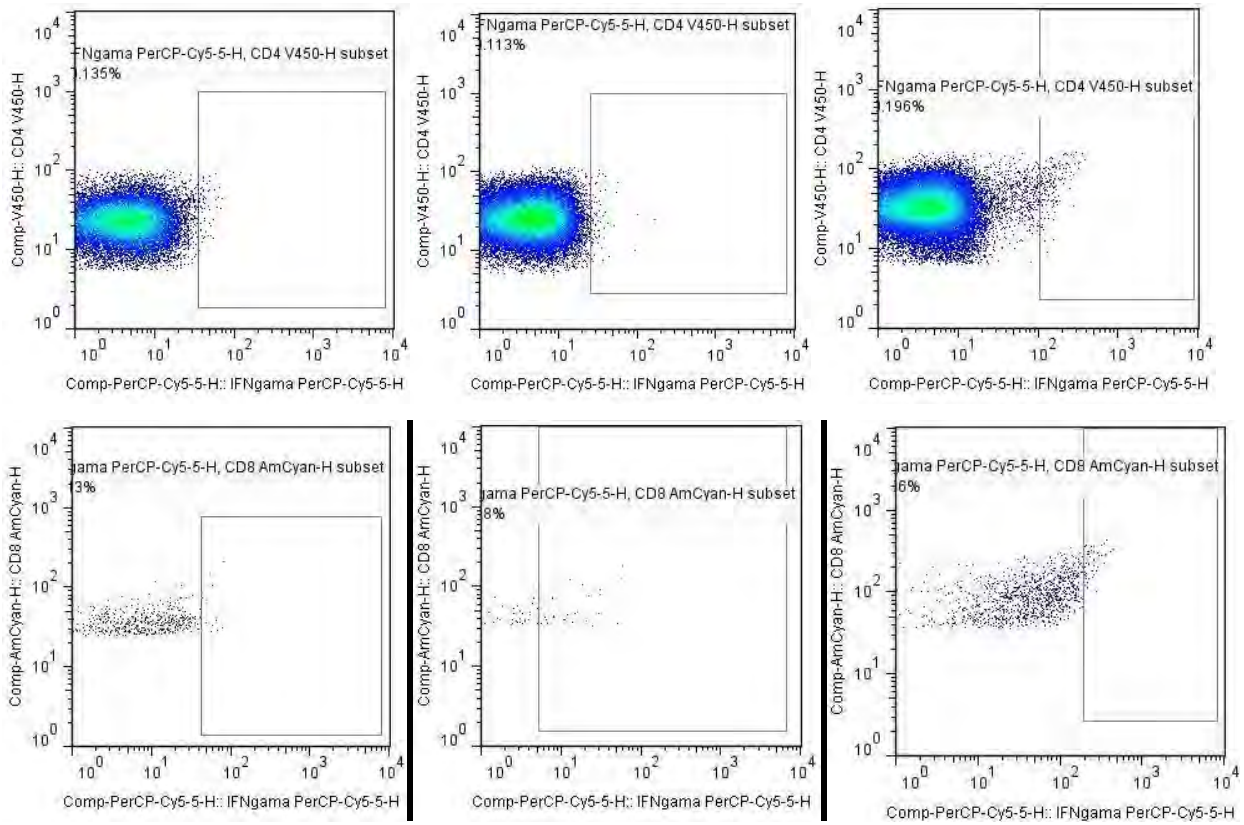

Based on the scatter plots indicated above, it was evident that when comparing helper T-cells with cytotoxic T-cells, the latter contained a reduced amount of cells responsible for the observed responses. When consulting the total percentage of helper T-cells and cytotoxic T-cells relative to the complete T-cell population across this patient's time points, the obtained proportions were 81.1% and 13.4% at day 0, 79.9% and 13.1% at week 8, and 74.8% and 17.7% at week 32, respectively. It was certainly apparent that as for patient DM, there was a much higher proportion of helper T-cells when compared to cytotoxic T-cells. As a means of verifying if these T-cell responses showed preliminary evidence of correlation to the array generated B-cell response, the matching MART-1/Melan-A responses were assessed. This data showed baseline titres of ~500 RFU, which gradually increased to ~600 RFU (week 8) and then ~950 RFU, with all titres below our significantly expressed threshold. When comparing these early findings to the graph indicated above right in green, these only match for the cytotoxic T-cells from day 0 to week 8, and no not match in the 3 additional instances, indicating that in this instance a B-cell response was somewhat indicative of a T-cell one, although this was not consistent across time points and cell types. Moreover, when including the temporal disease status of a partial response at week 8 and week 32, cytotoxic T-cells from day 0 to week 8 also respond in a similar manner, showing evidence

of increasing titres during a clinical response. However, the subsequent time point no longer matches the speculated titre increase with clinical efficacy. Therefore, specifically for patient KD, speculative evidence of a correlation was found between the generated B-cell, T-cell and clinical efficiency data for IFN-γ^+ cytotoxic T-cells, but only between day 0 and week 8.

Kinase inhibition – the specific treatment under investigation in this cohort – was designed to elicit both T-cell and antibody responses against melanoma-associated antigens in melanoma patients. Given that T-cell and B-cell responses are coordinated to some degree at the level of helper T-cells, agreement between these antigen-specific responses was expected. Yet, only two out of the eight tested patients presented with matching autoantibody responses. Amongst these, early evidence of a limited correlation was seen between T-cell and clinical data. However, due to the reduced number of array assayed temporal matching samples, this study was only conducted on a small subset of patients. Unfortunately, to be able to make accurate assumptions, larger patient numbers and possibly a longer stimulation period is required, limiting our possible data interpretation. Additionally, only 2 (NY-ESO-1 and MART-1/Melan-A) of our 123 antigens tested were available and functional for these assays, further limiting this assay.

4.3.2 Colorectal cancer patients who underwent pre- or post-operative chemotherapy/radiotherapy

A total of 62 serum samples, corresponding to sixty-two colorectal cancer patients undergoing pre- or post-operative chemotherapy/radiotherapy treatment were assayed, processed and analysed according to our pre-established CT100$^+$ microarray pipeline. The following settings were used for the CT100$^+$.jar processing and filtering steps: mean or median values = mean, noise threshold = 2 standard deviations of the background, replicate CV threshold = 20%, whole array filtering control = 10 ng/µL Cy5-biotin-BSA and whole array CV threshold = 21%. The initial stipulated research question was whether a pre- or post-operative therapy significantly altered the pattern of cancer-associated autoantibody titres in these patients, thereby potentially influencing the outcome of any subsequent treatment, which would provide us with a greater understanding of the interplay between chemotherapy/radiotherapy and anti-cancer autoimmune responses. For this cohort, data analysis was conducted based on the collected clinical information and each patient's resulting autoimmune profile, permitting the comparison between several of these parameters, as a means of possibly identifying diagnostic or prognostic biomarkers, or discovering that a therapy induced antigen expression deregulation might stimulate a beneficial cancer-specific autoimmunological effect post-therapy. However, it is important to note that only a single blood sample was available for each patient, signifying that no autoantibody responses progression across a time course may be measured, but rather a single profile for each patient. Hence,

our data analysis pipeline is distinct from those mentioned above. Furthermore, based on sample number-based power calculations indicated in Chapter 2, this cohort includes sufficient patient and sample numbers to be able to report statistically relevant results (power = 0.97).

Significant (> 1000 RFU) autoantibody titres were present in all 62 patients (*n* = 62/62, 100%), with signals ranging from 0 to ~23000 RFU. The majority of these patients (*n* = 40/62, 65%) displayed medium (between 2000 and 10000 RFU) signals, followed by 17/62 (27%) patients with low (between 1000 and 2000 RFU) signals, and 5/62 (8%) patients with high (above 10000 RFU) signal. In an attempt to verify if autoantibody levels were increased as a result of pre-operative chemotherapy/radiotherapy, patient distribution was assessed and no evident pattern was seen, with an equally divided pre- and post-operative subset of patients in each low (7 vs 7), medium (20 vs 19) and high (2 vs 2) signal group, respectively. Unfortunately, this finding did not infer any clarification in regards to whether higher autoantibody signals were associated with the presence of pre-operative chemotherapy/radiotherapy. When considering the presence or absence of recurrence, it was evident that the patients were distributed unequally across these same low (3 vs 11), medium (8 vs 29) and high (2 vs 2) autoantibody titre groups, respectively. This indicated that the majority of the recurring patients had medium autoantibody signals when tested. It seems unlikely therefore that this autoimmune profile would provide relevant information regarding likelihood of recurrence, due to the latter occurring at a much later temporal time point, and in a variable manner across patients. Additionally, in regards to cancer stage and site of disease, patient distribution was also assessed, with the majority of patients being stage II (*n* = 7/14, 50%) in the low group, stage III (*n* = 17/37, 46%) in the medium group, and both stage I (*n* = 2/4, 50%) and III (*n* = 2/4, 50%) in the high group. Cancer stage seemed to cluster quite randomly across signal groups, with lower autoimmune signals belonging to mainly stage II patients, medium signals to stage III, and higher signals to stages I and III. The main cancer types accumulating in each group were rectum (*n* = 8/14, 57%) and recto-sigmoid junction (*n* = 4/14, 29%) for low, rectum (*n* = 27/39, 69%) and caecum (*n* = 4/39, 10%) for medium, and rectum (*n* = 2/4, 50%) for high. Rectum was the main cancer site in each autoantibody signal group, which was most likely related to the fact that it is the most abundant cancer type of this cohort (65%), rather than an actual site-signal association. Interestingly, the patient displaying the highest autoantibody titres (~23000 RFU), CRC038, was a stage I rectum patient with pre-operative therapy. However, this patient also had disease recurrence, indicating that no likelihood of recurrence inference should be made, based on early array data.

Of the 123 cancer-associated antigens present on our CT100^{+} array, the most prevalent significant autoantibody titres (above 1000 RFU) detected in this cohort were towards 14 leading antigens. These were detected in at least 10 or more instances across all patients in this cohort, and most abundantly towards SILV/gp100 (*n* = 19/62, 31%) and p53 Q136X (*n* = 13/62, 21%), as indicated below in Fig. 4.16.

Figure 4.16: Most prevalent autoantibody titres detected across the pre- or post-operative therapy treatment cohort. This graph indicates the summed number of times autoantibody levels were detected towards the 14 leading antigens at titres above 1000 RFU.

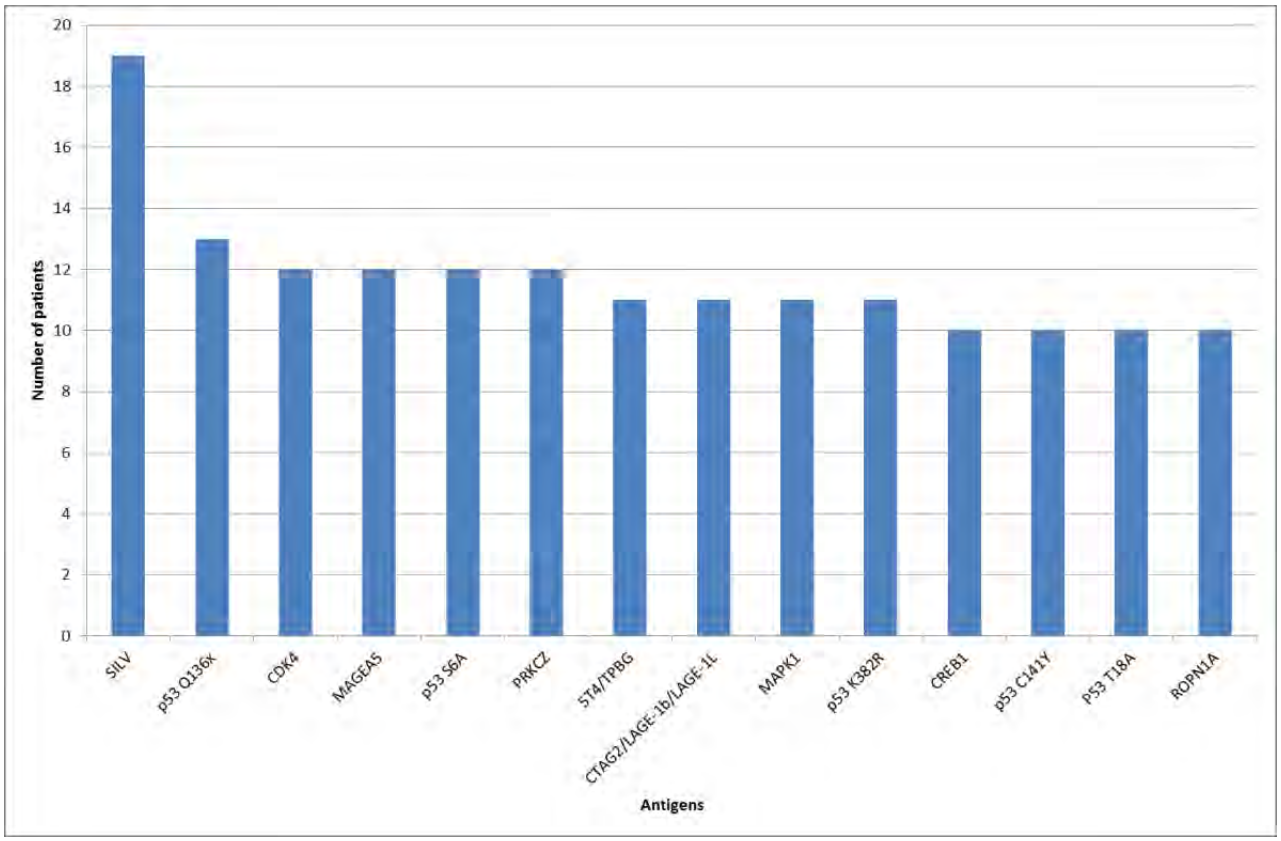

Based on this graph, it was evident that the most prevalent autoantibody titres towards a very interesting subset of leading antigens were present in at least ten patients. Besides from p53 Q136X, autoantibody titres towards an additional four p53 mutants were also amongst the top signals, thus arguing for upregulation of one form that shares a common epitope amongst these mutants. This finding strengthens a potential use for these, either diagnostic or therapeutic related. Additionally, the remaining prevalent titres were towards either CT antigens (MAGEA5, CTAG2/LAGE-b/LAGE-1L, ROPN1A), protein kinases (CDK4, PRKCZ, MAPK1) or other cancer-associated antigens (5T4/TPBG, CREB1).

As a means of defining whether the antigens with the most abundant autoantibody titres could be potential diagnostic or prognostic biomarkers, or even therapeutic targets, SILV/gp100 and p53 Q136X were investigated further.

SILV, also known as lineage-specific antigen gp100, is a type I transmembrane glycoprotein that plays a crucial role in the biogenesis of melanosomes (www.uniprot.com, www.ncbi.nlm.nih.gov/pubmedhealth). This protein is usually referred to as a melanoma or tumour-associated antigen, due to

its wide expression in melanomas, with early studies showing associated between an anti-SILV/gp100 response and cancer regression which is linked to the specific recognition by HLA-A2-restricted $CD8^+$ cytotoxic T-cells (Kawakami et al. 1994; Bakker et al. 1994). Hence, this protein was rapidly considered as an attractive melanoma diagnostic marker due to its restricted expression in melanocytes, and as a potential target for cellular immune responses against melanoma (Adema et al. 1994; Bakker et al. 1994; de Vries et al. 1997). A vast number of clinical trials followed this discovery, testing the efficacy of using a variety of SILV/gp100 peptides, either alone, or in combination with MART-1/Melan-A or IL-2, as a targeted melanoma immunotherapeutic, with promising results and continued testing to date (Zhai et al. 1996; Rosenberg et al. 1998; Di Pucchio et al. 2006; Schwartzentruber et al. 2011). However, all of the above and easily accessible literature is referent to melanoma, and this treatment cohort included solely colorectal cancer patients. When attempting to verify if a SILV/gp100-derived therapeutic vaccine had been tested in colorectal cancer, no records were found, indicating that this therapy has not yet been considered for colorectal cancer (Tartaglia et al. 2001; Xiang et al. 2013). This finding is of particular importance, as SILV/gp100 might be a potential novel therapeutic target for colorectal cancer, which has previously not been reported or tested. Therefore, the available data for SILV/gp100 across all patients was inspected, and an autoantibody titre trendline across this whole cohort was constructed, as indicated below in Fig. 4.17.

Figure 4.17: Anti-SILV/gp100 immunoglobulin titre trendline across all patients of the pre- or post-operative therapy treatment cohort. Threshold on graph indicates ~1000 RFU, as a means of facilitating view of most significant signals.

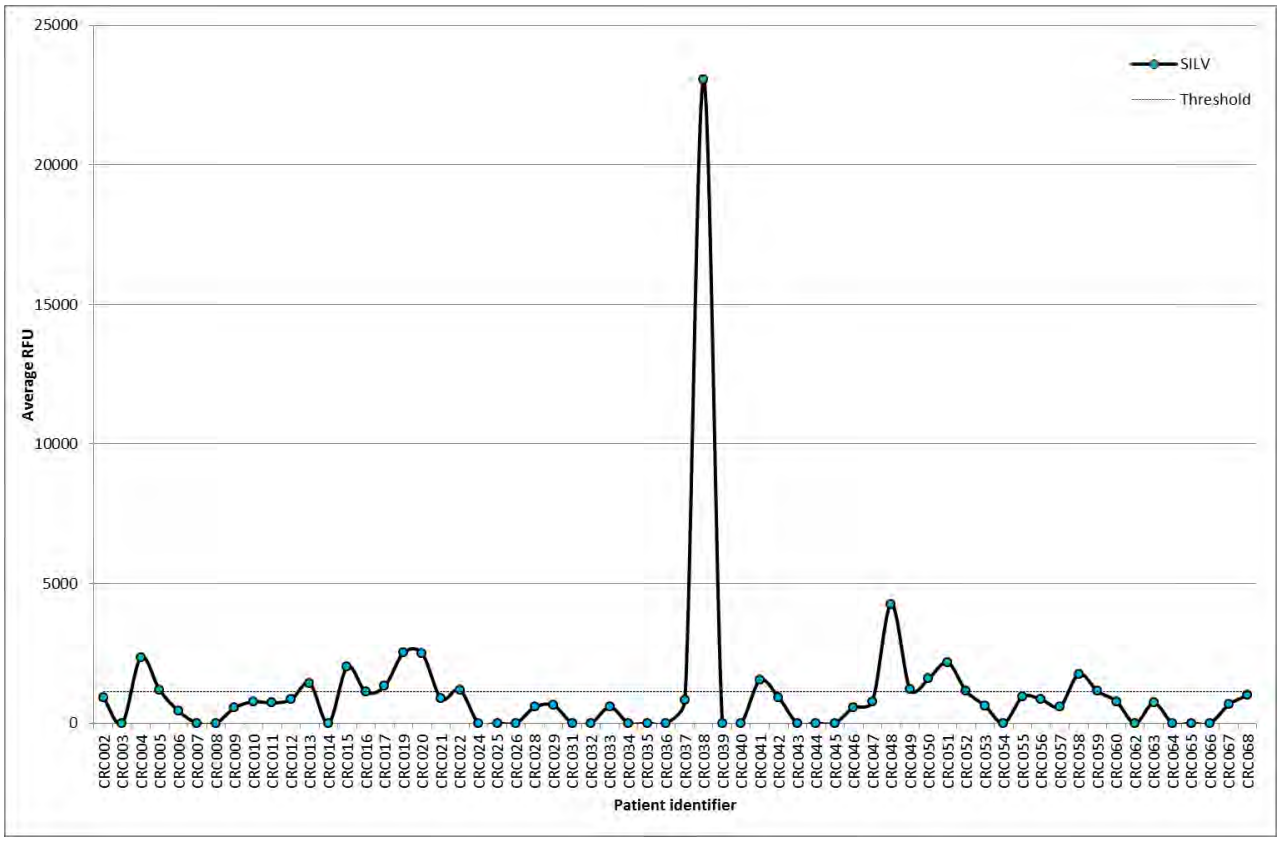

Visual inspection of this anti-SILV/gp100 immunoglobulin titre trendline indicates that autoantibody titres against SILV/gp100 are quite variable across our cohort, with two spikes for patients CRC038 (~23000 RFU, rectum, stage I, pre-operative therapy, and no disease recurrence) and CRC048 (~4500 RFU, rectum, stage IV, no pre-operative therapy, and no disease recurrence). In an attempt to verify if any particular disease site or stage, as well as presence or absence of pre-operative therapy and recurrence, was most prevalent across significant (> 1000 RFU) titres, these were accounted for. The most prevalent site and stage of disease was the rectum (*n* = 11/18, 61%) and stage II (*n* = 8/16, 50%), respectively. The latter seems to indicate that these titres don't seem to be related to a more advanced cancer type, but rather variably between stages I to IV. If this protein was in fact considered as a novel colorectal cancer therapeutic, the fact that it is expressed across all disease stages is certainly beneficial, as it implies a wider applicability. When considering pre-operative therapy, these patients were equally divided, with exactly half of them (*n* = 9/18, 50%) not having pre-operative therapy. Lastly, in regards to recurrence, it seemed that the majority of these patients did not have recurring disease (*n* = 13/17, 76%). This finding is of particular interest, as it might potentially indicate that the presence of

SILV/gp100 might be associated with a reduced likelihood of recurrent disease, warranting further studies.

In regards to the other most abundantly expressed protein, p53 Q136X, a similar analysis was conducted. The tumour suppressor p53 is known to play a crucial role in cell cycle regulation and induction of apoptosis, and common cancer-related mutations have been implicated with carcinogenesis, cancer progression, as well as possible diagnostic, prognostic and therapeutic uses. In regards to colorectal cancer in particular, the overexpression and mutation of p53 is also a known phenomenon, which validates our finding within this specific cancer type, amongst the several ones included in this treatment cohort (Rodrigues et al. 1990; Liu & Bodmer 2006). Additionally, p53 mutant overexpression has been linked to a poorer prognosis, decreased survival and even likelihood of tumour relapse, and therefore be considered an immunotherapeutic (Starzynska et al. 1992; Houbiers et al. 1995; Hammel et al. 1997; Kressner et al. 1998). Understandingly, p53 has been tested in a clinical trial setting across a variety of distinct cancer types, including colorectal cancer (www.clinicaltrials.gov). Therefore, the available data for p53 Q136X (a frame-shifted, inactivated mutant of p53) across all patients was inspected, and an autoantibody titre trendline across this whole cohort was constructed, as indicated below in Fig. 4.18.

Figure 4.18: Anti-p53 Q136X immunoglobulin titre trendline across all patients of the across pre- or post-operative therapy treatment cohort. Threshold on graph indicates ~1000 RFU, as a means of facilitating view of most significant signals.

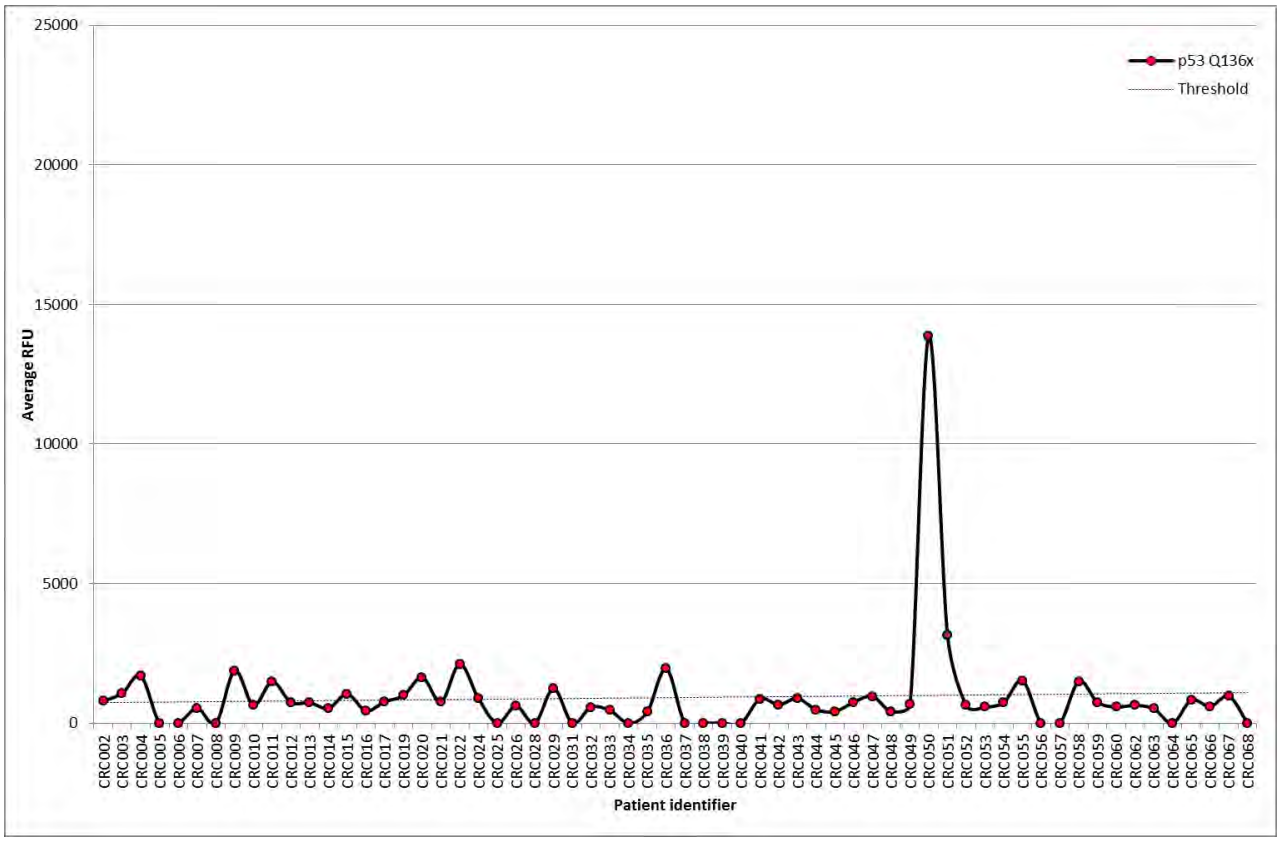

Visual inspection of this anti-p53 Q136X immunoglobulin titre trendline indicates that autoantibody titres against p53 Q136X are also variable across our cohort, with a spike for patient CRC050 (~14000 RFU, rectum, stage I, pre-operative therapy, and disease recurrence). In an attempt to verify if any particular disease site or stage, as well as presence or absence of pre-operative therapy and recurrence, was most prevalent across significant (> 1000 RFU) titres, these were accounted for. The most prevalent site and stage of disease was the rectum (*n* = 8/13, 62%) and stage III (*n* = 7/12, 58%), respectively. The latter seems to indicate that these autoantibody titres might be related to a more advanced cancer type, with gradually increasing patient numbers from stages I to III (no stage IV patient were present in this subset), which might indicate a potential use in identifying a more advanced cancer stage, warranting further studies. Remarkably, both this higher prevalence in rectum cancers and this increase in autoantibody titres related to increasing disease stage has been reported previously, which highly validates this finding (Starzynska et al. 1992). When considering pre-operative therapy, these patients were quite equally divided, with just over half of them (*n* = 7/13, 54%) not having pre-operative therapy. Lastly, in regards to recurrence, it seemed that the majority of these patients did not have recurring disease (*n* = 8/12, 67%). This finding might potentially indicate that the presence of p53 Q136X might

also be associated with a reduced likelihood of recurrent disease, however, this is contrary to what has been reported in the literature, and therefore warrants further study (Starzynska et al. 1992).

As a means of identifying the most interesting patient autoantibody titres across these most abundant antigens, a 3-D plot was constructed with all patients, and is indicated below in Fig. 4.19.

Figure 4.19: Most abundant autoantibody titres across pre- or post-operative therapy treatment cohort. This 3-D graph indicates the autoimmune profile of all patients across the most abundant antigens of this treatment cohort. Each antigen is indicated in a different colour, and each patient sample is indicated in the x-axis.

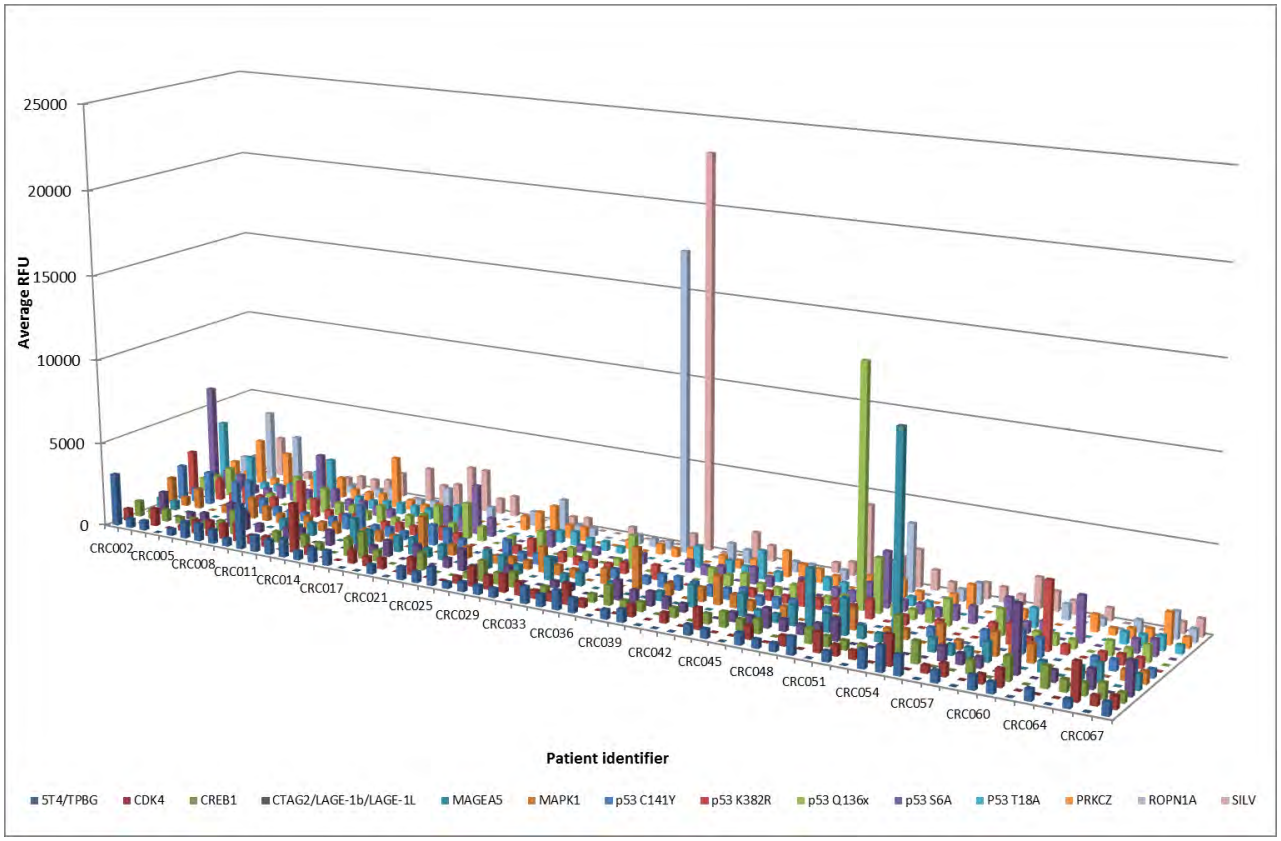

This data representation indicates that the majority of these patient signals are below 5000 RFU, with only five patients displaying signals between 5000 and 25000 RFU. These high signals were seen for p53 S6A (CRC002, rectum, stage II, pre-operative therapy, and no disease recurrence), ROPN1A (CRC037, proximal descending colon, stage III, no pre-operative therapy, and no disease recurrence), SILV/gp100 (CRC038, rectum, stage I, pre-operative therapy, and no disease recurrence), and MAGEA5 (CRC050, rectum, stage I, pre-operative therapy, and disease recurrence). It is particularly interesting to visualize that even amongst the same cancer type, stage and therapy, each patient's autoimmune profile and most commonly detected autoantibodies vary greatly, highlighting that each patient is a unique case,

and aiding in comprehending the distinct responses to treatment across a given cancer type. Thus, both variable genomic and proteomic profiles highlight the need for a personalised treatment approach for each patient.

We have applied our CT antigen microarray platform to the investigation of autoantibody profiles in a cohort of colorectal cancer patients who either underwent or not pre-operative chemotherapy or radiotherapy, and observed significant autoantibody titres across all patients. The main intent of this study was to assess whether pre-operative therapy altered patterns of autoantibody titres, thereby potentially influencing the outcome of subsequent therapy. In this regard, this cohort data showed that no apparent difference in autoantibody profiles was evident between patients who had undergone pre-operative therapy and those who hadn't, contrary to what was expected. However, it may be plausible that other factors, which we have yet to determined, may be contributing towards this lack of distinction. Such factors may include the presence of distinct cancer subtypes amongst this cohort, some of which may be immune suppressive in character, and thus potentially influencing the resulting autoimmune profiles (Sadanandam et al. 2013; Sanz-García et al. 2014). Although previous studies have demonstrated benefits when combining cancer therapeutics, we are unable to infer influences on subsequent treatment outcome of this specific cohort, due to the lack of evident differences amongst patients who underwent pre-operative therapy and those who did not (Hodi et al. 2010).

In this pre- or post-operative chemotherapy/radiotherapy cohort, we have successfully demonstrated that there are measurable differences in the autoantibody repertoires towards tumour-specific and –associated antigens amongst colorectal cancer patients. However, there was no evidence that these were potentially augmented or not by prior therapy. Furthermore, we identified SILV/gp100 – potential novel therapeutic target for colorectal cancer – and p53 Q136X – potential indicator of disease progression – as the two most abundantly detected autoantibodies amongst those tested, present across 31% and 21% patients, respectively. However, unlike with the kinase inhibition cohort, these titres are much less prevalent than desired to be considered as viable colorectal cancer biomarkers or cancer therapeutic targets with broad applicability. When considering patient sample numbers and relevant power calculations, although this cohort is quite diverse regarding age, the achieved statistical power is above recommended (power > 0.8), supporting the findings obtained in this cohort.

We therefore anticipate that our novel, quantitative, customizable CT antigen microarray platform may find usage in determining whether or not previous systemic therapy may aid in the efficacy of subsequent therapeutics, warranting confirmation using a pre-stipulated specifically focussed study and homogeneous cohort design using sufficient patient numbers according to an *a priori* power calculation estimate.

4.3.3 Myelodysplasia patients who underwent dual epigenetic modification

A total of 30 serum samples, corresponding to twelve MDS and AML patients before and after cycles 3 and 4 of treatment with panobinostat and azacitidine, were assayed, processed and analysed according to our established $CT100^+$ microarray pipeline. The following settings were used for the $CT100^+$.jar processing and filtering steps: mean or median values = mean, noise threshold = 2 standard deviations of the background, replicate CV threshold = 20%, whole array filtering control = 15 ng/µL Cy5-biotin-BSA and whole array CV threshold = 22%. The initial stipulated research question was whether the deregulation of the cancer-provoked epigenetic instability would create neo-antigens and subsequent expanded autoantibody responses. For this cohort, data analysis was conducted according to the available clinical information, which permitted the attribution of a disease status per time point, allowing for an optimal direct comparison between the patients clinical and immune responses towards the treatment. Furthermore, based on sample number-based power calculations indicated in Chapter 2, this cohort does not include sufficient patient and sample numbers to be able to report statistically relevant results (power = 0.35).

A significant (> 1000 RFU) autoantibody response was present in 11/12 (92%) patients, with the strongest response (~9000 RFU) seen, both quantifiably and visually, for patient 001-0002 (see Fig. 4.20 and 4.21).

Figure 4.20: Strongest patient autoimmune profile of the epigenetic modifier treatment cohort. This graph indicates the autoimmune profile of patient 001-0002 across two distinct time points (represented by different colours). As a means of clarifying the visualization of relevant titres, an insert of the magnified relevant data is indicated within this figure. *Statistically significant difference, P < 0.05 or **P < 0.01. D0: day 0; PR: partial response.

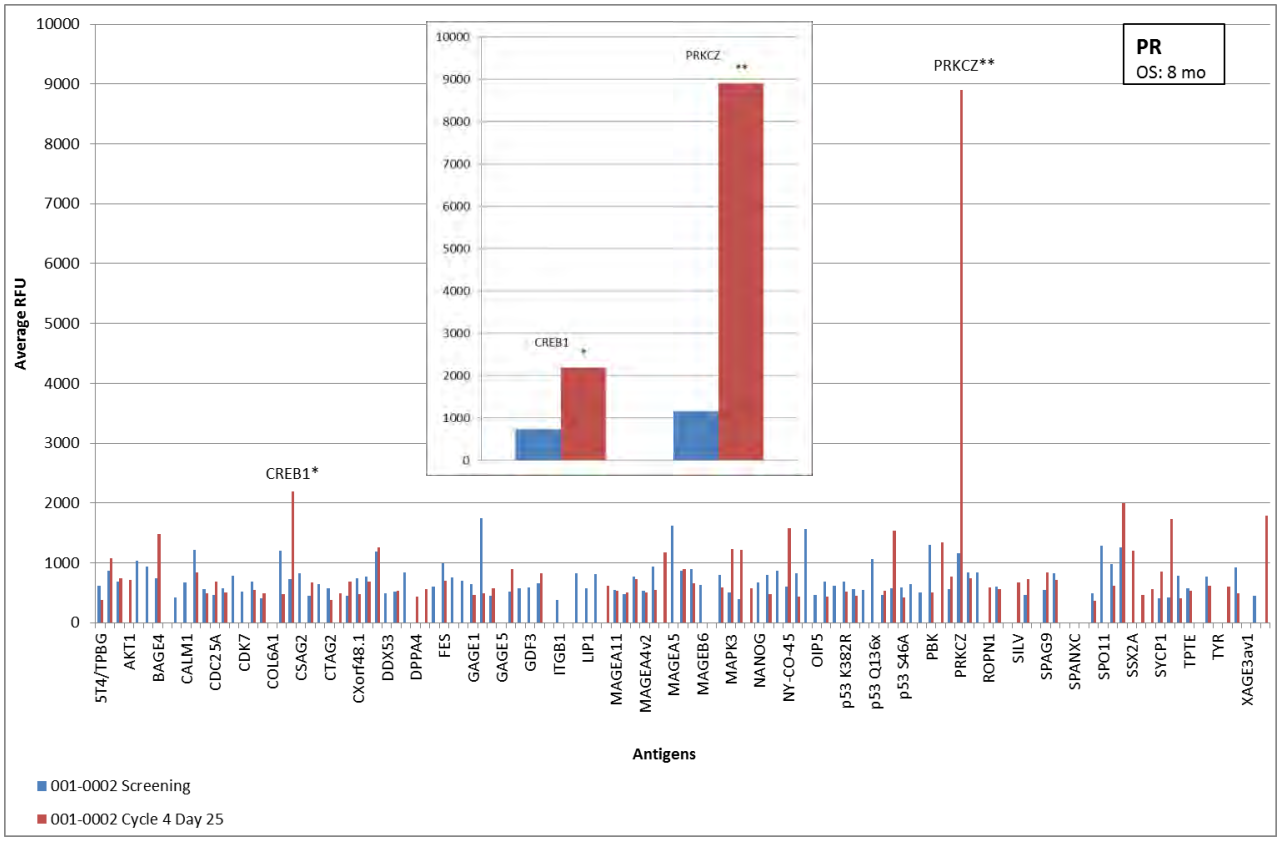

Figure 4.21: Strongest patient corresponding scanned array image of the epigenetic modifier treatment cohort. This figure indicates scanned array images of patient 001-0002 before (image on left at screening) and after (image on right at cycle 4, day 25) treatment, with visual evidence of an autoantibody response towards PRKCZ. Red box highlights triplicate PRKCZ positive signals.

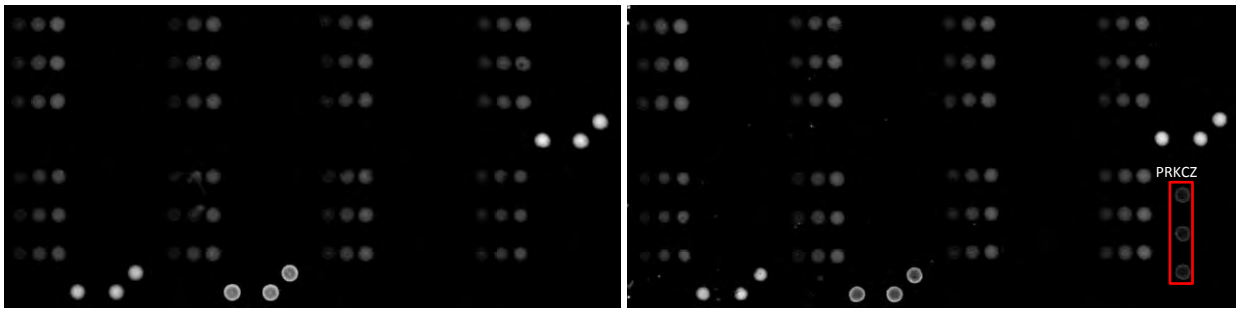

Patient 001-0002, diagnosed with AML-MRC, showed a statistically significant increase above 2000 RFU in CREB1 ($P < 0.05$) and PRKCZ ($P < 0.01$) in response to treatment. The fact that this patient shows such a drastic increase in autoimmune response to PRKCZ is of particular interest. PRKCZ, known as protein kinase C-zeta, is an atypical calcium- and diacylglycerol-insensitive isozyme of the protein kinase C family, a family of serine/threonine kinases that regulate several cell functions, such as proliferation, gene expression, cell cycle, differentiation, cytoskeletal organization cell migration and apoptosis (Teicher 2006; Way et al. 2000). Protein kinase C has been broadly targeted as a potentially attractive cancer therapy due to its potential role in carcinogenesis, being the receptor for tumour-promoting phorbol esters, with several studies aiming to understand how it regulates apoptosis and chemoresistence, as a means of reversing the latter (Bosco et al. 2011; Marengo et al. 2011; Pearson & Fabbro 2004; Teicher 2006). PRKCZ expression has been specifically linked to multiple myeloma and leukaemia, cancer types included in this treatment cohort, showing direct involvement in modulating hematopoietic neoplasms, which indicates a direct association and validation of this finding with the literature (Teicher 2006). Additionally, PRKCZ has recently shown to be essential for the regulation of cell motility, with direct involvement in the regulation of cancer cell migration and invasion, which may explain why an autoimmune response towards this protein was present for this patient (Xiao & Liu 2013).

When comparing the observed autoimmune profile for this patient with the overall disease status, PR, both showed preliminary evidence of agreement. However, to understand whether this response was indicative of a temporal clinical response (tumour regression and patient improvement), one must consider the disease status of the matched time point in question, rather than the patient's best or overall response, as this information will be more relevant. For that purpose, this particular question will be assessed further below. Additionally, to verify if this PRKCZ response was restricted to this patient (PR), all resulting autoimmune profiles were inspected, and three additional patients were found with a much lower (between 1000 and 2000 RFU) but relevant response, patients 001-00003 (CR), 001-0007 (R) and 001-0013 (SD), all of which presented with distinct overall disease statuses. Both patients 001-0002 and 001-0007 were diagnosed with AML-MRC, but the remaining two patients were diagnosed with MDS-Int2.

As a means to assist in comprehending the reason why some patients have a stronger immune response than others, the weakest response (~1500 RFU) was also of importance, and was seen for patient 001-0016 (see Fig. 4.22).

Figure 4.22: Weakest patient autoimmune profile of the epigenetic modifier treatment cohort. This graph indicates the autoimmune profile of patient 001-0016 across three distinct time points (represented by different colours). As a means of clarifying the visualization of relevant titres, an insert of the magnified relevant data is indicated within this figure. *Statistically significant difference, P < 0.05 or **P < 0.01.

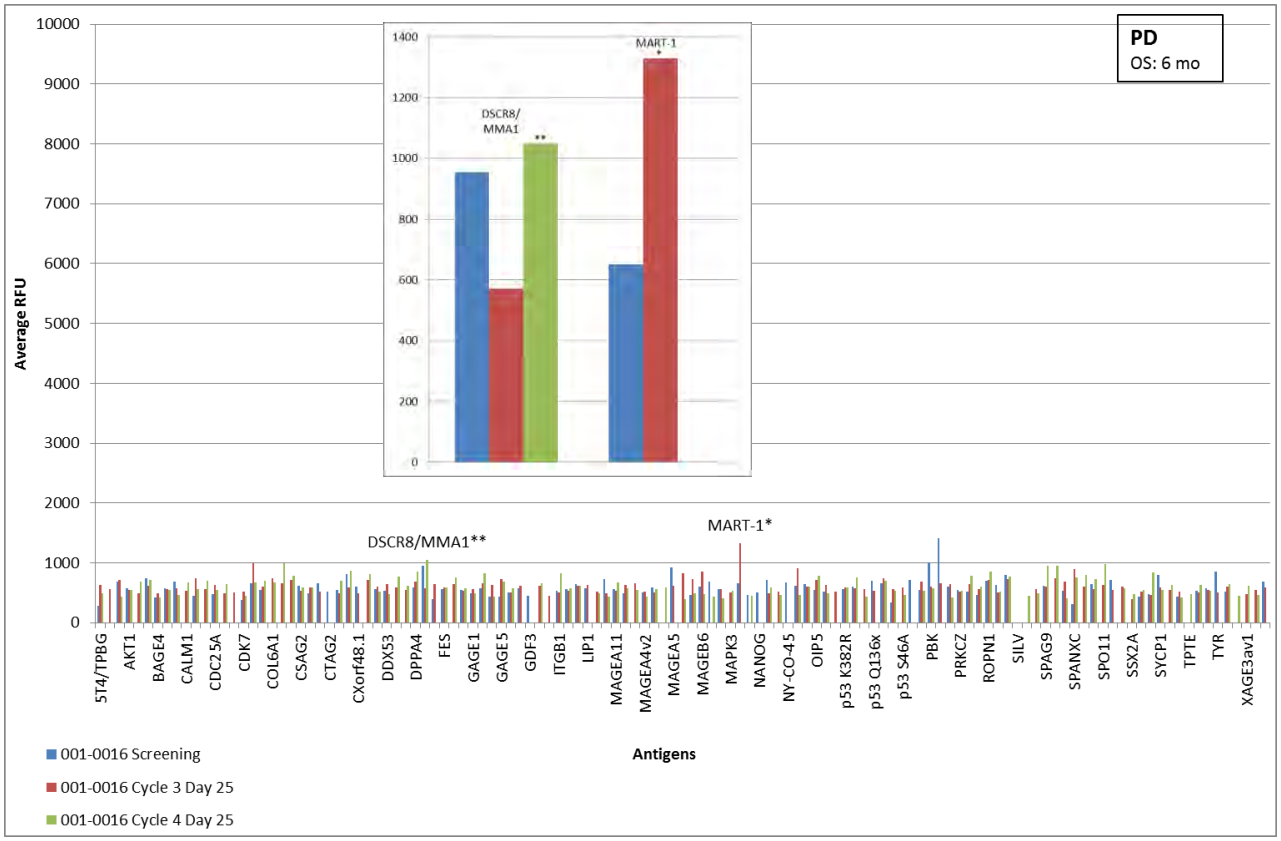

On the contrary to patient 001-0002, patient 001-0016, diagnosed with MDS-Int2, showed only a slight, but also statistically significant, increase above 1000 RFU in DSCR8/MMA1 (P < 0.01) and MART-1/Melan-A (P < 0.05) in response to treatment. When comparing this finding with the patient's overall disease status, PD, once again evidence of corroboration was made, as although a very weak response to treatment was present, the majority of these were below 1000 RFU, which was potentially indicative of a likely disease progression, rather than a suggested response.

Of this cohort, 12/12 (100%) patients showed autoantibody responses to treatment, although these responses were minor and below 2000 RFU for two patients, patient 001-0016 (see Fig. 4.22 above) and patient 001-0013 (see Fig. 4.23).

Figure 4.23: Patient with minor autoimmune responses of the epigenetic modifier treatment cohort. This graph indicates the autoimmune profile of patient 001-0013 across three distinct time points (represented by different colours).

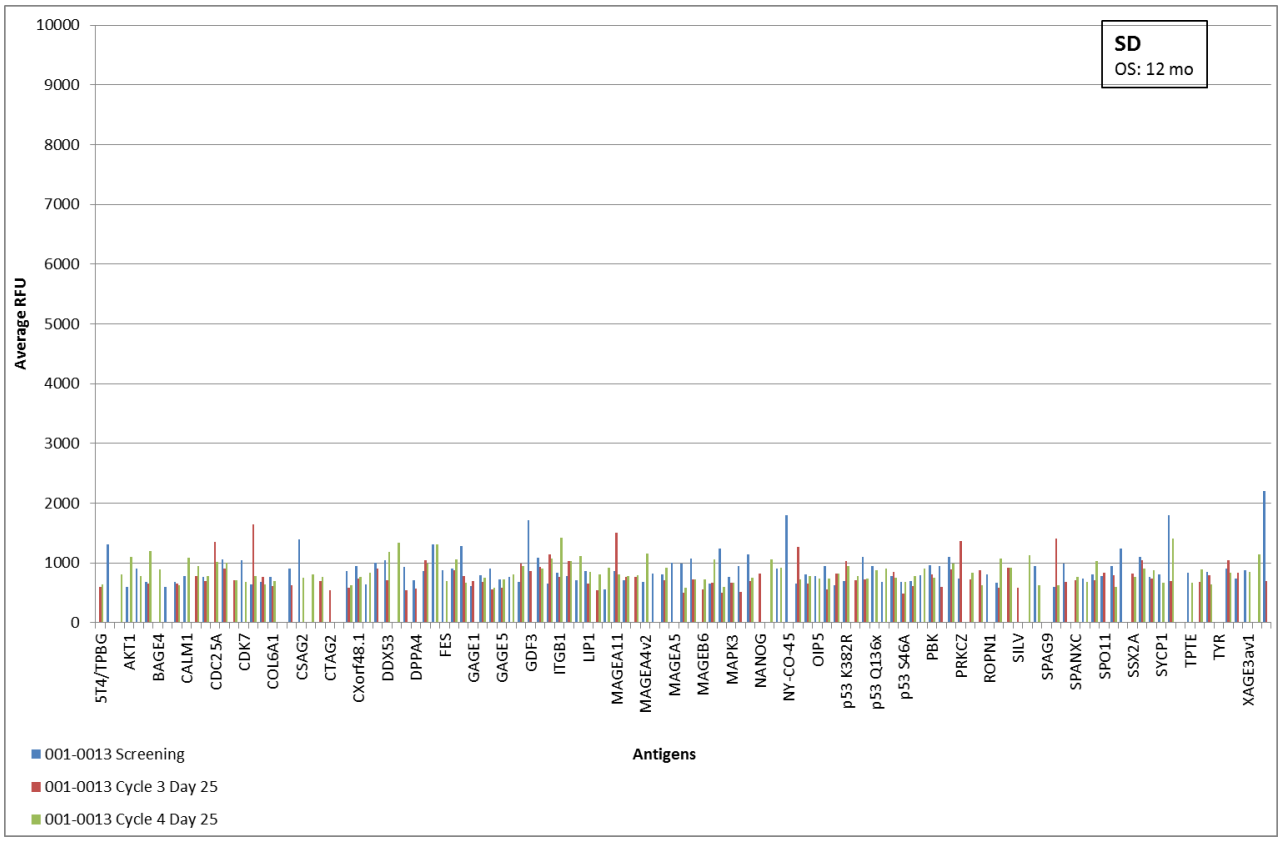

Patient 001-013, also diagnosed with MDS-Int2, showed several but minor increases in autoantibody signals in response to treatment, with overall stable titres across each time point. This patient's overall disease status was SD, which speculatively agreed with the observed autoimmune profile, as no major change was seen from screening to cycles 3 or 4 of treatment. However, when directly compared to patient 001-016, far more of these signals were above the 1000 RFU threshold (32 versus 2), which may account for the overall disease status difference (SD versus PD) between these two patients with seemingly similar autoimmune profiles.

Of the 123 cancer-associated antigens present on our CT100^{+} array, the most prevalent significant autoantibody titres (above 1000 RFU) detected in this cohort were towards 19 leading antigens. These were detected in at least six or more instances across all patient time points (screening or cycles of treatment) in this cohort, and most abundantly towards cytochrome P450 reductase and DSCR8/MMA1, as indicated below in Fig. 4.24.

Figure 4.24: Most prevalent autoantibody titres detected across the epigenetic modifier treatment cohort. This graph indicates the summed number of times autoantibody levels were detected towards the 19 leading antigens at titres above 1000 RFU, with distinction between S: screening; C3: cycle 3 of treatment; and C4: cycle 4 of treatment.

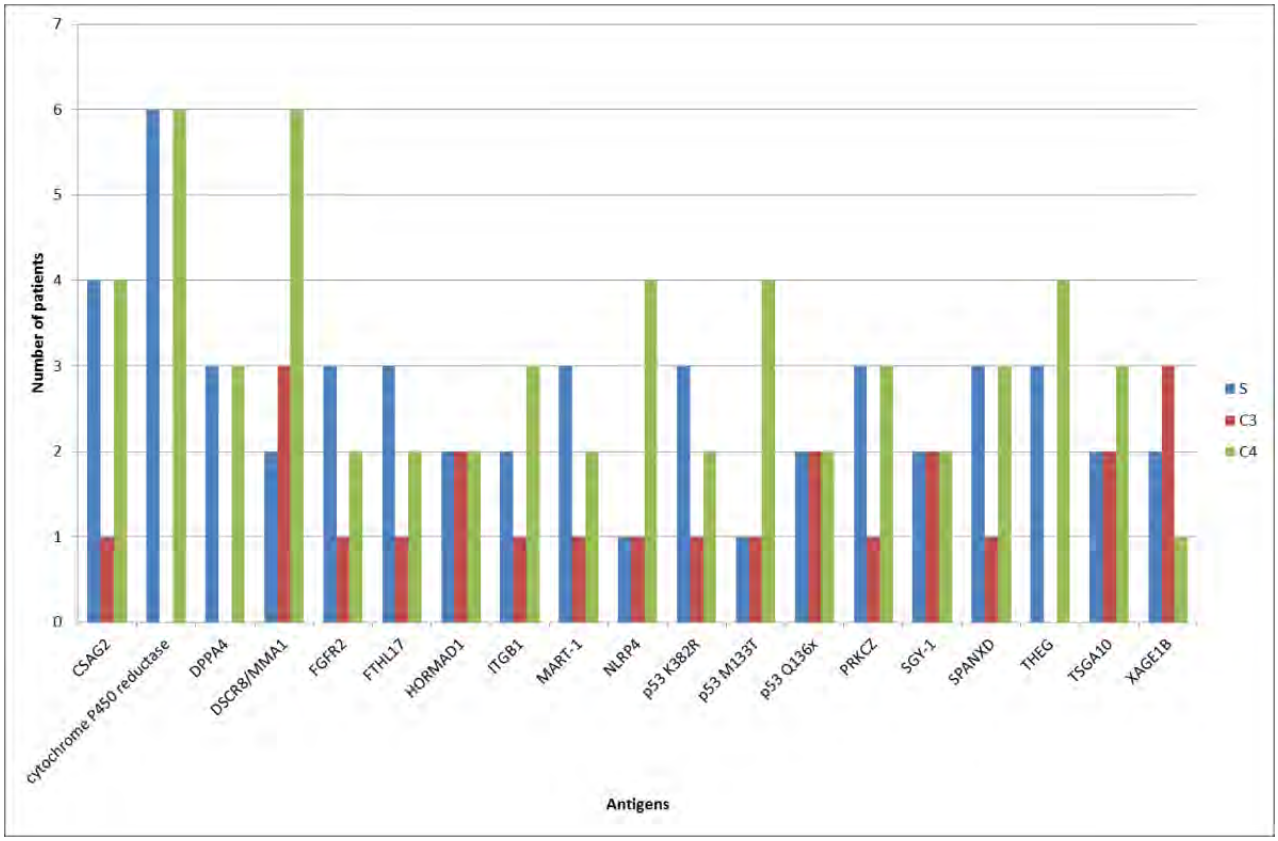

Based on this graph, it was evident that initially, when comparing screening to cycle 3 of treatment, the majority of these prevalent autoantibody responses towards these leading antigens were decreasing (*n* = 11/19, 58%), whilst the rest were either stable (*n* = 6/19, 32%) or increasing (*n* = 2/19, 10%). However, when comparing cycle 3 to cycle 4 of treatment, there was a clear shift in the opposite direction, with the majority of the prevalent autoantibody responses towards these leading antigens increasing (*n* = 15/19, 79%), whilst the remaining few were either stable (*n* = 3/19, 16%) or decreasing (*n* = 1/19, 5%). Based on the initially established research question, our interest was towards those that were augmented, as a result of treatment. Incidentally, the two most abundant autoantibodies of this set, when considering the cycle 3 and 4 comparison, both fell within this increasing responses subgroup, validating their potential.

Radar plots are typically used to represent a large number of variables in a two-dimensional chart, as a means of providing the viewer with a broad overview of the complete dataset. These plots can therefore be used to provide an overview of the distribution of autoantibody titres across a patient subset.

Therefore, for visual interpretation purposes, a radar plot of the detected autoantibody titres was constructed for all patients across the above-mentioned leading 19 antigens, to allow for a facilitated view of how patient responses are clustering across these antigens, and shown below in Fig. 4.25.

Figure 4.25: Radar plot of the prevalent autoantibody titres detected towards the leading 19 antigens across the epigenetic modifier treatment cohort. Each antigen is indicated by an axis, and each patient sample is indicated in a different colour. PRKCZ (~9000 RFU) for patient 001-0002, C4D25 and DSCR8/MMA1 (~8000 RFU) for patient 001-0006, C4D25 data points are omitted in this plot (outliers), due to an above average high intensity, to permit a better visualization of the majority of the signals.

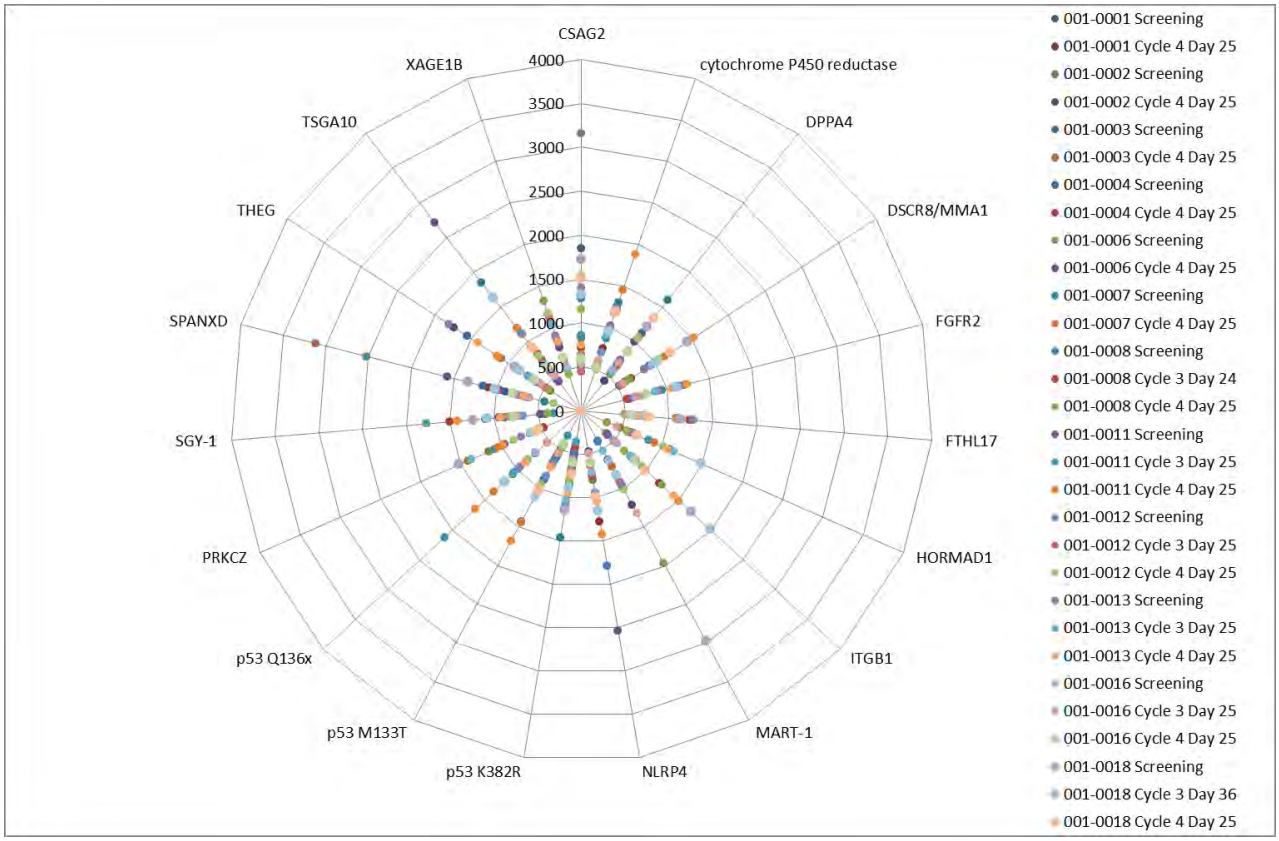

This radar plot provides a clear representation of why autoantibody titres towards these antigens are the most relevant of those tested, with multiple patients showing responses towards each of them. In a scenario where one would be seeking specific candidate biomarkers for a particular study, this finding would indicate that a potential biomarker would be amongst these 19 antigens, warranting further studies with a larger cohort.

As a means of interpreting these findings, and verifying their biological significance, the most abundant autoantibody titres detected, towards Cytochrome P450 reductase and DSCR8/MMA1, were investigated further. Cytochrome P450s can mediate the metabolism of several cancer therapeutic

drugs, being key enzymes in cancer treatment and even formation (Rodriguez-Antona & Ingelman-Sundberg 2006). Studies have shown that the polymorphic nature of the P450 genes affects an individual's drug response, highlighting the importance of considering this variability in cancer treatment (Ingelman-Sundberg et al. 2007). Cytochrome P450 reductase is a membrane bound protein that catalyses electron transfer from NADPH to all known cytochrome P450s, which is responsible for the oxidative metabolism of endogenous (fatty acids, steroids and prostaglandins) and exogenous (therapeutic drugs, environmental toxicants and carcinogens) compounds (Wang et al. 1997). Some P450 forms are selectively expressed in tumours, which could potentially aid the understanding of drug resistance mechanisms, or even indicate prospective therapeutic targets (Rodriguez-Antona & Ingelman-Sundberg 2006). To comprehend the presence of this enzyme in our cohort, it was essential to understand if these enzymes have an essential role in metabolizing the treatment undergone (azacitidine and panobinostat). Recent *in vitro* studies have shown that the metabolism of azacitidine is not mediated by P450s, as this drug is activated by intracellular phosphorylation, and although the exact metabolic fate of this drug is unknown, it is stated that clinically significant inhibitory or inductive effects on these enzymes is unlikely (Derissen et al. 2013; Chen et al. 2010). Panobinostat, on the other hand, is metabolized via multiple pathways (reduction, hydrolysis, oxidation and glucuronidation), with an oxidative metabolism mediated mainly by human cytochrome P450 CYP3A4 (70–98%) (with minor involvement of CYP2D6 and CYP2C19), indicating that if this drug was administered in combination with a CYP3A4 inhibitor, the end result would likely be clinical toxicity, as the anti-cancer therapeutic drug may not be metabolized (Hamberg et al. 2011). Moreover, it has been shown that the expression of some P450s may be affected by DNA methylation changes, which should occur when treating patients with the hypomethylating agent azacitidine, occurring mainly in genes of importance for the metabolism of endogenous compounds (Ingelman-Sundberg et al. 2007). With this in mind, the available data for cytochrome P450 reductase and 3A4 across all patients was inspected, and those patients exhibiting a relevant (> 1000 RFU) signal were plotted along with their overall disease status and OS, as indicated below in Fig. 4.26.

Figure 4.26: Anti-cytochrome P450 (reductase and 3A4) immunoglobulin titres across relevant patients. This graph indicates anti-cytochrome P450-3A4 (in blue) and -reductase (in red) immunoglobulin titres across all patients and time points, highlighting those with statistical significance. CR: complete response, PR: partial response, PD: progressive disease, R: resistant, SD: stable disease.

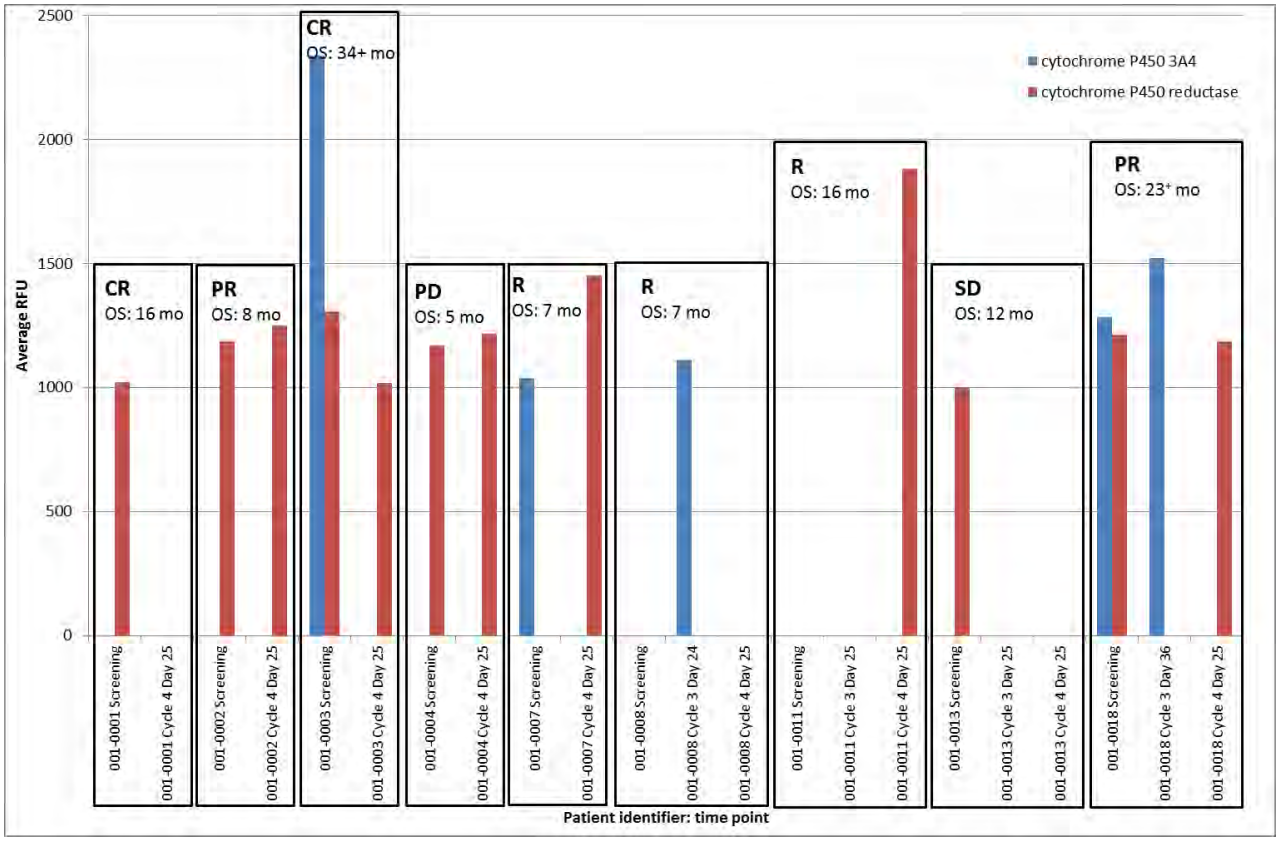

It was apparent that 9/12 (75%) patients showed relevant signals towards these two antigens, without evidence of any particular exclusivity for a disease status (CR, PR, PD, R and SD) or average survival (ranging from 5 to 34+ months). Although there is a known link between P450s and cancer treatment resistant mechanisms, as mentioned above, a clear link was not seen in this cohort, possibly related to the limited number of patients. However, further studies using a larger cohort may be able to verify this assumption.

DSCR8/MMA1, known as Down syndrome critical region protein 8/malignant melanoma-associated protein 1, is another member of the CT antigen family, CT25, with unknown function (www.uniprot.org) (De Wit et al. 2002). Although DSCR8/MMA1 expression was initially found in melanoma, it has been specifically linked to other tumour types, such as lung, liver, bladder, sarcoma, uterus, and multiple myeloma, the latter being a cancer type closest to this treatment cohort (De Wit et al. 2002; Risinger et al. 2007; van Duin et al. 2011). Therefore, the available data for DSCR8/MMA1 across all patients was

inspected, and those patients exhibiting a relevant (> 1000 RFU) signal were plotted along with their overall disease status and OS, as indicated below in Fig. 4.27.

Figure 4.27: anti-DSCR8/MMA1 immunoglobulin titres across relevant patients. This graph indicates anti-DSCR8/MMA1 immunoglobulin titres across all patients and time points, highlighting those with statistical significance. CR: complete response, R: resistant, PR: partial response, SD: stable disease, PD: progressive disease.

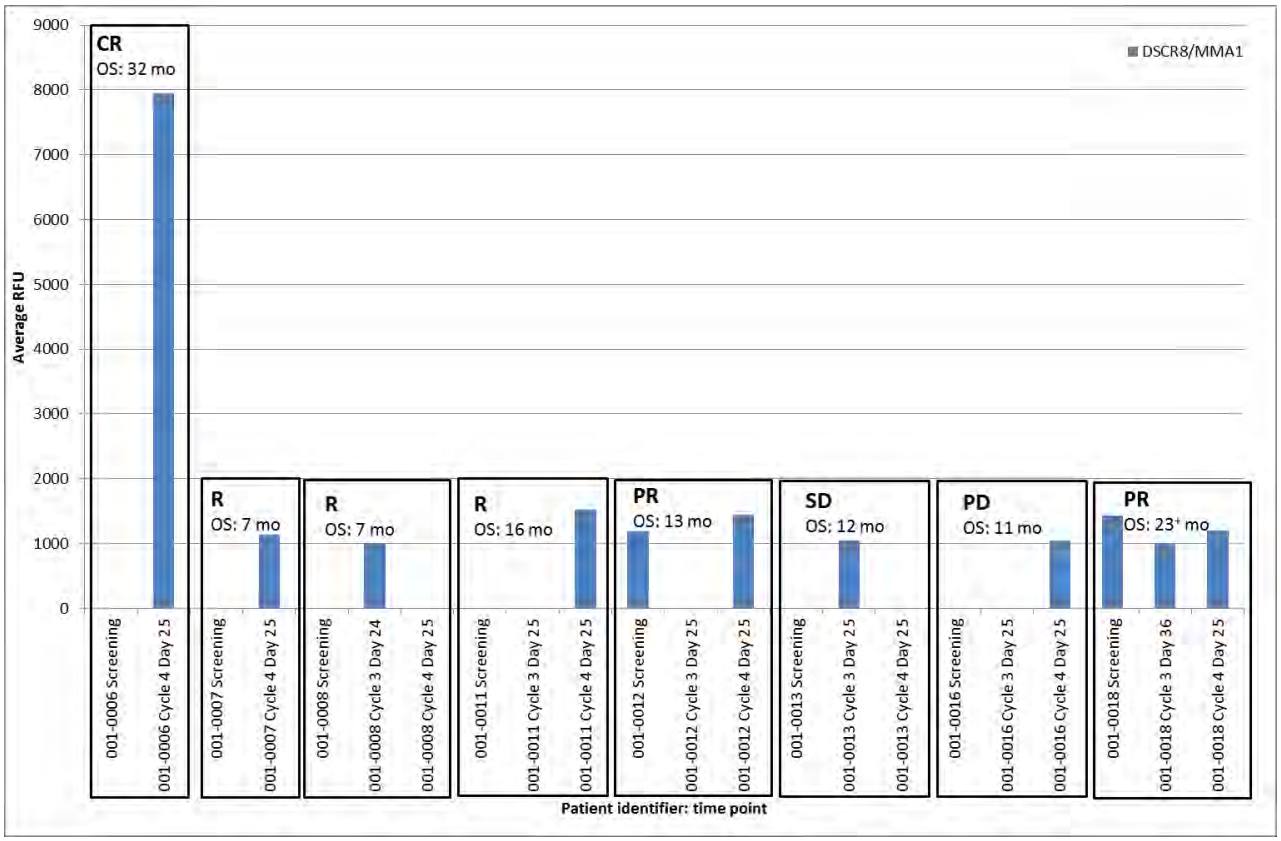

It was apparent that 8/12 (67%) patients showed responses towards this protein, without any particular exclusivity for a disease status (CR, R, PR, SD and PD) or average survival (ranging from 7 to 32 months). Although no clear evidence was apparent between DSCR8/MMA1 and disease status, this could possibly related to the limited number of patients. Hence, it may be of interest to conduct further studies using a larger cohort, as a means of verifying a potential use for this protein.

As a means of further understanding how DSCR8/MMA1 interacts with other proteins, which could potentially infer details regarding its unknown function, a STRING (search tool for the retrieval of interacting genes/proteins v9.1, http://string-db.org) analysis was performed, and the resulting network is indicated in Fig. 4.28 (Franceschini et al. 2013).

Figure 4.28: Network of STRING resulting associations with DSCR8/MMA1. This network is the evidence view using Homo sapiens, and each line colour represents the types of evidence for the association. Black line: coexpression; Green line: textmining.

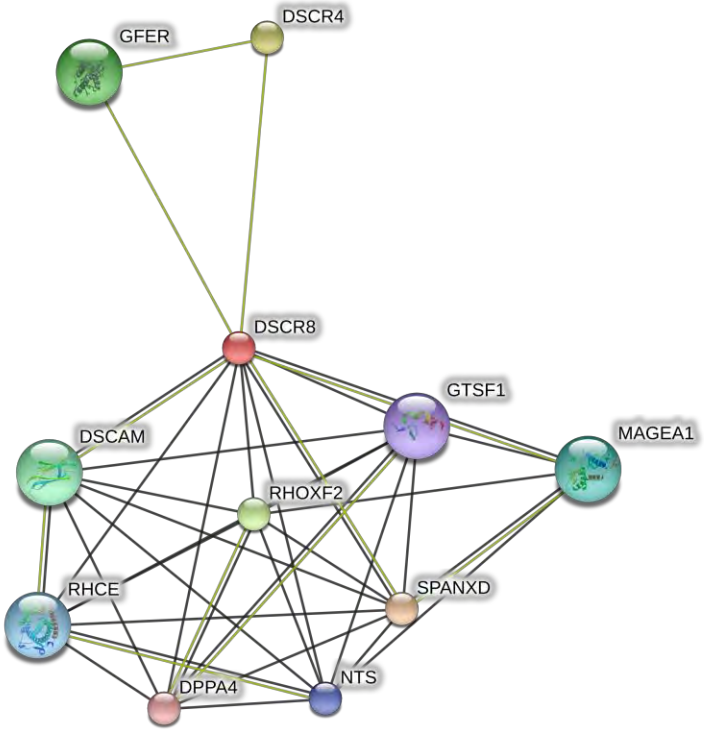

When visually inspecting this association, interestingly two other proteins that appeared as the 19 most significantly and abundantly expressed in this cohort, SPANXD (SPANX family, member E, unknown specific function) and DPPA4 (developmental pluripotency associated 4, may play a role in maintaining cell pluripotentiality) appear here as predicted functional partners (scores: 0.856 and 0.661, respectively). This prediction strengthens our findings made above for this treatment cohort, but does not necessarily clarify the function of DSCR8/MMA1.

Additionally, a BLAST (basic local alignment search tool) analysis against the *Homo sapiens* database using UniProtKB was conducted, with the intent of verifying which proteins shared a similar sequence with DCSR8 (Altschul et al. 1990; Altschul et al. 1997). The resulting alignments were ordered by E-value and score, and the best alignment, after excluding protein isoforms, was for Actin-related protein 10, with an E-value of $3e^{-6}$, a score of 110 and an identity of 68%. This protein has been reported to be involved in microtubule-based movement. When ordering the resulting alignments by identity, the best alignment was for Zinc finger matrin-type protein 1, with an E-value of $8e^{-3}$, a score of 81, and an identity of 82%. This protein has been reported to have a possible role in the p53-dependent growth

regulatory pathway, which is of particular interest, as p53 mutant autoantibody titres are also amongst the 19 most significantly detected of this cohort, possibly implying that p53 might also be a component of a network with DSCR8/MMA1 (Hellborg et al. 2001).

As mentioned above, to understand whether the observed autoimmune responses were speculatively indicative of temporal clinical responses, a matched disease status per time point must be assessed. For this purpose, on a patient-by-patient basis, each autoimmune profile was directly compared to the patient's clinical status at that time point, as a means of suggesting a biological significance of our generated data. When observing the autoimmune profile of patient 001-0002, which is mentioned above in Fig. 4.20 (and corresponding array images indicated in Fig. 4.21), it was indicated that at C4D25 (cycle 4, day 25), the patient was responding to treatment. This is in agreement with the array data which shows a statistically significant increase in CREB1 and PRKCZ autoantibody levels from screening to cycle 4 of epigenetic modification, whilst other signals remain more or less stable, which shows evidence of a matching partial response measured by bone marrow assessment. For patient 001-0016, whose immune profile is mentioned above in Fig. 4.22, clinical notes indicated a slight deterioration at C3D25 (cycle 3, day 25), followed by disease progression at C4D25 (cycle 4, day 25) of treatment, which is somewhat in agreement with the observed autoimmune responses. Although a slight – but statistically significant – increase (although below 1500 RFU) in MART-1/Melan-A levels is observed from screening to cycle 3, these levels drop below our noise threshold at cycle 4 of treatment and all other responses are below 1000 RFU. Hence, at the latter time point, the observed autoimmune profile suggests a complete lack of significant autoantibody level for this patient, which is in agreement with the matching reported disease progression. Lastly, when considering patient 001-013, whose autoimmune profile is indicated in Fig 4.23, clinical notes are not available for C3D25 (cycle 3, day 25), but indicate stable disease/no deterioration at C4D25 (cycle 4, day 25). This patient's autoantibody levels remain stable across all time points, including from screening to cycle 4 of treatment, showing evidence of a matching reported stable disease after epigenetic modification. Hence, in these three instances, the preliminary data suggests that temporal clinical statuses were in partial or complete agreement with observed autoimmune responses, which may indicate that the presence or absence of an autoimmune response might suggest the presence or absence of a clinical response.

When assessing the agreement between our array data and the temporal clinical data for the remaining nine patients of this treatment cohort, four patients (001-0001, 001-0003, 001-0006 and 001-0018) showed evidence of a complete agreement and one additional patient (001-0012) of partial agreement, indicating speculative evidence of partial or complete matching data across 8/12 (66.7 %) patients in this cohort. By contrast, the autoantibody levels observed for the remaining four patients (001-0004, 001-0007, 001-0008 and 001-0011) suggested no agreement with temporal clinical responses, or lack thereof, indicating no agreement across 4/12 (33.3%) patients. Interestingly, all patients that were

deemed clinically resistant to treatment (001-0007, 001-0008 and 001-0011) showed no evidence of agreement between array and temporal clinical data, whilst all patients that were indicated as complete responders (001-0001, 001-0003 and 001-0006) showed evidence of complete agreement. Hence, it is plausible that the patients that are deemed resistant to treatment, may be displaying some sort of immune evasion and associated suppression, and are thus displaying autoimmune profiles with limited possible inferences regarding immune efficacy. These findings suggest potential biological significance of our generated $CT100^{+}$ array data, as well as its prospective utility as a tool to monitor clinical responses to treatment. However, it is essential to note that all measurements require a baseline reference, as relative and not absolute changes are being assessed. Furthermore, these findings require further studies using a larger cohort, as the limited patient numbers do not allow for statistically significant inferences to be made.

We have applied our CT antigen microarray platform to the investigation of autoantibody profiles in a cohort of myelodysplasia patients undergoing epigenetic modification, and observed a large number (92% of the cohort) of autoantibody responses – statistically significant changes in autoantibody titres – to treatment. The main intent of this study was to assess whether epigenetic modification created neo-antigens and subsequent expanded antibody responses. In this regard, we identified autoantibody titres towards 19 potential antigens abundantly detected across this cohort. However, amongst these, no specific autoantibody titre appeared to be exclusively induced as a result to treatment. An expanded immune response after epigenetic treatment was evident across the majority of all patients, of which 67% of the cohort presented with preliminary evidence of a matching array and clinically reported responses. Furthermore, evidence of the lack of agreement between array and clinical data across all resistant patients suggests that immunoevasion – an emerging cancer hallmark – may be occurring, and thus possibly contributing towards cancer progression in these cases (Hanahan & Weinberg 2011).

In this epigenetic modification treatment cohort, we have successfully demonstrated that there are measurable differences in the autoantibody repertoires towards tumour-specific and –associated antigens between pre- and post-treated myelodysplasia patients, with preliminary evidence of possible correlation to the likelihood of clinical response. When considering patient sample numbers and relevant power calculations, the achieved statistical power is well below recommended (power > 0.8), which does not support the findings obtained in this cohort. Therefore although these results provide preliminary insight into this cohort, these warrant further confirmation across a larger group of patients.

We therefore anticipate that our novel, quantitative, customizable CT antigen microarray platform may find usage once again in monitoring patient responses to treatment, with potential therapy resistance inferences, warranting confirmation using a pre-stipulated specifically focussed study and homogeneous cohort design using sufficient patient numbers according to an *a priori* power calculation estimate.

4.3.4 Variable cancer type patients who underwent survivin treatment

A total of 103 serum samples, corresponding to forty-eight variable cancer patients with advanced solid tumours undergoing survivin treatment were assayed, processed and analysed according to our established CT100^{+} microarray pipeline. The following settings were used for the CT100^{+}.jar processing and filtering steps: mean or median values = mean, noise threshold = 2 standard deviations of the background, replicate CV threshold = 20%, whole array filtering control = 10 ng/µL Cy5-biotin-BSA and whole array CV threshold = 20%. The initial stipulated research question was whether the observed T-cell responses against survivin peptides were indicative of an expanded B-cell response, an autoantibody response detected by our CT100^{+} array. For this cohort, data analysis was conducted according to the available clinical information, which permitted the attribution of a best overall tumour response to treatment and presence of a post-vaccination immunological response for each patient, allowing for a comparison between our generated array data (B-cell responses) and the reported tumour and T-cell responses towards survivin. However, it is important to note that both the tumour and immunological data was sourced from the complete study, whilst the generated array data is based only on either baseline only, baseline and one post-vaccination time point or baseline and two post-vaccination time points, with no temporal data available, indicating that the provided blood samples could be from anytime between weeks 0 and 24. Therefore, comparison between these is not as direct as desired, as it is unknown what tumour or T-cell response was present at the matching array data time point. Nonetheless, these data were compared, based in the assumption that the array data represents baseline, 1st vaccination and 2nd vaccination. Furthermore, based on sample number-based power calculations indicated in Chapter 2, this cohort includes sufficient patient and sample numbers to be able to report statistically relevant results (power = 0.92).

A significant (> 1000 RFU) autoantibody response to treatment (increase in autoantibody titres above baseline) was present in 29/44 (66%) patients, with the remaining 4 patients having only a baseline blood sample. The strongest autoimmune response (~35000 RFU) was seen, both quantifiably and visually, for patient C05P005 (see Fig. 4.29 and 4.30).

Figure 4.29: Strongest patient autoimmune profile of the survivin cohort. This graph indicates the autoimmune profile of patient C05-P005 across two distinct time points (represented by different colours). As a means of clarifying the visualization of relevant titres, an insert of the magnified relevant data is indicated within this figure. *Statistically significant difference, $P < 0.05$ or **$P < 0.01$.

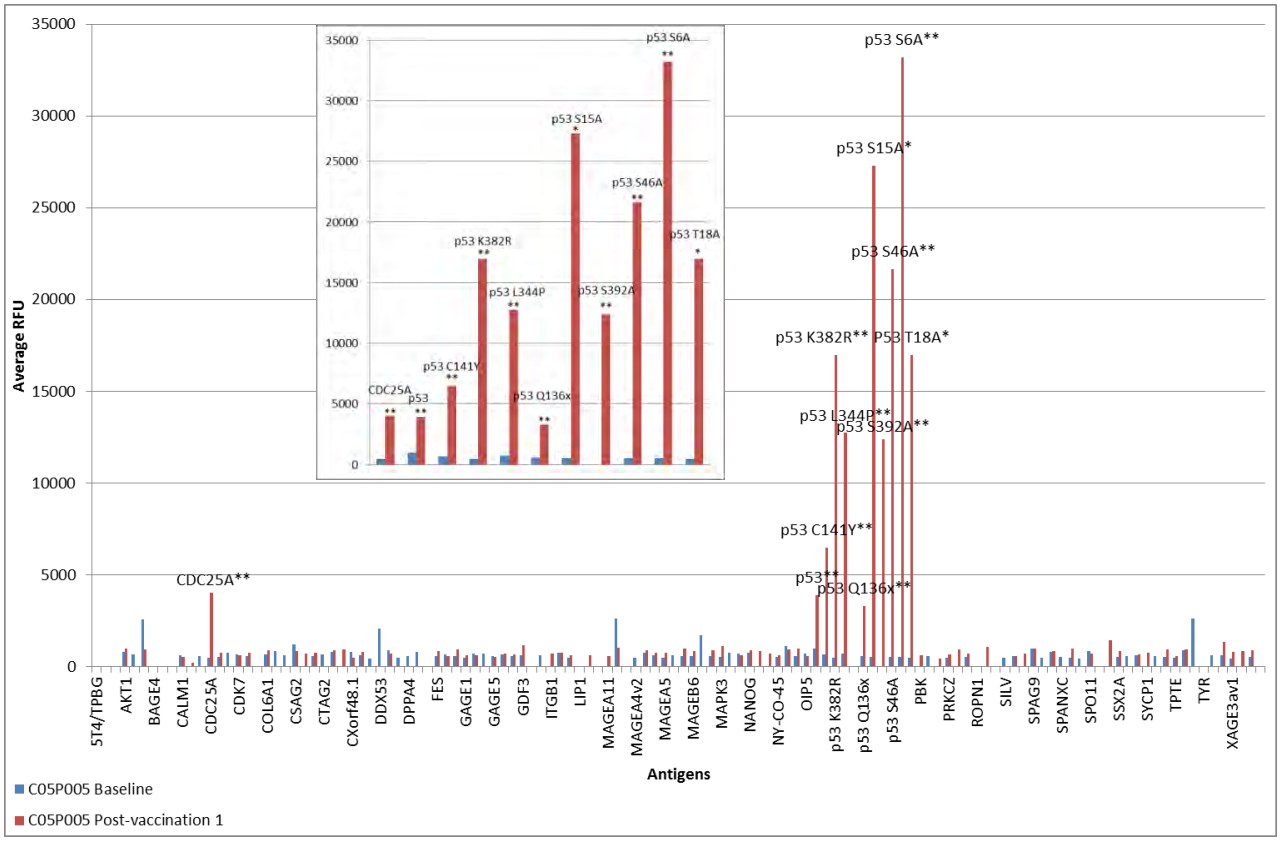

Figure 4.30: Strongest patient corresponding scanned array images of the survivin cohort. This figure indicates scanned array images of patient C05P005 before (image on left at baseline) and after (image on right at post-vaccination 1) treatment, with visual evidence of an autoantibody response towards many different p53 forms, either wild-type or mutant. Red boxes highlight triplicate p53 S392A, p53 K382R, p53 S46A, p53 S6A, p53 T18A, p53 S15A and p53 L344P positive signals.

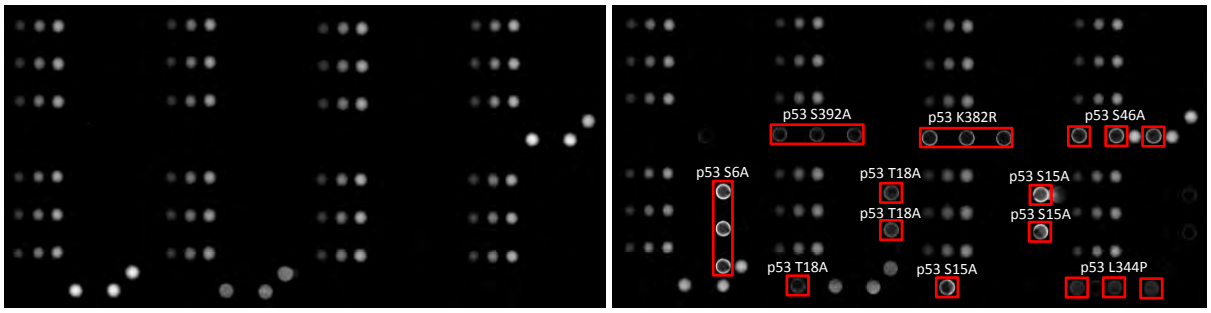

Patient C05P005, diagnosed with ovarian cancer, showed a statistically significant increase above 2000 RFU in CDC25A ($P < 0.01$) and in p53 ($P < 0.01$), p53 S6A ($P < 0.01$), p53 C141Y ($P < 0.01$), p53 S15A ($P < 0.01$), P53 T18A ($P < 0.01$), p53 Q136X ($P < 0.01$), p53 S46A ($P < 0.01$), p53 K382R ($P < 0.01$), p53 S392A ($P < 0.01$), p53 L344P ($P < 0.01$) in response to treatment. The fact that this patient shows autoimmune responses to nearly all p53s (with exception of p53 M133T), wild type and mutants, is most likely indicative of one form – most simply, wild type p53 – that shares a common epitope amongst these mutants. p53, also known as cellular tumour antigen p53, acts as a tumour suppressor in many distinct tumour types, with specific functions related to cell cycle regulation and induction of apoptosis (www.uniprot.org) (El-Deiry et al. 1993). p53 mutations are common in cancer, which has led to the extensive study of these abnormalities in regards to carcinogenesis and the ability to potentiate cancer progression, as well as their possible diagnostic, prognostic and therapeutic implications (Greenblatt et al. 1994; Risch 1998). In regards to ovarian cancer in particular, the overexpression and mutation of p53 is a known phenomenon, which is consistent with our finding within this specific cancer type, amongst the several ones included in this treatment cohort (Kupryjańczyk et al. 1993; Marks et al. 1991). It has also been shown that in ovarian cancer these mutations are linked to chemotherapy resistance, early relapse and shortened overall survival (Reles et al. 2001).

A comparison between the observed autoimmune profile and the best observed clinical response for this patient was not possible, as the latter was non-evaluable. However, when assessing this patient's immunological response, no T-cell response against survivin as a result of treatment was detected. When comparing the obtained autoimmune profile for this patient with the overall reported clinical and T-cell responses, these are not in agreement, as these latter data seem to indicate no response towards treatment. This lack of preliminary correspondence may be due to the lack of temporal matching of the array data with the reported clinical and T-cell responses. As a means to verify if the p53 autoimmune responses were restricted to this patient, all other autoimmune profiles were inspected, and two additional patients were found with a similar response, C01P028 (PD) and C01P0029 (PD). Interestingly, these two patients were also diagnosed with ovarian cancer, which supports this finding, yet neither patient presented a clinical response to treatment. However, patient C01P028 did have a T-cell response to treatment, which could be explained by either a younger age (44) or the presence of 3 HLA types (A01, A03 and B07), when compared to patients C05P005 (63 years of age, HLA type A01) and C01P029 (67 years of age, HLA types A02 and A03), respectively. Due to the limited amount of ovarian cancer patients in this cohort, an additional study using a larger patient cohort should be performed, as a means of verifying if these findings hold true across a significant number of patients.

Of the remaining 15 patients, a significant decrease in autoantibody response to treatment (decrease in autoantibody titres above baseline) was present in 7/44 (16%) patients, whilst 8/44 (18%) patients presented with stable autoimmune levels. A decrease in autoantibody titres was seen for patients

C01P007 (colorectal cancer, PD, survivin T-cell response), C01P012 (colorectal cancer, PD, survivin T-cell response), C01P040 (mesothelioma, PD, no survivin T-cell response), C03P009 (melanoma, PD, survivin T-cell response), C03P012 (colorectal cancer, NE, no survivin T-cell response), C03P020 (melanoma, PD, no survivin T-cell response) and C05P017 (neuroendocrine tumour, SD, survivin T-cell response). Once again, no evidence of a correlation is seen between the reported overall patient characteristics and the autoimmune profile, probably due to the lack of comparison between temporal clinical and immunological responses. The patients who presented with stable autoantibody titres across all assayed array time points included C01P013 (sarcoma, PD, survivin T-cell response), C01P024 (colorectal cancer, SD, no survivin T-cell response), C02P003 (melanoma, PD, no survivin T-cell response), C02P008 (outstanding clinical information), C03P002 (NSCLC, PD, survivin T-cell response), C03P005 (NSCLC, SD, survivin T-cell response), C03P014 (breast cancer, PD, survivin T-cell response) and C04P013 (melanoma, PD, no survivin T-cell response). As indicated above, no correlation is seen between the reported overall patient characteristics and the autoimmune profile.

Of the 123 cancer-associated antigens present on our CT100^{+} array, the most prevalent significant autoantibody titres (above 1000 RFU) detected in this cohort were towards 20 leading antigens. These were detected in at least nine or more instances across all patient time points (baseline or post-treatment) in this cohort, and most abundantly towards NY-ESO-1 and CTAG2/LAGE-1b/LAGE-1L, as indicated below in Fig. 4.31.

Figure 4.31: Most prevalent autoantibody titres detected across the survivin treatment cohort. This graph indicates the summed number of times autoantibody levels were detected towards the 20 leading antigens at titres above 1000 RFU , with distinction between B: baseline; V1: post-vaccination 1; and V2: post-vaccination 2.

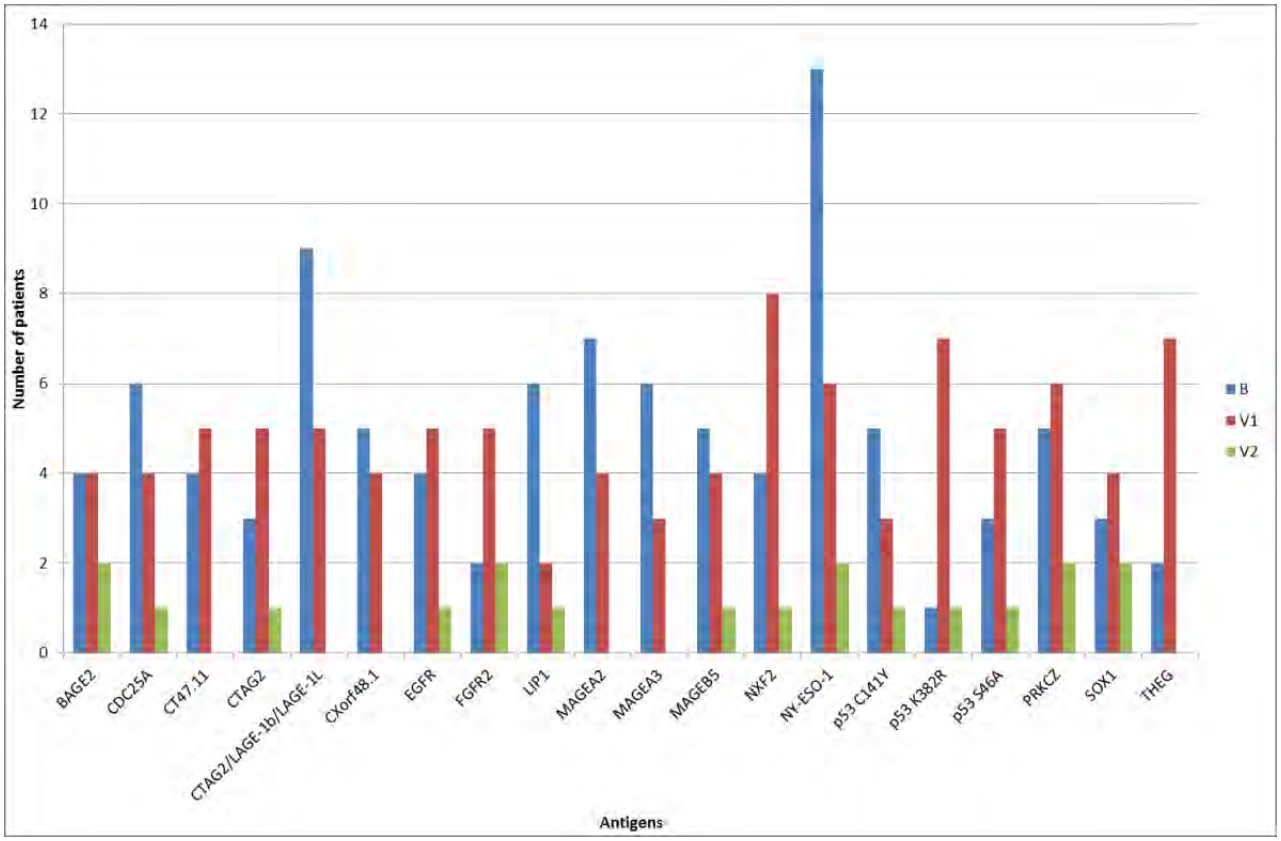

Based on this graph, it was evident that initially, when comparing baseline to post-vaccination 1, half of these prevalent autoantibody responses towards these leading antigens were increasing (*n* = 10/20, 50%), whilst the rest were either decreasing (*n* = 9/20, 45%) or stable (*n* = 1/20, 5%). When comparing post-vaccination 1 to 2, all prevalent autoantibody responses towards these leading antigens decrease (*n* = 20/20, 100%), however, this is most likely a function of only 10/48 (21%) patients possessing the post-vaccination 2 time point, as the majority of the patients included in our cohort have only two time points. Based on the initially established research question, our interest was towards those autoantibody titres that were both augmented and decreased as a result to treatment, as we wanted to assess whether the observed T-cell responses were indicative of an autoantibody response. The two most abundant autoantibody titres of this set are decreasing from baseline to post vaccination time points 1 and 2.

As a means of defining whether these most abundant autoantibody titres were clustering within a specific cancer type, radar plots were constructed for the three most abundant cancer types in this

cohort, melanoma (*n* = 9/46, 20%), colorectal cancer (*n* = 8/46, 17%) and ovarian cancer (*n* = 7/46, 15%), and are indicated below in Fig. 4.32, 4.33 and 4.34.

Figure 4.32: Radar plot of the prevalent autoantibody titres detected towards the leading 20 antigens across melanoma patients of the survivin cohort. Each antigen is indicated by an axis, and each patient sample is indicated in a different colour.

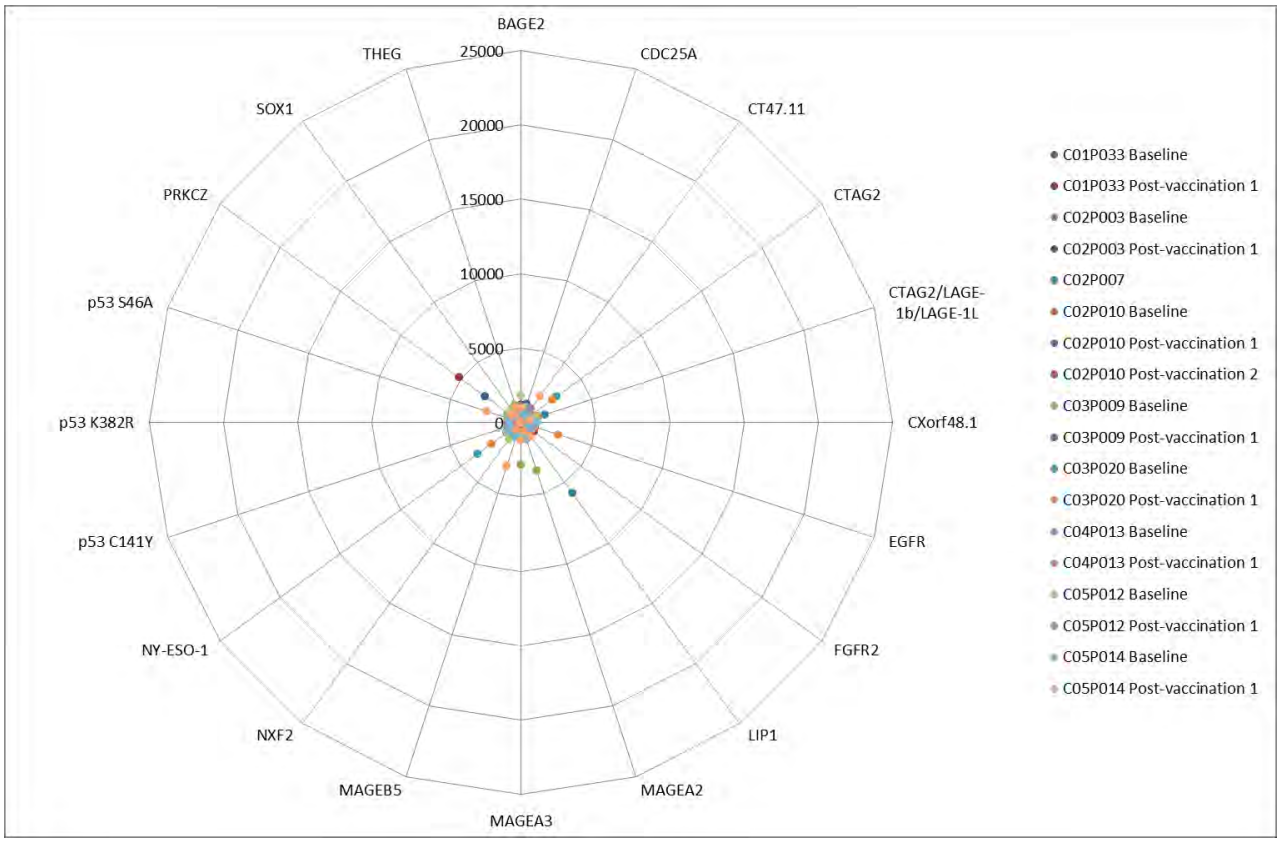

Figure 4.33: Radar plot of the prevalent autoantibody titres detected towards the leading 20 antigens across colorectal cancer patients of the survivin cohort. Each antigen is indicated by an axis, and each patient sample is indicated in a different colour. NY-ESO-1 (˜45000 RFU) for patient C01P007 at baseline was omitted in this plot (outlier), due to an above average high intensity, to permit an equal axis range amongst cancer type radar plots.

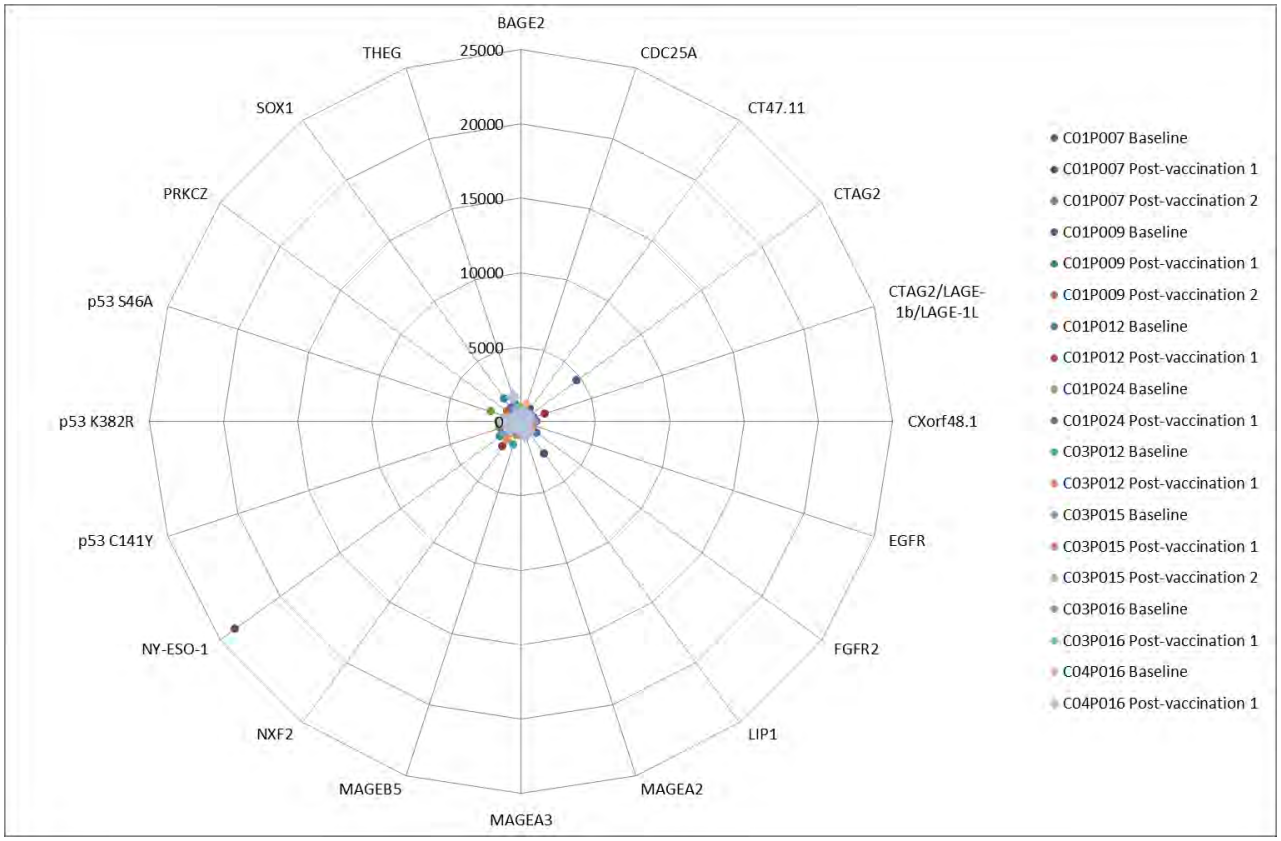

Figure 4.34: Radar plot of the prevalent autoantibody titres detected towards the leading 20 antigens across ovarian cancer patients of the survivin cohort. Each antigen is indicated by an axis, and each patient sample is indicated in a different colour.

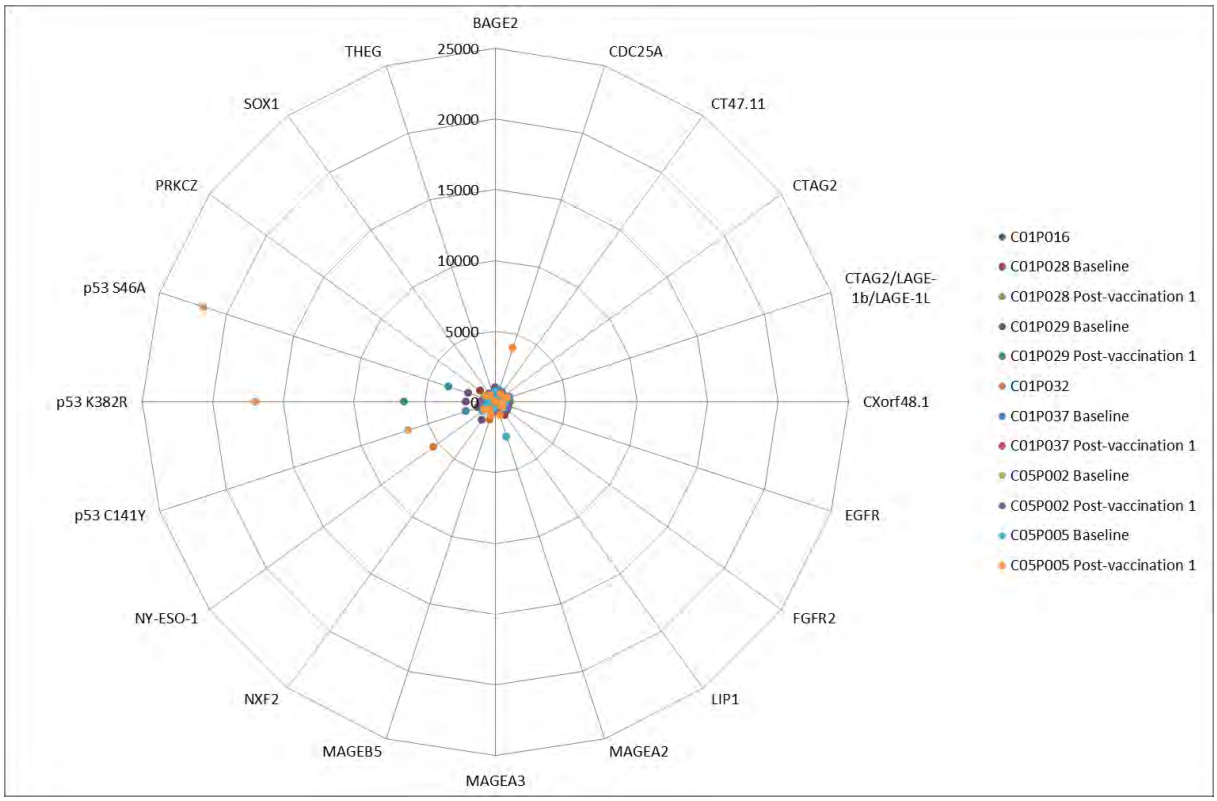

In regards to melanoma (see Fig. 4.32), it was evident that this cancer type presented the overall lowest autoantibody signals in comparison to colorectal and ovarian cancer, with the highest intensity being only 6000 RFU. The highest autoantibody titres were towards LIP1 (~6000 RFU), PRKCZ (~5000 RFU) and NY-ESO-1 (~3500 RFU), along with the expected melanoma antigens, MAGEA2, MAGEA3 and MAGEB5 (~3000 RFU). When assessing the resulting radar plot for the colorectal cancer patients (see Fig. 4.33), it was clear that this cancer type presented the overall highest signals, with intensities reaching ~45000 RFU. The antigens that presented with the highest autoantibody titres were NY-ESO-1 (~45000 RFU) and CTAG2 (~4500 RFU), as well as LIP1 (~2500 RFU). The NY-ESO-1 and CTAG2 pair usually appears together due to their high sequence homology (77%). In regards to ovarian cancer (see Fig. 4.34), the highest autoantibody titre reached ~21500 RFU, with evidence of accumulative p53 mutant (p53 C141Y, p53 K382R and p53 S46A) autoantibody titres ranging from ~2000 to ~21500 RFU. Whether or not these mutant forms correspond to multiple mutations or simply a shared epitope of one form remains to be determined, warranting further genomic testing. Besides from these, NY-ESO-1 (~5500 RFU) and CDC25A (~4000 RFU) were also amongst the highest titres. When combining these findings, it seems that only NY-ESO-1 was present in all three cancer types, which interestingly coincide with the most

abundant protein of this treatment cohort. The second most abundant protein, CTAG2/LAGE-1b/LAGE-1L, was a CTAG2 isoform, which also explains why this pair arose as the most abundant amongst the 20 antigens reported here.

As a means of interpreting these findings, and verifying their biological significance, the most abundant autoantibody titres towards NY-ESO-1 and CTAG2/LAGE-1b/LAGE-1L, were investigated further.

NY-ESO-1, a CT antigen member broadly described in Section 4.3.1 in regards to the kinase inhibition treatment cohort, has once again appeared as one of the most significant autoantibody titres. CTAG2/LAGE-1b/LAGE-1L, a CTAG2 (NY-ESO-2) isoform usually reported as LAGE-1b, is evidently yet another member of the CT antigen family. LAGE-1b has also been reported as an attractive immunotherapeutic target, mainly due to similarities with NY-ESO-1, and has been reported to have both prognostic and predictive value in cancers (Lethé et al. 1998; Odunsi et al. 2003; Dyrskjøt et al. 2012). Furthermore, survivin cancer treatment, as the one administered to the patient in this treatment cohort, has been reported to induce frequent, robust and multifunctional $CD4^+$ T-cell responses amongst vaccinated patients, which have been shown to be essential for the induction and maintenance of cytotoxic T-cell responses (Widenmeyer et al. 2012). Therefore, the available data for NY-ESO-1 and CTAG2/LAGE-1b/LAGE-1L across all patients was inspected, and those patients exhibiting relevant (> 1000 RFU) signals were plotted along with their presence or absence of T-cell and clinical response, as indicated below in Fig. 4.35.

Figure 4.35: Anti-NY-ESO-1 and -CTAG2/LAGE-1b/LAGE-1L immunoglobulin titres across relevant patients. This graph indicates anti-NY-ESO-1 (in red) and -CTAG2/LAGE-1b/LAGE-1L (in blue) immunoglobulin titres across all patients and time points, highlighting those with statistical significance. PD: progressive disease; SD: stable disease.

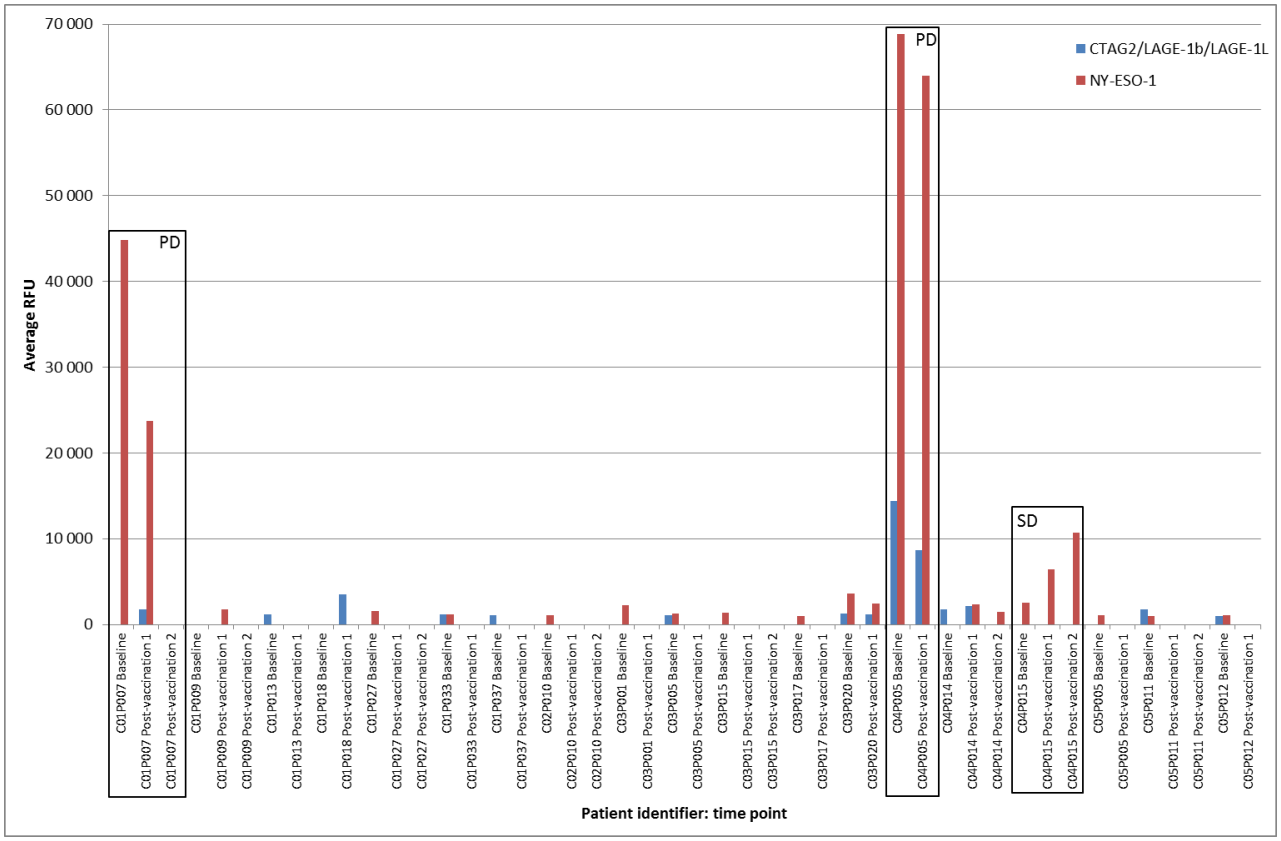

It was apparent that 17/48 (35%) patients showed responses towards NY-ESO-1, with the majority of these presenting clinically as stable disease (*n* = 9/17, 53%), followed by progressive disease (*n* = 7/17, 41%) and one non-evaluable case (*n* = 1/17, 6%). After treatment, these responses mainly decreased (*n* = 13/17, 76%), with only a few increases (*n* = 3/17, 18%), and a patient with a single time point (*n* = 1/17, 6%). Amongst the three patients who showed an increase in autoantibody titres after survivin treatment, all three were deemed as clinically stable throughout the clinical trial. However, although an additional six patients were also stable, their titres decreased as a result to treatment, which is difficult to explain without further clinical studies, but may suggest that either the anti-NY-ESO-1 antibody response is not clinically relevant here, or that there are distinct subtypes of cancer, some of which may be immune suppressive in character (Sadanandam et al. 2013; Sanz-García et al. 2014; The Cancer Genome Atlas Reserach Network 2013; Konecny et al. 2014).

In regards to CTAG2/LAGE-1b/LAGE-1L, responses were seen towards 12/48 (25%) patients, with the majority of these presenting clinically with progressive disease (*n* = 8/12, 67%), the remaining patients

remaining stable (*n* = 4/12, 33%). Once again, the majority of these are decreasing as a result of treatment (*n* = 8/12, 67%), with only a few increases (*n* = 3/12, 25%), and one patient with a single time point (*n* = 1/12, 8%). Amongst the three patients with increasing titres, two are classified as having progressive disease, and solely one as stable. By contrast, the additional three stable patients presented a decrease in autoantibody titres.

It is difficult to compare the resulting autoimmune profiles with the clinical and immunological reported findings of this clinical trial, due to lack of temporal and peptide match between the latter and the array data. However, an attempt to compare these might still provide some relevant information. Based on the array data, it was clear that complete agreement between clinical and survivin T-cell responses was also not obtained.

When considering the clinical responses, amongst the 14/46 (30%) patients classified as having stable disease, 10/14 (71%) of those presented with autoantibody responses to treatment. An equal number of 10/14 (71%) of these patients also presented with survivin T-cell responses post-vaccination, although of these only 7/10 (70%) patients presented with matching expanded B-cell and survivin T-cell responses. Amongst the 27/46 (59%) patients classified as progressive disease, 14/27 (52%) of those presented with elevated autoantibody responses to treatment, while 4/27 (15%) could not be evaluated (single time point). A slightly higher number of 15/27 (55%) of those patients also presented with survivin T-cell responses post-vaccination, although only 9/15 (60%) of these presented with matching expanded B-cell and survivin T-cell responses. This indicates that 9/27 (33%) patients classified as progressive disease also did not present elevated autoantibody responses to treatment.

In regards to the survivin T-cell responses, amongst the 29/46 (63%) patients classified as having a survivin T-cell response post-vaccination, 17/29 (59%) of those presented with autoantibody responses to treatment, while 4/29 (14%) could not be evaluated (single time point). Amongst the 17/46 (40%) patients classified as non- survivin-T-cell responders post-vaccination, 11/17 (65%) of those presented with autoantibody responses to treatment. This indicates that 6/17 (35%) patients classified as non-survivin-T-cell responders also did not present autoantibody responses to treatment.

Hence, it appeared that the array generated data showed speculative evidence of 71% (SD) and 33% (PD) agreement with the reported clinical data, and 59% (survivin T-cell responders) and 35% (non-survivin-T-cell responders) agreement with the reported T-cell data. The lack of correspondence in the lower percentages may be related to lack of temporal equality of the array generated data. However, it is of note that 52% of the patients presenting with progressive disease and 65% of the patients classified as non-survivin-T-cell responders presented an expanded B-cell responses to treatment. Unfortunately, survivin was not present on our CT100^{+} array, but it would be interesting to verify if a matching anti-survivin B-cell response was present in the patients reported as having a T-cell response against survivin.

Nonetheless, these results indicate that a possible expanded B-cell immunological response towards cancer-associated antigens might be occurring as a result of survivin vaccination in 29/44 (66%) patients in this cohort, most likely due to survivin therapy leading to tumour lysis, which in turn leads to an increase in circulating cancer antigens, and therefore resulting in an increase in detected autoantibody responses towards those antigens. Whether such increases actually signify a clinical efficient immune response to therapy or are simply symptomatic remains to be determined.

We have applied our CT antigen microarray platform to the investigation of autoantibody profiles in a cohort of variable cancer type patients undergoing survivin treatment, and observed a defined number (66% of the cohort) of autoantibody responses – statistically significant increases in autoantibody titres – to treatment. The main intent of this study was to assess whether the induction of an autoantibody response correlated with reported induced survivin-specific T-cell responses post-treatment amongst these patients. In this regard, it is interesting that our CT antigen array data suggests evidence of direct correlation between our observed autoantibody responses and the survivin-specific T-cell reported ones across a subset of patients (59% of the cohort). Hence, this proposes that a potential expanded B-cell immunological response may be occurring as a result to treatment, as although a survivin-specific therapeutic is administered a variety of autoantibody responses towards other cancer-associated antigens are observed. Furthermore, a direct correlation between our data the reported clinical benefit was also observed, across a larger subset of patients (71%). Nonetheless, these findings warrant further investigation due to the lack of exact temporal matching between antibody, T-cell and clinical responses.

In this survivin treatment cohort, we have successfully demonstrated that there are measurable differences in the autoantibody repertoires towards tumour-specific and –associated antigens between pre- and post-treated patients, with preliminary evidence of possible correlation to the likelihood of clinical and T-cell response. Furthermore, we have successfully identified a well-established therapeutic target – NY-ESO-1 – and an isoform of its homologous pair (CTAG2), CTAG2/LAGE-1b/LAGE-1L, which were the two most abundant antigens toward which autoantibody titres were detected, present across 35% and 25% patients, respectively. The fact that both these antigens share the majority of their sequence and have common epitopes suggests that autoantibody responses are probably towards one of these forms in particular (most likely NY-ESO-1). When considering patient sample numbers and relevant power calculations, although this cohort is quite diverse regarding patient age and tumour type , the achieved statistical power is above recommended (power > 0.8), supporting the findings obtained in this cohort.

We therefore anticipate that our novel, quantitative, customizable CT antigen microarray platform may find usage in future cancer research in monitoring patient expanded autoantibody responses to treatment and identifying novel therapeutic targets, warranting confirmation using a pre-stipulated

specifically focussed study and homogeneous cohort design using sufficient patient numbers according to an *a priori* power calculation estimate.

4.3.5 Colorectal cancer patients with unresectable liver metastasis who underwent SIRT treatment

A total of 25 serum samples, corresponding to eleven colorectal cancer patients with unresectable liver metastasis undergoing selective internal radiotherapy were assayed, processed and analysed according to our pre-established CT100^{+} microarray pipeline. The following settings were used for the CT100^{+}.jar processing and filtering steps: mean or median values = mean, noise threshold = 2 standard deviations of the background, replicate CV threshold = 20%, whole array filtering control = 10 ng/µL Cy5-biotin-BSA and whole array CV threshold = 20%. The initial stipulated research question was to assess the effect of selective internal radiotherapy on a patient's autoimmune profile, thereby potentially inferring a successful clinical response to treatment. For this cohort, data analysis was conducted based on the available clinical trial and sample information, which permitted comparison between patient autoimmune profiles before and after SIRT treatment, as a means of verifying the immunological efficacy of this treatment. However, it is important to note that due to the absence of basic clinical information and the resulting clinical efficacy or inefficacy, speculative clinical inference and correlation with immunological data may not be made, therefore limiting this analysis. Furthermore, based on sample number-based power calculations indicated in Chapter 2, this cohort does not include sufficient patient and sample numbers to be able to report statistically relevant results (power = 0.32).

A significant (> 1000 RFU) autoantibody response to treatment (increase in autoantibody titres above baseline) was present in 6/11 (55%) patients, while the remaining four patients showed a decrease in autoantibody titres as a response to treatment. As previous studies have reported a clinical efficacy of up to 90%, a relatively high clinical response rate is predicted (Stubbs et al. 2001; Stubbs & Wickremesekera 2004). However, if that clinical response is suggested to be correlated with an immune one, a much lower speculated response rate is seen here for this treatment cohort. The highest autoantibody titres detected both quantifiably and visually were for patient SIRT027 (~60000 RFU), although these decrease from baseline to each successive time points after treatment (see Fig. 4.36 and 4.37).

Figure 4.36: Strongest patient autoimmune profile of the SIRT cohort. This graph indicates the autoimmune profile of patient SIRT027 across three distinct time points (represented by different colours). As a means of clarifying the visualization of relevant titres, an insert of the magnified relevant data is indicated within this figure. **Statistically significant difference, P < 0.01.

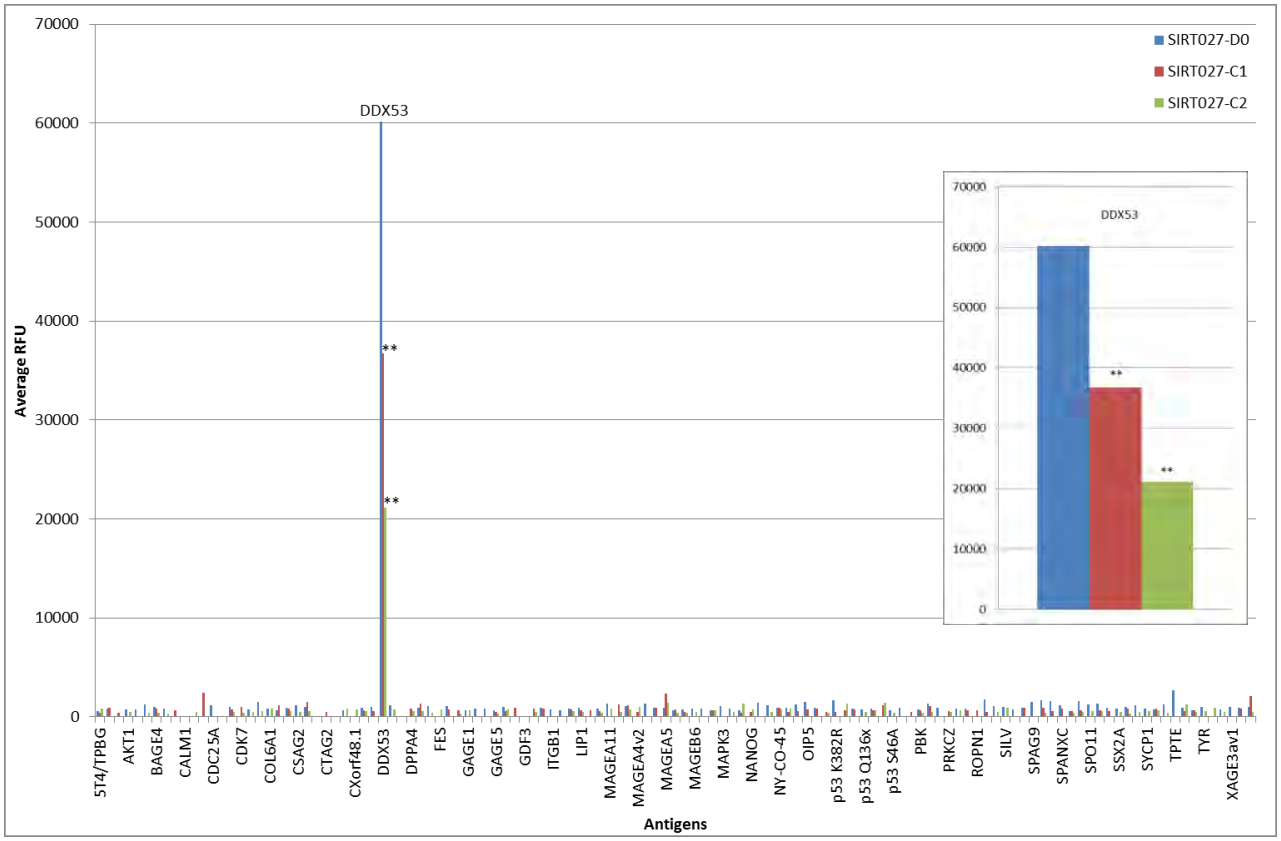

Figure 4.37: Highest autoantibody titres patient's corresponding scanned array images of the SIRT cohort. This figure indicates scanned array images of patient SIRT027 before (image on left at baseline) and after treatments (image in middle at cycle 1, and image on right at cycle 2), with visual evidence of a decreasing autoantibody response towards DDX53. Red boxes highlight triplicate DDX53 positive signals.

Patient SIRT027 showed a statistically significant decrease in DDX53 (P < 0.01) from an initial high signal of ~60000 RFU at baseline, to ~37000 RFU at cycle 1 of treatment, and then to ~21000 RFU at cycle 2 of treatment, showing a progressive decrease in autoantibody titres as a response to treatment. DDX35, a

known CT antigen also known as CAGE, has a known catalytic function involved in both ATP and RNA binding (www.uniprot.com). This decrease in autoantibody titres could either signify that antibody-antigen complexes have formed resulting in less free circulating antibodies available for detection using our array platform (which seems unlikely), or that there is a possible decrease in clinical efficacy. It is essential to note that due to the nature of this treatment, it is unknown whether a cancer-specific immune response is expected, as this treatment consists of radiotherapy rather than immunotherapy. Furthermore, a study has reported that immediate levels of serum CEA (carcinoembryonic antigen) after treatment might be a misleading indication of clinical efficacy, as these levels only gave the best and most indicated information only 2-3 months after treatment administration (Stubbs & Wickremesekera 2004). However, due to the lack of clinical efficacy information, the true reasoning as to whether an immune response may be indicative of a clinical one remains to be determined.

Of the 123 cancer-associated antigens present on our CT100^{+} array, the most prevalent significant autoantibody titres (above 1000 RFU) detected in this cohort were towards 12 leading antigens. These were detected in at least six or more instances across all patient time points (baseline or cycles of treatment) in this cohort, and most abundantly towards CSAG2, as indicated below in Fig. 4.38.

Figure 4.38: Most prevalent autoantibody titres detected across the SIRT treatment cohort. This graph indicates the summed number of times autoantibody levels were detected towards the 12 leading antigen at titres above 1000 RFUs, with distinction between D0: baseline; C1: cycle 1; and C2: cycle 2.

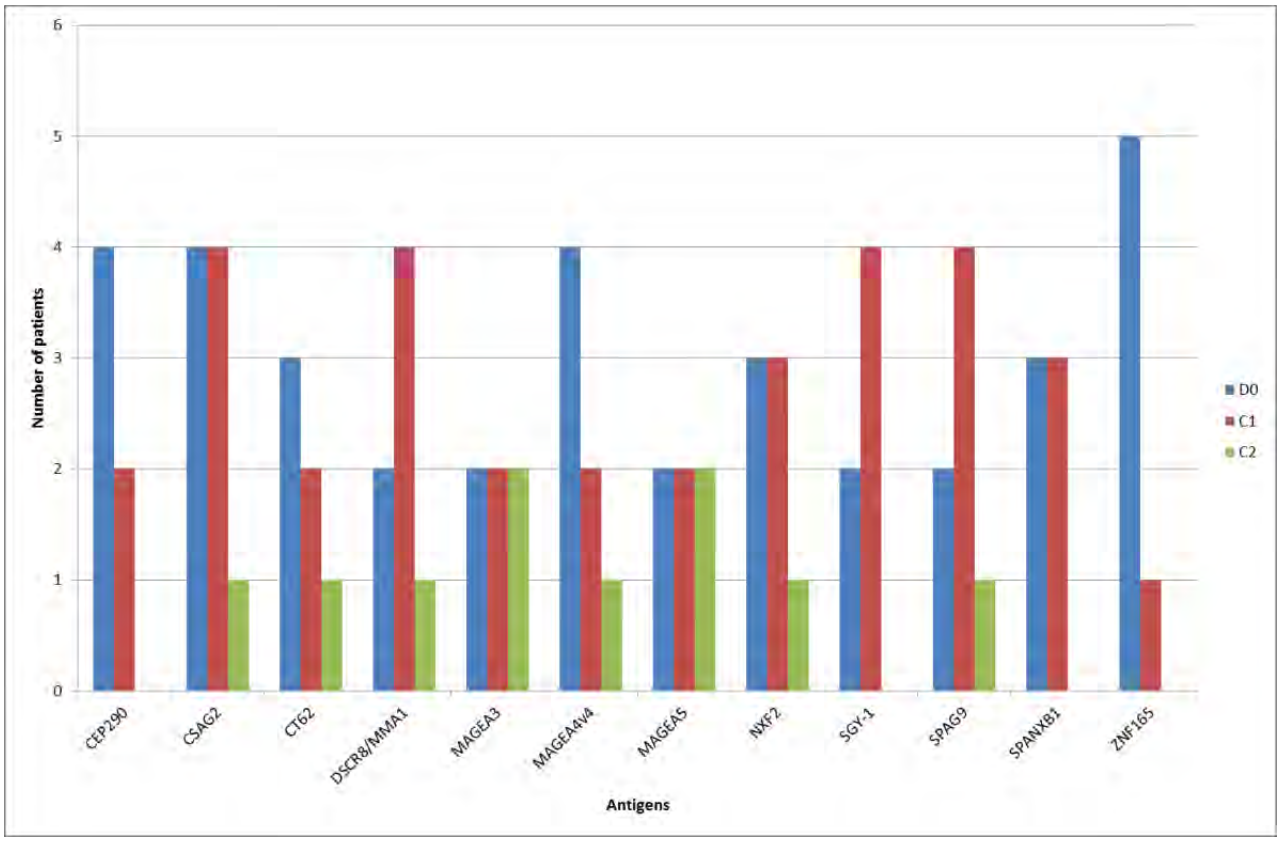

Based on this graph, it was evident that initially, when comparing baseline to cycle 1 of treatment, the majority of these prevalent autoantibody responses towards these leading antigens were stable (*n* = 5/12, 42%), whilst the rest were either decreasing (*n* = 4/12, 33%) or increasing (*n* = 3/12, 25%). When comparing cycle 1 to 2, the majority of the prevalent autoantibody responses decrease (*n* = 10/12, 83%), while the remaining two (*n* = 2/12, 17%) remain stable. This is most likely a function of only 3/12 (25%) patients possessing the cycle 2 time point, as the majority of the patients included in our cohort have only two time points. Based on the initially established research question, our interest was towards those autoantibody titres that were both augmented and decreased as a result to treatment, as we wanted to assess the effect of selective internal radiotherapy on a patient's autoimmune profile, thereby potentially inferring a successful clinical response to treatment. The most abundant autoantibody of this set, towards the CT antigen CSAG2, was initially stable from baseline to cycle 1 of treatment, but then decreased from cycles 1 to 2. Interestingly, both CSAG2 and the remaining eleven (CEP290, CT62, DSCR8/MMA1, MAGEA3, MAGEA4v4, MAGEA5, NXF2, SGY-1, SPAG9, SPANXB1 and ZNF165) most abundantly detected autoantibody titres of this treatment cohort were all CT antigens

(CTdatabase: www.cta.lncc.br). The fact that the most relevant antigens in this cohort were all CT antigens serves as a validation of our vast CT antigen selection for this array platform.

As a means of comprehending what role CSAG2 plays in this advanced cancer type or therapy, it was investigated further. Chondrosarcoma-associated gene 2/3 protein (CSAG2), also known as taxol-resistant-associated gene 3 protein (TRAG-3), is a drug resistance related protein, with its expression being associated with chemotherapy resistant, neoplastic and possibly malignant phenotype (www.uniprot.com). CSAG2 expression was first reported in ovarian carcinoma cell lines, but a study using colorectal cancer cell lines also confirmed its expression in the cancer type of this treatment cohort (Duan et al. 1999; Nimmrich et al. 2000). The clinical impact of this overexpression was studied in ovarian carcinoma patients, and it was demonstrated that an overall progression-free survival was increased for those who expressed a weak CSAG2 signal, making this protein a prognostic factor for the prediction of clinical outcome after chemotherapy (Materna et al. 2007). Furthermore, this protein has been found to be co-expressed with the fellow CT antigen MAGE family (Lin et al. 2002). This finding validates the fact that three distinct members of the MAGE family, MAGEA3, MAGEA4v4 and MAGEA5, were alongside with CSAG2 amongst the antigens towards which autoantibody titres were most abundantly detected in the SIRT treatment cohort. As a means to further assess the levels of CSAG2 autoantibodies in this cohort, the available data for CSAG2 across all patients was inspected, and an autoantibody trendline across this whole cohort was constructed, as indicated below in Fig. 4.39.

Figure 4.39: Anti-CSAG2 immunoglobulin titre trendline across SIRT treatment cohort. Threshold on graph indicates ~1000 RFU, as a means of facilitating view of most significant signals.

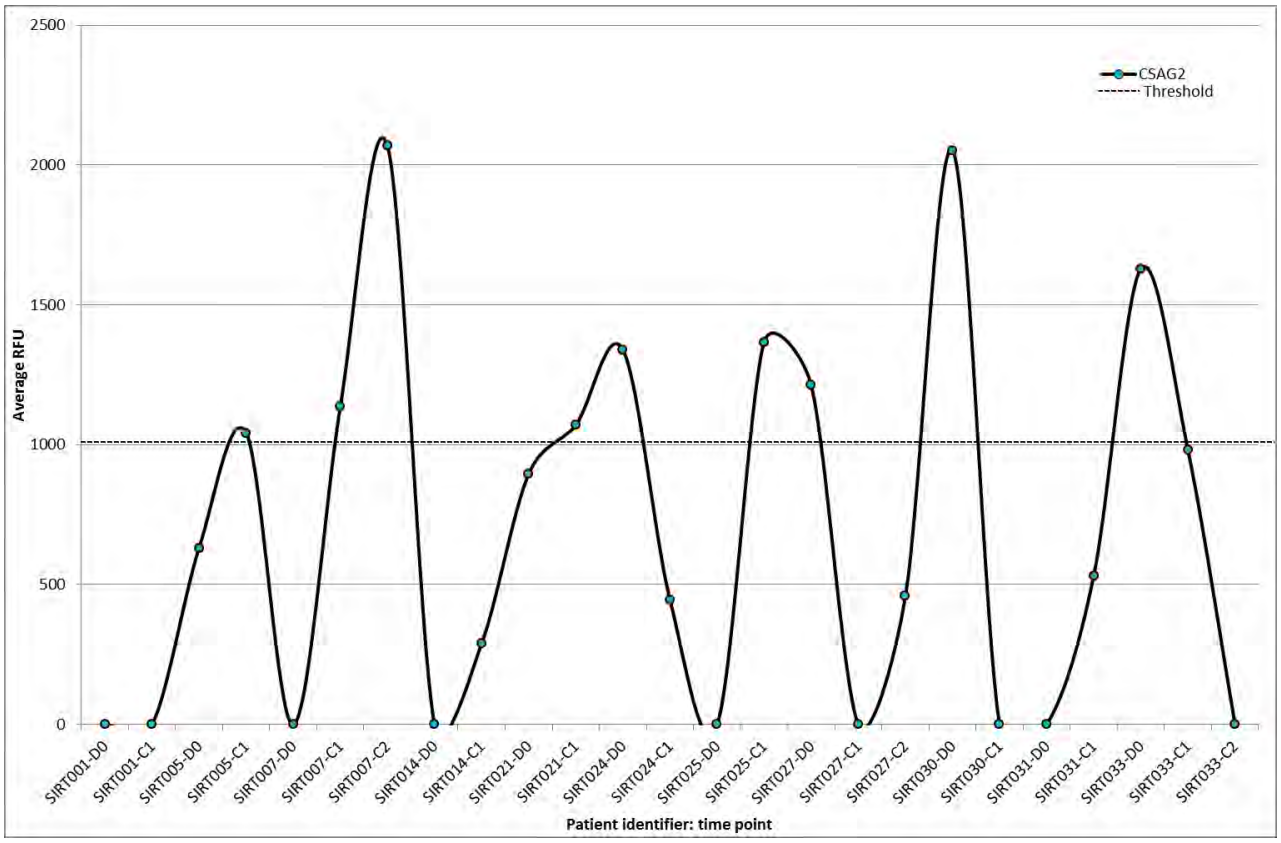

Visual inspection of this anti-CSAG2 immunoglobulin titre trendline indicated that autoantibody titres against CSAG2 were quite variable across our cohort, with two spikes above 2000 RFU for patients SIRT007 at cycle 2 and SIRT030 at baseline. Oddly, these spikes occurred at opposite time points, with the first being induced as a result of treatment, and the second being present at baseline, but then drastically reduced. Therefore, one might assume that the potential clinical effect were contrary in these two patients, although this has not been confirmed. When comparing these two patient's complete autoimmune profiles, it was evident that patient SIRT007 presented an overall autoimmune response to treatment, with an increase in autoantibody titres from baseline to cycle 1, whilst patient SIRT030 did not, showing a drop in autoantibody titres from baseline to cycle 1 of treatment. This further adds to our assumption of clinical efficacy on regards to patient SIRT007. As mentioned above, high levels of this protein prior to therapy are indicative of a poorer overall and progression free survival, indicating a poor prediction of clinical outcome after therapy (Materna et al. 2007). Hence, this further verifies our assumption regarding poor predicted clinical efficacy in patient SIRT030. However, this prediction cannot be verified due to restricted access to clinical efficacy results, and most importantly, due to the limited patient numbers in this cohort. An additional study using a larger patient cohort may be relevant to assess if any clinical significance of this finding is true.

As a means of identifying the most interesting autoantibody titres across these 13 leading antigens, a 3-D plot was constructed with all patients, and is indicated below in Fig. 4.40.

Figure 4.40: Most abundant autoantibody titres towards antigens across SIRT treatment cohort. This 3-D graph indicates the autoimmune profile of all patients across the most abundant antigens of this treatment cohort. Each antigen is indicated in a different colour, and each patient sample is indicated in the x-axis. D0: baseline; C1: cycle 1; C2: cycle 2.

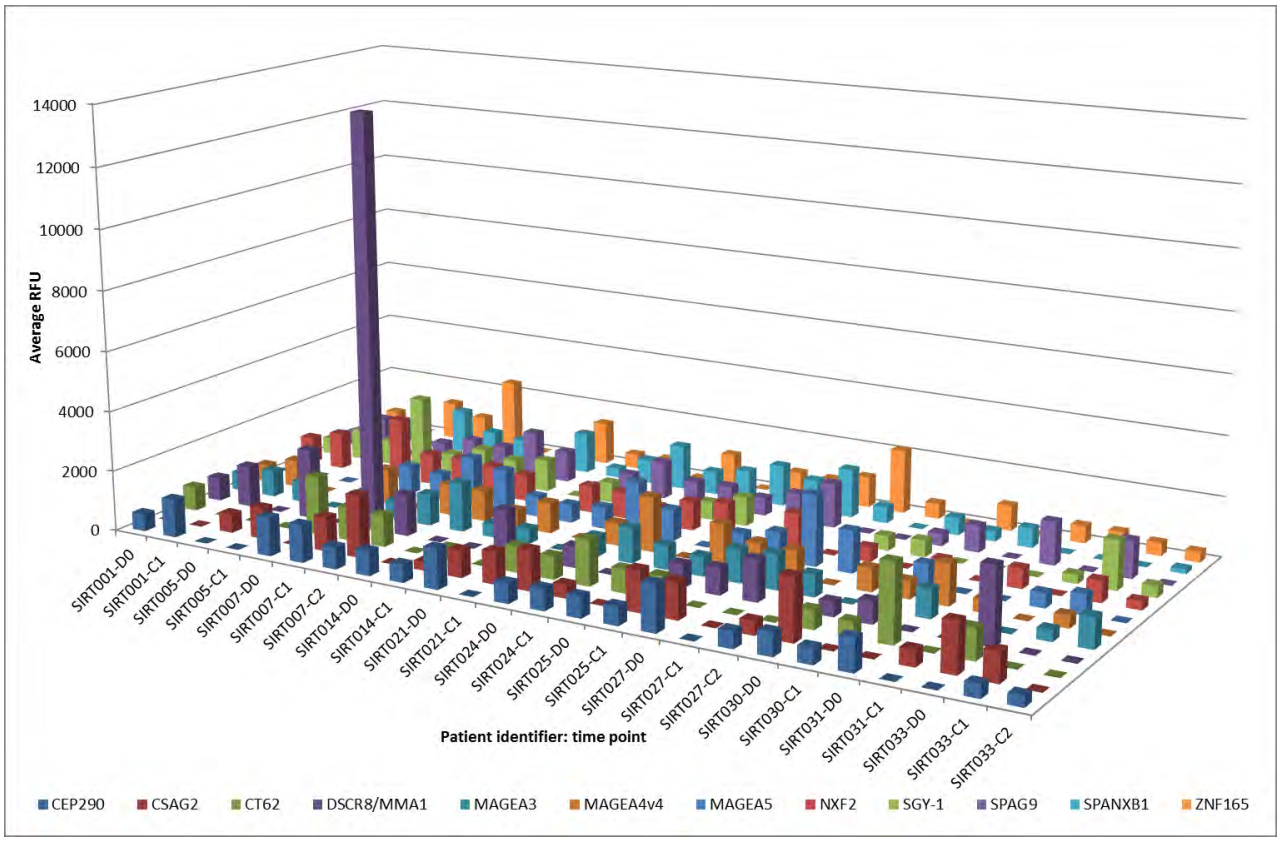

This data representation indicates that the majority of these patient signals are below 2500 RFU, with only one patient displaying a very above average signal of ~14000 RFU. This was seen for patient SIRT007 at cycle 1 of treatment against the DSCR8/MMA protein. This protein was discussed previously for the epigenetic modification cohort (Section 4.3.3), highlighting its immunotherapeutic potential, as well as a possible role in conferring a complete clinical response in patients when previously absent titres are greatly induced as a response to treatment. Based on this, one might assume that a possible highly beneficial clinical response for this patient was present, although this has not been confirmed for the reasons given above.

As mentioned above, although previously studies have reported clinical responses of up to 90%, the limited access to patient characteristics and clinical responses to treatment of this particular cohort, and

the limited patient numbers, meant that no further analysis or data interpretation could be conducted here.

We have applied our CT antigen microarray platform to the investigation of autoantibody profiles in a cohort of metastatic colorectal cancer patients who presented with liver metastasis and are undergoing SIRT. The main intent of this study was to assess the effect of SIRT on autoantibody levels, and if these changes were able to speculatively infer successful clinical response to treatment. In this regard, it is interesting that our CT antigen array data suggests evidence of observed autoantibody responses – statistically significant increases in autoantibody titres – across 55% of the cohort to treatment, an immune response rate much lower than clinical responses previously reported in other studies. Once again, due to the fact that all patients present with metastatic disease, tumour-induced systemic immune suppression may be occurring, which could in turn lead to lower autoantibody responses to treatment than expected (Nicholaou et al. 2009). Additionally, it may also be likely that this specific therapy does not necessarily induce a cancer-specific autoantibody response, but rather a distinct response that might be mediating clinical improvement.

In this SIRT treatment cohort, we have successfully demonstrated that there are measurable differences in the autoantibody repertoires towards tumour-specific and –associated antigens between pre- and post-treated metastatic colorectal cancer patients, with speculative preliminary evidence of possible correlation to the likelihood of clinical response. Furthermore, we have successfully identified CSAG2 – a well reported indicator of chemotherapeutic resistance - as the most abundantly expressed protein amongst those tested, present across 73% of patients. This clinical trial in particular tested the efficacy of combining chemotherapy with SIRT, which indicates the need to potentiate chemotherapeutic responses to therapy, and is thus in agreement with the suggested lack of chemotherapeutic efficacy associated with anti-CSAG2 immunoglobulin titres. However, when considering patient sample numbers and relevant power calculations, the achieved statistical power is well below recommended (power > 0.8), which does not support the findings obtained in this cohort. Therefore although these results provide preliminary insight into this cohort, these warrant further confirmation across a larger group of patients.

We therefore anticipate that our novel, quantitative, customizable CT antigen microarray platform may find usage in monitoring patient responses to treatment, with potential therapy resistance inferences, warranting confirmation using a pre-stipulated specifically focussed study and homogeneous cohort design using sufficient patient numbers according to an *a priori* power calculation estimate.

4.3.6 Malignant melanoma patients who underwent standard or no treatment

A total of 98 serum samples, corresponding to eighty-eight malignant melanoma patients undergoing a variety of distinct cancer treatments (surgery, chemotherapy, radiotherapy, immunotherapy or none), either in a clinical trial setting or not, were assayed, processed and analysed according to our pre-established CT100^{+} microarray pipeline. The following settings were used for the CT100^{+}.jar processing and filtering steps: mean or median values = mean, noise threshold = 2 standard deviations of the background, replicate CV threshold = 20%, whole array filtering control = 10 ng/µL Cy5-biotin-BSA and whole array CV threshold = 21%. The initial stipulated research question was whether this retrospective study could potentially identify diagnostic or prognostic biomarkers, as well as to assess whether and how different therapies significantly alter autoimmune titres. For this purpose, data analysis was conducted based on the collected clinical information and each patient's resulting autoimmune profile, permitting the comparison between several of these parameters. However, although eight patients have multiple sample time points undergoing distinct treatments which may allow therapy efficacy comparisons, it is important to note that the majority of these patients only have a single blood sample, signifying that no autoantibody responses progression across a time course may be measured for these, but rather a single profile for each patient. Hence, our data analysis pipeline is distinct from those mentioned above. Furthermore, based on sample number-based power calculations indicated in Chapter 2, this cohort includes sufficient patient and sample numbers to be able to report statistically relevant results (power = 0. 996).

Significant (> 1000 RFU) autoantibody titres were present in the majority of all samples (*n* = 93/98, 95%), with only five patients displaying titres below 1000 RFU, with signals ranging from 0 to ~289000 RFU. The latter were patients 581576 (male, surgery, stage III, not deceased), 568788 (female, no treatment, stage II, not deceased), 228343 (female, unknown treatment, stage III, deceased), 735678 (female, no treatment, stage III, deceased), 584655 (male, surgery, stage IV, not deceased), with no apparent consistent pattern. It is of note, however, that of the four of these five patients who had treatment information, none were undergoing chemotherapy, radiotherapy or immunotherapy, but rather had no treatment or surgery only. When grouping these patients based on treatment undergone, the highest autoantibody titres were observed for patients undergoing no treatment (~289000 RFU towards CTAG2), followed by those undergoing immunotherapy (~140000 RFU towards CTAG2), chemotherapy (~90000 RFU towards NY-ESO-1), and surgery (~26000 RFU towards NY-ESO-1), with the overall lowest titres seen for patients undergoing radiotherapy (~2500 RFU towards CTNNB1). These levels of autoantibody titres are quite peculiar, as they indicate that counterintuitively no therapy yields the highest autoimmune levels, even though this subset includes forty-seven patients. This may be due to the fact that many of the patients in this subset have previously undergone some previous therapy at an earlier time point, although the captured information is limited to the specific treatment each patient

was having at the time of the sample collection. Alternatively, as many cancer treatments suppress the immune system, these patients may be displaying a more responsive immune system due to not having undergone any previous harsh treatment. On the other hand, patients undergoing radiotherapy presented the lowest autoantibody titres, although this data was limited to only three patients, and therefore not allowing an adequate representation of this treatment type. In regards to the antigens indicating highest autoantibody titres, both CTAG2 and NY-ESO-1 appear twice in these treatment subsets. However, further analysis is required to verify if these might have a larger significance in this cohort. As a means of further interpreting the largest and most interesting subset of patients undergoing no treatment, a radar plot was constructed displaying autoantibody titres across all antigens, and is indicated below in Fig. 4.41.

Figure 4.41: Radar plot of the autoantibody titres detected towards all antigens across patients undergoing no treatment of the other treatments cohort. Each antigen is indicated by an axis, and each patient sample is indicated in a different colour.

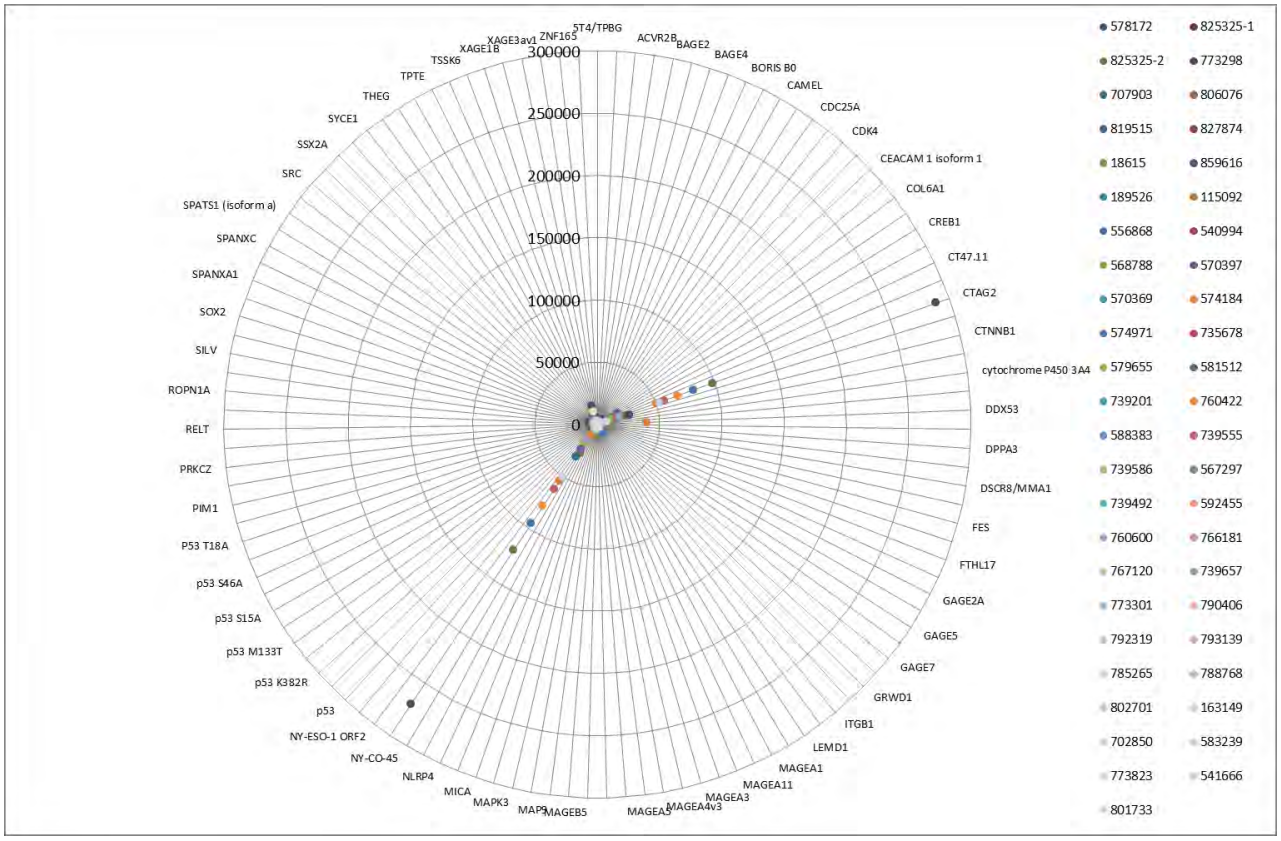

Based on this radar plot, it was evident that patient autoantibody titres are repeatedly clustering against both CTAG2 and NY-ESO-1 for matching patient samples. A paired response towards NY-ESO-1 and CTAG2 is certainly expected, due to the high sequence homology between them, as previously

mentioned above. It would certainly be informative to verify if the seven patients displaying the extremely high autoantibody signals (between 50000 and 300000 RFU) towards these two antigens were in fact undergoing some form of immunotherapy at a previous time-point. As one of the immunotherapies includes NY-ESO-1 vaccination, it seems as if this might be the most likely previous therapy undergone. Alternatively, those instances could be patients with naturally occurring high autoantibody titres, independent of any therapy. These seven included patients 773298 (female, stage III, deceased), 825325-2 (female, stage IV, deceased), 574971 (female, stage IV, deceased), 760422 (male, stage IV, deceased), 739555 (male, stage IV, deceased), 702850 (male, stage IV, deceased), and 574184 (female, stage IV, unknown). The most prevalent characteristic of these seven patients were disease stage IV (*n* = 6/7, 86%), and deceased (*n* = 6/6, 100%). These are in line with a very advanced disease phase, where not much can be done except attempt to prolong the short predicted survival time for metastatic melanoma patients.

Of the 123 cancer-associated antigens present on our CT100^{+} array, the most prevalent significant autoantibody titres (above 1000 RFU) detected in this cohort were towards 17 leading antigens. These were detected in at least 27 or more instances across patient samples in this cohort, and most abundantly towards NY-ESO-1 (*n* = 48/98, 49%) and CTAG2 (*n* = 45/98, 46%), as indicated below in Fig. 4.42.

Figure 4.42: Most prevalent autoantibody titres detected across the other treatments cohort. This graph indicates the summed number of times autoantibody levels were detected towards the 17 leading antigens at titres above 1000 RFU.

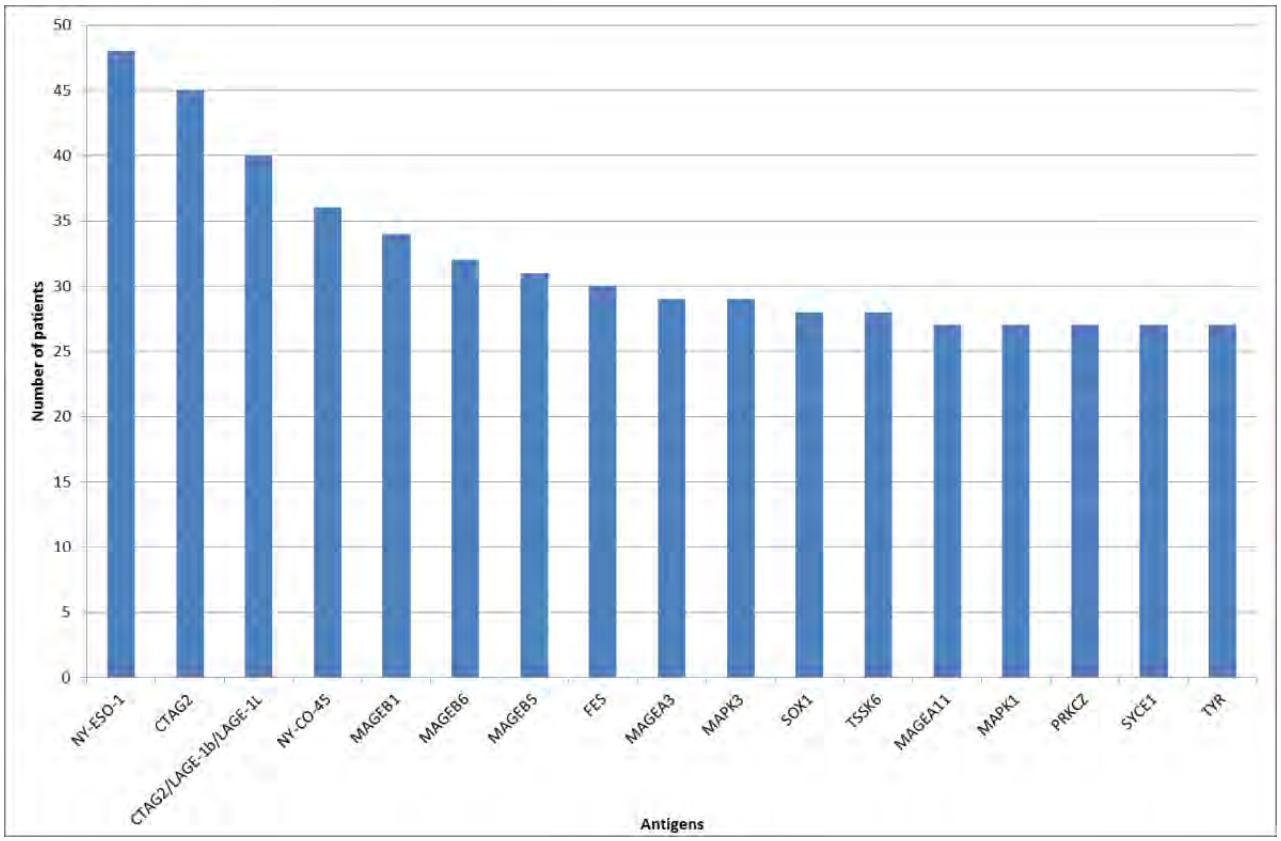

Based on this graph, it was evident that a very interesting subset of prevalent autoantibody titres was present in at least 27/98 (28%) patient samples. Besides from prevalent titres towards the NY-ESO-1 and CTAG2 common leading antigen pair, as well as CTAG2/LAGE-1b/LAGE-1L, a CTAG2 isoform, many autoantibody titres were towards CT antigens, such as members of the expected melanoma antigen (MAGE) family, MAGEB1, MAGEB6, MAGEB5, MAGEA3, MAGEA11, as well as NY-CO45, TSSK6 and SYCE1. Additionally, a few protein kinases are also present, such as FES, MAPK3, MAPK1 and PRKCZ, and other non-CT antigens such as SOX1 and TYR, which are quite a wide range of distinct antigen groups. As a means of defining whether abundant titres towards these leading antigens could be potential diagnostic or prognostic biomarkers, or even therapeutic targets, the NY-ESO-1 and CTAG2 pair was investigated further.

NY-ESO-1 has been broadly discussed above in Sections 4.3.1 and 4.3.4, as abundant autoantibody titres were detected towards this antigen in both the kinase inhibition and the survivin treatment cohorts. The high level of sequence homology (77%) between the NY-ESO-1/CTAG2 pair has also been mentioned, which justifies the matching titres towards these two antigens mentioned above. Particularly, in

melanoma, NY-ESO-1 has received a great deal of interest as an attractive immunotherapeutic target (NY-ESO-1 ISCOMATRIX vaccine), and has also been tested in a clinical trial setting, with initial promise due to a treatment triggered induction of immune responses (Davis et al. 2004; Maraskovsky 2004). However, although strong vaccine-induced responses were shown in early disease stages, advanced melanoma patients showed little to no clinical responses to vaccination, which was possible due to a tumour-induced systemic immune suppression driven by regulatory T-cells (Nicholaou et al. 2009). Hence, NY-ESO-1 therapies have been somewhat overshadowed by kinase inhibitors, due to more beneficial clinical responses to treatment, even amongst advanced melanoma patients (Vanneman & Dranoff 2012). Nonetheless, the available data for both NY-ESO-1 and CTAG2 across all patients was inspected, and a dual autoantibody titre trendline across this whole cohort was constructed, as indicated below in Fig. 4.43.

Figure 4.43: Anti-NY-ESO-1 and -CTAG2 immunoglobulin titre trendlines across other treatments cohort. Anti-NY-ESO-1 immunoglobulin titres are indicated in red, and anti-CTAG2 immunoglobulin titres are indicated in blue, with both trendlines showing nearly complete overlap.

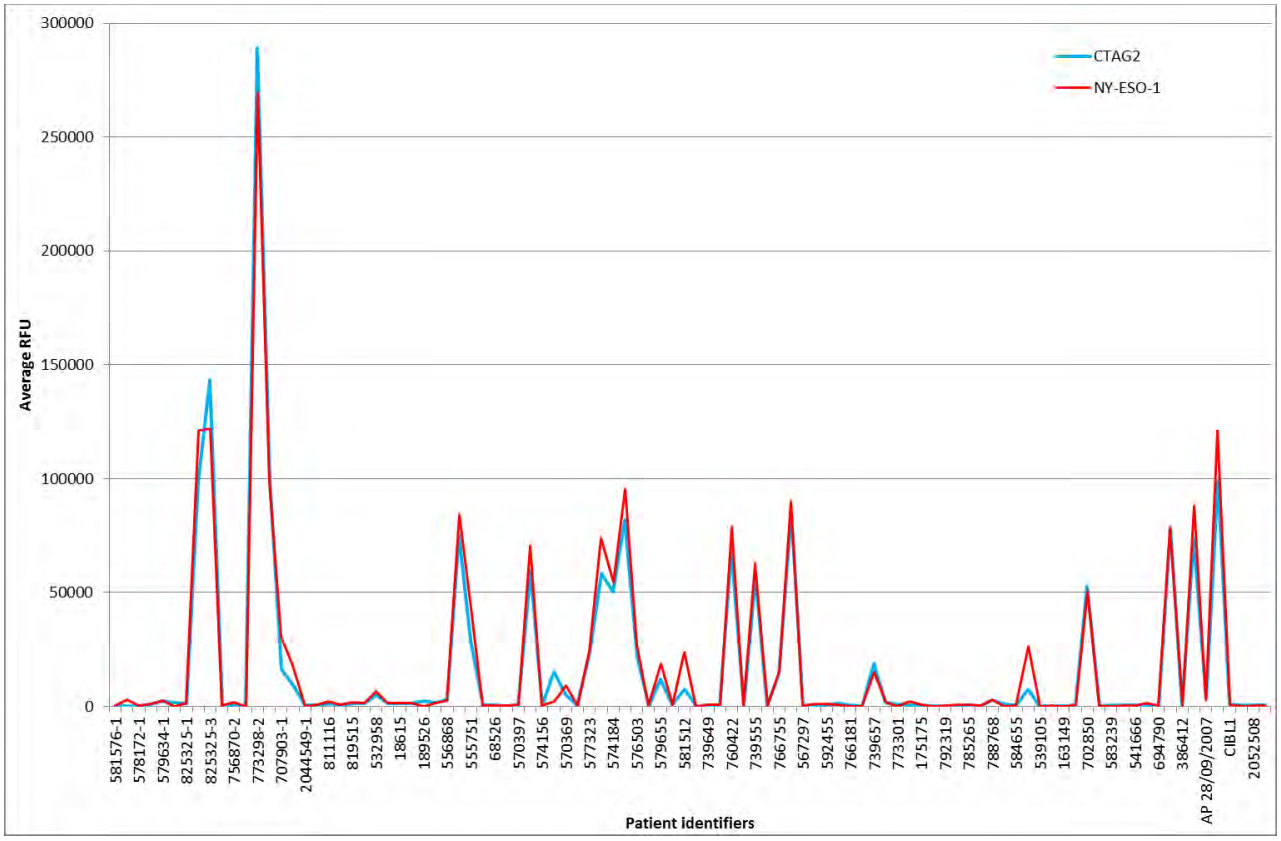

Visual inspection of these anti-NY-ESO-1 and -CTAG2 immunoglobulin titre trendlines indicate a nearly complete overlap and paired NY-ESO-1/CTAG2 autoantibody titre across this cohort, which serves as a

very robust validation of our array platform, methodology, data analysis pipeline, and reported autoantibody responses. Additionally, this indicates autoantibody responses amongst these patients are certainly occurring in NY-ESO-1/CTAG2 shared epitope regions. When inspecting the three most intense autoantibody titres above 100000 RFU, these occur for patients 825325-2/3 (female, stage IV, undergoing no treatment (2) or immunotherapy (3), deceased), 773298-2 (female, stage II, undergoing no treatment, deceased) and C 6/3/1996 (no available information). The first two patients were certainly enrolled in immunotherapeutic trials in between no-treatment breaks, which might explain the presence of such high titres. Due to such a high number of patient samples (*n* = 48/98, 49%) expressing significantly high autoantibody titres towards NY-ESO-1, this protein certainly has diagnostic biomarker potential. Previous studies have identified this protein as a predictive biomarker of response, showing an improved clinical benefit prediction for seropositive NY-ESO-1 melanoma patients (Yuan et al. 2011). However, due to the lack of complete clinical information, and available temporal sample information instead, it is unknown whether these patients did in fact have an improved clinical response to immunotherapy, although this prediction is likely. Furthermore, due to the high levels of NY-ESO-1 amongst our mostly advanced malignant melanoma cohort, perhaps researchers should re-focus interest in understanding why vaccination with this protein was not effective in advanced cases, and attempt to change that.

We have applied our CT antigen microarray platform to the investigation of autoantibody profiles in a cohort of metastatic malignant melanoma patients undergoing a variety of different treatments, and observed significant autoantibody titres across 95% of this cohort. The main intent of this study was to retrospectively assess whether potential diagnostic or prognostic biomarkers could be identified, and whether distinct therapeutic options generated specific autoantibody titres or patterns. In this regard, it is interesting that our CT antigen array data successfully identified a melanoma-specific well-established therapeutic target – NY-ESO-1– and its homologous pair, CTAG2, which were the two antigens towards which the most abundant autoantibody titres were detected, present across 49% and 46% patients, respectively. Once again, due to the increased sequence homology amongst this pair, it remains to be determined whether the observed responses are towards a shared epitope. However, the nearly complete overlap of autoantibody responses of this pair across this cohort are most likely indicative of such. Additionally, when considering treatment specific autoantibody patterns, the highest autoantibody levels were observed for patients undergoing no treatment, which may be due to the absence of immune-aggressive previous therapeutics leading to more responsive immune systems. However, clinical history is not available amongst these patients, and thus inferences may not be made.

In this variable treatment cohort, we have successfully demonstrated that there are measurable differences in the autoantibody repertoires towards tumour-specific and –associated antigens between malignant melanoma patients. Furthermore, we have successfully identified a melanoma-specific well-

established therapeutic target – NY-ESO-1– and its homologous pair, CTAG2, which were the two antigens towards which the most abundant autoantibody titres were detected, present across 49% and 46% patients, respectively. The fact that both these antigens share the majority of their sequence and have common epitopes suggests that autoantibody responses are probably towards one of these forms in particular (most likely NY-ESO-1). When considering patient sample numbers and relevant power calculations, although this cohort is quite diverse regarding demographics (age and gender) and treatment undergone , the achieved statistical power is above recommended (power > 0.8), supporting the findings obtained in this cohort.

We therefore anticipate that our novel, quantitative, customizable CT antigen microarray platform may find usage in identifying diagnostic or prognostic biomarkers, as well as novel therapeutic targets, warranting confirmation using a pre-stipulated specifically focussed study and homogeneous cohort design using sufficient patient numbers according to an *a priori* power calculation estimate.

5 CONCLUSIONS

5.1 Conclusions

In this work, we have developed and validated a novel protein microarray platform, the CT100^{+}, containing CT antigens, and other cancer-associated antigens of interest. Our microarray is mainly composed of CT antigens due to their attractive and highly reported potential as cancer biomarkers and their restricted overexpression in a variety of distinct cancer types with potential applications in many cancers. Initially, slide coating and cloning procedures were improved, resulting in a much more homogenous assay surface as a result of the newly developed immersion technique, and reduced non-specific binding following transfer of all protein expression to insect cells. The array layout was developed to include additional cancer-related antigens, as well as incorporating a means to measure total IgG levels per array. Printing and assaying procedures were optimized with the intent of obtaining consistently reproducible and robust data. Printing settings involving the number of stamps, buffer standardization and pin washing procedures were adjusted to obtain equal-sized and spaced spots, excluding the usual printing-associated issues such as pin sticking, spot running, carryover, and non-specific binding. Post-printing slide storage was altered to improve storage time and slide viability, and consisted of using a dry storage refrigerated method.

Once an optimal process was in place, the platform was assessed to verify its linear range and detection limit, as a means of inferring potential applications and best assaying concentrations, obtaining a previously unreported low detection limit in the pg/mL range, with linearity over at least three orders of magnitude. Hence, only 1 µL amount of patient serum was required for each assay, which is

advantageous when dealing with precious and limited patient samples, which is usually the case, and suggesting that in the future assays could be run on a pin prick of blood. Quality control steps were developed as a means of assuring robust and highly reproducible results amongst repeatedly generated data. These included verifying that printing was successful, and that both patient serum and detection antibody were added to each array, as well as testing for array specificity towards cancer using pooled cancer and healthy samples, and were required to be as stipulated in order to accept with high confidence the resulting data of that print run. Reproducibility studies were also performed with the intent of verifying that consistent resulting data was obtained repeatedly, even when amongst different sample dilution preparations. Additionally, a new bioinformatic tool, the $CT100^{+}$.jar, was developed to enable robust pre-processing and objective quality control of raw data files.

Once this complete, optimized, thorough and robust pipeline was in place, serum based immune responses could be assessed, which was done across six distinct cohorts undergoing different treatments, and including several cancer types, with the intent of either supporting or refuting our original hypothesis. We thus aimed to verify whether or not there were measurable differences in autoantibody repertoires towards tumour-specific and –associated antigens between pre- and post-treated cancer patient samples, which could potentially correlate with associated T-cell or clinical responses, thus exploring different potential uses of this platform.

The resulting data of the first cohort including thirty-six malignant melanoma patients undergoing kinase inhibition, identified abundant autoantibody titres towards two antigens, NY-ESO-1 and MAGEB1, that were present in 61% (*n* = 22/36) and 56% (*n* = 20/36) of all patients, respectively, both of which have been identified previously as cancer therapeutic targets and are currently being tested in a clinical trial setting. In regards to the stipulated research question – whether the induction of an autoantibody response correlated with T-cell responses and clinical improvements post-treatment amongst these patients – our CT antigen array data suggests limited evidence of correlating T-cell responses, but preliminary evidence of correlation between our observed autoantibody responses and the clinically reported ones across a subset of patients (35% of the cohort). Although this cohort was quite diverse regarding patient demographics (age and gender) and treatments undergone (single vs. dual kinase inhibition treatment), the achieved statistical power was above recommended (power > 0.8), supporting the findings obtained in this cohort.

The resulting data of the second cohort included sixty-two colorectal cancer patients undergoing pre- or post-operative chemotherapy/radiotherapy treatment, identified abundant autoantibody titres towards two antigens, SILV/gp100 and p53 Q136X, across 31% (*n* = 19/62) and 21% (*n* = 13/62) of all patients, identifying potential novel therapeutic targets for colorectal cancer and a possible indicator of advanced disease stage, respectively. In regards to the main intent of this study – to assess whether pre-operative therapy altered patterns of autoantibody titres, thereby potentially influencing the outcome of

subsequent therapy – this cohort data showed that no difference in autoantibody profiles was evident between patients who had undergone pre-operative therapy and those who hadn't, contrary to what was expected, thus limiting subsequent inferences to be made. Although this cohort was quite diverse regarding age, the achieved statistical power was above recommended (power > 0.8), supporting the findings obtained in this cohort.

The third cohort included twelve myelodysplasia patients undergoing dual epigenetic modification treatment, and identified abundant autoantibody titres towards two antigens, cytochrome P450 reductase and DSCR8/MMA1, that were present in 75% (*n* = 9/12) and 67% (*n* = 8/12) of all patients. However, due to the limited number of patients in this cohort, no inferences could be made regarding a potential link to resistance and a possible novel therapeutic target, respectively. In regards to the main intent of this study – to assess whether epigenetic modification created neo-antigens and subsequent expanded autoantibody responses – we identified abundant autoantibody titres towards 19 potential antigens with expanded autoantibody response towards cancer-associated antigens as a result to treatment, but no specific responsible neo-antigen. Furthermore, preliminary evidence of an expanded immune response after epigenetic treatment was evident across the majority of all patients, of which 67% of the cohort presented with matching array and clinically reported responses. Unfortunately, this cohort did not achieve the required statistical power (power > 0.8), and thus the findings obtained could not be statistically supported. Therefore although these results provide preliminary insight into this cohort, these warrant further confirmation across a larger group of patients.

The data obtained on the fourth cohort including forty-eight variable cancer patients undergoing survivin treatment, identified a known potential link between p53 mutant-associated chemotherapy resistance, early relapse and shortened overall survival in ovarian cancer patients, warranting further genomic studies. However, this possible association requires verification using a larger dedicated ovarian cancer cohort, as a means of verifying significance. Additionally, abundant autoantibody titres towards two antigens, NY-ESO-1 and CTAG2/LAGE-1b/LAGE-1L, were identified. This homologous pair was present in 35% (*n* = 17/48) and 25% (*n* = 12/48) of all patients, respectively, and have been identified previously as cancer immunotherapeutic targets with potential prognostic and predictive value. In regards to the main intent of this study – to assess whether the induction of an autoantibody response correlated with reported induced survivin-specific T-cell responses post-treatment amongst these patients – our CT antigen array data suggests evidence of direct correlation between our observed autoantibody responses and the survivin-specific T-cell reported ones across a subset of patients (59% of the cohort). Furthermore, preliminary evidence of a correlation between our data and the reported clinical benefit was also observed, across a larger subset of patients (71%), warranting further investigation. Although this cohort was quite diverse regarding patient age and tumour type, the

achieved statistical power was above recommended (power > 0.8), supporting the findings obtained in this cohort.

The fifth and smallest cohort included eleven colorectal cancer patients with unresectable liver metastasis undergoing selective internal radiotherapy, identified abundant autoantibody titres towards an antigen, CSAG2, across 73% (*n* = 8/11) of all patients. However, the limited patient numbers in this cohort, and lack of their clinical information, do not allow speculative inferences to be made regarding a potential link to poor clinical efficacy to treatment. In regards to the main intent of this study – to assess the effect of SIRT on autoantibody levels and to potentially infer clinical responses to treatment – our CT antigen array data suggests an immune response rate much lower than clinical responses previously reported in other studies. Unfortunately, this cohort did not achieve the required statistical power (power > 0.8), and thus the findings obtained could not be statistically supported. Therefore although these results provide preliminary insight into this cohort, these warrant further confirmation across a larger group of patients.

The sixth and final cohort included eighty eight malignant melanoma patients undergoing a variety of distinct cancer treatments. In regards to the stipulated research question of this study - whether potential diagnostic or prognostic biomarkers could be identified, and whether distinct therapeutic options generated specific autoantibody titres or patterns – our CT antigen array data successfully identified abundant autoantibody titres towards two antigens, NY-ESO-1 and CTAG2, a homologous pair expressed across 49% (*n* = 48/98) and 46% (*n* = 45/98) of all patients, respectively, with reported diagnostic and clinical efficacy predictive biomarker potential. Additionally, when considering treatment specific autoantibody patterns, the highest autoantibody levels were observed for patients undergoing no treatment, which may be due to treatment-related, or lack thereof, more responsive immune systems. Furthermore, the overlap in autoantibody titres of this pair validated our array platform, showing consistency amongst our obtained results across patients. Although this cohort was quite diverse regarding demographics (age and gender) and treatment undergone, the achieved statistical power was above recommended (power > 0.8), supporting the findings obtained in this cohort.

In sum, it was evident that some of the treatment cohorts assessed in this work were limited by low patient numbers and/or lack of access to clinical information, making robust statistically relevant conclusions difficult. Furthermore, inter- and intra-cohort variability was prevalent, even amongst the same cancer type and stage, , indicating that if patients are known to respond differently to treatment, a personalised treatment and disease management approach should also be used. However, the main objective of this thesis was to develop a protein microarray platform capable of robustly measuring differences in autoantibody repertoires using cancer patient serum, and to then explore its potential utility across a range of cancers and treatments; rather than attempting to identify robust clinically valuable and applicable findings, using pre-stipulated specifically focussed studies and homogeneous

cohort designs with adequate patient numbers. Additionally, our findings have successfully supported our research hypothesis, by demonstrating that there are in fact measurable differences in the autoantibody repertoires towards tumour-specific and –associated antigens amongst cancer patients, which usually differ between pre- and post-treatment time points. Although these autoantibody levels showed preliminary evidence of correlation with associated T-cell and clinical responses across some of the assayed pilot cohorts, larger focussed studies using sufficient patient numbers according to an *a priori* power calculation estimates are required to verify significant and clinically applicable findings.

Additionally, it is essential to mention that amongst all treatment cohorts, a subset of patients presented with an overall lack of significant autoantibody titres towards the assessed tumour-specific and –associated antigens. The absence of these titres may be related to a number of immunosuppressive or immunoregulatory cancer mechanisms, as the majority of these patients have undergone numerous therapeutics and present with advanced cancers. As a result, these may potentially lead to a dysfunctional cellular immunity, which would negatively affect autoantibody production. Although this may be considered to be a limitation in the application of this method in the future, this overall lack of an autoimmune repertoire still provides essential information which may aid in comprehending a lack of clinical response to therapy, and thus guide alternative therapeutic planning, such as attempting to use an immunotherapeutic that may reverse regulatory pathways (e.g. immune checkpoint blockade therapy) instead.

In conclusion, we have shown that our novel protein microarray platform thus represents a sensitive, high-throughput and readily customizable means to detect and quantify the presence of large panels of cancer-specific human autoantibodies in serum, obtaining consistently robust, high quality and reproducible data, and demonstrating its potential feasibility and inferred biological significance. Although patient-specific autoantibody profiles may correlate with treatment responses, further validation is required. Nonetheless, without doubt, these profiles do inform on patient-specific autoantibody titres towards antigens, which may be useful in stratification of treatment options in the future.

5.2 Potential applications

This work has shown that our robust, highly reproducible, sensitive and specific $CT100^{+}$ protein microarray platform has great potential clinical applicability. Applications of this tool include the potential use to identify novel diagnostic, disease progression, prognostic, treatment resistant and even predictive biomarkers, which could aid in the detection and management of cancer. Most importantly, these could lead to the discovery of novel cancer therapeutic targets, which are certainly a topic of great importance and necessity in the cancer field. This biomarker discovery approach is applicable to a

variety of distinct cancer types, broadening its possible use. Additionally, the identification of novel biomarkers that could be used in patient stratification prior to chemotherapy, radiotherapy or immunotherapy, as a means to improve clinically efficacy of the therapeutic being tested, is also a possibility. In addition, this platform has the potential to serve as a means of monitoring cancer patient responses to chemotherapy, radiotherapy or immunotherapy, indicating a prospective and promising utility as an immune monitoring tool in a clinical trial setting, allowing for easily and rapidly obtainable patient clinical efficiency inferential information without use of laborious, costly and unpleasant medical tests.

Based on the results obtained in this Thesis, the potential application that may hold the most promise is the biomarker discovery approach, specifically the identification of novel diagnostic or prognostic biomarkers. This assumption is based on the fact that amongst the four cohorts that contained an acceptable sample number and the recommended statistical power, we were able to detect abundant autoantibody titres towards previously well reported antigens, namely NY-ESO-1, CTAG2, CTAG2/LAGE-1b/LAGE-1L, MAGEB1, SILV/gp100 and p53 Q136X. These antigens have been identified as potential diagnostic or prognostic biomarkers across specific cancer types, or have either been or continue to be used as potential cancer therapeutics in a clinical trial setting, thus validating our reported findings.

5.3 Future work

The CT100^{+} protein microarray platform could potentially be developed even further, mainly regarding the inclusion of additional cancer-associated antigens of interest, as our array layout and format allows for the triplicate printing of up to 170 individual protein types. These could be selected based on current literature in this field, or specific assays developed for this purpose. Additionally, our protein microarray bioinformatic tool, the CT100^{+}.jar, could be enhanced to include an optional graphing and clustering tool, as well as the possibility to conduct varied statistical analysis, as a means of allowing a user-friendly standardized data analysis procedure for all users. Alternatively, this protein microarray principle could be applicable to other immune system diseases, such as tuberculosis, warranting further research.

In addition, it is apparent from the work described in this Thesis that perhaps a more advanced approach is needed to understand the complexity of the observed cancer-specific autoimmune responses. In particular, genomic experiments are now revealing specific subtypes of cancer with very different inflammatory or immunosuppressive phenotypes; it remains to be seen though whether our serology data provides a non-invasive means to identify cancer subtypes.

6 REFERENCES

Adema, G.J. et al., 1994. Molecular characterization of the melanocyte lineage-specific antigen gp100. *The Journal of biological chemistry*, 269(31), pp.20126–33.

Alberts, B. et al., 2002. B Cells and Antibodies. In *Molecular Biology of the Cell*. New York: Garland Science.

Altieri, D.C., 2003. Validating survivin as a cancer therapeutic target. *Nature reviews. Cancer*, 3(1), pp.46–54.

Altschul, S.F. et al., 1990. Basic local alignment search tool. *Journal of molecular biology*, 215(3), pp.403–10.

Altschul, S.F. et al., 1997. Gapped BLAST and PSI-BLAST: a new generation of protein database search programs. *Nucleic acids research*, 25(17), pp.3389–402.

Ambrosini, G., Adida, C. & Altieri, D.C., 1997. A novel anti-apoptosis gene, survivin, expressed in cancer and lymphoma. *Nature Medicine*, 3(8), pp.917–921.

Andersen, B.M. & Ohlfest, J.R., 2012. Increasing the efficacy of tumor cell vaccines by enhancing cross priming. *Cancer Letters*, 325(2), pp.155–164.

Anderson, K.S. & LaBaer, J., 2005a. The sentinel within: Exploiting the immune system for cancer biomarkers. *Journal of Proteome Research*, 4(4), pp.1123–1133.

Anderson, K.S. & LaBaer, J., 2005b. The sentinel within: exploiting the immune system for cancer biomarkers. *Journal of proteome research*, 4(4), pp.1123–33.

Atadja, P., 2009. Development of the pan-DAC inhibitor panobinostat (LBH589): successes and challenges. *Cancer letters*, 280(2), pp.233–41.

Athappilly, F.K. & Hendrickson, W. a, 1995. Structure of the biotinyl domain of acetyl-coenzyme A carboxylase determined by MAD phasing. *Structure (London, England : 1993)*, 3(12), pp.1407–1419.

Ausubel, F.M. et al., 1999. Short Protocols in Molecular Biology. In *Current Protocols in Molecular Biology*. Wiley, New York.

Bakker, A.B. et al., 1994. Melanocyte lineage-specific antigen gp100 is recognized by melanoma-derived tumor-infiltrating lymphocytes. *The Journal of experimental medicine*, 179(3), pp.1005–9.

Balboni, I. et al., 2006. Multiplexed protein array platforms for analysis of autoimmune diseases. *Annual review of immunology*, 24, pp.391–418.

Balch, C.M. et al., 2009. Final version of 2009 AJCC melanoma staging and classification. *Journal of clinical oncology : official journal of the American Society of Clinical Oncology*, 27(36), pp.6199–206.

Beeton-Kempen, N. et al., 2014. Development of a novel, quantitative protein microarray platform for the multiplexed serological analysis of autoantibodies to cancer-testis antigens. *International journal of cancer. Journal international du cancer*, 135(8), pp.1842–51.

Bendandi, M., 2009. Idiotype vaccines for lymphoma: proof-of-principles and clinical trial failures. *Nature reviews. Cancer*, 9(SepTemBer), pp.675–681.

Berrade, L., Garcia, A.E. & Camarero, J.A., 2011. Protein Microarrays : Novel Developments and Applications. *Pharmaceutical Research*, pp.1480–1499.

Beyer, M. & Schultze, J.L., 2006. Regulatory T cells in cancer. *Blood*, 108(3), pp.804–811.

Blackburn, J.M. & Shoko, A., 2011. Protein Function Microarrays for Customised Systems-Oriented Proteome Analysis. In U. Korf, ed. *Methods in Molecular Biology*. Humana Press, pp. 305–330.

Blackburn, J.M., Shoko, A. & Beeton-Kempen, N., 2012. Miniaturized, microarray-based assays for chemical proteomic studies of protein function E. D. Zanders, ed. *Methods in Molecular Biology*, 800, pp.133–162.

Blank, C.U. et al., 2011. Combination of targeted therapy and immunotherapy in melanoma. *Cancer Immunol Immunother*, 60, pp.1359–1371.

Bolstad, B.M. et al., 2003. A comparison of normalization methods for high density oligonucleotide array data based on variance and bias. *Bioinformatics (Oxford, England)*, 19(2), pp.185–93.

Boni, A. et al., 2010. Selective BRAFV600E inhibition enhances T-cell recognition of melanoma without affecting lymphocyte function. *Cancer Research*, 70(9), pp.5213–5219.

Bosset, J.-F. et al., 2006. Chemotherapy with preoperative radiotherapy in rectal cancer. *The New England journal of medicine*, 355(11), pp.1114–23..

Boutell, J.M. et al., 2004. Analysis of the effect of clinically-relevant mutations on p53 function using protein microarray technology. *Proteomics*, 4, pp.1950–1958.

Bradford, M.M., 1976. A rapid and sensitive method for the quantitation of microgram quantities of protein utilizing the principle of protein-dye binding. *Analytical biochemistry*, 72, pp.248–54.

Bray, F. et al., 2013. Global estimates of cancer prevalence for 27 sites in the adult population in 2008. *International journal of cancer. Journal international du cancer*, 132(5), pp.1133–45.

Büssow, K. et al., 2001. Protein Array technology: Potential Use in Medical Diagnostics. *Am J Pharmacogenomics*, 1(1), pp.1–7.

Caballero, O.L. & Chen, Y., 2009. Cancer/testis (CT) antigens : Potential targets for immunotherapy. *Cancer Science*, 100(11), pp.2014–2021.

Causton, H.C., Quackenbush, J. & Brazma, A., 2004. Microarray gene expression data analysis: a beginners guide. In *Yeast*. Blackwell Publishing, pp. 973–974.

Cebon, J., 2010. Cancer vaccines: Where are we going? *Asia-Pacific journal of clinical oncology*, 6 Suppl 1, pp.S9–15.

Chapman, P.B. et al., 2011. Improved survival with vemurafenib in melanoma with BRAF V600E mutation. *The New England journal of medicine*, 364(26), pp.2507–16.

Chapman-Smith, A. & Cronan, J.E., 1999. The enzymatic biotinylation of proteins: a post-translational modification of exceptional specificity. *Trends in Biochemical Sciences*, 24(9), pp.359–363.

Chen, Y. et al., 2010. In vitro assessment of cytochrome P450 inhibition and induction potential of azacitidine. *Cancer chemotherapy and pharmacology*, 65(5), pp.995–1000.

Choi-Rhee, E. & Cronan, J.E., 2003. The biotin carboxylase-biotin carboxyl carrier protein complex of Escherichia coli acetyl-CoA carboxylase. *The Journal of Biological Chemistry*, 278(33), pp.30806–12.

Cohen, J., 1988. Statistical Power Analysis for the Behavioral Sciences. In *Psychology*. pp. 273–406.

Curtin, J.A. et al., 2005. Distinct sets of genetic alterations in melanoma. *The New England journal of medicine*, 353(20), pp.2135–47.

Danna, E.A. et al., 2004. Surgical Removal of Primary Tumor Reverses Tumor-Induced Immunosuppression Despite the Presence of Metastatic Disease. *Cancer Research*, 64, pp.2205–2211.

Davies, H. et al., 2002. Mutations of the BRAF gene in human cancer. *Nature*, 417(6892), pp.949–54.

Davies, M.A. et al., 2011. Prognostic factors for survival in melanoma patients with brain metastases. *Cancer*, 117(8), pp.1687–1696.

Davis, I.D. et al., 2004. Recombinant NY-ESO-1 protein with ISCOMATRIX adjuvant induces broad integrated antibody and CD4(+) and CD8(+) T cell responses in humans.

Proceedings of the National Academy of Sciences of the United States of America, 101(29), pp.10697–702.

Derissen, E.J.B., Beijnen, J.H. & Schellens, J.H.M., 2013. Concise Drug Review: Azacitidine and Decitabine. *The Oncologist*, 18, pp.619–624.

Disis, M.L. et al., 2009. Concurrent trastuzumab and HER2/neu-specific vaccination in patients with metastatic breast cancer. *Journal of Clinical Oncology*, 27(4), pp.4685–4692.

Dougan, M. & Dranoff, G., 2009. Immune therapy for cancer R. Wang, ed. *Annu Rev Immunol*, 27, pp.83–117.

Drake, C.G., Lipson, E.J. & Brahmer, J.R., 2014. Breathing new life into immunotherapy: review of melanoma, lung and kidney cancer. *Nature Reviews Clinical Oncology*, 11(1).

Dranoff, G., 2004. Cytokines in cancer pathogenesis and cancer therapy. *Nature reviews. Cancer*, 4(January), pp.11–22.

Duan, Z. et al., 1999. TRAG-3, a novel gene, isolated from a taxol-resistant ovarian carcinoma cell line. *Gene*, 229(1-2), pp.75–81.

Duarte, J. et al., 2013. Protein Function Microarrays: Design, Use and Bioinformatic Analysis in Cancer Biomarker Discovery and Quantitation. In X. Wang, ed. *Bioinformatics of Human Proteomics, Translational Bioinformatics 3*. Springer Netherlands, pp. 39–74.

Van Duin, M. et al., 2011. Cancer testis antigens in newly diagnosed and relapse multiple myeloma: prognostic markers and potential targets for immunotherapy. *Haematologica*, 96(11), pp.1662–9.

Dyrskjøt, L. et al., 2012. Expression of MAGE-A3, NY-ESO-1, LAGE-1 and PRAME in urothelial carcinoma. *British journal of cancer*, 107(1), pp.116–22.

Edge, S.B. & Byrd, D.R., 2010. *AJCC Cancer Staging Manual* 7th Editio., Springer SBM.

El-Deiry, W.S. et al., 1993. WAF1, a potential mediator of p53 tumor suppression. *Cell*, 75(4), pp.817–25.

Esteller, M., 2008. Epigenetics in cancer. *The New England journal of medicine*, 358(11), pp.1148–59.

Falchook, G.S. et al., 2012. Dabrafenib in patients with melanoma, untreated brain metastases, and other solid tumours: a phase 1 dose-escalation trial. *Lancet*, 379(9829), pp.1893–901.

Fang, Y., Lahiri, J. & Picard, L., 2003. G protein-coupled receptor microarrays for drug discovery. *Drug Discovery Today*, 8(16), pp.755–61.

Faul, F. et al., 2007. G*Power 3: a flexible statistical power analysis program for the social, behavioral, and biomedical sciences. *Behavior research methods*, 39(2), pp.175–191.

Faul, F. et al., 2009. Statistical power analyses using G*Power 3.1: tests for correlation and regression analyses. *Behavior research methods*, 41(4), pp.1149–1160.

Ferlay, J. et al., 2015. Cancer incidence and mortality worldwide: Sources, methods and major patterns in GLOBOCAN 2012. *International journal of cancer. Journal international du cancer*, 136(5), pp.E359–86.

Flaherty, K.T. et al., 2012. Combined BRAF and MEK inhibition in melanoma with BRAF V600 mutations. *The New England journal of medicine*, 367(18), pp.1694–703.

Franceschini, A. et al., 2013. STRING v9.1: protein-protein interaction networks, with increased coverage and integration. *Nucleic acids research*, 41(Database issue), pp.D808–15.

Frank, R. & Hargreaves, R., 2003. Clinical biomarkers in drug discovery and development. *Nature Reviews*, 2(7), pp.566–580.

Fukuda, S. & Pelus, L.M., 2006. Survivin, a cancer target with an emerging role in normal adult tissues. *Molecular cancer therapeutics*, 5(5), pp.1087–98.

Garcia-lora, A., Algarra, I. & Garrido, F., 2003. MHC Class I Antigens , Immune Surveillance , and Tumor Immune Escape. *Journal of Cellular Physiology,* , 355, pp.346–355.

Germano, S. et al., 2012. MAGE-D4B is a novel marker of poor prognosis and potential therapeutic target involved in breast cancer tumorigenesis. *International journal of cancer. Journal international du cancer*, 130(9), pp.1991–2002.

Gibbs, P. et al., 2014. Selective Internal Radiation Therapy (SIRT) with yttrium-90 resin microspheres plus standard systemic chemotherapy regimen of FOLFOX versus FOLFOX alone as first-line treatment of non-resectable liver metastases from colorectal cancer: the SIRFLOX study. *BMC cancer*, 14(1), p.897.

Greenberg, P. et al., 1997. International Scoring System for Evaluating Prognosis in Myelodysplastic Syndromes. *Blood*, 89(6), pp.2079–2088.

Greenblatt, M.S. et al., 1994. Mutations in the p53 tumor suppressor gene: clues to cancer etiology and molecular pathogenesis. *Cancer research*, 54(18), pp.4855–78.

Halama, N. et al., 2011. Localization and density of immune cells in the invasive margin of human colorectal cancer liver metastases are prognostic for response to chemotherapy. *Cancer Research*, 71(17), pp.5670–5677.

Hall, D.A., Ptacek, J. & Snyder, M., 2007. Protein microarray technology. *Mechanisms of ageing and development*, 128(1), pp.161–7.

Hamberg, P. et al., 2011. Effect of ketoconazole mediated CYP3A4 inhibition on clinical pharmacokinetics of panobinostat (LBH589), an orally active histone deacetylase inhibitor. *Cancer Chemotherapy and Pharmacology*, 68(3), pp.805–813.

Hammel, P. et al., 1997. Detection and monitoring of serum p53 antibodies in patients with colorectal cancer. *Gut*, 40(3), pp.356–61.

Hanahan, D. & Weinberg, R.A., 2011. Hallmarks of cancer: the next generation. *Cell*, 144(5), pp.646–74.

Hanahan, D. & Weinberg, R.A., 2000. The hallmarks of cancer. *Cell*, 100(1), pp.57–70.

Hardiman, G., 2003. Microarray technologies - an overview. In *Pharmacogenomics*. pp. 251–6.

Hellborg, F. et al., 2001. Human wig-1, a p53 target gene that encodes a growth inhibitory zinc finger protein. *Oncogene*, 20(39), pp.5466–74.

Hodi, F.S. et al., 2010. *Improved survival with ipilimumab in patients with metastatic melanoma.*,

Holliday, R., 1987. The inheritance of epigenetic defects. *Science*, 238(4824), pp.163–170.

Houbiers, J.G. et al., 1995. Antibodies against p53 are associated with poor prognosis of colorectal cancer. *British journal of cancer*, 72(3), pp.637–41.

Houghton, A.N. & Guevara-Patiño, J.A., 2004. Immune recognition of self in immunity against cancer. *The Journal of clinical investigation*, 114(4), pp.468–71.

Hunder, N.N. et al., 2008. Treatment of Metastatic Melanoma with Autologous CD4+ T Cells against NY-ESO-1. *N Engl J Med*, 358(25), pp.2698–2703.

Ingelman-Sundberg, M. et al., 2007. Influence of cytochrome P450 polymorphisms on drug therapies: pharmacogenetic, pharmacoepigenetic and clinical aspects. *Pharmacology & therapeutics*, 116(3), pp.496–526.

Islam, A. et al., 2000. High expression of Survivin, mapped to 17q25, is significantly associated with poor prognostic factors and promotes cell survival in human neuroblastoma. *Oncogene*, 19(5), pp.617–23.

Jäger, E. et al., 1999. Humoral immune responses of cancer patients against "Cancer-Testis" antigen NY-ESO-1: correlation with clinical events. *International journal of cancer. Journal international du cancer*, 84(5), pp.506–10.

Jemal, A. et al., 2011. Global cancer statistics. *CA: a cancer journal for clinicians*, 61(2), pp.69–90.

Jones, P.A. & Laird, P.W., 1999. Cancer epigenetics comes of age. *Nature genetics*, 21(february), pp.163–167.

Kapiteijn, E. et al., 2001. Preoperative radiotherapy combined with total mesorectal excision for resectable rectal cancer. *The New England journal of medicine*, 345(9), pp.638–46.

Kawakami, Y. et al., 1994. Identification of a human melanoma antigen recognized by tumor-infiltrating lymphocytes associated with in vivo tumor rejection. *Proceedings of the National Academy of Sciences of the United States of America*, 91(14), pp.6458–62.

Kim, K.B. et al., 2013. Phase II study of the MEK1/MEK2 inhibitor Trametinib in patients with metastatic BRAF-mutant cutaneous melanoma previously treated with or without a BRAF

inhibitor. *Journal of clinical oncology : official journal of the American Society of Clinical Oncology*, 31(4), pp.482–9.

Klein, J.B. & Thongboonkerd, V., 2004. Overview of Proteomics. In *Proteomics in Nephrology*. pp. 1–10.

Kodadek, T., 2001. Protein microarrays : prospects and problems. *Chemistry & biology*, 8(2), pp.105–115.

Konecny, G.E. et al., 2014. Prognostic and Therapeutic Relevance of Molecular Subtypes in High-Grade Serous Ovarian Cancer. *JNCI Journal of the National Cancer Institute*, 106, pp.dju249–dju249.

Koopmann, J.-O. & Blackburn, J., 2003. High affinity capture surface for matrix-assisted laser desorption/ionisation compatible protein microarrays. *Rapid communications in mass spectrometry : RCM*, 17(5), pp.455–62.

Kressner, U. et al., 1998. Increased serum p53 antibody levels indicate poor prognosis in patients with colorectal cancer. *British journal of cancer*, 77(11), pp.1848–51.

Kruit, W.H. et al., 2008. Immunization with recombinant MAGE-A3 protein combined with adjuvant systems AS15 or AS02B in patients with unresectable and progressive metastatic cutaneous melanoma: A randomized open-label phase II study of the EORTC Melanoma Group (16032- 18031). *ASCO Meeting Abstracts*, 25(15).

Kufe, D.W. et al. eds., 2003. *Holland-Frei Cancer Medicine* 6th editio., Hamilton: BC Decker.

Kupryjańczyk, J. et al., 1993. p53 gene mutations and protein accumulation in human ovarian cancer. *Proceedings of the National Academy of Sciences of the United States of America*, 90(11), pp.4961–5.

Lennerz, V. et al., 2014. Immunologic response to the survivin-derived multi-epitope vaccine EMD640744 in patients with advanced solid tumors. *Cancer immunology immunotherapy*, 63(4), pp.381–94.

Lesterhuis, W.J. et al., 2011. Route of administration modulates the induction of dendritic cell vaccine-induced antigen-specific T cells in advanced melanoma patients. *Clinical Cancer Research*, 17(3), pp.5725–5735.

Lethé, B. et al., 1998. LAGE-1, a new gene with tumor specificity. *International journal of cancer.*, 76(6), pp.903–8.

Li, F. et al., 1998. Control of apoptosis and mitotic spindle checkpoint by survivin. *Nature*, 396(December), pp.580–584.

Li, M., Yuan, Y. & Han, Y., 2005. Expression Profile of Cancer-Testis Genes in 121 Human Colorectal Cancer Tissue and Adjacent Normal Tissue. *Clinical Cancer Research*, pp.1809–1814.

Lin, C. et al., 2002. Cancer/testis antigen CSAGE is concurrently expressed with MAGE in chondrosarcoma. *Gene*, 285(1-2), pp.269–78.

Liu, M.A., 2011. DNA vaccines: an historical perspective and view to the future. *Immunol Rev*, 239, pp.62–84.

Liu, Y. & Bodmer, W.F., 2006. Analysis of P53 mutations and their expression in 56 colorectal cancer cell lines. *Proceedings of the National Academy of Sciences of the United States of America*, 103(4), pp.976–81.

Long, G. V. et al., 2014. Combined BRAF and MEK inhibition versus BRAF inhibition alone in melanoma. *The New England journal of medicine*, 371(20), pp.1877–88.

MacBeath, G. & Schreiber, S.L., 2000. *Printing Proteins as Microarrays for High-Throughput Function Determination*,

Madoz-Gúrpide, J. et al., 2008. Integral protein microarrays for the identification of lung cancer antigens in sera that induce a humoral immune response. *Molecular & cellular proteomics : MCP*, 7(2), pp.268–281.

Maraskovsky, E., 2004. NY-ESO-1 Protein Formulated in ISCOMATRIX Adjuvant Is a Potent Anticancer Vaccine Inducing Both Humoral and CD8+ T-Cell-Mediated Immunity and Protection against NY-ESO-1+ Tumors. *Clinical Cancer Research*, 10(8), pp.2879–2890.

Marchand, M. et al., 1999. Tumor regressions observed in patients with metastatic melanoma treated with an antigenic peptide encoded by gene MAGE-3 and presented by HLA-A1. *International journal of cancer. Journal international du cancer*, 80(2), pp.219–30.

Marks, J.R. et al., 1991. Overexpression and mutation of p53 in epithelial ovarian cancer. *Cancer research*, 51(11), pp.2979–84.

Matarraz, S. et al., 2011. New technologies in cancer. Protein microarrays for biomarker discovery. *Clin Transl Oncol*, 13, pp.156–161.

Materna, V. et al., 2007. Taxol-resistance-associated gene-3 (TRAG-3/CSAG2) expression is predictive for clinical outcome in ovarian carcinoma patients. *Virchows Archiv : an international journal of pathology*, 450(2), pp.187–94.

McArthur, G.A. et al., 2014. Safety and efficacy of vemurafenib in BRAF(V600E) and BRAF(V600K) mutation-positive melanoma (BRIM-3): extended follow-up of a phase 3, randomised, open-label study. *The Lancet. Oncology*, 15(3), pp.323–32.

Merrell, K. et al., 2004. Analysis of low-abundance, low-molecular-weight serum proteins using mass spectrometry. *Journal of biomolecular techniques : JBT*, 15(4), pp.238–248.

Michaud, G. et al., 2003. Analyzing antibody specificity with whole proteome microarrays. *Nature Biotechnology*, 21(12), pp.1509–12.

Neller, M.A., López, J.A. & Schmidt, C.W., 2008. Antigens for cancer immunotherapy. *Seminars in Immunology*, 20, pp.286–295.

Nicholaou, T. et al., 2006. Directions in the immune targeting of cancer: lessons learned from the cancer-testis Ag NY-ESO-1. *Immunology and cell biology*, 84(3), pp.303–17.

Nicholaou, T. et al., 2009. Regulatory T-cell-mediated attenuation of T-cell responses to the NY-ESO-1 ISCOMATRIX vaccine in patients with advanced malignant melanoma. *Clinical cancer research : an official journal of the American Association for Cancer Research*, 15(6), pp.2166–2173.

Nimmrich, I. et al., 2000. Seven genes that are differentially transcribed in colorectal tumor cell lines. *Cancer letters*, 160(1), pp.37–43.

Nutt, S.L. et al., 2015. The generation of antibody-secreting plasma cells. *Nature Reviews Immunology*, 15(3), pp.160–171.

O'Kane, S.L., O'Brien, J.K. & Cahill, D.J., 2011. Optimized Autoantibody Profiling on Protein Arrays. In U. Korf, ed. *Methods in Molecular Biology*. Methods in Molecular Biology. Humana Press, pp. 331–341.

Odunsi, K. et al., 2003. NY-ESO-1 and LAGE-1 cancer-testis antigens are potential targets for immunotherapy in epithelial ovarian cancer. *Cancer research*, 63(18), pp.6076–83.

Peled, N. et al., 2009. MAGE A3 antigen-specific cancer immunotherapeutic. *Immunotherapy*, 1(1), pp.19–25.

Perales, M.-A. et al., 2002. Strategies to overcome immune ignorance and tolerance. *Seminars in cancer biology*, 12(1), pp.63–71.

Peyssonnaux, C. & Eychène, A., 2001. The Raf/MEK/ERK pathway: new concepts of activation. *Biology of the cell / under the auspices of the European Cell Biology Organization*, 93(1-2), pp.53–62.

Predki, P.F., 2004. Functional protein microarrays: ripe for discovery. *Current Opinion in Chemical Biology*, 8(1), pp.8–13.

Di Pucchio, T. et al., 2006. Immunization of stage IV melanoma patients with Melan-A/MART-1 and gp100 peptides plus IFN-alpha results in the activation of specific CD8(+) T cells and monocyte/dendritic cell precursors. *Cancer research*, 66(9), pp.4943–51.

Quackenbush, J., 2001. Computational Analysis of Microarray Data. *Genetics*, 2(June).

Quoix, E. et al., 2011. Therapeutic vaccination with TG4010 and first-line chemotherapy in advanced non-small-cell lung cancer: A controlled phase 2B trial. *The Lancet Oncology*, 12(12), pp.1125–1133.

Reles, A. et al., 2001. Correlation of p53 mutations with resistance to platinum-based chemotherapy and shortened survival in ovarian cancer. *Clinical cancer research : an official journal of the American Association for Cancer Research*, 7(10), pp.2984–97.

Restifo, N.P., Dudley, M.E. & Rosenberg, S.A., 2012. Adoptive immunotherapy for cancer: harnessing the T cell response. *Nature reviews. Immunology*, 12(4), pp.269–81.

Rifai, N., Gillette, M.A. & Carr, S.A., 2006. Protein biomarker discovery and validation: the long and uncertain path to clinical utility. *Nature Biotechnology*, 24(8), pp.971–983.

Risch, H.A., 1998. Hormonal etiology of epithelial ovarian cancer, with a hypothesis concerning the role of androgens and progesterone. *Journal of the National Cancer Institute*, 90(23), pp.1774–86.

Risinger, J.I. et al., 2007. Global expression analysis of cancer/testis genes in uterine cancers reveals a high incidence of BORIS expression. *Clinical cancer research : an official journal of the American Association for Cancer Research*, 13(6), pp.1713–9.

Rodrigues, N.R. et al., 1990. p53 mutations in colorectal cancer. *Proceedings of the National Academy of Sciences of the United States of America*, 87(19), pp.7555–9.

Rodriguez-Antona, C. & Ingelman-Sundberg, M., 2006. Cytochrome P450 pharmacogenetics and cancer. *Oncogene*, 25(11), pp.1679–91.

Rodríguez-Paredes, M. & Esteller, M., 2011. Cancer epigenetics reaches mainstream oncology. *Nature medicine*, 17(3), pp.330–9.

Roitt, I.M., Brostoff, J. & Male, D.K. eds., 2001. *Immunology* 6th editio., Mosby.

Rosenberg, S.A. et al., 1998. Immunizing patients with metastatic melanoma using recombinant adenoviruses encoding MART-1 or gp100 melanoma antigens. *Journal of the National Cancer Institute*, 90(24), pp.1894–900.

Rosenberg, S.A. et al., 1998. Immunologic and therapeutic evaluation of a synthetic peptide vaccine for the treatment of patients with metastatic melanoma. *Nature medicine*, 4(3), pp.321–7.

Sadanandam, A. et al., 2013. A colorectal cancer classification system that associates cellular phenotype and responses to therapy. *Nat Med*, 19(5), pp.619–625.

Safari Serufuri, J.-M., 2010. *Development of computational methods for Custom protein arrays analysis . A case study on a 100 protein (" CT100 ") cancer / testis antigen array .*

Sanchez-Carbayo, M., 2011. Antibody Microarrays as Tools for Biomarker Discovery. In U. Korf, ed. *Methods in Molecular Biology*. Methods in Molecular Biology. Humana Press, pp. 159–182.

Sanz-García, E. et al., 2014. Prognosis and Therapeutic Implications for Emerging Colorectal Cancer Subtypes. *Current Colorectal Cancer Reports*, 10, pp.55–61.

Sauer, R. et al., 2004. Preoperative versus postoperative chemoradiotherapy for rectal cancer. *The New England journal of medicine*, 351(17), pp.1731–40.

Scanlan, M.J. et al., 2002. Cancer/testis antigens: an expanding family of targets for cancer immunotherapy. *Immunological reviews*, 188(3), pp.22–32.

Scarcella, D.L. et al., 1999. Expression of MAGE and GAGE in high-grade brain tumors: a potential target for specific immunotherapy and diagnostic markers. *Clinical cancer research : an official journal of the American Association for Cancer Research*, 5(2), pp.335–41.

Schlom, J., 2012. Therapeutic cancer vaccines: Current status and moving forward. *Journal of the National Cancer Institute*, 104, pp.599–613.

Schwartzentruber, D.J. et al., 2011. gp100 peptide vaccine and interleukin-2 in patients with advanced melanoma. *The New England journal of medicine*, 364(22), pp.2119–27.

Schweitzer, B., Predki, P. & Snyder, M., 2003. Microarrays to characterize protein interactions on a whole-proteome scale. *Proteomics*, 3(11), pp.2190–2199.

Scott, A.M., Wolchok, J.D. & Old, L.J., 2012. Antibody therapy of cancer. *Nature Reviews Cancer*, 12(April), pp.278–287.

Shiku, H. et al., 1977. Cell surface antigens of human malignant melanoma. III. Recognition of autoantibodies with unusual characteristics. *The Journal of experimental medicine*, 145, pp.784–789.

Shin, S. et al., 2001. An Anti-apoptotic Protein Human Survivin Is a Direct Inhibitor of Caspase-3 and -7. *Biochemistry*, 40(4), pp.1117–1123.

Simpson, A.J.G. et al., 2005. Cancer/testis antigens, gametogenesis and cancer. *Nature reviews. Cancer*, 5(8), pp.615–25.

Starzynska, T. et al., 1992. Prognostic significance of p53 overexpression in gastric and colorectal carcinoma. *British journal of cancer*, 66(3), pp.558–62.

Stockert, E. et al., 1998. A survey of the humoral immune response of cancer patients to a panel of human tumor antigens. *The Journal of experimental medicine*, 187(8), pp.1349–54.

Stubbs, R.S., Cannan, R.J. & Mitchell, A.W., 2001. Selective internal radiation therapy with yttrium-90 microspheres for extensive colorectal liver metastases. *Journal of gastrointestinal surgery : official journal of the Society for Surgery of the Alimentary Tract*, 5(3), pp.294–302.

Stubbs, R.S. & Wickremesekera, S.K., 2004. Selective internal radiation therapy (SIRT): a new modality for treating patients with colorectal liver metastases. *HPB : the official journal of the International Hepato Pancreato Biliary Association*, 6(3), pp.133–9.

Sumimoto, H. et al., 2006. The BRAF-MAPK signaling pathway is essential for cancer-immune evasion in human melanoma cells. *The Journal of experimental medicine*, 203(7), pp.1651–1656.

Swana, H.S. et al., 1999. Tumor content of the antiapoptosis molecule survivin and recurrence of bladder cancer. *The New England journal of medicine*, 341(6), pp.452–3.

Tabi, Z., 2009. Cancer Vaccines. In Y. Lu & R. I. Mahato, eds. *Pharmaceutical Perspectives of Cancer Therapeutics*. Springer US, pp. 365–397.

Tamm, I. et al., 1998. IAP-Family Protein Survivin Inhibits Caspase Activity and Apoptosis Induced by Fas (CD95), Bax, Caspases, and Anticancer Drugs. *Cancer research*, 58, pp.5315–5320.

Tan, E.M., 2001. Autoantibodies as reporters identifying aberrant cellular mechanisms in tumorigenesis. *Journal of Clinical Investigation*, 108(10), pp.1411–1415.

Tan, H.T. et al., 2009. Serum autoantibodies as biomarkers for early cancer detection. *FEBS Journal*, 276, pp.6880–6904.

Tan, P. et al., 2014. Dual epigenetic targeting with panobinostat and azacitidine in acute myeloid leukemia and high-risk myelodysplastic syndrome. *Blood cancer journal*, 4(e170).

Tartaglia, J. et al., 2001. Therapeutic vaccines against melanoma and colorectal cancer. *Vaccine*, 19(17-19), pp.2571–5.

Terwilliger, T.C., Stuart, D. & Yokoyama, S., 2009. Lessons from Structural Genomics. *Annu Rev Biophys*, 38, pp.371–383.

The Cancer Genome Atlas Reserach Network, 2013. Integrated genomic characterization of endometrial carcinoma. *Nature*, 497(53), pp.67–73.

Thompson, C., 1995. Apoptosis in the pathogenesis and treatment of disease. *Science*, 267(5203), pp.1456–1462.

Thurner, B. et al., 1999. Vaccination with mage-3A1 peptide-pulsed mature, monocyte-derived dendritic cells expands specific cytotoxic T cells and induces regression of some metastases in advanced stage IV melanoma. *The Journal of experimental medicine*, 190(11), pp.1669–78.

Ueda, H. et al., 2003. Association of the T-cell regulatory gene CTLA4 with susceptibility to autoimmune disease. *Nature*, 423(6939), pp.506–511.

Ulloa-Montoya, F. et al., 2013. Predictive gene signature in MAGE-A3 antigen-specific cancer immunotherapy. *Journal of clinical oncology : official journal of the American Society of Clinical Oncology*, 31(19), pp.2388–2395.

Vanneman, M. & Dranoff, G., 2012. Combining immunotherapy and targeted therapies in cancer treatment. *Nature Reviews \ Cancer*, 12(April), pp.237–251.

Vansteenkiste, J. et al., 2007. Final results of a multi-center, double-blind, randomized, placebo-controlled phase II study to assess the efficacy of MAGE-A3 immunotherapeutic as adjuvant therapy in stage IB/II non-small cell lung cancer (NSCLC). J. Clin. Oncol.25. *ASCO Meeting Abstracts*, 25(18), p.7554.

Vigil, C., Martin-Santos, T. & Garcia-Manero, G., 2010. Safety and efficacy of azacitidine in myelodysplastic syndromes. *Drug Design, Development and Therapy*, pp.221–229.

Vigneron, N. et al., 2013. Peptide database: T cell-defined tumor antigens. *Cancer Immunity*.

Vivier, E. et al., 2012. Targeting natural killer cells and natural killer T cells in cancer. *Nature Reviews Immunology*, 12(4), pp.239–252.

De Vries, T.J. et al., 1997. Heterogeneous expression of immunotherapy candidate proteins gp100, MART-1, and tyrosinase in human melanoma cell lines and in human melanocytic lesions. *Cancer research*, 57(15), pp.3223–9.

Wang, M. et al., 1997. Three-dimensional structure of NADPH – cytochrome P450 reductase : Prototype for FMN- and FAD-containing enzymes. *Proc Natl Acad Sci USA*, 94(August), pp.8411–8416.

Wang, X. et al., 2005. Autoantibody signatures in prostate cancer. *The New England journal of medicine*, 353(12), pp.1224–1235.

Whitehurst, A.W., 2014. Cause and consequence of cancer/testis antigen activation in cancer. *Annual review of pharmacology and toxicology*, 54, pp.251–72.

Widenmeyer, M. et al., 2012. Promiscuous survivin peptide induces robust CD4+ T-cell responses in the majority of vaccinated cancer patients. *International journal of cancer. Journal international du cancer*, 131(1), pp.140–9.

De Wit, N.J.W. et al., 2002. Expression profiling of MMA-1a and splice variant MMA-1b: new cancer/testis antigens identified in human melanoma. *International journal of cancer*, 98(4), pp.547–53.

Wolf-Yadlin, A., Sevecka, M. & MacBeath, G., 2009. Dissecting protein function and signaling using protein microarrays. *Current Opinion in Chemical Biology*, 13(4), pp.398–405.

World Health Organization, 2002. *National Cancer Control Programmes - Policies and managerial guidelines*,

Xiang, B. et al., 2013. Colorectal cancer immunotherapy. *Discovery medicine*, 15(84), pp.301–8.

Xiang, R. et al., 2008. Oral DNA vaccines target the tumor vasculature and microenvironment and suppress tumor growth and metastasis. *Immunological Reviews*, 222, pp.117–128.

Xu, Y.-W. et al., 2014. Autoantibodies as potential biomarkers for the early detection of esophageal squamous cell carcinoma. *The American journal of gastroenterology*, 109(1), pp.36–45.

Yang, Y. et al., 1993. Construction of recombinant DNA by exonuclease recession. *Nucleic Acids Research*, 21(8), pp.1889–1893.

Yuan, J. et al., 2011. Integrated NY-ESO-1 antibody and CD8+ T-cell responses correlate with clinical benefit in advanced melanoma patients treated with ipilimumab. *Proceedings of the National Academy of Sciences of the United States of America*, 108(40), pp.16723–8.

Zhai, Y. et al., 1996. Antigen-specific tumor vaccines. Development and characterization of recombinant adenoviruses encoding MART1 or gp100 for cancer therapy. *Journal of immunology (Baltimore, Md. : 1950)*, 156(2).

Zhao, Y., Chapman, D.A.G. & Jones, I.M., 2003. Improving baculovirus recombination. *Nucleic Acids Research*, 31(2), pp.1–5.

Zheng, J. et al., 2005. Strong repulsive forces between protein and oligo (ethylene glycol) self-assembled monolayers: a molecular simulation study. *Biophysical Journal*, 89(1), pp.158–66.

Zhu, H. et al., 2000. Analysis of yeast protein kinases using protein chips. *Nature Genetics*, 26(3), pp.283–9.

Zhu, H. et al., 2001. Global analysis of protein activities using proteome chips. *Science (New York, N.Y.)*, 293(5537), pp.2101–5.

Zhu, X., Gerstein, M. & Snyder, M., 2006. ProCAT : a data analysis approach for protein microarrays. *Genome Biology*, 7(11), p.R110.

Zou, W., 2006. Regulatory T cells, tumour immunity and immunotherapy. *Nature reviews. Immunology*, 6(April), pp.295–307.